Vector-meson interactions, dynamically generated molecules, and the hadron spectrum

Dissertation
zur
Erlangung des Doktorgrades (Dr. rer. nat.)
der
Mathematisch-Naturwissenschaftlichen Fakultät
der
Rheinischen Friedrich-Wilhelms-Universität Bonn

von
Dilege Gülmez
aus
Ankara, Turkey

Bonn, 21.06.2018

Dieser Forschungsbericht wurde als Dissertation von der Mathematisch-Naturwissenschaftlichen Fakultät der Universität Bonn angenommen und ist auf dem Hochschulschriftenserver der ULB Bonn `http://hss.ulb.uni-bonn.de/diss_online` elektronisch publiziert.

1. Gutachter:	Prof. Dr. Ulf-G. Meißner
2. Gutachterin:	Prof. Dr. Cristoph Hanhart
Tag der Promotion:	27.07.2018
Erscheinungsjahr:	2018

Abstract

We study the lowest-lying vector-meson interactions and dynamically generated bound states. Therefore, these bound states are studied as hadronic molecules. We demonstrate that some unitarization methods are not well-defined to study the pole structures of amplitudes in the region far from the threshold. We employ an improved unitarization method based on a covariant formalization that is necessary to study the pole structures of amplitudes in the region far from the threshold. In this work, first, we study the analysis of the covariant $\rho\rho$ scattering in a unitarized chiral theory and then extend it to the strange sector, i.e. SU(3) chiral symmetry. We demonstrate that the on-shell factorization of the Bethe-Salpeter equation is not suitable away from the threshold. Moreover, the left-hand cuts would overlap the right-hand cuts for the coupled-channel unitarization of the Bethe-Salpeter equation. It makes unitarized amplitudes non-analytical and the poles of amplitudes, associated to possible bound states or resonances, unreliable. To avoid this difficulty, we employ the first iterated solution of the N/D method and investigate the possible dynamically generated resonances and bound states. A comparison with the non-relativistic calculation is provided as well.

Contents

Preface

In the beginning of 1930s, the deuterium, and then the neutron were discovered. In 1935, Yukawa proposed pions to explain nucleon-nucleon interactions in a field theoretical approach, via one pion exchange. Even though this description is not the true microscopic picture of nature, Yukawa brought in a new approach to particle physics which has evolved into many different effective field theories. Twelve years later, in 1947, the pion was observed, and the kaon discovery followed it in the same year. Since then, many more hadrons have been observed as higher energies were probed.

Starting with the discovery of kaons, particle physicists started to suspect the elementary nature of these particles. This idea received increasing support as the hadron spectrum expanded. It was realized that most of these hadrons are actually resonances and the first unified framework of hadrons, the quark model, was proposed in 1964 by Gell-Mann and Zweig. After this, hadrons were not considered as elementary, but as composite particles of quarks. An underlying theory of strong interactions was proposed ten years later as a non-abelian gauge theory. However, the quark model, due to its simplicity, has always been studied to understand the hadron spectrum. With the failure to explain the lowest-lying scalar nonet, Jaffe proposed the tetraquark picture in 1977, which goes beyond the classical quark model. As the hadron spectrum was investigated more, it has been realized that some hadrons cannot be explained by static multi-quark states and were studied as colored diquark correlations or as dynamically generated hadronic molecules.

The identification of the structure of a hadron state is not always straightforward. The analyses can take years, which are conducted by many independent groups, as in the case of the $\sigma(500)$ or $\Lambda(1405)$. There are several hadron states with open questions, and numerous research groups are debating about their structures. Therefore, the study of the hadron spectrum is a rich field with intense ongoing research. The chosen methods to study the open questions should be considered carefully since each method comes with its limitations and drawbacks.

In this work, we study the low-energy dynamics of the lowest-lying vector-mesons and dynamically generated hadronic molecules via their interactions. The study combines chiral perturbation theory (ChPT), which is the effective field theory (EFT) of quantum chromodynamics (QCD) at low energies, and the hidden gauge symmetry formalism to build an effective chiral Lagrangian to include vector-mesons. To be able to study dynamically generated molecules, we need to employ a unitarization method of scattering amplitudes. This leads to the chiral unitary approach, which allows us to study the structures appearing via vector-meson vector-meson scattering processes, like bound states and resonances. By using the chiral unitary approach, we are able to perform calculations which require only one free parameter for each channel. Even though the chiral unitary approach allows us to study the energy regimes and structures where the chiral effective Lagrangians by themselves are not applicable, it has limitations. Therefore, while employing these methods and studying the dynamically generated bound states and resonances, we scrutinize early works on the issue by accentuating those limitations.

In the first chapter of this work, we give a brief introduction on the basic ideas of quantum field theory (QFT) and QCD, the QFT of strong interactions. In particular, we study the symmetry properties of its Lagrangian, how one of these symmetries, the chiral symmetry is spontaneously broken and the

consequences of this symmetry breaking. In the second chapter, we study how to build a low energy effective theory of QCD, ChPT, based on the dynamics of chiral symmetry breaking. We need this new scheme besides QCD since perturbative methods are not applicable in the low-energy regime of this theory. At the end of the second chapter, a chiral Lagrangian is studied to include vector-mesons by using the hidden local gauge formalism based on the ideas of EFTs. In the next chapter, we study properties of the S-matrix theory such as unitarity and causality to understand the pole structures in strong interaction amplitudes. The consequences of these properties are then applied to unitarize scattering amplitudes obtained from the chiral effective Lagrangian. Moreover, we briefly explain a few unitarization methods to understand the limitations of each method by going over the assumptions and the simplifications of each method.

The last chapter of this work is dedicated to covariant scattering calculations of $SU(2)$ and $SU(3)$ sectors of vector-meson interactions. First, we use the on-shell factorization method of the Bethe-Salpeter equation, and its limitations are examined. It is shown that this method violates analytic properties of the scattering amplitude far away from the threshold of the interactions and results are unreliable. Hence, we employ a more general method, the N/D method. We get the correct analytic properties for scattering amplitudes and investigate the possibility of dynamically generated resonances and bound states in each partial wave channel. Finally, these results are compared to the non-relativistic calculations.

Most of the content of this thesis has been published in

1. D. Gülmez, U.-G. Meißner and J.A. Oller, A chiral Covariant approach to $\rho\rho$ scattering, Eur.Phys.J. C **77** (2017) no.7, 460 [arXiv:1611.00168]

2. M.-L Du, F.-K. Guo, D. Gülmez, U.-G. Meißner, Q. Wang, Covariant vector-meson vector-meson interactions and dynamically generated resonances,
In preparation for publication

CHAPTER 1

Introduction

The Standard Model explains the strong and electroweak interactions of elementary particles. Before the discovery of the Higgs boson, the validity of the Standard Model was thought to be up to around 1 TeV. With the discovery of the Higgs boson, the range of validity has potentially increased to far above that limit. The theory has demonstrated its predictive power and precision, and it explains nearly all the data in Particle Data Group book (PDG) [1]. It predicted the Higgs, W, and Z bosons, the top and charm quarks, and the gluon before they had been observed. Other major examples of its prediction and precision are the anomalous magnetic moment of the electron and muon, and the mass of the Z boson.

Albeit its success, there are pending problems which the Standard Model is unable to answer. Some of these problems are, for instance, its 26 unexplained free parameters [1], which demand a deeper understanding of nature, the hierarchy problem (it is open to debate if this is a problem at all), dark energy and dark matter, and gravity (the Standard Model is constructed with flat spacetime). Thus, there is a need for a more general theory but we already know that to study low-energy scale physics of particles (low with respect to the Planck scale, $\Lambda_{Planck} = 10^{19}$ GeV) any theory can be realized as a QFT since quantum phenomena at these scales can be understood in terms of a quantum field theory [3].

Given that the Standard Model examines the low-energy scale with respect to the Planck scale, it is also a QFT. Any QFT needs to satisfy Lorentz invariance (causality), unitarity and cluster decomposition. A QFT has to be gauge invariant. Otherwise, a massless spin-1 particle violates Lorentz invariance due to the coupling of these fields [4]. The gauge symmetry of the Standard model is $SU(3) \otimes SU(2) \otimes U(1)$, which is spontaneously broken by the Higgs field. Another important property of the Standard Model is its renormalizability at the scale at which it works very well. The model gets its predictive power from this property, since a renormalizable QFT depends on a finite number of parameters and renormalization provides a systematic approach of the theory for higher energy scale physics, such that we can assign a cutoff Λ for new physical phenomena to occur and effects of these phenomena are suppressed by orders of $1/\Lambda$ below the cutoff region.

The Standard Model is expressed in the Lagrangian formalism like any other QFT, since symmetries are manifest in the Lagrangian formalism. The degrees of freedom of the theory are various fundamental fields. The variety of those fields is not explained in the theory and excitations of these fields are considered as elementary particles. There are no reasons to consider these particles as composite particles at the energy scale of the Standard Model since there is no experimental evidence of it.

[1] These are the electromagnetic coupling constant, strong coupling constant, 9 Yukawa coupling constants, Higgs potential coupling constant (or the Higgs mass), the Weinberg angle, the electroweak symmetry breaking scale, the three mixing angles and the CP-violating phase of the Cabbibo-Kobayashi-Maskawa (CKM) matrix, the strong CP-violating factor, three neutrino masses, the three mixing angles and the CP-violating phase of the Pontecorvo-Maki-Nakagawa-Sakata (PMNS) matrix, for further details see [2].

The particle spectrum of the Standard Model includes quarks (u, d, s, c, b, t) and leptons $(e, \mu, \tau, \nu_e, \nu_\mu, \nu_\tau)$, the fermionic content of matter which obey Fermi-Dirac statistics with half integer spins, and bosons $(H, W^\pm, Z, \gamma)$, obeying Bose-Einstein statistics with integer spins. The charged leptons (e, μ, τ) and quarks interact electromagnetically via its force mediator, the photon (γ). All leptons interact weakly via the $W^\pm$ and Z bosons. These two forces are unified in the Standard Model as the electroweak force with the symmetry group $SU(2) \otimes U(1)$. In addition to their electric charge, quarks also carry color charge. As a consequence, they interact strongly via gluons. Unlike photons, gluons carry charge, the color charge. Thus, they can interact amongst themselves. This property makes their symmetry group non-commutative. Therefore, strong interactions, with the gauge group $SU(3)$, is a non-abelian gauge theory called Quantum ChromoDynamics (QCD).

In this work, we work with hadrons (composite particles made of quarks) and their strong interactions at energies of the order GeV, to be called the low-energy regime from now on. Except conformal field theories, all field theories have running coupling constants, meaning their values change with respect to the energy scale. At the order of one GeV, the interactions of hadrons are dominated by the strong interaction. Accordingly, we take into account solely the QCD part of the Standard Model. However, QCD is non-perturbative in this region. Non-perturbative theories are still unsolvable analytically and different methods have been developed to understand the nature of QCD in this energy regime.

The main numerical approach is lattice QCD, where QCD is solved numerically in a discretized spacetime lattice and the required entities are calculated numerically, and then the zero lattice spacing limit is taken [5–8]. There are other approaches like holographic models [9–12].

The most successful/commonly used analytic method is to exploit the symmetry properties of the theory in the low-energy regime, and some EFTs can be built using these properties. These EFTs make it possible to use perturbation theory to perform calculations of hadronic interactions at that energy regime by using hadrons as the degrees of freedom instead of the degrees of freedom of QCD, quarks and gluons [13–19].

With the development of EFTs, many properties of low-energy hadronic interactions are now understood and many predictions have been made regarding their properties and hadronic spectrum. As its usefulness has been revealed, the method is now applied to other energy regimes. Hence, new phenomenological Lagrangians have been constructed to study new degrees of freedoms.

In the rest of this chapter, we give a brief introduction to QCD and its low-energy regime properties. The units and conventions used in this work can be found in Appendix A.

1.1 QCD

Quarks

QCD is built on the idea that quarks are the fundamental particles, not hadrons. Whether they are real objects or not was still open to debate in the beginning of the 1970s [2]. By then, the idea of quarks was prevalent but there were also theories which studied hadrons independent of any QFT scheme. It is not clear who proposed the idea of quarks first [20], but it is officially accepted that they are envisioned by Gell-Mann and Zweig [22, 23]. The conclusive experimental result was announced by the SLAC collaboration with their experiment on the deep inelastic scattering of leptons on nucleons [24]. The properties of the six known quarks are shown in Table 1.1.

Since the top quark has an extremely short lifetime ($O(10^{-25})$ s) it decays to another quark (mostly to the $b-$quark) before it can hadronize. Therefore, it is not considered in this work. Moreover, this work

[2] For a brief overview of that period [20] and for a detailed one [21].

	Mass [MeV]	Charge [e]	Isospin	Strangeness
u	$2.2^{+0.6}_{-0.4}$	$2/3$	$1/2$	0
d	$4.7^{+0.5}_{-0.4}$	$-1/3$	$1/2$	0
s	96^{+8}_{-4}	$-1/3$	0	1
c	1280 ± 30	$2/3$	0	0
b	$4180^{+40}_{-30} \pm 40$	$-1/3$	0	0
t	173210 ± 510	$2/3$	0	0

Table 1.1: Properties of quarks [1].[3]

is focused on the low-energy regime of QCD, around 1 GeV. Hence, the $c-$ and $b-$quarks are not of interest in this work as well. On the other hand, the $u-$, $d-$, and $s-$quarks have much lower mass values with respect to the GeV scale. Therefore, we will be dealing with only these three flavors which are categorized as light quarks. Decoupling of the heavy quarks from QCD is mentioned in Section 2.1.1.

Color

There are two types of hadrons; mesons and baryons. Mesons are $q\bar{q}$ states (bosonic) whereas baryons are qqq states (fermionic) (There are also exotic states like tetraquark and pentaquark hadrons [4] [26–30]). Quark spin alignment of baryons has two possibilities: spin $1/2$ and spin $3/2$. Spin $1/2$ formation is an anti-symmetric formation whereas $3/2$ is symmetric. Moreover, the three quark state of baryons includes space and flavor states which are symmetric. As a result, spin $3/2$ baryons (historically, the Δ was the first of these) are totally symmetric. Fermions have anti-symmetric ground states since they obey Fermi-Dirac statistics. Hence, a spin 3/2 totally symmetric wave function is contradictory. This problem was named as the spin-statistics problem and it was resolved with introduction of a new quantum number, the color charge.

This new quantum number is not an observable, thus hadrons must be color neutral, 'colorless'. For mesons, $q\bar{q}$ states, it is easy to obtain colorless states just by assigning opposite charges to them, like red and anti-red. The same is not the case for baryons. To obtain a color neutral state for a three quark state, there should be three different color quantum numbers (red, green and blue). The combination of red, green, and blue gives a colorless state similar to the red and anti-red combination. Hence, it is only possible to obtain an anti-symmetric ground state for baryons with spin $3/2$ with three color charges.

Although, the spin statistics problem was not the only problem indicating a new quantum number. QCD was found to be renormalizable only if there are three differently charged quarks. Otherwise, some gauge anomalies occur [31]. Hadronic τ decays also give clear evidence of three different color charges [32]. The observed rate of the π^0 decay to two photons can only be explained if there are three species of quarks[5], and there are more examples to be found in the literature [32, 34].

Asymptotic Freedom

Despite deep inelastic scattering of leptons off nucleons leading the way to quarks, an unexpected result was discovered [24]. At large momentum transfer, nucleons turn out to have a noninteracting internal structure. This result indicated that the nucleon structure consists of Feynman's partons [35]. This

[3] The quark masses are scheme- and scale-dependent, see [1] and the discussion therein [25].

[4] There is no restriction in adding more quarks to the theory as long as the wave-function symmetries are respected.

[5] In the first calculation of this decay, protons and neutrons were used [33]. Because, it was done before the discovery of quarks. Therefore, the result was in agreement with the experiment without the knowledge of number of color charges.

structure turned out to be quarks and the short distance behaviour of quarks was later explained via asymptotic freedom [36, 37]. It simply dictates that as the energy scale increases, interactions of particles weaken in an asymptotically free theory. As a result of this, we can conclude that the QCD coupling constant is also a running coupling constant like in QED, but in the opposite direction. In QED, the interaction or the effective charge of the particle increases with energy due to a phenomenon called charge screening whereas in QCD the coupling constant decreases as energy increases.

To understand this concept, consider the running coupling constant of any gauge coupling up to leading order (in the perturbative energy regime):

$$\alpha_s(Q^2) = \frac{\alpha_s(\mu^2)}{1 + \frac{\beta_0}{(4\pi)^2}\alpha_s(\mu^2)\ln Q^2/\mu^2} \tag{1.1}$$

where α is the running coupling constant, Q is the energy scale, and μ is the renormalization scale. Here, β_0 characterizes the interaction. If it has a negative value, the gauge theory is like QED, it is infrared (IR) stable. If it has a positive value, as Q^2 increases $\alpha_s(Q^2)$ approaches to zero, it is ultraviolet (UV) stable. This is to say it is an asymptotically free theory. This difference between QED and QCD is due to the fact that, the photon does not have any electric charge whereas the gluon has color charge. Therefore, gluons can interact with one another. Before the Nobel prized publications of Politzer and, Gross and Wilczek [36, 37] [6], it was thought that no quantum field theory could be asymptotically free [39].

In perturbative QCD, the coupling constant varies with the energy scale μ as in eq. (1.1). For calculations in the perturbative regime, we need to choose a convenient energy regime and deduce the coupling constant value in that regime. One way to do this is to set $\mu = m_Z^2$. There is another way in which a dimensionful parameter is introduced via

$$\ln \frac{Q^2}{\Lambda^2} = -\int_{\alpha_s(Q^2)}^{\infty} \frac{dx}{\beta(x)}\,, \tag{1.2}$$

which shows the divergence scale of the coupling outside the perturbative energy regime. It is found to be around $\Lambda = 200$ MeV which implies that perturbative method is not valid for QCD at scales of $Q \sim 1$ GeV [40]. Confinement, chiral symmetry breaking and hadronization occurs in this region. Therefore, we need different methods in the low-energy regime of QCD to understand these problems.

Confinement

There is one more significant characteristic of QCD, which is confinement of quarks and gluons. It dictates that there can be no colorful state. To put it in another way, quarks cannot be observed freely but only in bound states. Color is a gauge degree of freedom, therefore it cannot be understood experimentally (since it cannot be observed), hence it should be analyzed analytically. Although confinement lacks an analytical proof until now, it can be understood partially by considering two static quarks (test charges) with a gauge field (a gluon) connecting them so that the system is gauge invariant. When the total energy of the state is calculated with respect to the distance between the quarks, it has the form [40]:

$$V(r) = a + b\alpha/r + \sigma r + O(r^2)\,, \tag{1.3}$$

where a and b are real constants and σ behaves like a string tension. The Coulomb potential like term behaves as in QED, so to say as in a perturbative theory. However, the perturbative region of QCD exhibits

[6] We should emphasize the work of 't Hooft here as well [38].

asymptotic freedom, so it consists of hadrons. On the other hand, confinement is a non-perturbative phenomenon. The term linear in r has a string-like behaviour since it leads to an increase in energy as the distance between a quark and an antiquark pair increases. At some point (depending on the value of σ), the potential energy of the pair will be so large that another pair of quark and antiquark is created, forming a new pair of bound state with the initial quarks. QCD string tension, $\sigma \sim 400$ MeV [41], makes it impossible to observe a single quark or gluon but only a colorless bound state.

1.1.1 QCD Lagrangian

Gauge Invariance

To have a gauge invariant QCD let us start with a massive free quark Lagrangian:

$$\mathcal{L}_0 = \bar{\psi}(x) i \not{\partial} \psi(x) - m \bar{\psi}(x) \psi(x) \,. \tag{1.4}$$

This Lagrangian is invariant under the global $U(1)$ phase transformation[7]

$$\psi(x) \to \psi'(x) = e^{-iQ\epsilon} \psi(x) \,. \tag{1.5}$$

Here, Q and ϵ are real constants. To check whether this transformation is same at different points of spacetime, let $\epsilon \equiv \epsilon(x)$. It is obvious that the mass term is still invariant whereas the kinetic term transforms as

$$\partial_\mu \psi(x) \to e^{-iQ\epsilon(x)} (\partial_\mu - iQ\partial_\mu \epsilon(x)) \psi(x) \,. \tag{1.6}$$

Hence, it is not invariant. As a result, the phase should be global and not local to preserve invariance. A spin-1 field A_μ and a covariant derivative D_μ have to be introduced if local invariance and the gauge invariance is insisted. The form of the covariant derivative is:

$$D_\mu(x) = (\partial_\mu + iQA_\mu(x)) \psi(x) \,. \tag{1.7}$$

The newly introduced objects transform under the local transformation as:

$$A_\mu(x) \quad \to \quad A'_\mu(x) = A_\mu(x) + \partial_\mu \epsilon(x) \,, \tag{1.8}$$

$$D_\mu \psi(x) \quad \to \quad (D_\mu \psi)'(x) = e^{-iQ\epsilon(x)} D_\mu \psi(x) \,. \tag{1.9}$$

As a result, demanding local $U(1)$ transformation invariance (gauge invariance) has generated a vector field-spinor field interaction in the Lagrangian:

$$\mathcal{L} = \bar{\psi}(x)(i \not{D} - m)\psi(x) = \mathcal{L}_0 - QA_\mu(x) \bar{\psi}(x) \gamma^\mu \psi(x) \,. \tag{1.10}$$

To explain the dynamics of the vector field Lagrangian needs a vector propagation term. A mass term cannot be assigned to this vector field since $m_V^2 A_\mu A^\mu$ is not gauge invariant. Introducing a kinetic term and using the gauge invariant field strength tensor (the gauge must be fixed, for details see [4, 31]) $F_{\mu\nu} = \partial_\mu A_\nu - \partial_\nu A_\mu$, the full Lagrangian gets the form:

$$\mathcal{L} = \bar{\psi}(x)(i \not{D} - m)\psi(x) - \frac{1}{4} F^{\mu\nu} F_{\mu\nu} \,. \tag{1.11}$$

This is the form of a general gauge invariant Lagrangian with one fermion and one gauge field.

[7] The transformation has an exponential form since they are unitary, $U^\dagger U = I$.

QCD Lagrangian

The free quark Lagrangian with three flavors (f) and each flavor with three colors (i) has a very similar form like the one in eq. (1.4)

$$\mathcal{L}_0 = \bar{q}_{i,a}(i\not{\partial} - m_{q_a})q_{i,a}\,, \tag{1.12}$$

where repeated indices are summed over and spacetime dependence is not stated.

If we study global transformations which leave quark fields invariant, we end up with $SU(3)$ transformations. This corresponds to eight independent transformations of $SU(3)$. The $SU(3)$ group elements and properties can be found in Appendix B.1. The main difference between $U(1)$ and $SU(3)$ transformations occurs when gauge invariance is demanded. The details of sustaining gauge invariance in $SU(3)$ and gauge fixing procedure are studied in Appendix B.2. The gauge invariant QCD Lagrangian has the form (before gauge fixing):

$$\mathcal{L}_{\text{QCD}} = -\frac{1}{2}\langle F_i^{\mu\nu}F^i_{\mu\nu}\rangle + \bar{q}^i_f(i\not{D}_{ij} - m_f\delta_{ij})q^j_f\,. \tag{1.13}$$

Here, $\langle\rangle$ refers to the trace and $F^{\mu\nu}$ has the form as in eq. (B.12).

Any QFT (localized Lorentz invariant gauge theories) should conserve CPT(Charge-Parity-Time) symmetry which is the combination of the discrete symmetries together. QCD, eq. (1.13), conserves, in addition to the local gauge symmetry (which ensures renormalizability of QCD), each discrete symmetry C, P, and T separately.

Strong CP problem

There is an omitted gauge invariant term in eq. (1.13) which violates CP invariance,

$$\mathcal{L}_\theta = \frac{\theta g^2}{64\pi^2}\epsilon^{\mu\nu\alpha\beta}F^i_{\mu\nu}F_{i,\alpha\beta}\,, \tag{1.14}$$

where ϵ is the Levi-Civita tensor, g is the strong coupling constant and θ is the chiral phase or field mixing angle. This term is the analog of $E\cdot B$ interaction in QED and appears due to the non-trivial vacuum structure of QCD. This term violates the CP symmetry/T symmetry but this violation has never been observed in strong interaction experiments. The current limit on θ is $\theta \lesssim 7.4\times10^{-11}$ [42], which is obtained by using the experimental limit on the electric dipole moment of the neutron [43]. The question, "Why θ has such a small value?" leads to the strong CP problem. The value can be set to zero directly, however if we require real mass terms in the Standard Model, this term can be regenerated via weak interactions. There are different solutions to the strong CP problem. One of them is the Peccei-Quinn theory, where θ is a scalar field called axion [44], and for another solution which does not introduce a new particle can be checked in [45]. Since this term can be written as a total divergence, it is absent from the Feynman rules in the context of perturbative QCD[8]. In this work, the experimental limit on θ ensures us that it can be neglected[9].

1.1.2 Chiral Symmetry in QCD

We have already stated that QCD has a gauge symmetry with gauge group $SU(3)_c$ and it is invariant under parity transformations. If we ignore the θ term which has never been observed in experiments, it is

[8] In the case of non-Abelian theories, there are finite action configurations which does not allow the surface term to be neglected. These terms are called instantons and θ term can cause physical effects due to instantons [46].

[9] For a study of finite θ dependence of resonances, see [47]

invariant under CP transformations as well. Therefore, it is also invariant under T symmetry (due to the CPT theorem). Moreover, there are some approximate symmetries of the QCD Lagrangian which can be exploited and they turn out to be beneficial. We will take into account chiral symmetry which has a crucial role in this work.

Let us consider only the kinetic terms of eq. (1.13):

$$\mathcal{L}_{\text{kinetic}} = -\frac{1}{2}F_i^{\mu\nu}F^i_{\mu\nu} + \bar{q}^i_f(i\not{D}_{ij})q^j_f\,. \tag{1.15}$$

Using the projection operators $P_{R/L} = \frac{1}{2}(1\pm\gamma_5)$, the right- and left-handed quark fields (chiral components) can be defined as:

$$q_{R/L} = \frac{1}{2}(1 \pm \gamma_5)q\,. \tag{1.16}$$

Eq. (1.15) can be written as (color indices and quark independent parts are dropped):

$$\mathcal{L}_{\text{q,kinetic}} = \bar{q}_{f,L}(i\not{D})q_{f,L} + \bar{q}_{f,R}(i\not{D})q_{f,R}\,. \tag{1.17}$$

It can be seen that this Lagrangian does not have a term which mixes the flavors (the covariant derivative is flavor independent) or left- and right-handed quarks. Therefore, the independent transformations R, L of right- and left-handed quark fields $q_{R/L} \rightarrow R/L\, q_{R/L}$, leave $\mathcal{L}_{\text{q,kinetic}}$ invariant. Hence, there exists a global transformation for each flavor. The symmetry group of the left- and right-handed quark transformations (chiral transformations) is $U(3)_L \otimes U(3)_R$. It is already stated that the masses of light quarks and heavy quarks have a big scale difference. Moreover, heavy quarks can be integrated out in the low-energy regions. Hence, let us just consider the light quarks as massless (chiral limit);

$$m_u = m_d = m_s = 0 \quad \& \quad m_c = m_b = m_t = \infty\,. \tag{1.18}$$

Therefore, the symmetry of eq. (1.17) takes the form:

$$SU(3)_L \otimes SU(3)_R \otimes U(1)_V \otimes U(1)_A\,. \tag{1.19}$$

$SU(3)_L \otimes SU(3)_R$ is called the chiral symmetry group.

When there is an exact global symmetry of a Lagrangian, due to Noether's theorem, there should be a conserved current ($\partial_\mu J^\mu = 0$) where the charge (Q) of that current is conserved ($dQ/dt = 0$), e.g., translation symmetry in time and space refers to energy-momentum conservation. We consider Noether's theorem briefly in appendix C.1

When Noether's theorem is applied, the conserved currents of the chiral symmetry are

$$L^a_\mu = \sum_{q=u,d,s} \bar{q}_L \frac{\lambda^a}{2}\gamma_\mu q_L\,, \qquad R^a_\mu = \sum_{q=u,d,s} \bar{q}_R \frac{\lambda^a}{2}\gamma_\mu q_R\,, \tag{1.20}$$

with the corresponding conserved charges Q^a_L and Q^a_R. These currents can be rewritten as

$$V^a_\mu = R^a_\mu + L^a_\mu = \bar{q}\gamma_\mu \frac{\lambda_a}{2} q \quad , \qquad A^a_\mu = R^a_\mu - L^a_\mu = \bar{q}\gamma_\mu\gamma_5 \frac{\lambda_a}{2} q \tag{1.21}$$

$$\partial^\mu V^a_\mu = 0 \quad , \qquad \partial^\mu A^a_\mu = 0 \tag{1.22}$$

$$Q^a_V \xrightarrow[\text{parity}]{P} Q^a_V \quad , \qquad Q^a_A \xrightarrow{P} -Q^a_A\,. \tag{1.23}$$

Eq. (1.22) is briefly explained in appendix C.1.1.

There is also the singlet part of chiral symmetry which occurs under the same phase transformation for all left/right handed quarks:

$$V_0^\mu = \bar{q}_R \gamma^\mu q_R + \bar{q}_L \gamma^\mu q_L = \bar{q}\gamma^\mu q \quad , \qquad A_0^\mu = \bar{q}_R \gamma^\mu q_R - \bar{q}_L \gamma^\mu q_L = \bar{q}\gamma^\mu \gamma_5 q \tag{1.24}$$

$$\partial_\mu V_0^\mu = 0 \quad , \qquad \partial_\mu A_0^\mu \neq 0 \,. \tag{1.25}$$

Here, the conserved charge of V_0^μ is the baryon number. A_0^μ is only conserved in the classical theory. Thus, $U(1)_A$ is not an actual symmetry of the theory. The symmetry is broken due to an anomaly appearing in the quantizaton process [31]. Anomalies are beyond the scope of this work. For a detailed discussion, the interested reader can refer to [19, 34] and references therein. As a result, the symmetry is reduced to

$$SU(3)_L \otimes SU(3)_R \otimes U(1)_V \,. \tag{1.26}$$

When QCD is considered with the assumption in eq. (1.18), we realize that there is only one parameter in the Lagrangian. It is the coupling strength of a quark, g. Since $g^2 \propto \ln(r\Lambda_{\mathrm{QCD}})^{-1}$, there are no free dimensionless parameters, which makes the assumption very powerful.

1.1.3 Spontaneous Symmetry Breaking

Consider eqs. (1.22), (1.23). Since the corresponding charges are conserved, they commute with the Hamiltonian.

$$\begin{aligned} H_{\text{chiral QCD}}|\psi\rangle &= E|\psi\rangle, \\ Q_V|\psi\rangle = E|\psi\rangle \quad &, \quad Q_A|\psi\rangle = E|\psi\rangle \,. \end{aligned} \tag{1.27}$$

Therefore, chiral symmetry leads to bound states with opposite parity but same mass. This is not observed in the hadron spectrum. For example, the parity partner of the nucleon ($m_N \sim 940$ MeV) is $N(1535)$. According to chiral symmetry they should have the same mass whereas in reality $N(1535)$ is much heavier. The resolution to this problem comes with the realization of the spontaneous breaking of chiral symmetry, which was explained by Nambu and Goldstone [48, 49]. We briefly study symmetry realization in QCD and spontaneous symmetry breaking in appendix C.2.2.

For spontaneous symmetry breaking to occur, a continuous symmetry should be realized in the Lagrangian of a theory. However, the symmetry is not shared by the vacuum or the particle spectrum of the theory (like in chiral symmetry of QCD). Therefore, the chiral symmetry of the Hamiltonian should not be a symmetry of the vacuum:

$$Q_V|0\rangle = 0 \,, \quad Q_A|0\rangle \neq 0 \,. \tag{1.28}$$

The reason for the axial charge to be non-invariant is the Wafa-Witten theorem [50]. This theorem states that there is no spontaneous parity breaking in theories with vector-like fermions (fermions that transform in the same way under L and R). Thence, the lowest energy state of a gauge theory is invariant only under the vector charges. The lowest energy state that QCD forms is quark condensate, $\langle 0|\bar{q}q|0\rangle$. This condensate mixes the opposite handed quark fields in the following way

$$\langle 0|\bar{q}q|0\rangle = \langle 0|\bar{q}_L q_R + \bar{q}_R q_L|0\rangle \overset{m_q \to 0}{=} \langle 0|\bar{u}u|0\rangle = \langle 0|\bar{d}d|0\rangle = \langle 0|\bar{s}s|0\rangle \,. \tag{1.29}$$

Mixing of left- and right-handed quarks breaks the chiral symmetry of QCD. The spontaneous symmetry

breaking of QCD has no analytical proof in QCD itself, but both phenomenology and Lattice QCD confirms it. Eq. (1.29) in the chiral limit shows that massless QCD is flavor blind[10]. Therefore, the vector part is left as a symmetry of the theory whereas the axial symmetry is broken.

Goldstone's theorem states that if a symmetry is spontaneously broken, there will be massless, spin 0 particles (Nambu-Goldstone bosons), corresponding to the generators of the spontaneously broken symmetry. This can be understood in a brief explanation as follows: Since chiral symmetry is a continuous symmetry of the QCD Lagrangian, the corresponding charge should be conserved, $[H, Q^i_{V,A}] = 0$, where i corresponds to each generator of the symmetry in consideration. The axial part of chiral symmetry is spontaneously broken. Thus, the axial current creates eight degenerate states [11] from the vacuum: $Q^i_A|0\rangle = |\phi\rangle$. Using $[H, Q^i] = 0$, we get:

$$H|\phi\rangle = HQ^i_A|0\rangle = Q^i_A H|0\rangle = 0\,. \tag{1.30}$$

Therefore, these degenerate states, $|\phi\rangle$, are massless pseudoscalars (since they are created via axial charge) and there are 8 of them. They are called Nambu-Goldstone bosons.

As a result, when chiral symmetry is spontaneously broken, the symmetry is reduced to:

$$SU(3)_V \otimes U(1)_V \tag{1.31}$$

and there are eight pseudoscalar Goldstone bosons. In the QCD particle spectrum, lightest octet of hadrons are pseudoscalars ($\pi^\pm, \pi^0, K^\pm, K^0, \bar{K}^0, \eta$), corresponding to the Goldstone bosons indeed (in case of taking only u and d quarks ($SU(2)$) in the chiral limit there are 3 Goldstone bosons which are π multiplet).

However, these eight pseudoscalar mesons are not massless in nature. Chiral symmetry only reveals itself in the massless quark limit, hence it is not an exact symmetry of nature. When quark masses are considered, chiral symmetry is explicitly broken and pseudoscalar mesons become massive.

1.1.4 Quarks with Mass and Explicit Symmetry Breaking

When $\mathcal{L}_{\text{QCD}}$ is considered under chiral rotations, the mass term breaks this invariance by mixing left- and right-handed fields:

$$\mathcal{L}_m = m_f(\bar{q}_{f,R}q_{f,L} + \bar{q}_{f,L}q_{f,R})\,. \tag{1.32}$$

When the quark mass matrix ($\mathcal{M} = \text{diag}(m_u, m_d, m_s)$) is introduced, vector and axial currents are no longer conserved:

$$\partial_\mu V^\mu = \frac{i}{2}\bar{q}(\mathcal{M}\lambda - \lambda\mathcal{M})q = \frac{i}{2}\bar{q}[\mathcal{M}, \lambda]q\,,\ \partial_\mu A^\mu = \frac{i}{2}\bar{q}(\mathcal{M}\lambda + \lambda\mathcal{M})q = \frac{1}{2}i\bar{q}\{\mathcal{M}, \lambda\}\gamma_5 q\,, \tag{1.33}$$

$$\partial_\mu V^\mu_0 = 0,\ \partial_\mu A^\mu_0 = 2i\bar{q}\mathcal{M}\gamma_5 q + \text{anomaly term}\,. \tag{1.34}$$

When quark masses are considered, we can see that the $U(1)_A$ symmetry is broken even if the anomaly is not considered. All quark masses are different from each other. Therefore, only the diagonal currents are conserved since mass matrix is also diagonal. Therefore, $U(1)_V$ symmetry, $V^\mu_0 = \bar{q}\gamma^\mu q$ is the only symmetry which survives. Moreover, each individual flavor current is also conserved, e.g. $\bar{u}\gamma_\mu u$,...

[10] The vacuum of QCD should preserve main symmetries of QCD, like Lorentz invariance, parity, etc. Hence, only scalar operators can lead to vacuum expectation values which are not zero. Moreover, the vacuum expectation value of an operator can be non zero only if it commutes with the Hamiltonian. As a result, there is only one option left, the quark condensate.

[11] Any $SU(N)$ theory has $N^2 - 1$ generators.

Even though quarks are massive, their values are small (we consider only light quarks). Hence explicit symmetry breaking is small and can be treated perturbatively. Thus, how much it deviates from the exact symmetry is proportional to the masses of quarks. For simplicity, let us consider two flavors, u and d:

$$\mathcal{L}_m = m_u \bar{u}u + m_d \bar{d}d = \frac{1}{2}[(m_u + m_d)(\bar{u}u + \bar{d}d) + (m_u - m_d)(\bar{u}u - \bar{d}d)]\,, \tag{1.35}$$

where $\bar{q}q = \bar{q}_R q_L + \bar{q}_L q_R$. The first term does not lead to isospin breaking since the mass matrix is diagonal whereas the second term breaks the isospin symmetry. Since up and down quark masses are very close to each other, the mass difference term is very small with respect to the scale. Therefore, these quark masses can be assumed to be equal. In this case, the second term gives zero and the isospin breaking is avoided.

In case of three flavors, $m_s - m_d$ term appears with the relation $(m_s - m_d) \gg (m_d - m_u)$. However, this difference can also be considered as small with respect to the energy scale in consideration. Therefore, we can take all three quark masses to be equal. So, if only $m_u = m_d$ is assumed, it is the isospin $SU(2)$ symmetry and the symmetry is reduced to:

$$SU(3)_V \otimes U(1)_V \to SU(2) \otimes U(1)_V \otimes U(1)\,. \tag{1.36}$$

The last $U(1)$ is responsible for the strangeness conservation. If all three flavors are considered to be equal, $m_u = m_d = m_s$, it is called $SU(3)$ flavor symmetry:

$$SU(3) \otimes U(1)_V\,. \tag{1.37}$$

This symmetry is evidently approximate, since in the particle spectrum we have singlets, octets and decouplets. These groups of particles are the representation of the $SU(3)$ group where zero mass degeneracy is broken with respect to quark mass differences.

Gell-Mann-Oakes-Renner Relation

The chiral condensate is renormalization group dependent; hence it is not an observable quantity. On the other hand $m_q\langle\bar{q}q\rangle$ is independent of the renormalization group, so it is a physical quantity. We can relate this quantity with the scaling of the pion mass via Gell-Mann-Oakes-Renner (GMOR) relation which can be derived from eq. (1.42):

$$m_\pi^2 = -\frac{(m_u + m_d)\langle 0|\bar{q}q|0\rangle}{f_0^2}\,, \tag{1.38}$$

where f_0 is called the pion decay constant. It is determined experimentally, via pion weak decay to leptons and their neutrinos, to be $f_\pi \sim 92.1$ MeV [1]. Here, we have to be careful. If quarks are considered to be massless or different from their real value, the experimental value would be different from the theoretical value. That is why we have f_0 instead of f_π in eq. (1.38). This issue will be discussed later in section 2.2.3. Eq. (1.38) states that the squared Goldstone mass is proportional to the quark condensate when there is no exact chiral symmetry.

Partially Conserved Axial-Vector Current (PCAC)

One of the consequences of spontaneous symmetry breaking is that for each generator of the broken symmetry group, there is a Goldstone boson (π):

$$\langle 0|J_\mu(0)|\pi\rangle \neq 0\,. \tag{1.39}$$

That means, Goldstone bosons couple with the vacuum through the current of the spontaneously broken symmetry since their quantum numbers are identical. The corresponding spontaneously broken current in chiral QCD is the axial vector current A_μ:

$$\langle 0|A_\mu(0)|\pi(p)\rangle \neq 0\,. \tag{1.40}$$

Moreover, the Goldstone theorem indicates that Goldstone fields have only derivative couplings. Therefore, they have zero scattering amplitudes for zero momenta. These are all contained in:

$$\langle 0|A^a_\mu(0)|\pi_b(p)\rangle = ie^{-ipx}\delta^a_b p^\mu f_0\,. \tag{1.41}$$

This equation tells us that f_0 represents the strength of a Goldstone boson decay via axial vector current.

Taking the divergence of eq. (1.41) yields:

$$\langle 0|\partial^\mu A^a_\mu(0)|\pi_b(p)\rangle = i\delta^a_b m^2_\pi f_0\,. \tag{1.42}$$

We already stated that in the chiral limit quarks have no mass and the axial vector current is conserved. This statement can be realized first in eq. (1.38), which lets $m_\pi = 0$, and then for that value, eq. (1.42) shows the conservation of the axial current. Moreover, eq. (1.42) says that $\partial^\mu A_\mu$ and π correspond to the same field (to be discussed in Section 2.2.2). This refers to partially conserved axial current (PCAC) which says that in the limit of small momenta, one particle singularities dominate the interaction [51].

Let us clarify this statement with an example. In the chiral limit, $\partial_\mu A^\mu = 0$ and $m_\pi = 0$. Therefore,

$$ip^\mu\langle 0|A^a_\mu(0)|\pi_b(p)\rangle = 0\,. \tag{1.43}$$

Consider the amplitude $\mathcal{M}^\mu = \langle\pi^a(q_1)\pi^b(q_2)\pi^c(q_3)|A^\mu_d(x)|0\rangle$ in the chiral limit. The second vertex of diagram, fig.1.1(b), can be considered as $\pi\pi$ scattering, $T(q_1, q_2, q_3, q)$. Therefore,

$$i\mathcal{M}^\mu = iR^\mu + iq^\mu\frac{if_0}{q^2}iT(q_1, q_2, q_3, q)\,. \tag{1.44}$$

Since axial current is conserved, $\partial_\mu\mathcal{M}^\mu = 0$. Hence, $q_\mu\mathcal{M}^\mu = 0$. This implies:

$$\lim_{q\to 0} q_\mu\mathcal{M}^\mu = \lim_{q\to 0} R^\mu - \lim_{q\to 0} f_0 T(q_1, q_2, q_3, q). \tag{1.45}$$

Since the left hand side is zero, $T(q_1, q_2, q_3, q) = 0$ when R^μ is assumed to include no singularities [12]. As a result, at vanishing momenta, Goldstone bosons do not interact as stated in the Goldstone theorem. However, since chiral symmetry is not exact, there will be corrections of order $q^2 = m^2_\pi$ when quarks are massive.

(a) diagram with no singularities. (b) diagram with a Goldstone boson exchange.

Figure 1.1: Axial current to 3π coupling

[12] In reality, this term has multi-pion exchange singularities or includes resonances with mass.

It is said that one particle singularities dominate over the rest (R^μ) with respect to PCAC which can be seen from eq. (1.45). In this case, f_0 becomes a characteristic property of low-energy interactions of Goldstone bosons. It represents the low-energy scale. Since that term dominates in low-energy interactions, $T(q_1, q_2, q_3, q)$ can be expanded in terms of Goldstone boson momenta. However, the exchange of Goldstone bosons can create singularities due to poles, e.g., four point function with pion exchange. Even though the expansion in terms of momenta would fail (starting at zero momentum limit for a massless theory), these singularities are considered to be of higher orders of the expansion due to PCAC. They appear in loop diagrams and are called chiral logs. These logarithms occur since pion exchange is a long-range interaction in chiral limit.

An important conclusion of PCAC is that the interaction of Goldstone bosons at low energies is weak whereas it is the opposite for quarks and gluons. Therefore, these interactions can be treated perturbatively unlike in QCD. we can set a framework where quarks and gluons are exchanged with Goldstone bosons as degrees of freedom to make use of perturbation theory. Theories with this framework are called effective field theories and with a careful treatment they can represent the main theory in a certain energy regime. In the next chapter we discuss properties of EFTs, and their equivalence with the underlying theory in a certain regime within the framework of chiral effective theory.

CHAPTER 2

Chiral Effective Field Theory

As mentioned already, the low-energy regime of QCD (approximately below 1 GeV) is non-perturbative due to the large value of the running coupling constant (eq. (1.1)). Therefore, we need a different framework which is in agreement with the symmetry principles of QCD. Phenomenological methods were used even before the QCD era to understand the spontaneous chiral symmetry breaking of strong interactions [51]. In the language of field theory, the leading order results for the low-energy regime of QCD (e.g. scattering of pions) were already known in the late sixties (phenomenological models and current algebra method). The first systematic treatment of these phenomenological models was discussed by Weinberg [13]. In this work, it was clarified how to calculate corrections to the leading order and how these corrections can be classified to be suppressed at each order. This scheme was applied to the low-energy regime of QCD and a systematic order by order calculation (with additionally introduced coupling constants) was first introduced by Gasser and Leutwyler for $SU(2)$ and for $SU(3)$ respectively in [14, 15].

Loop calculations which are divergent take place in the systematic expansion. Hence, a sound regularization is demanded as well. To achieve this and for robust phenomenological applications, the values of the introduced coupling constants should be known accurately. However, these constants should be determined for the energy regime where QCD is not perturbative. As a result, they should be determined from a different approach.

There are different methods to understand the low-energy behaviour of QCD. A few of them are chiral effective field theories [16, 19, 52–54], sum rules [55–57], dispersion relations [58], Dyson-Schwinger equations [59–61] as analytic approaches and lattice QCD [11, 62, 63] as a numerical method to solve QCD Lagrangian directly. Each of them has its own strengths and weaknesses. However, chiral effective Lagrangians and lattice QCD are the most commonly used ones. Some of them also offer a scheme to relate nuclear physics with QCD [64–66].

In this work, we will be using low-energy effective field theory of QCD, chiral perturbation theory (ChPT). The operators, respecting the symmetries of QCD, can be included in the action and this can be done in a systematic way in terms of perturbation theory. Therefore, we expect ChPT to describe strong interaction phenomena in the low-energy regime. Since these effective theories are limited to a certain range of energies and calculations are needed up to a few perturbative orders, they are less restricted in terms of renormalizability. Hence, already mentioned additional parameters are needed to be introduced at each order which need to be fixed. These constants play a free parameter role in the effective theory and they are most likely fixed by an experiment or by lattice simulations [67].

2.1 Effective Field Theories

Particle physics includes the study of phenomena in very different scales of time, energy or length. In some scales relativistic effects are important whereas in others, classic limits, or stationary states are precise enough depending on the purpose of a calculation. This is a very intuitive feature. We can calculate motions of Newtonian objects, up to very precise orders without the need for special relativity or calculate the hydrogen atom without including muon or top quark dynamics into the theory. Therefore, while studying some particular regime of energy we can omit the "unrelated" part. A systematic scheme of work is needed to be able to perform calculations safely and rigorously to make sure that the missing physics do not have much of an effect on the result. This is done by effective field theories. In the modern understanding of QFT, even the Standard Model is an effective field theory.

An effective field theory (EFT) aims to study the small energies of the light modes of some physical phenomena with respect to a given scale. Therefore, the first thing to understand is where to set the scale. This scale is usually called the hard scale and represented by Λ, which separates the notion of low and high energies and what the degrees of freedom, light modes below that scale are. This has to be done to make sure that the physics of high energy scales can be eliminated systematically. Otherwise, high energy physics or heavy modes may have uncontrolled effects on the phenomena. As a result, the EFT would lose its predictive power and reliability. Once a scale of an EFT is set, all modes with higher masses can be integrated out. The effects of these heavy modes are included either in generated operators from the decoupling procedure or in the coupling constants of EFT via a renormalization procedure. An EFT with a well separated scale ensures that higher energy effects are suppressed inversely in the power of heavy field masses or the defined energy scale. Exploiting this, we can perform calculations with a model-independent approach in the non-perturbative regime of QCD or have simpler ways to calculate observables of a theory.

If an EFT of a fundamental or more underlying theory is studied, we must investigate the symmetries of the fundamental theory and their behaviour in the defined energy regime of EFT. On the other hand, if an EFT does not have a more fundamental theory, the assumed symmetry principles should be considered and realized (if they are broken or not, and if yes, how?). Once these principles are known, we can construct an EFT. This requirement is known as the 'folk theorem' of Weinberg [13] [1]:

> ...although individual quantum field theories have of course a good deal of content, quantum field theory itself has no content beyond analyticity, unitarity, cluster decomposition, and symmetry. This can be put more precisely in the context of perturbation theory: if one writes down the most general possible Lagrangian, including all terms consistent with assumed symmetry principles, and then calculates matrix elements with this Lagrangian to any given order of perturbation theory, the result will simply be the most general possible S-matrix consistent with analyticity, perturbative unitarity, cluster decomposition and the assumed symmetry principles. As I said, this has not been proved, but any counterexamples would be of great interest, and I do not know of any.
>
> With this "theorem", one can obtain and justify the results of current algebra simply by writing down the most general Lagrangian consistent with the assumed symmetry principles, and then deriving low-energy theorems by a direct study of the Feynman graphs, without operator algebra.

After the construction of such a general Lagrangian, a perturbative expansion (in terms of momentum, mass, etc.) should be organized. Later on, a finite set of parameters should be fixed order by order.

[1] This has been proven for ChPT (all possible interactions consistent with the parity, charge conjugation and approximate chiral symmetry) by Leutwyler in [68].

Finally, Feynman diagrams of a process can be calculated up to desired order. This method gives a systematic approach and model-independent blueprint to EFTs.

As a very brief historical example, we can consider a leptonic electroweak decay process via a weak gauge boson (W) exchange, with a total energy much smaller than the energy scale $\Lambda \equiv M_W$. If it is calculated from the Standard model Lagrangian,

$$\frac{g^2}{2}\frac{g^{\mu\nu} - \frac{k^\mu k^\nu}{M_W^2}}{M_W^2 - k^2} \times (\text{vertex contr.}) \tag{2.1}$$

where g is the coupling constant, 'vertex contr.' indicates contribution from each leptonic electroweak process tree level diagram vertex and the rest is just the propagator of the gauge boson. Since the lepton mass is much smaller than the gauge boson mass, the propagator can be expanded in powers of $\frac{k^2}{M_W^2}$ in the low-energy region. Thus, at lowest order it simplifies to $\frac{g^2}{2M_W^2} \times$ (vertex cont). This can be obtained from an effective Lagrangian of the form [69, 70]

$$\mathcal{L} = 2\sqrt{2}G_F(\bar{l}\gamma_\mu P_L \nu_l)(\bar{\nu_{l'}}\gamma^\mu P_L \nu_{l'}) + \text{h.c.}\,. \tag{2.2}$$

where the terms inside the parenthesis correspond to (vertex contr.) in eq. (2.1) and G_F is called the Fermi constant which is the only parameter of the effective Lagrangian. This parameter includes information of the coupling constant g, gauge boson mass M_W, the excluded heavy field in this case, and other coefficients. It was historically set from the experimental value of the muon mean life. The interpretation of the difference in terms of Feynman diagrams would be that eq. (2.1) corresponds to a tree level process while eq. (2.2) corresponds to an effective contact interaction

2.1.1 Integrating Out a Heavy Field

Let us say that there is a general action $S[\phi_l, \phi_h]$ (a full theory which is known) which includes both a light (ϕ_l) and a heavy (ϕ_h) field with $m_{\phi_l} \ll m_{\phi_h} \equiv \Lambda$:

$$S[\phi_l, \phi_h] = \int d^4x \mathcal{L}(\phi_l, \phi_h) = S[\phi_l] + S[\phi_l, \phi_h]\,.^2 \tag{2.3}$$

Integrating out heavy fields refers to separation of the integration process to first integration over the heavy fields for fixed values of the light modes. Then, an effective action can be defined as:

$$e^{iS_{\text{eff}}[\phi_l]} = \int d\phi_h e^{iS[\phi_l,\phi_h]} = e^{iS[\phi_l]} \int d\phi_h e^{iS[\phi_l,\phi_h]}\,. \tag{2.4}$$

Notice that the outcome of the last integral depends only on ϕ_l. As a result, the effective action will have the form:

$$S_{\text{eff}}[\phi_l] = \int d^4x \mathcal{L}_{\text{eff}}(\phi_l) = S[\phi_l] + S_{\text{non-dec}}[\phi_l] + S_{\text{dec}} \tag{2.5}$$

where the last term includes the decoupling terms which are suppressed by $1/m_{\phi_h}$ or $1/\Lambda$.

Heavy fields have two effects. They renormalize the infrared (IR) couplings and they cause new non-renormalizable interactions which are inversely proportional to the heavy field mass. Therefore, as the limit $m_{\phi_h} \to \infty$ is taken, these terms decouple.

[2] For an introduction to the path integral formalism [71].

Decoupling Theorem

The formulation of decoupling for any QFT is done by Appelquist and Carrazone [72]. They have stated:

> If the remaining low-energy theory is renormalizable, then all effects of heavy particles appear either as a renormalization of the coupling constants in the theory or else are suppressed by powers of the heavy particles masses.

This theorem, for gauge theories, allows all heavy fermions to decouple. For example in QCD, all heavy quarks can be integrated out. This is intuitive. If heavy modes had effects on the low energy limit, we would be able to predict heavy quarks in the low-energy limit via experimental results in that region, which is never the case.

2.1.2 Constructing an EFT Lagrangian

We demand our effective theory to exhibit the symmetries of a more general theory. The degrees of freedom of the effective theory will be different but they still should be invariant under the same symmetry transformations. Without any prescription, we can write the most general effective Lagrangian consistent with these transformations and symmetries, as stated in the folk theorem:

$$\mathcal{L}_{\text{fund.th.}}[\text{d.o.f.}] \rightarrow \mathcal{L}_{\text{eff}}[\text{eff. d.o.f.}]\,. \tag{2.6}$$

It might seem like there would be infinitely many possible terms and yet effective theories can be expanded in terms of momenta. This lets us to manage perturbatively all the possible terms order by order:

$$\mathcal{L}_{\text{eff}} = \mathcal{L}_{\text{eff}}^{\mathcal{O}(1)} + \mathcal{L}_{\text{eff}}^{\mathcal{O}(2)} + \cdots\,. \tag{2.7}$$

Each higher order coefficients of operators are suppressed by $1/\Lambda$, where Λ is the energy scale of an effective theory. As a result, each vertex contribution from these terms will have E^n/Λ^{n-4} (from dimensional analyses) order contributions. In a low-energy effective field theory, since the energy is smaller than the characteristic hard scale, higher order contributions are guaranteed to be smaller with respect to the lower order contributions. At each order, terms will come with some extra unknown coefficients which should be determined either from experiment or from phenomenology.

2.1.3 Weinberg's Power Counting

According to the procedure above, we need a dimensional counting scheme for loop diagrams. Some of the momentum terms of a particular order term can be included in a loop diagram which need to be integrated over. Therefore, these terms would turn out to have a smaller order with respect to their originated order. Hence, if we do not insist on such a particular counting rule, there might be contributions to a lower order calculation from an arbitrarily higher order. This would destroy the systematic expansion which we demand for a theory of bosons with derivative couplings This scheme, proposed by Weinberg, is the so called Weinberg's power counting theorem [13].

Consider a diagram with N_V total vertices: $N_V = \sum_n N_n$ with N_n being number of vertices of nth derivative term of an effective theory, p^n, m^n. So, the mass scale (scale in the coefficients of the effective Lagrangian) dimension should be $N_C = \sum_n N_n(d-n)$ where d is the dimension which comes from dimensional regularization (so that we can count the mass, energy dimension), which will be taken as 4 from now on. Consider that there are N_I internal lines and N_E external lines and each internal line is

formed with a contraction of two fields. Moreover, the Euler identity gives:

$$N_I = N_L + N_V - 1\,. \tag{2.8}$$

where N_L is the number of independent loops.

Therefore, a calculated amplitude will be in the order of:

$$\text{mass}^{4-N_E} = \Lambda^{\sum_n N_n(4-n)-N_E-2N_L-2\sum_n N_n+2}(m \text{ or } p)^D\,. \tag{2.9}$$

This gives us:

$$D = 2 + \sum_n N_n(n-2) + 2N_L\,. \tag{2.10}$$

In terms of rescaling of momenta ($p_i \to tp_i$) and masses ($m_i \to t^2 m_i$) and amplitude, this refers to:

$$\mathcal{M}(tp_i, t^2 m_i) = t^D \mathcal{M}(p_i, m_i) \quad \text{where: } 0 < t \leq 1 \tag{2.11}$$

Eq. (2.10) and eq. (2.11) imply that each added vertex or loop increases the dimension of m or p. Notice that $D \geq 2$. Eq. (2.10) is called Weinberg's power counting. It says that a Feynman diagram will be at the order of $O\left(\frac{p}{4\pi f_0}\right)^D$ where f_0 is a leading order constant of the theory. Therefore, at the leading order, a diagram with one loop has $O\left(\frac{p}{4\pi f_0}\right)^2$ contribution. This scheme makes sure that only a small number of loops is needed at low energies. As the number of loops is increased in a diagram, contributions will become less important.

2.2 Constructing the Chiral Effective Lagrangian

While constructing the Lagrangian, first we must define the symmetries of the theory. In the low-energy regime of QCD, the dominating properties are chiral symmetry, spontaneous and explicit symmetry breaking of chiral symmetry and anomalous symmetry breaking of $U(1)$ axial symmetry. Moreover, as stated several times, due to confinement, hadrons are the observables, instead of quarks and gluons. Therefore, hadrons are the degrees of freedom of the chiral effective Lagrangian. As a result, low energy interactions are described by Goldstone bosons which form the pseudoscalar meson octet. In chiral limit, they are massless. Since there are no massless particles other than photons and gluons, pions would have a long life time in chiral limit since there is nothing else for them to decay to. This leads to long range interaction behaviour of pion exchange. But, since there is explicit symmetry breaking, the pion is massive and the pion exchange is a short range interaction, like QCD itself. Low energy chiral Lagrangians were first studied by Weinberg [73] and more general frameworks of how to construct spontaneously broken effective theories were studied in [14, 15, 74, 75]. For an introduction to ChPT with different applications [54, 76–81] and for a detailed introduction to the topic [16, 19, 82] are suggested to the interested reader.

2.2.1 Goldstone Boson Representation

Since the degrees of freedom are Goldstone bosons, we want first to find a representation of the meson fields. Our Lagrangian has $SU(3)_L \times SU(3)_R$ chiral symmetry which is spontaneously broken to $SU(3)_V$ ($SU(3)_V \subset SU(3)_L \times SU(3)_R$). Consider R as a representation of $SU(3)_L \times SU(3)_R$, the Goldstone bosons then transform accordingly:

$$\pi \to \pi' = R(s, \pi)\,, \tag{2.12}$$

where $\pi \equiv (\pi_1, \pi_2, ..., \pi_8)$ and $s \in SU(3)_L \times SU(3)_R$. Since $SU(3)_V$ leaves the vacuum invariant, $R(v, 0) = 0$, $\forall v \in SU(3)_V$. Therefore, if e is considered as the unit element ($R(e, a) = a$) of $SU(3)_L \times SU(3)_R$, $R(e, 0) = 0 \Rightarrow e \in SU(3)_V$. Moreover,

$$R(ev, 0) = R(e, R(v, 0)) = R(e, 0)\,. \tag{2.13}$$

Therefore, the representation R maps the coset space $SU(3)_L \times SU(3)_R / SU(3)_V$ (isomorphic to $SU(3)_L \times SU(3)_R$) elements onto all field configurations of π. Every element of $SU(3)_L \times SU(3)_R$ can be represented as

$$s = (s_L, s_R) = (1, s_R S_L^{-1})(s_L, s_L) \equiv cv\,, \qquad c \in SU(3)_L \times SU(3)_R / SU(3)_V\,. \tag{2.14}$$

The action of $SU(3)_L \times SU(3)_R$ on $SU(3)_L \times SU(3)_R / SU(3)_V$ gives:

$$(L, R)(1, s_R s_L^{-1}) = (L, R s_R s_L^{-1}) = (1, R s_R s_L^{-1} L^{-1})(L, L)\,. \tag{2.15}$$

Here, $L, R \in SU(3)_{L,R}$ and the same relation holds for $s_L s_R^{-1}$ as well. As a result, every element of $SU(3)_L \times SU(3)_R / SU(3)_V$ can be represented as:

$$U := s_L s_R^{-1} \quad \text{or} \quad U := s_R s_L^{-1}\,. \tag{2.16}$$

Hence, π can be represented by matrix valued fields $U(x) \in SU(3)$. Under chiral symmetry transformation, the behaviour of U is:

$$\begin{aligned} (1, U) \to (1, U') \quad &= \quad (L, R)(1, U) = (L, RU) = (1, RUL^\dagger)(L, L) \\ U \quad &\to \quad U' = RUL^\dagger\,. \end{aligned} \tag{2.17}$$

A particular representation is

$$U = \exp\left(\frac{i\lambda_a \pi_a}{f_0}\right), \tag{2.18}$$

where a is summed over, λ_a are the Gell-Mann matrices (Appendix B.1) and

$$\phi = \lambda_a \pi_a = \sqrt{2} \begin{pmatrix} \frac{1}{\sqrt{2}}\pi^0 + \frac{1}{\sqrt{6}}\eta & \pi^+ & K^+ \\ \pi^- & -\frac{1}{\sqrt{2}}\pi^0 + \frac{1}{\sqrt{6}}\eta & K^0 \\ K^- & \bar{K}^0 & -\frac{2}{\sqrt{6}}\eta \end{pmatrix}. \tag{2.19}$$

2.2.2 The Leading Order $O(p^2)$

According to eq. (2.6),

$$\mathcal{L}_{\text{QCD}}[q, \bar{q}, F] \to \mathcal{L}_{\text{ChPT}}[U, \partial U, \partial^2 U, \dots], \tag{2.20}$$

where C, P, T, Lorentz and chiral symmetries are respected. Due to Lorentz invariance, only terms with even powers of momentum are allowed (this is the reason for the first term in eq. (2.7) to vanish). At the zeroth momentum order, the only term which respects all the symmetries is $U^\dagger U = \mathbb{1}$. This term has no effect on the equations of motion. Therefore, it can be omitted. The next order is the second order. There

is only one term which respects all of the symmetries[3]:

$$\mathcal{L}^{(2)} = \frac{f_0^2}{4}\langle \partial_\mu U^\dagger \partial^\mu U \rangle \,. \tag{2.21}$$

This term by itself defines a specific model called the non-linear sigma model [85]. The coefficient is chosen such that normalized bosons are reproduced when we expand U in powers of ϕ:

$$U = 1 + i\frac{\phi}{f_0} - \frac{\phi^2}{2f_0^2} + \cdots \,, \tag{2.22}$$

$$\mathcal{L}^{(2)} = \partial_\mu \pi^+ \partial^\mu \pi^- + \partial_\mu K^+ \partial^\mu K^- + \cdots \,. \tag{2.23}$$

The Noether currents of eq. (2.21) are:

$$V_a^\mu = \frac{if_0^2}{4}\langle \lambda_a [\partial_\mu U, U^\dagger] \rangle \,, \qquad A_a^\mu = \frac{if_0^2}{4}\langle \lambda_a \{\partial_\mu U, U^\dagger\} \rangle \,. \tag{2.24}$$

These currents are to be described within the effective field theory since they include one pion exchange. However, if the low-energy expansion is applied, these currents will have more than one current for each vertex (one-particle reducible). Therefore, by defining a single current as in eq. (2.24), we can not explain one-particle reducible diagrams. By using the external source method (we will study this in next section), we can establish all vertices on the same ground and the higher order terms can contain more than one current. Moreover, the Ward identities obtain a very simple form when external sources are used.

PCAC in ChPT

Taking eq. (2.24) into account, we get

$$\partial^\mu A_\mu^k = f_\pi m_\pi^2 \pi^k + \cdots \,. \tag{2.25}$$

This tells us that Goldstone bosons can be described either by π or by $\partial^\mu A_\mu$. Here, we have used f_π instead of f_0 to indicate that we are considering the physical value which is determined from the pion decay (for the relation in between f_0 and f_π see section 2.2.3).

External Sources

In order to study a current, a corresponding classical, external source term can be introduced in the Lagrangian: $\mathcal{L}[\phi, S] = \mathcal{L}[\phi] + JS$. The generating functional with an external source S and corresponding current J then has the form:

$$Z[S] = \int D\phi \exp\left(i \int d^4x \mathcal{L}[\phi, S] \right), \tag{2.26}$$

$$\langle 0|J(x)|0\rangle = \frac{1}{Z[0]} \left(\frac{-i\delta Z[S]}{\delta S(x)} \right)\Bigg|_{S=0} \,. \tag{2.27}$$

[3] For a formal proof of this correspondence [83, 84], it will be explained later in this section.

External sources can be introduced as traceless and hermitian matrices in flavor space:

$$\text{Scalar:} \qquad s = \lambda_a s_a \,, \tag{2.28}$$

$$\text{Pseudoscalar:} \qquad p = \lambda_a p_a \,, \tag{2.29}$$

$$\text{Vector:} \qquad v^\mu = \frac{\lambda_a}{2} v_a^\mu \,, \tag{2.30}$$

$$\text{Axial-Vector:} \qquad a^\mu = \frac{\lambda_a}{2} a_a^\mu \,. \tag{2.31}$$

In this case, the singlet parts of the external sources are excluded since vector and axial currents are chosen to be traceless in flavor space (they couple to right- and left-handed currents and $\langle l_\mu \rangle = \langle r_\mu \rangle = 0$ as we will see. Moreover, the singlet axial current has an anomaly (for more details see [82]). However, the singlet parts for scalar and pseudoscalar sources can be introduced. A tensor source can also be introduced in case of need [86].

The inclusion of external sources changes the global chiral symmetry to a local symmetry ($U(x) \rightarrow R(x)U(x)L^\dagger(x)$) [4]. As these external sources are introduced, the QCD Lagrangian takes the form:

$$\begin{aligned} \mathcal{L}_{\text{QCD,ext.}} &= -\frac{1}{2}\langle F^{\mu\nu} F_{\mu\nu} \rangle + \bar{q} i \not{D}_{ij} q + \bar{q}\gamma^\mu (v_\mu + \gamma^5 a_\mu) q - \bar{q}(s - i\gamma^5 p) q \,, & (2.32)\\ &= \mathcal{L}_{\text{QCD}} + \bar{q}\gamma^\mu (v_\mu + \gamma^5 a_\mu) q - \bar{q}_R m(x) q_L - \bar{q}_L m^\dagger(x) q \,, & (2.33)\\ &= \mathcal{L}_{\text{QCD}} + \bar{q} J[s, p, v, a] q \,. & (2.34) \end{aligned}$$

The generating functional with external sources has the form [68]:

$$Z[J(s,p,v,a)] = \int dF dq d\bar{q} \exp\left(\int i d^4x (\mathcal{L}_{\text{QCD}}(q, \bar{q}, F) + \bar{q} J[s, p, v, a] q) \right), \tag{2.35}$$

which can be replaced, via Weinberg's conjecture, by the effective Lagrangian path integral:

$$Z[J(s,p,v,a)] = \int dU \exp\left\{ i \int d^4x \left(\mathcal{L}_{\text{ChPT}}(U, \partial U, \ldots, J[v, a, s, p]) \right) \right\}. \tag{2.36}$$

This equation tells us the connection of the effective Lagrangian with the underlying theory. The left hand side has the generating functional of QCD whereas the right hand side includes only ChPT terms. Thence, the value of the generating functional of QCD under a set of external fields represents the dynamics of QCD and this is equivalent to the effective theory in the presence of the same external sources. Therefore, the ChPT Lagrangian now has pion fields and external sources at any order. The higher order terms for external sources represent diagrams with more than one current.

[4] The introduced external sources are demanded to be local since when generating functionals are invariant under their local transformation, this invariance is equivalent to the Ward identities [82].

Eq. (2.32) is invariant under local transformations:

$$q(x) \rightarrow q'(x) = L(x)\frac{1-\gamma^5}{2}q(x) + R(x)\frac{1+\gamma^5}{2}q(x)\,, \tag{2.37}$$

$$s \rightarrow s' = R(x)sL^\dagger(x)\,, \tag{2.38}$$

$$p \rightarrow s' = R(x)pL^\dagger(x)\,, \tag{2.39}$$

$$v_\mu + a_\mu = r_\mu \rightarrow r'_\mu = R(x)r_\mu R^\dagger(x) + iR(x)\partial_\mu R^\dagger(x)\,, \tag{2.40}$$

$$v_\mu - a_\mu = l_\mu \rightarrow l'_\mu = L(x)l_\mu L^\dagger(x) + iL(x)\partial_\mu L^\dagger(x)\,. \tag{2.41}$$

Moreover, we can choose $p = v_\mu = a_\mu = 0, s = \mathcal{M} = \mathrm{diag}(m_u, m_d, m_s)$ to generate eq. (1.13) from eq. (2.32). We should note that eq. (2.35) is not invariant under these transformations at each order. It has anomalies, including the so called $U(1)$ axial anomaly which was mentioned before, due to the fermion transformation in the path integral formalism [82]. Also, chiral anomalies are present (Wess-Zumino term). However, chiral anomalies occur only at the next-to-leading order in the chiral power counting scheme [82].

Chiral Transformations

According to this, $\mathcal{L}_{\mathrm{ChPT}}$ with external sources should also be invariant under the local chiral symmetry. Therefore, a covariant derivative should be defined:

$$D_\mu U = \partial_\mu U - i[v_\mu, U] - i\{a_\mu, U\} = \partial_\mu U + iUl_\mu - ir_\mu U\,, \tag{2.42}$$

with the chiral transformation ($R\partial_\mu R^\dagger = -(\partial_\mu R)R^\dagger$ is used):

$$\begin{aligned} D_\mu U &\rightarrow \partial(RUL^\dagger) + i(RUL^\dagger)(Ll_\mu L^\dagger + i(L\partial_\mu L^\dagger)) - i(Rr_\mu R^\dagger + i(R\partial_\mu R^\dagger))(RUL^\dagger) \\ &= (\partial_\mu R)UL^\dagger + R(\partial_\mu U)L^\dagger + RU\partial_\mu L^\dagger + iRUl_\mu L^\dagger - RU\partial_\mu L^\dagger - iRr_\mu UL^\dagger - (\partial_\mu R)UL^\dagger \\ &= R(\partial_\mu U + iUl_\mu - ir_\mu U)L^\dagger = R(D_\mu U)L^\dagger\,. \end{aligned} \tag{2.43}$$

The field strength tensors of the external fields are defined as:

$$f^R_{\mu\nu} := \partial_\mu r_\nu - \partial_\nu r_\mu - i[r_\mu, r_\nu] \rightarrow R(x)f^R_{\mu\nu}R^\dagger(x)\,, \tag{2.44}$$

$$f^L_{\mu\nu} := \partial_\mu l_\nu - \partial_\nu l_\mu - i[l_\mu, l_\nu] \rightarrow L(x)f^L_{\mu\nu}L^\dagger(x)\,. \tag{2.45}$$

Since $\langle r_\mu\rangle = \langle l_\mu\rangle = \langle [r_\mu/l_\mu, r_\nu/l_\nu]\rangle = 0$, $f^{L,R}_{\mu\nu}$ are also traceless. As a convention used by Gasser and Leutwyler [14, 15], $\chi = 2B_0(s+ip)$ is introduced where B_0 is a constant to be determined.

All structures up to $O(p^2)$ are described. Since the vector and axial-vector external currents are at the same level as the derivative operator, they have chiral order 1. This makes the field strength tensor of chiral order 2. As seen in QCD, the scalar external field can be assigned with the mass matrix. In eq. (1.38), it is stated that the mass matrix is proportional to the squared mass of mesons, so it has chiral order 2. That is the reason why mass rescales as $m_i \rightarrow t^2 m_i$ in the power counting. See table 2.1 to see all the building block structures up to second chiral order.

To construct an effective Lagrangian from these elements, we need to be sure that the Lagrangian obeys the symmetry transformations. Therefore, besides their chiral transformation rules in eq. (2.37),

Chiral Order	Building Elements
$O(p^0)$	$U(x)$
$O(p^1)$	$D_\mu U(x)$, r_μ, l_μ
$O(p^2)$	$D_\mu D_\nu U(x)$, $f^R_{\mu\nu}$, $f^L_{\mu\nu}$, χ

Table 2.1: Chiral orders of the building elements up to second order

their P and C transformation rules are needed to respect all symmetries of QCD[5]. We will give some examples and then list chiral, C, and P transformation rules for the structures up to second chiral order in table 2.2.

Let us consider $U(x)$ first. For simplicity, let us assume we have $SU(2)$ symmetry rather than $SU(3)$ symmetry. Then,

$$U(x) = \exp\left\{i\begin{pmatrix} \pi^0 & \sqrt{2}\pi^+ \\ \sqrt{2}\pi^- & -\pi^0 \end{pmatrix}\right\}. \tag{2.46}$$

Its charge conjugate is simply the transpose of itself:

$$U(x) \xrightarrow{C} CU(x)C^{-1} = U^T(x) = \exp\left\{i\begin{pmatrix} \pi^0 & \sqrt{2}\pi^- \\ \sqrt{2}\pi^+ & -\pi^0 \end{pmatrix}\right\}. \tag{2.47}$$

Next, chirally transformed U can be considered:

$$R/L \xrightarrow{C} CR/LC^{-1} = (L^\dagger/R^\dagger)^T, \tag{2.48}$$

$$\begin{aligned} RUL^\dagger &\xrightarrow{C} C(RUL^\dagger)C^{-1} = CRC^{-1}CUC^{-1}CL^\dagger C^{-1} \\ &= (L^\dagger)^T U^T R^T = (RUL^\dagger)^T. \end{aligned} \tag{2.49}$$

As a last example, we will check the covariant derivative under charge transformation by using $r_\mu \xrightarrow{C} -l_\mu^T$ and $l_\mu \xrightarrow{C} -r_\mu^T$:

$$\begin{aligned} D_\mu U &\xrightarrow{C} C(\partial_\mu U + iUl_\mu - ir_\mu U)C^{-1} \\ &= \partial_\mu U^T - iU^T r_\mu^T + il_\mu^T U^T \\ &= (\partial_\mu U + iUl_\mu - ir_\mu U)^T = (D_\mu U)^T. \end{aligned} \tag{2.50}$$

Chiral invariant combinations should be formed out of these elements. Since any element a transforms as $RaL^\dagger$, chirally invariant combinations are of the form ($\langle ab\rangle = \langle ba\rangle$ is used):

$$\langle ab^\dagger\rangle \to \langle RaL^\dagger(RbL^\dagger)^\dagger\rangle = \langle RaL^\dagger Lb^\dagger R^\dagger\rangle = \langle ab^\dagger\rangle. \tag{2.51}$$

This can be generalized to $\langle ab^\dagger cd^\dagger\rangle$, $\langle ab^\dagger\rangle\langle cd^\dagger\rangle$. Therefore, we can generate the zeroth order chiral invariant term as $\langle UU^\dagger\rangle = \langle \mathbb{1}\rangle$, which is equal to the number of flavors. There are two options with the chiral order one: $\langle (D_\mu UU^\dagger)\rangle = -\langle U(D_\mu U)^\dagger\rangle = 0$. We have more possibilities at the second chiral order: $\langle f^{R/L}_{\mu\nu}\rangle = 0$, $\langle (D_\mu D_\nu U)U^\dagger\rangle = -\langle (D_\nu U)(D_\mu U)^\dagger\rangle = \langle U(D_\nu D_\mu U)^\dagger\rangle$, $\langle \chi U^\dagger\rangle$, and $\langle U\chi^\dagger\rangle$. Clearly, there is no term to be used to describe Goldstone bosons or external forces at the zeroth or first chiral order. Finally,

[5]Due to the CPT theorem, if P and C symmetries are respected, T symmetry is automatically respected.

Structure	Chiral Transformation	C	$P\ (\bar{x} = (t, -x))$
$U(x)$	$R(x)U(x)L^\dagger(x)$	$U^T(x)$	$U^\dagger(\bar{x})$
$D_\mu U(x)$	$R(x)(D_\mu U(x))L^\dagger(x)$	$(D_\mu U(x))^T(x)$	$(D_\mu U(x))^\dagger(\bar{x})$
$D_\mu D_\nu U(x)$	$R(x)(D_\mu D_\nu U(x))L^\dagger(x)$	$(D_\mu D_\nu U(x))^T(x)$	$(D_\mu D_\nu U(x))^\dagger(\bar{x})$
$\chi(x)$	$R(x)\chi(x)L^\dagger(x)$	$\chi^T(x)$	$\chi^\dagger(\bar{x})$
$(r_\mu/l_\mu)(x)$	$(R/L)(x)(r_\mu/l_\mu)(R/L)^\dagger(x) + i(R/L)(x)\partial_\mu(R/L)^\dagger(x)$	$-(l_\mu/r_\mu)^T(x)$	$(l^\mu/r^\mu)(\bar{x})$
$f_{\mu\nu}^{R/L}(x))$	$(R/L)(x)f_{\mu\nu}^{R/L}(R/L)^\dagger(x)$	$-(f_{\mu\nu}^{L/R})^T(x)$	$f_{L/R}^{\mu\nu}(\bar{x})$

Table 2.2: Transformation rules for the building elements up to second order

to ensure Lorentz invariance, Lorentz indices have to be contracted. This also excludes the first order or any odd number of order terms. As a result, we are left with three terms: $\langle (D_\mu U)(D^\mu U)^\dagger \rangle$, $\langle U\chi^\dagger \rangle$, $\langle \chi U^\dagger \rangle$. The last two can be combined as: $\langle U\chi^\dagger \pm \chi U^\dagger \rangle$, but the '$-$' sign does not conserve parity. Therefore, we are left with only two terms and their coefficients for the lowest order chiral Lagrangian. As a result, the most general chiral invariant effective Lagrangian of Goldstone bosons up to leading order can be written as:

$$\mathcal{L}^{(2)} = \frac{f_0^2}{4}\left(\langle (D_\mu U)(D^\mu U)^\dagger \rangle + \langle \chi U^\dagger + U\chi^\dagger \rangle\right). \tag{2.52}$$

The first term is the generalized version of eq. (2.21), invariant under local $SU(2)_R \times SU(2)_L$ as well. The second term introduces the quark masses. Hence, it is responsible for the explicit symmetry breaking. Notice that, there are no terms with $f_{\mu\nu}^{R/L}$. The last thing to be noticed is that there are two coefficients at the leading order, f_0 and B_0 (hidden in χ in the second term). These are called the low-energy coefficients (LECs) which are parameters of the Lagrangian. f_0 is a measure of the spontaneous symmetry breaking of QCD (see eq. (1.42)) whereas B_0 is a measure of the quark condensate (see eq. (2.55). They are determined either from experiment or phenomenology (meson resonance saturation, the extended NJL model or lattice QCD). By a redefinition of LECs and fields from the second and fourth chiral orders, UV-divergent contributions of the loop diagrams from second chiral order vertices can be absorbed in these coefficients.

Goldstone Boson Masses

As aforementioned, ChPT can reproduce QCD Green functions perturbatively in small momenta and quark masses. Therefore, ChPT Green functions can be related to QCD Green functions perturbatively. Consequently, matrix elements can be related as well [13, 15]. For example, consider the generating functional of ChPT at the lowest order:

$$Z^{(2)}[s, p, v, a] = \int \mathcal{D}U \exp\left(i \int d^4x \mathcal{L}^{(2)}[U, s, p, v, a]\right). \tag{2.53}$$

If we take $p = v = a = 0$, and $s = \mathcal{M}$, it can be related to the quark condensate. Consider a scalar source in which an auxiliary field (φ) is defined. This source acts as a perturbation of the quark mass in

consideration:

$$\begin{aligned}
\langle 0|\bar{q}q|0\rangle &= \frac{1}{Z^{(2)}[\mathcal{M},0,0,0]}\left(i\frac{\delta}{\delta\varphi}\right)Z^{(2)}[\mathcal{M}_\varphi,0,0,0]\Big|_{\varphi=0} \\
&= \frac{1}{Z^{(2)}[\mathcal{M},0,0,0]}\int \mathcal{D}U\frac{-f_0^2B_0}{2}(U^\dagger+U)\exp\left(i\int d^4x\mathcal{L}^{(2)}[U,\mathcal{M},0,0,0]\right) \\
&= \frac{-f_0^2B_0}{Z^{(2)}[\mathcal{M},0,0,0]}\int \mathcal{D}U\left(1-\frac{\pi^2}{f_0^2}+\cdots\right)\exp\left(i\int d^4x\mathcal{L}^{(2)}[U,\mathcal{M},0,0,0]\right) \\
&= -f_0^2B_0+O(\mathcal{M}+\cdots)
\end{aligned} \tag{2.54}$$

Therefore,

$$\langle 0|\bar{u}u|0\rangle = \langle 0|\bar{d}d|0\rangle = \langle 0|\bar{s}s|0\rangle = -f_0^2B_0+O(\mathcal{M})+\cdots . \tag{2.55}$$

Since B_0 is proportional to the quark condensate, it can be considered as the chiral symmetry breaking parameter. So, at the leading order, the quark condensates are degenerate.

Let us determine the masses of the Goldstone bosons at the leading order. Again, let's set $p = v = a = 0$, and $s = \mathcal{M}$. What is left from the symmetry breaking part is

$$\mathcal{L}_m^{(2)} = -\frac{B_0}{2}\langle\phi^2\mathcal{M}\rangle \tag{2.56}$$

$$\begin{aligned}
&= -\frac{B_0}{2}(2(m_u+m_d)\pi^+\pi^- + 2(m_u+m_s)K^+K^- + 2(m_d+m_s)K^0\bar{K}^0 + (m_u+m_d)\pi^0\pi^0 \\
&+ \frac{1}{3}(m_u+m_d+4m_s)\eta^2 + \frac{2}{\sqrt{3}}(m_u-m_d)\pi^0\eta)\,.
\end{aligned} \tag{2.57}$$

The last term refers to $\pi^0-\eta$ mixing [41], proportional to the $SU(2)$ isospin symmetry breaking which is proportional to the mass difference of up and down quarks. Using this, we can deduce the Gell-Mann, Oakes, and Renner relations [87]:

$$\begin{aligned}
m_{\pi^0}^2 &= 2B_0m - \frac{B_0}{4}\frac{(m_u-m_d)^2}{m_s-m}\,, & m_{\pi^\pm}^2 &= 2B_0m\,, \\
m_{K^0}^2 &= B_0(m_d+m_s)\,, & m_{K^\pm}^2 &= 2B_0(m_u+m_S)\,, \\
m_\eta^2 &= \frac{2}{3}B_0(m+m_s)+\frac{B_0}{4}\frac{(m_u-m_d)^2}{m_s-m}\,, & m &= \frac{m_u+m_d}{2}\,.
\end{aligned} \tag{2.58}$$

By considering the quark-antiquark density dependence of B_0 (eq. (2.55)), we can say that B_0 is responsible for the spontaneous symmetry breaking whereas terms like (m_u+m_d) are responsible for the explicit symmetry breaking. For example, if we preserve the $SU(2)$ isospin limit, $m_u = m_d = m \neq m_s$, this gives us eq. (1.38):

$$m_\pi^2 = 2B_0m\,, \quad m_K^2 = B_0(m+m_s)\,, \quad m_\eta^2 = \frac{2}{3}B_0(m+2m_s)\,. \tag{2.59}$$

We can reduce these three relations into one and we get the Gell-Mann Okubo mass formula [88, 89] which is independent of B_0 and quark masses:

$$3m_\eta^2 = 4m_K^2 - m_\pi^2\,. \tag{2.60}$$

Using m_K and m_π as inputs, we get $m_\eta \sim 566$ MeV. This is the prediction of eq. (2.60) whereas the

empirical value is 547 MeV [1].

The first thing to be observed from eq. (2.59) is that we cannot deduce a value for B_0 or for boson masses. However, mass ratios for quarks can be obtained:

$$\begin{aligned} \frac{M_K^2}{M_\pi^2} &= \frac{m+m_s}{2m} \quad \Rightarrow \quad \frac{m_s}{m} = 25.9\,, \\ \frac{M_\eta^2}{M_\pi^2} &= \frac{m+2m_s}{3m} \quad \Rightarrow \quad \frac{m_s}{m} = 24.3\,, \\ \frac{M_K^2 - M_{K^0}^2 + M_{\pi^+}^2}{-M_K^2 + M_{K^0}^2 + M_{\pi^+}} &= \frac{m_u}{m_d} \quad \Rightarrow \quad \frac{m_u}{m_d} \sim 0.66\,. \end{aligned} \tag{2.61}$$

If $SU(2)$ symmetry breaking is turned off, $m_u = m_d = 0$, the pion mass disappears. This explains why squared boson masses are very different. It is appreciated that ChPT can be used to extrapolate the quark masses to their physical values if the GMOR is checked on lattice. Moreover, $\mathcal{L}_m^{(2)}$ shifts the vacuum energy which is related to squared boson mass via B_0.

2.2.3 Higher Order Corrections

We said that ChPT has a systematic expansion with a Weinberg counting rule. Therefore, there are higher order tree level terms as well as loop diagrams contributing to particle interactions. Typically, these loop diagrams have UV divergences. When they are regularized with a regularization method which respects the symmetries, there will be counter terms that are required by the regularization process. By construction, respecting the "folk" theorem, ChPT contains all terms needed. However, there are infinitely many, hence there are infinitely many parameters. Nevertheless, Weinberg's counting scheme ensures that we can calculate physical processes up to needed order without having problems from the higher order contributions.

When the leading order diagram ($O(p^2)$, fig.2.1(a)) and the loop diagram ($O(p^4)$, fig.2.1(b)) are taken into account, at least tree diagrams with one vertex from $\mathcal{L}^{(4)}$ ($O(p^4)$, fig.2.1(c)) should also be considered so that by renormalization, infinities of the loop diagrams of $\mathcal{L}^{(2)}$ can be absorbed by the LECs of $\mathcal{L}^{(4)}$. Hence, ChPT is a renormalizable theory in the 'modern' sense [90].

For building a power counting scheme, $\mathcal{L}_{\text{ChPT}}$ can be organized in powers of Goldstone boson masses and momenta due to the low-energy scale. This is called chiral power counting scheme. For a systematic expansion, an energy scale should be set which is relatively high with respect to Goldstone boson masses and momenta. Spontaneous chiral symmetry breaking has a scale around $\Lambda_\chi \sim 4\pi f_\pi \sim 1.2\,\text{GeV}$, which is set as the chiral scale. The reason for this value will be explained later. Actually, any limit around the order of $m_{\text{resonance}}$ is justifiable since ChPT fails to explain resonances.

As in the construction of the leading order terms, higher order terms can be constructed by respecting gauge invariance, Lorentz invariance, P and C symmetries and chiral symmetry. The form of the fourth

order chiral Lagrangian is [15][6]:

$$\begin{aligned}\mathcal{L}^{(4)} &= L_1\langle D_\mu U(D^\mu U)^\dagger\rangle^2 + L_2\langle D_\mu U(D_\nu U)^\dagger\rangle\langle D^\mu U(D^\nu U)^\dagger\rangle \\ &+ L_3\langle D_\mu U(D^\mu U)^\dagger D_\nu U(D^\nu U)^\dagger\rangle + L_4\langle D_\mu U(D^\mu U)^\dagger\rangle\langle \chi U^\dagger + U\chi^\dagger\rangle \\ &+ L_5\langle D_\mu U(D^\mu U)^\dagger(\chi U^\dagger + U\chi^\dagger)\rangle + L_6\langle \chi U^\dagger + U\chi^\dagger\rangle^2 \\ &+ L_7\langle \chi U^\dagger - U\chi^\dagger\rangle^2 + L_8\langle U\chi^\dagger U\chi^\dagger + \chi U^\dagger\chi U^\dagger\rangle \\ &- iL_9\langle f_{\mu\nu}^R D^\mu U(D^\nu U)^\dagger + f_{\mu\nu}^L (D^\mu U)^\dagger D^\nu U\rangle + L_{10}\langle U f_{\mu\nu}^L U^\dagger f_R^{\mu\nu}\rangle \\ &+ H_1\langle f_{\mu\nu}^R f_R^{\mu\nu} + f_{\mu\nu}^L f_L^{\mu\nu}\rangle + H_2\langle \chi\chi^\dagger\rangle\,. \end{aligned} \tag{2.62}$$

Here, L_i are the LECs similar to the leading order constants f_0 and B_0. So, ten more parameters are needed to perform calculations up to $O(4)$[7].These parameters contain properties of the non-perturbative properties of QCD which are disregarded or not computable. Notice that L_1, L_2, and L_3 survive in the chiral limit whereas all the other terms disappear. H_1 and H_2 do not contain any information about Goldstone bosons but only about the external sources. Therefore, they have no physical implication. However, they are required in the renormalization processes as counter terms for one loop graphs [15]. There is one more term, $L_x\langle D_\mu U(D_\nu U)^\dagger D^\mu U(D^\nu U)^\dagger\rangle$, which is invariant for all symmetries only if $N_f > 4$ [15].

Besides the terms in eq. (2.62), loop diagrams with second order vertices contribute at the fourth order[8]. They contribute to the fourth order due to eq. (2.10). These one loop diagrams contain UV divergences. By a redefinition of LECs (except for L_3 and L_7), H_i, and fields, these UV divergent terms can be absorbed in LECs when loop diagrams are renormalized. Therefore, besides the non-perturbative properties of QCD, the fourth order LECs also contain divergences of the loop diagrams produced by the second order terms. We can see from the pattern that it is actually generalized and higher order LECs contain divergences of diagrams constructed with lower order terms.

To understand the chiral ordering of the leading and next-to-leading order, consider eq. (2.10) and elastic $\pi\pi$ scattering in Table 2.3.

Table 2.3: Chiral ordering of $\pi\pi$ scattering.

Lagrangian	n (# of derivatives)	N_n (# of vertices)	N_L (# of loops)	D (Chiral Order)	Diagrams
$\mathcal{L}^{(2)}$	2		0	2	fig. 2.1(a)
$\mathcal{L}^{(2)}$	2		1	4	fig. 2.1(b)
$\mathcal{L}^{(4)}$	4	1	0	4	fig. 2.1(c)
$\mathcal{L}^{(2)}$	2		2	6	fig. 2.1(d)
$\mathcal{L}^{(4)}$	4	1	1	6	fig. 2.1(e)
$\mathcal{L}^{(4)}$	4	2	0	6	fig. 2.1(f)
$\mathcal{L}^{(6)}$	6	1	0	6	fig. 2.1(g)

[6]For the $SU(2)$ version see [14]

[7]The number of parameters depend on the number of flavors (N) included in the chiral symmetry ($SU(N)$).

[8]There is also contribution from an anomaly at this order which was first studied by Wess and Zumino [91] and later by Witten [92].

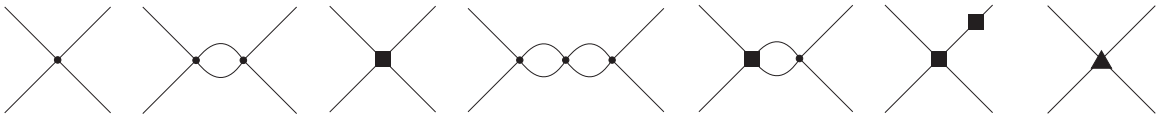

(a) $O(p^2)$ (b) $O(p^4)$ (c) $O(p^4)$ (d) $O(p^6)$ (e) $O(p^6)$ (f) $O(p^6)$ (g) $O(p^6)$

Figure 2.1: some $\pi\pi$ scattering diagrams with different chiral orders.

f_0, B_0, and Λ_χ

f_0 is determined from the matrix element of the axial-vector current, $A_{\mu,a} = R_{\mu,a} - L_{\mu,a} = i\frac{f_0^2}{4}\langle\lambda_a[\partial_\mu U, U^\dagger]\rangle$, with the vacuum and a Goldstone boson field:

$$\langle 0|A^\mu|\phi\rangle = ip^\mu f_0 \,. \tag{2.63}$$

This gives us the decay of a Goldstone boson to leptonic sector in the chiral limit. Therefore, f_0 can be set from $\pi \to l\nu_l$ (see [1]):

$$f_0 = f_\pi = 92.1 \text{ MeV} \,. \tag{2.64}$$

However, usually we are not in the chiral limit and we consider quark masses. Hence, there will be corrections to f_0 due to quark masses. Thus, the accurate relation is:

$$f_\pi = f_0(1 + O(m_q) + \cdots) \,. \tag{2.65}$$

At the next-to-leading order, there should be a logarithmic contribution from the loop diagram as well.

B_0 is related to the quark condensate via eq. (2.55). Up to the leading order, the value of B_0 is set via the value of $f_0 = f_\pi$ and the sum rule calculation of $\langle 0|q\bar{q}|0\rangle = -(250 \text{ MeV})^3$ [56] leads us to a value of around

$$B_0 \backsimeq 1830 \text{ MeV} \,. \tag{2.66}$$

Like in eq. (2.65), B_0 and the quark condensate relation actually has the form:

$$\langle 0|\bar{q}q|0\rangle = -f_0^2 B_0(1 + O(m_q) + \cdots) \,. \tag{2.67}$$

Each loop increases the chiral order by two. When any next-to-leading order loop is calculated, it receives a factor of $1/(4\pi)^2$ and a factor of $1/f_0^2$ from the expansion of $U = e^{i\frac{\phi}{f_0}}$. Therefore, each chiral order will add an extra factor of $(4\pi f_0)^{-1}$ to the expansion. Therefore, this value is set as the hard scale for spontaneous chiral symmetry breaking:

$$\Lambda_\chi = 4\pi f_\pi \backsimeq 1200 \text{ MeV} \,. \tag{2.68}$$

Thus, it is considered to be the scale of Goldstone boson masses and momentum power expansion, e.g. p^2/Λ_χ^2, m_π^2/Λ_χ^2.

Renormalized LECs

An appropriate renormalization of LECs and H_is are [15]:

$$L_i = L_i^r(\mu) + \Gamma_i L \,, \qquad (i = 1, \ldots, 10) \tag{2.69}$$

$$H_i = H_i^r(\mu) + \Delta_i L \,, \qquad (i = 1, 2) \,. \tag{2.70}$$

Here, $L = \frac{\mu^{d-4}}{32\pi^2}(\frac{2}{d-4} - \ln(4\pi) + \gamma_E - 1)$ with $\gamma_E = -\Gamma'(1) = 0.577$ the Euler constant and d is the spacetime dimension from dimensional regularization. With these renormalized LECs, the second order terms and its loop diagrams become finite at $d = 4$. After renormalization, the LECs become scale (μ) dependent due to dimensional regularization:

$$L_i^r \mu = L_i^r(\mu_0) + \frac{\Gamma_i}{32\pi^2} \ln\left(\frac{\mu_0^2}{\mu^2}\right). \tag{2.71}$$

However, the scale dependence of LECs and loop diagram terms cancel in such a way that observable quantities remain scale-independent. In Table 2.4, we give the values for renormalized LECs at the ρ mass scale ($\mu = m_\rho$) and Γ_i values.

Table 2.4: Renormalized low-energy coupling constants L_i^r for $SU(3)$ [67, 93, 94].

LEC	Empirical Value (10^{-3})	Γ_i	Process
L_1^r	0.4 ± 0.3	$\frac{3}{32}$	$\pi\pi \to \pi\pi$
L_2^r	1.35 ± 0.3	$\frac{3}{16}$	$\pi\pi \to \pi\pi$
L_3^r	-3.5 ± 1.1	0	$K_{l_4}, \pi\pi \to \pi\pi$
L_4^r	-0.3 ± 0.5	$\frac{1}{8}$	Zweig Rule, Lattice
L_5^r	1.4 ± 0.5	$\frac{3}{8}$	F_K/F_π, Lattice
L_6^r	-0.2 ± 0.3	$\frac{11}{144}$	Zweig Rule, Lattice
L_7^r	-0.4 ± 0.2	0	$\eta - \eta'$ mixing
L_8^r	0.9 ± 0.3	$\frac{5}{48}$	$M_{K^0} - M_{K^+}$, L_5, Lattice
$-iL_9^r$	6.9 ± 0.7	$\frac{1}{4}$	π e.m. radius, Lattice
L_{10}^r	-5.5 ± 0.7	$\frac{-1}{4}$	$\pi \to l\nu\gamma$, Lattice

There is an important reason for setting $\mu = m_\rho$. If we perform calculations at the energy which is around the mass of resonances, they will have noticeable contributions to the LECs. Therefore, even if the heavy states are not considered in the theory, their effect can be seen. For example, in a $\pi\pi$ scattering if the lowest lying resonance, the rho-meson, is considered to be produced, the contribution will be proportional to $\frac{g^2}{s-m_\rho^2}$. If the momentum exchange is low with respect to m_ρ, the contribution of the

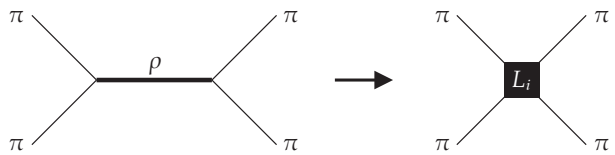

Figure 2.2: Contribution to LECs from heavier resonances in the low energy.

resonance to the scattering amplitude is hidden in the LECs of the form:

$$L_i \sim \frac{g^2}{m_\rho^2} + O(p^2) + \cdots. \tag{2.72}$$

Hence, if the resonance mass is low, its contribution to L_i is higher. The contributions to the LECs can be considered by integrating out vector (V), scalar (S), singlet-scalar (S_1) multiplets from a general, chirally invariant Lagrangian as:

$$L_i = L_i^V + L_i^S + L_i^{S_1} . \tag{2.73}$$

As the contribution from each channel is controlled, we observe a vector-meson dominance by $\rho(770)$ meson [95–97]. Moreover, as expected, LEC values are saturated by the lowest lying multiplet of the corresponding channel. Regardless of the existence of $f_0(500)$, the scalar contribution starts at around ≥ 1 GeV[9].

Mass terms at Higher Orders

If the pion mass is considered up to chiral order $O(4)$, there are three diagrams contributing to the pion self-energy: the free pion propagator, tadpoles from the leading order Lagrangian and the pion self-energy contribution from the next-to-leading order Lagrangian, see fig.2.3. The first is the result of

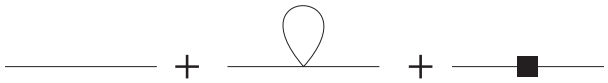

Figure 2.3: π self-energy diagrams up to next-to-leading order

the leading order calculation in eq. (2.59), the second one has a divergent loop integral and the last one has a contribution at the order of $O(p^4)$. Therefore, the result for m_π has the form:

$$m_\pi^2 = B_0(m_u + m_d) + A_\pi I + B_\pi(L_i) . \tag{2.74}$$

Here, A_π and B_π are real and of order $O(p^2)$ and $O(p^4)$ respectively. L_i are the related LECs contributing to B_π and I is the divergent loop integral. This loop integral should be regularized. In dimensional regularization the divergent part of that integral at $d = 4$ dimensions should be absorbed in renormalized LECs. Notice that the divergent term appeared due to $\mathcal{L}^{(2)}$ and is absorbed by the LECs of $\mathcal{L}^{(4)}$. As a result, the GMOR relation, up to next-to-leading order has the form:

$$m_\pi^2 = B_0(m_u + m_d)[1 + A'_\pi(\log)] + B'_\pi(L_i^r) . \tag{2.75}$$

Limits of ChPT

ChPT offers very accurate results for pseudoscalar mesons around the momentum scale of $100-200$ MeV. It is found to give very good estimations of the masses of the pseudoscalar mesons, $\pi\pi$, πK scatterings, π, η, K decays and some other properties [99–104]. Moreover, baryons can be included in ChPT and we can get reasonable results for some static and dynamic properties of baryons [16]. This useful applicability of ChPT beyond the low-energy region can be used in higher energy regimes only if there are no resonances appearing in dynamical interactions. Hence, pseudoscalar interaction channels, free of vector resonances, may be explained within ChPT as well in this region. However, it fails for spin 1 channels due to the low-lying vector resonances, which are not explicable by ChPT itself [105–107], see fig.2.4.

This energy region is still below the perturbative region of QCD but above the low-energy regime. However, there are different ways to reconcile these resonances in the theory to study this energy region.

[9] The $f_0(500)$ is not studied in this work. A detailed discussion and review can be found in [98].

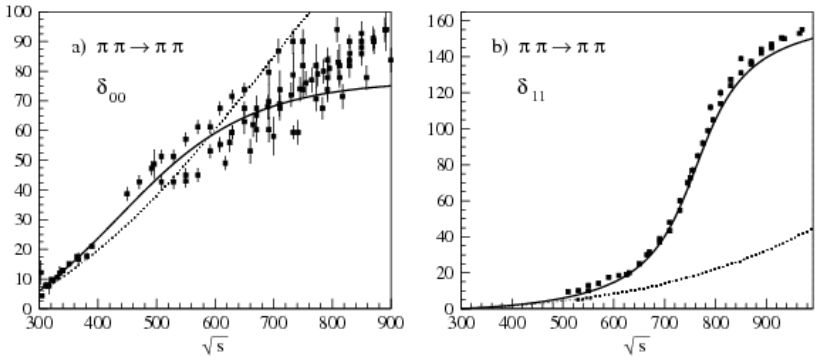

Figure 2.4: ChPT results (represented by dashed lines) vs experimental pion-pion scattering data whereas solid lines represent IAM fit. This figure is taken from [108].
It is clear to see that in the vector channel, ChPT does not explain the resonance behaviour of the phase shift [106, 107].

Obviously, all these methods should be in agreement with ChPT in the low-energy regime. There are several different methods like the N/D method [109], inverse amplitude method [110], using the Bethe-Salpeter equation [111, 112] and so on. Each of these methods has its drawbacks and range of applicability, respectively. We will go over these issues in the next section.

On the other hand, we can generalize ChPT by including additional degrees of freedom. As a result, we can get phenomenological chiral Lagrangians. For example, we can add the lowest lying vector-mesons, by obeying the symmetries of the low-energy theorem and having a proper counting scheme. Moreover, integrating out these resonances should be possible since at the low-energy regime ChPT should be reproduced:

$$\int dV \exp\left(i \int d^4x \mathcal{L}_V(V,U,s,p,v,a)\right) = Z_{\text{ChPT}}(U,s,p,v,a)\,. \tag{2.76}$$

There are several different approaches to add vector-mesons. In general, they can be introduced as vector matrices, as hidden gauge particles of the non-linear σ model or as a second rank tensor field [53, 113, 114] which are all equivalent [53, 95, 96]. Since they are massive spin-1 particles, they have three degrees of freedom. Additional degrees of freedom generates constraints on the coefficients of the Lagrangian. Introducing these fields generates non-linear chiral symmetry. Therefore, they should transform as:

$$V \to V' = T(L,R,U)VT^{\dagger}(L,R,U)\,. \tag{2.77}$$

Here, V is the representation for the vector-meson octet. For example, if we use second rank tensors and respecting all the symmetries, they are included in the Lagrangian as:

$$\mathcal{L}_V = \frac{-1}{4}\langle V_{\mu\nu}V^{\mu\nu}\rangle\,, \tag{2.78}$$

$$V_{\mu\nu} = \partial_\mu V_\nu - \partial_\nu V_\mu - ig[V_\mu, V_\nu]\,, \tag{2.79}$$

where g represents the coupling constant in between the vector-mesons.

In general, the tensor field formulation is preferable for constructing chiral-invariant building blocks. However, we will use the hidden local gauge symmetry formulation in this work. This choice is not due to the formalism itself but it was used in [115, 116]. We want to stick with this choice for convenience

since we examine these results and compare them with ours.

2.3 Hidden Local Gauge Symmetry

The addition of massive particles introduces a new scale to ChPT. This violates the power counting scheme around the mass of the lowest lying vector-meson which appears as a resonance in the scattering. To preserve the counting scheme, spin-1 fields should be regularized in the infrared region. This is a cumbersome procedure, but it is possible. We refer to [117, 118] for the interested reader. We will use the hidden gauge symmetry method to include vector-mesons. This procedure is explained below. Moreover, the introduced coupling constants are not constrained. Although each unconstrained parameter needs an experimental input, there are not enough available experimental input for all the processes. Hidden gauge symmetry offers a successful framework for this problem.

The hidden symmetry approach exploits the fact that any nonlinear sigma model with a manifold G/H is gauge equivalent to another one with $G_{\text{global(g)}} \otimes H_{\text{local(l)}}$ where H_{l} is the hidden local symmetry. That hidden symmetry introduces composite gauge bosons as gauge fields [119]. The first realization of these bosons as rho-mesons was by Bando et al. [119]. The idea is that, since the non-linear sigma model is a low-lying effective theory of massless QCD with $U(3)_L \otimes U(3)_R$ global symmetry, which is spontaneously broken to $U(3)_V$ local symmetry, the rho-meson can be realized as the dynamical gauge boson, which is composed of quarks.

It is well known that the rho-meson is a $q\bar{q}$ state and not a gauge field. However, using the ideas in [73] and relying on the phenomenological success of vector-meson dominance in [120], associating the rho-meson as the gauge field of a hidden local symmetry and assuming the kinetic term to be generated by this hidden symmetry end up in generation of the rho-meson mass via Higgs-like mechanism with the spontaneous breaking of this hidden local symmetry. Moreover, the vector-meson dominance and the Kawarabayashi, Suzuki, Riazuddin and Fayyazuddin relation (KSRF) [121, 122] can be achieved as well. All this can be achieved with only one free parameter. We will summarize these ideas, starting with two flavors and generalizing it to three flavor case following the procedure in [53, 119]. For more details on this issue, we refer to [53].

2.3.1 ρ Meson as a Dynamical Gauge Boson

Let us first consider the Lagrangian with $G/H = (SU(2)_L \otimes SU(2)_R)_g/(SU(2)_V)_l$:

$$\mathcal{L} = \frac{f_\pi^2}{4}\langle \partial_\mu U \partial^\mu U^\dagger \rangle, \tag{2.80}$$

where U represents the pions, $U(x) = e^{i\pi(x)/f_\pi}$ and $\pi = \pi^a \tau^a$ where τ^a are the $SU(2)$ generators. As we have seen before, this Lagrangian is invariant under the global chiral transformation $U(x) \to LU(x)R^\dagger$.

The linear model can be constructed with two independent terms of $SU(2)_V$ (ξ_L and ξ_R) as:

$$U(x) = \xi_L^\dagger \xi_R, \tag{2.81}$$

and parametrized as:

$$\xi_{L,R} = e^{i\sigma(x)/f_\pi} e^{\mp i\pi(x)/f_\pi}. \tag{2.82}$$

The transformation of these two terms under $(SU(2)_L \otimes SU(2)_R)_g/(SU(2)_V)_l$ is as follows:

$$\xi_{L,R}(x) \to h(x)\xi_{L,R}(L,R)^\dagger, \tag{2.83}$$

where $h(x) \in (SU(2)_V)_l$. Respectively, the covariant derivative can be defined as

$$D_\mu \xi_{L,R}(x) = \partial_\mu \xi_{L,R}(x) - iV_\mu(x)\xi_{L,R}(x). \tag{2.84}$$

Here, $V_\mu = V_\mu^a \tau^a/2$ is a non-Abelian gauge field for $SU(2)_V$ which is to be realized as the rho-meson later on. It transforms under $(SU(2)_L \otimes SU(2)_R)_g/(SU(2)_V)_l$ as (where V_μ is rescaled to gV_μ):

$$V_\mu \to (i/g)h(x)\partial_\mu h^\dagger(x) + h(x)V_\mu(x)h^\dagger(x). \tag{2.85}$$

There are two independent covariant forms that can be written and their transformations are:

$$D_\mu \xi_L(x)\xi_L^\dagger(x) + D_\mu \xi_R(x)\xi_R^\dagger(x) \quad \to \quad h(x)(D_\mu \xi_L(x)\xi_L^\dagger(x) + D_\mu \xi_R(x)\xi_R^\dagger(x))h^\dagger(x), \tag{2.86}$$

$$D_\mu \xi_L(x)\xi_L^\dagger(x) - D_\mu \xi_R(x)\xi_R^\dagger(x) \quad \to \quad h(x)(D_\mu \xi_L(x)\xi_L^\dagger(x) - D_\mu \xi_R(x)\xi_R^\dagger(x))h^\dagger(x). \tag{2.87}$$

Thus, if we enforce chiral symmetry and parity conservation, a Lagrangian with lowest order of derivatives of ξ (second order) can be written in terms of these two linearly independent terms:

$$\mathcal{L}_V = -\frac{f_\pi^2}{4}\langle D_\mu \xi_L(x)\xi_L^\dagger(x) + D_\mu \xi_R(x)\xi_R^\dagger(x)\rangle^2, \tag{2.88}$$

$$\mathcal{L}_A = -\frac{f_\pi^2}{4}\langle D_\mu \xi_L(x)\xi_L^\dagger(x) - D_\mu \xi_R(x)\xi_R^\dagger(x)\rangle^2. \tag{2.89}$$

If the definition of the covariant derivative is used as in eq. (2.84), we get

$$\mathcal{L}_V = f_\pi^2\langle gV_\mu - \frac{1}{2i}(\partial_\mu \xi_L \xi_L^\dagger + \partial_\mu \xi_R \xi_R^\dagger)\rangle^2 , \tag{2.90}$$

$$\mathcal{L}_A = f_\pi^2\langle \frac{1}{2i}(\partial_\mu \xi_L \xi_L^\dagger - \partial_\mu \xi_R \xi_R^\dagger)\rangle^2 . \tag{2.91}$$

The equation of motion of V_μ is

$$gV_\mu^a = -\frac{i}{2}\langle \tau^a(\partial_\mu \xi_L \xi_L^\dagger + \partial_\mu \xi_R \xi_R^\dagger)\rangle \backsimeq -\frac{1}{2f_\pi^2}(\pi \times \partial_\mu \pi)^a + \cdots . \tag{2.92}$$

If this equation is used in eq. (2.90), $\mathcal{L}_V$ vanishes and therefore this term can be multiplied by an arbitrary parameter, a. Regarding this, the general Lagrangian has the form:

$$\mathcal{L} = \mathcal{L}_A + a\mathcal{L}_V. \tag{2.93}$$

Also, notice that if we fix the local gauge by setting $\xi_L^\dagger = \xi_R = \xi$, which is called the unitary gauge (represented as $e^{-i\pi/f_\pi}$), eq. (2.91) becomes equal to eq. (2.80). By using this, we set $\sigma = 0$ which eliminates the scalar degrees of freedom.

In some nonlinear sigma models hidden gauge fields are generated via quantum effects where the poles of these fields are generated as well [123]. Hence, we can assume that the kinetic term for V_μ is dynamically generated via QCD, pion dynamics or quantum effects of quarks [124]. Thus, the kinetic

term is added directly [10] to have a phenomenological Lagrangian. So, eq. (2.93) becomes

$$\mathcal{L} = \mathcal{L}_A + a\mathcal{L}_V - \frac{1}{4}F^{\mu\nu}F_{\mu\nu}\,, \tag{2.94}$$

where $F_{\mu\nu}$ is the non-Abelian field strength tensor: $F_{\mu\nu} = \partial_\mu V_\nu - \partial_\nu V_\mu + gV_\mu \times V_\nu$. If ξ is expanded to obtain the physical modes, $\xi(x) = 1 + \frac{i}{2f_\pi}\tau\cdot\pi(x) + \cdots$, we obtain

$$\mathcal{L}_A = \frac{f_\pi^2}{4}\langle\partial_\mu U\partial^\mu U^\dagger\rangle, \tag{2.95}$$

$$\mathcal{L}_V = f_\pi^2\langle gV_\mu - i[\pi,\partial_\mu\pi]/(2f_\pi^2) + \cdots\rangle^2. \tag{2.96}$$

As a result, eq. (2.94) becomes

$$\mathcal{L} = \frac{f_\pi^2}{4}\langle\partial_\mu U\partial^\mu U^\dagger\rangle + \frac{a}{2}g^2f_\pi^2V_\mu^2 + \frac{a}{2}gV_\mu\cdot(\pi\times\partial^\mu\pi) - \frac{1}{4}F^{\mu\nu}F_{\mu\nu} + \cdots\,, \tag{2.97}$$

$$= \frac{1}{2}(\partial_\mu\pi)^2 + \frac{a}{2}g^2f_\pi^2V_\mu^2 + \frac{a}{2}gV_\mu\cdot(\pi\times\partial^\mu\pi) - \frac{1}{4}F^{\mu\nu}F_{\mu\nu} + \cdots\,. \tag{2.98}$$

If V_μ^a is identified with the rho-meson, we can assign the mass of the rho-meson and the $\rho\pi$ coupling constant from this Lagrangian:

$$m_\rho^2 = ag^2f_\pi^2\,, \tag{2.99}$$

$$g_{\rho\pi\pi} = \frac{1}{2}ag. \tag{2.100}$$

Notice that eq. (2.99) is in the form of spontaneous symmetry breaking mechanism. As this indicates, the mass of the rho-meson is indeed realized via spontaneous breaking of $(SU(2)_V)_l$ symmetry. Unphysical modes are the scalar modes (σ) which are absorbed by the rho.

Here, the parameter a is independent of any symmetry discussions. However, for $a = 2$ the KSRF relation [121, 122] (version 2)[11] can be realized, which relates the rho-meson and the pion decay,

$$m_\rho^2 = 2g^2f_\pi^2, \tag{2.101}$$

and the universality of the rho coupling is accomplished:

$$g = g_{\rho\pi\pi}. \tag{2.102}$$

Numerically, the value for $g_{\rho\pi\pi}$ can be deduced from decay of the rho to two pions.

2.3.2 Introducing External Gauge Bosons

Since the global symmetry part $(SU(2)_L \otimes SU(2)_R)$ can be freely gauged in this framework, we can introduce gauge fields $(\mathcal{V}_\mu, \mathcal{A}_\mu)$. Isospin and hypercharge can be identified as the charges of the global

[10] Addition of the kinetic term by hand is the main assumption of this approach. Notice that adding the kinetic term has no effect on the low-energy dynamics of the theory.

[11] Here, we specified the rule as version 2 since a independent relation, version 1, says $g_\rho = 2f_\pi^2 g_{\rho\pi\pi}$. This relation is found if we include the external gauge bosons. a independent relation underlies the symmetry structure of the formalism since it is derived purely from symmetry consideration. Moreover, two versions become equivalent when the rho-meson dominance of the photon coupling is assumed ($a = 2$ dictates it) [119].

symmetry. Therefore, $\mathcal{V}_\mu, \mathcal{A}_\mu$ can be referred to the photon, W and Z bosons. Hence, there are two different types of gauge bosons: external ones ($\mathcal{V}_\mu, \mathcal{A}_\mu$) and hidden ones ($V_\mu$) which are coupled to two different charges where sources are the global and local symmetries independently. The coupling of the photon with V_μ leads to vector-meson dominance.

The charge can be written in terms of hypercharge and isospin as $Q = I_3 + Y/2$. The generalization to the electroweak model can be seen in detail in [53, 124]. In this case $Y = 0$ and the electromagnetic gauge field is denoted by B_μ referring to $U(1)$ global symmetry. Hence, the covariant derivative is

$$D_\mu \xi_{L/R} = (\partial_\mu - igV_\mu)\xi_{L/R} + ie_0 \xi_{L/R} B_\mu \tau^3, \tag{2.103}$$

where e_0 is the coupling constant of the global gauge interaction. Eq. (2.98) is generalized to (using eqs. (2.101), (2.102))

$$\begin{aligned}\mathcal{L} = {} & \frac{f_\pi^2}{4}\langle \partial_\mu U \partial^\mu U^\dagger \rangle - \frac{1}{4}\langle F_{\mu\nu}^2 \rangle - \frac{1}{4}\langle B_{\mu\nu}^2 \rangle + \frac{1}{2} m_\rho^2 \langle V_\mu^2 \rangle - \frac{e_0 m_\rho^2}{g}\langle V_\mu^3 B^\mu \rangle \\ & + \frac{e_0^2}{2g^2} m_\rho^2 \langle B_\mu^2 \rangle + \frac{ag}{2}\langle V_\mu \cdot (\pi \times \partial^\mu \pi) \rangle - \frac{a-2}{2} e_0 \langle B_\mu \cdot (\pi \times \partial^\mu \pi)_3 + \rangle \cdots .\end{aligned} \tag{2.104}$$

When a is set to 2, this Lagrangian gives us $\rho^0 - \gamma$ mixing which corresponds to the Lagrangian leading to the vector-meson dominance in [125]. Accordingly, the rho-meson dominance is explained with no further assumption rather than the assumption of hidden gauge symmetry approach itself and set of the parameter a. The free parameter $a = 2$ value gives not only the vector-meson dominance but also the KSRF relation and the universality of the rho-meson coupling. If we diagonalize the mass matrix of the V_μ^3-B_μ mixing term, we get

$$m_\gamma^2 = 0\ , \qquad m_{\rho^0}^2 = a(g^2 + e_0^2) f_\pi^2\ , \qquad m_{\rho^\pm}^2 = a g^2 f_\pi^2\ . \tag{2.105}$$

Accordingly, mass eigenstates can be found as

$$\begin{aligned} A_\mu &= (g^2 + e_0^2)^{-1/2}(g B_\mu + e_0 V_\mu^3)\,, \\ V_\mu^0 &= (g^2 + e_0^2)^{-1/2}(g V_\mu^3 - e_0 B_\mu)\,, \end{aligned} \tag{2.106}$$

where the electromagnetic charge is taken as $e = \frac{g e_0}{\sqrt{g^2 + e_0^2}} \approx e_0$. Thus, $\rho^0 - \gamma$ mixing is analogous to the Higgs mechanism of the electroweak gauge symmetry and the conserved charge is the electromagnetic charge. For $a = 2$, we get

$$g_{\gamma\pi\pi} = 0 \tag{2.107}$$

$$g_{\gamma\rho} = m_\rho^2/g\,. \tag{2.108}$$

Using eqs. (2.99), (2.100), (2.107) and (2.108) we can get

$$\frac{g_{\rho\pi\pi}}{m_\rho^2} = \frac{1}{2g f_\pi^2}\,, \qquad \frac{g_{\rho\gamma}}{m_\rho^2} = \frac{1}{g} \tag{2.109}$$

which lead to

$$\frac{g_{\rho\gamma}}{g_{\rho\pi\pi}} = 2 f_\pi^2\,. \tag{2.110}$$

This is the famous KSRF relation [121, 122] (version 1; see [11]) which can be regarded as the low-energy theorem of the hidden local symmetry framework [119]. Notice that this relation is independent of the parameter a.

2.3.3 $U(3)$ Extension of thes Hidden Local Symmetry

The $U(3)$ extension was first done by Bando et al. in [126]. If we want to include only the ω-meson, introducing it as a $U(1)$ gauge is more practical [127]. In this case, the hidden symmetry is extended to $(SU(2)_V \otimes U(1))_l\ (SU(2)_L \otimes SU(2)_R)_g/(SU(2)_V)_l$. If we want to include all of the vector-meson octet, the symmetry is extended to $(U(3)_L \times U(3)_R)_g/(U(3)_V))l$. This extension includes the vector-meson nonet as the dynamical gauge bosons and the nonet of pseudoscalar mesons as well. t^a become generators of $U(3)$ where a runs from 1 to 9. Moreover, $h(x) \in U(3)_V$, $(L, R) \in (U(3)_{L,R})_g$, and $f_\pi = f_k$ [53]. The Lagrangian has the same form as in the previous case but with different structure for the elements. After a gauge fixing procedure as before (unitary gauge), including external gauge bosons[12] and expanding the Lagrangian in terms of physical modes, we get:

$$\begin{aligned} \mathcal{L}_A &= \langle \partial_\mu \pi + ie_0[\pi, Q]B_\mu + \cdots \rangle^2 , \\ a\mathcal{L}_V &= af_{\pi^2}\langle gV_\mu - e_0 QB_\mu - \frac{1}{2f_\pi^2}[\pi, \partial_\mu \pi] + \cdots \rangle^2 . \end{aligned} \tag{2.111}$$

From these equations, masses and couplings for V_μ and B_μ can be deduced:

$$m_V^2 = ag^2 f_\pi^2, \tag{2.112}$$

$$g_{V\pi\pi} = \frac{1}{2}ag , \tag{2.113}$$

$$m_B^2 = ae_0^2 f_\pi^2 2\langle Q^2 \rangle , \tag{2.114}$$

$$g_{B\pi\pi} = \frac{a-2}{2}e_0 . \tag{2.115}$$

From the vector part of the Lagrangian, we get

$$g_{V^a\gamma} = agf_\pi^2\langle t^a Q\rangle = \frac{m_V^2}{g}2\langle t^a Q\rangle = 4g_{V\pi\pi}f_\pi^2\langle t^a Q\rangle . \tag{2.116}$$

The $(U(3)_V)_l \otimes U(1)_Q$ symmetry is spontaneously broken to $U(1)_{\text{em}}$ and electromagnetic charge is $Q_{\text{em}} = Q + Q_{\text{hidden}}$.

a independent relations ($U(3)$ breaking is taken into account [126]) can be written as:

$$\frac{g_\rho}{m_\rho^2} = \frac{3g_\omega}{m_\omega^2} = -\frac{3g_\phi}{\sqrt{2}m_\phi^2} = \frac{1}{g}. \tag{2.117}$$

[12] In three-flavor case, the electromagnetic charge has the form $Q = I_3^L + I_3^R + \frac{1}{2}(Y^L + Y^R)$ with isospin and hypercharge for the global symmetry so the source charges of V_μ and B_μ do not mix as in the two flavor case.

2.3.4 General Form of the Hidden Local Symmetry Lagrangian

The Lagrangian of the hidden local symmetry considering the vector-meson nonet as the dynamical gauge bosons and the photon as the external gauge boson can be written as [124]:

$$\begin{aligned}\mathcal{L} = &-\frac{1}{4}\langle F_{\mu\nu}^2\rangle - \frac{1}{4}\langle B_{\mu\nu}^2\rangle + \frac{1}{4}f_\pi^2\langle \partial_\mu U \partial^\mu U^\dagger\rangle + \frac{1}{2}\langle (m_\rho^2 V_\mu^2 - 2eg_{\rho\gamma}V_\mu^3 B^\mu + m_B^2 B_\mu^2)\rangle \\ &+ g_{\rho\pi\pi}\langle V^\mu \cdot (\pi \times \partial_\mu \pi)\rangle + g_{\gamma\pi\pi}\langle B^\mu (\pi \times \partial_\mu \pi)_3\rangle + \cdots .\end{aligned} \tag{2.118}$$

e is the electromagnetic coupling constant, m_V is the mass matrix of the vector-meson nonet, $m_{\mathcal{B}}$ is the primary photon mass and $\mathcal{B}_\mu$ is the primary photon field. As we have seen in eq. (2.105), after diagonalization of mass matrices the photon becomes massless. We can extend the hidden gauge formalism to include axial-vector mesons as well [124, 128].

CHAPTER 3

S-Matrix Theory and Unitarization of ChPT

During the pre-QCD era, and even before the quark model was introduced, hadrons were known to exist. In particular, pion properties and scattering were studied in a wide range of aspects like pion-pion partial waves, form factors, correlations with resonances, etc. One of the obstacles to study the strong interactions was to apply perturbative methods. Therefore, a different approach was needed.

If we do not consider fields as the main element of the theory but transition amplitudes of the required interactions, we can apply the S-matrix method (first proposed by Heisenberg [129]). This method is based on the idea to exploit the general properties of the interaction in question without use of explicit field definitions. It was built to satisfy principles of quantum mechanics, special relativity and causality. Since the theory is dealing with asymptotic states, the short-range nature of the strong force should also be one of the general properties of the interaction. Consideration of causality leads to the analytic properties of scattering amplitudes. These analytic properties can be verified order by order in a perturbative expansion or in axiomatic field theory. Therefore, after the well-established perturbative method of field theories and dispersion relations, starting from the late 1950s, relativistic S-matrix theory was applied rigourously and it is now understood that it brings a series of restrictions on the high energy behaviour of hadrons. With the success of effective field theories in the low-energy regime, the S-matrix theory started to receive a lot of attention again and turned out to be very useful. In this section, properties of the S-matrix theory will be discussed and the application of S-matrix theory to ChPT will follow. We follow mostly [98, 130].

3.1 S-Matrix Theory

3.1.1 S-Matrix

Since we are dealing with short range interactions, particles separated far enough in space are considered to be free. These particles are considered to be incoming and outgoing states which are the states defined long-enough before and after scattering such that they can be taken as free states. These states can be described in terms of creation and annihilation operators [1]

$$a_{\text{in}}(\mathbf{p})|0\rangle = 0\,, \qquad a_{\text{out}}(\mathbf{p})|0\rangle = 0\,. \tag{3.1}$$

[1] For rigour, there should be two vacuum states which are proven to be equal to each other by a phase factor since initial and final states are associated to the Poincaré group.

The commutation relations for these operators are

$$[a_{\text{in/out}}(\mathbf{p}), a^{\dagger}_{\text{in/out}}(\mathbf{p}')] = (2\pi)^3 \delta(\mathbf{p} - \mathbf{p}') \,. \tag{3.2}$$

Incoming and outgoing particle operators are related to each other by a unitary transformation [131] (the S-matrix is considered to be Lorentz invariant):

$$S^{\dagger} a_{\text{in}}(\mathbf{k}) S = a_{\text{out}}(\mathbf{k}) \,, \tag{3.3}$$

$$S^{\dagger} S = S S^{\dagger} = \mathbb{1} \,. \tag{3.4}$$

Hence, the free states, which are created by the creation operators defined in eq. (3.2) (momentum eigenstates), are also related to each other via the S-matrix. Therefore, matrix elements of S are transition probabilities of these states:

$$|\mathbf{p}_1, \ldots, \mathbf{p}_n\rangle_{\text{in}} = S\, |\mathbf{p}_1, \ldots, \mathbf{p}_n\rangle_{\text{out}} \,, \tag{3.5}$$

$${}_{\text{out}}\langle \mathbf{p}'_1, \ldots, \mathbf{p}'_n | \mathbf{p}_1, \ldots, \mathbf{p}_n\rangle_{\text{in}} = {}_{\text{out}}\langle \mathbf{p}'_1, \ldots, \mathbf{p}'_n | S\, |\mathbf{p}_1, \ldots, \mathbf{p}_n\rangle_{\text{out}} \,. \tag{3.6}$$

Asymptotic States

If we need to introduce asymptotic fields:

$$\Phi_{\text{in/out}}(x) = \frac{1}{(2\pi)^3} \int \frac{d^3\mathbf{k}}{\sqrt{2k_0}} \left(a^{\dagger \text{in/out}} e^{-ikx} + a^{\text{in/out}} e^{ikx} \right) , \tag{3.7}$$

and they are related to each other as

$$\Phi_{\text{out}}(x) = S^{\dagger} \Phi_{\text{in}} S \,. \tag{3.8}$$

These fields can be considered to be free fields of a Lorentz invariant field $\Phi(x)$ with $x = (t = \pm\infty, \mathbf{x})$. Hence, for any state, these fields should satisfy the asymptotic condition

$$\lim_{t \to \mp\infty} \langle \phi_a | (\Phi(x) - \Phi_{\text{in/out}}(x)) | \phi_b \rangle = 0 \,. \tag{3.9}$$

3.1.2 Unitarity

The S-matrix can be considered in terms of its elements which indicate transition of an initial state i to a final state f as

$$S_{fi} = \delta_{fi} + i(2\pi)^4 \delta^4(p_f - p_i) T_{fi} \,. \tag{3.10}$$

T is responsible for the interaction part and the factor in front of T is called the energy-momentum conservation factor, where δ_{fi} is the part where the final state is unperturbed and identical to the initial state. This separation is possible since initial and final states are momentum eigenstates. Therefore, the position information is absent in the S-matrix. This makes it possible for the particles to be distant enough and not interact at all. In the interaction part, T is related to the Lorentz invariant scattering amplitude $\mathcal{M}$ with the choice of normalization factors of the states,

$$T_{fi} = \prod_{a \in i} \frac{1}{\sqrt{2p_{0a}}} \prod_{b \in f} \frac{1}{\sqrt{2p_{0b}}} \mathcal{M}_{fi} \,. \tag{3.11}$$

The square of T gives the probability density of the reaction.

If we consider eqs. (3.4) and (3.10), then unitarity takes the form:

$$T_{fi} - T_{if}^{\dagger} = i(2\pi)^4 \sum_n \delta^4(p_n - p_i) T_{fn}^{\dagger} T_{ni}\,, \tag{3.12}$$

where n are all possible intermediate states which are physically accessible (states that can be produced at a given energy). The strong interaction is invariant under time reversal, therefore the S-matrix should also be time symmetric, $T_{fi} = T_{if}$. Hence, eq. (3.12) becomes

$$T_{fi} - T_{fi}^{\dagger} = 2\mathrm{Im}T_{fi} = (2\pi)^4 \sum_n \delta^4(p_n - p_i) T_{fn}^{\dagger} T_{in}\,, \tag{3.13}$$

and when $f = i$ (elastic scattering):

$$2\mathrm{Im}T_{ii} = (2\pi)^4 \sum_n \delta^4(p_n - p_i) |T_{ni}|^2\,. \tag{3.14}$$

We can use the intermediate state phase space, $\rho(s) = \frac{2p_n}{\sqrt{s}}$ of state n with the center-of-mass momentum p_n from eq. (D.5) and using the Mandelstam variables (described in appendix D),

$$s = (p_1 + p_2)^2\,, \qquad t = (p_1 - p_3)^2\,, \qquad u = (p_1 - p_4)^2\,, \tag{3.15}$$

to write eq. (3.14) in a more compact form:

$$\mathrm{Im}T(s) = \rho(s)|T(s)|^2\,. \tag{3.16}$$

If a two particle interaction is considered, we can project amplitudes into partial waves by integrating out the 3-momenta angles of initial and final states and using the Legendre polynomials, and spherical harmonics properties (the partial wave formalism is explained in detail in appendix E):

$$\mathrm{Im}t_l^{fi}(s) = \sum_n \rho(s) t_l^{fn}(s) t_l^{ni}(s)^*\,. \tag{3.17}$$

This can be written in the matrix form as:

$$\mathrm{Im}T(s) = T(s)\Sigma(s)T(s)^*\,, \tag{3.18}$$

where $\Sigma(s)$ is the diagonal phase space matrix. For elastic scattering, eq. (3.17) becomes:

$$\mathrm{Im}t_l(s) = \rho(s)|t_l(s)|^2\,. \tag{3.19}$$

3.1.3 Causality and Analyticity

If we demand causality, it is usually taken to be represented as the commutator of field operators at two spacetime points with space-like separation to be zero:

$$[\Phi(x), \Phi(y)] = 0\,, \qquad \text{for} \qquad (x-y)^2 < 0\,. \tag{3.20}$$

This means that the space-like separated fields are statistically independent. This property is named locality. A rigorous proof for the connection of causality and analyticity can only be stated in the non-relativistic formalism and is studied in detail in [132]. There is no general proof for the relativistic

theory. We can only make deductions from perturbation theory or axiomatic field theory. The connection between causality and analyticity in relativistic theory is called the Mandelstam hypothesis [133, 134] [2].

Interaction amplitudes are objects of the S-matrix which contain the physical dynamics of scattering processes. In the coordinate space, they are related to the time ordered vacuum expectation value which describes the absorption of a particle in one spacetime point and creation of another one in another spacetime point[3]:

$$\langle 0|T\{\Phi(x)\Phi(y)\}|0\rangle = \langle 0|\Theta(y^0 - x^0)[\Phi(y), \Phi(x)] \pm \Phi(x)\Phi(y)|0\rangle \,. \tag{3.21}$$

Θ is the Heaviside step function. Due to eq. (3.20), $\langle 0|[\Phi(y), \Phi(x)]|0\rangle = \Theta((y-x)^2)f(y)$ where $f(y)$ is the integrand of the interaction amplitude. The latter part is the sum over all possible intermediate states with total momenta p_n:

$$\langle 0|\Phi(x)\Phi(y)|0\rangle = \sum_n \mid C_n \mid^2 e^{-ip_n(x-y)} \,. \tag{3.22}$$

This term vanishes when it is integrated over four momenta to get the scattering amplitude since both the incoming and intermediate states should have a positive definite energy. Therefore, the amplitude has the form

$$\tilde{T}(E) = \int d^4y T(y)\Theta(y^0)\Theta(y^2)e^{ipy} = \int d^3\mathbf{y} \int dt e^{iEt}e^{-i\mathbf{py}} \,. \tag{3.23}$$

The Heaviside functions dictate that $t > 0$ and the total phase of the exponential is positive as well. If the integral in eq. (3.23) converges, it also converges for complex E with $\mathrm{Im}(E) > 0$. This is due to the fact that the latter condition converges faster than the former one due to the exponentially decreasing factor $e^{-\mathrm{Im}(E)t}$. As a result of this, $\tilde{T}$ is an analytic function in the upper half plane of complex plane. Therefore, analytic continuation to positive imaginary values of the energy is possible. Defining E as having a real and positive imaginary part corresponds to generating the future light-cone.

Let us consider only the time part, $T(t)$, and consider the Fourier transform of it:

$$T(t) = \int_{-\infty}^{\infty} dE e^{-iEt}\tilde{T}(E) \,. \tag{3.24}$$

Due to causality we should get $T(t < 0) = 0$. Therefore, $\tilde{T}(E)$ cannot increase exponentially in the complex plane due to eq. (3.24). For large enough negative t, this might not be the case. Therefore, the interaction amplitude should be restricted to be bounded for a finite N as:

$$\mid \tilde{T}(E) \mid < \mid s \mid^N \,. \tag{3.25}$$

The analyticity of the interaction amplitude is related to crossing symmetry and dispersion relations while the analyticity of the vacuum expectation value is related to the CPT theorem and to spin-statistics [130].

In the perturbative method, the scattering amplitude is given by a series of Feynman diagrams and contains all the dynamics of the process. Therefore, if individual perturbative elements are analytic, analytic continuation of the amplitude is possible [135]. Hence, all analyticity discussions of the dynamics are contained in the Feynman diagrams. Moreover, if an analytic function has singularities, their structures are very important physically. Once it is realized that all the singularities of Feynman graphs have physical origins, an amplitude of an interaction can be investigated by investigating analytic

[2] For a detailed study, see [131]

[3] It is an anti-commutator for fermions.

properties of the corresponding perturbative diagrams (whether they are formally Feynman diagrams or not) [135]. In addition, there are also kinematic singularities which should be taken into account.

Dispersion Relations

Since $\tilde{T}(E)$ can be analytically continued to the positive complex plane of E, we can apply Cauchy's theorem for real E and get

$$\tilde{T}(E + i\epsilon) = \frac{1}{2\pi} \oint_C \frac{\tilde{T}(E')dE'}{E' - E - i\epsilon}\,, \tag{3.26}$$

and we assume that $\tilde{T}(E) \to 0$ as $r \to \infty$ where $E = re^{i\theta}$ to ensure that the curve of the contour integral does not contribute.

3.1.4 Crossing-Symmetry

In the non-relativistic case, we can solve the radial Schrödinger equation for an arbitrary scattering potential and make sure that solutions are asymptotic so that they are superpositions of incoming and outgoing waves. Then, as mentioned, we can derive analyticity of the solutions rigorously and investigate analytic properties of these solutions. Further details on this issue can be found in [130, 131]. On the other hand, in a relativistic theory, the interaction potential cannot be arbitrary and restricted by unitarity and causality. While examining relativistic features, we also need to consider crossing symmetry which has important consequences on the relativistic potential.

In a two-body scattering process there are two Lorentz invariant independent parameters (Appendix D). In the center-of-mass frame (cms), these parameters can be defined to be the total momentum transfer (q) and the scattering angle (θ) [4]. We can use the Mandelstam variables, eq. (3.15), to describe a $2 \to 2$ scattering. There are only two independent parameters since the Mandelstam variables are connected via energy-momentum conservation and the mass-shell conditions. Hence, they satisfy

$$s + t + u = \sum_i m_i^2\,, \tag{3.27}$$

As a result, they lie on the same plane and there is a physical region for each scattering as indicated in fig.D.1.

From field theory, it is known that particles with the same mass and opposite propagation direction can be considered as anti-particles of each other (negative energy is assigned to an anti-particle). Therefore, a scattering amplitude $T_{ab\to cd}$ of $a(\mathbf{p_1}) + b(\mathbf{p_2}) \to c(\mathbf{p_3}) + d(\mathbf{p_4})$ in a specific physical region on the Mandelstam plane is equal to scattering of $T_{a\bar{c}\to\bar{b}d}$ with $a(\mathbf{p_1}) + \bar{c}(-\mathbf{p_3}) \to \bar{b}(-\mathbf{p_2}) + d(\mathbf{p_4})$ and $T_{a\bar{d}\to\bar{b}c}$ with $a(\mathbf{p_1}) + \bar{d}(-\mathbf{p_4}) \to \bar{b}(-\mathbf{p_2}) + c(\mathbf{p_3})$ in different physical regions as in fig.D.1. Due to causality, all three amplitudes are analytic. The Mandelstam hypothesis says that these three amplitudes are connected by analytic continuation to unphysical region, hence there is a single analytic function $T(s,t,u)$:

$$T(s,t,u) = \begin{cases} T_{ab\to cd}(s,t,u)\,, & s = (p_1 + p_2)^2 \geq (m_a + m_b)^2\,, t \leq 0\,, u \leq 0 \quad \text{s-channel,} \\ T_{a\bar{c}\to\bar{b}d}(t,s,u)\,, & t = (p_1 + \bar{p}_3)^2 \geq (m_a + m_c)^2\,, s \leq 0\,, u \leq 0 \quad \text{t-channel,} \\ T_{a\bar{d}\to\bar{b}c}(u,t,s)\,, & u = (p_1 + \bar{p}_4)^2 \geq (m_a + m_d)^2\,, s \leq 0\,, t \leq 0 \quad \text{u-channel.} \end{cases} \tag{3.28}$$

The scattering amplitude $T(s,t,u)$ has to satisfy the unitarity condition for all three physical amplitudes which are different in every physical region.

[4] For $n_1 \to n_2$ reaction, counting the number for Lorentz invariant independent parameters is given by $3(n_1 + n_2) - 10$.

Moreover, the CPT theorem says that the interaction $a + b \to c + d$ is the same as $\bar{c} + \bar{d} \to \bar{a} + \bar{b}$. So, if we consider both CPT and PT invariances (reversing the interaction direction), $T(s,t,u)$ represents 12 different interactions in total.

3.2 Singularities of the Scattering Amplitude

There are two types of singularities of the S-matrix. One type is due to the kinematic properties of the scattering, mainly characterized by the masses of the scattered particles, e.g. triangle singularities. They are called branch points. The other type is due to the dynamics of the interaction and named as poles. An observed structure in an experiment is identified as a physical state if and only if it is explained by a pole in the S-matrix theory [136].

We considered analyticity and unitarity of single parameter functions. Also, Cauchy's theorem applies only to single variable complex functions but it is stated that a two-particle scattering amplitude has two independent parameters. To be able to apply Cauchy's theorem we have two options. Either, we should fix one of the parameters (keeping s as a variable where t is fixed) or we should consider partial waves since the scattering angle is integrated out and there is only one independent parameter left in the partial wave formalism.

3.2.1 Branch Points and Branch Cuts

Free Propagator

Let us consider the two-point function of scalar fields, as in eq. (3.21) but this time by using the fields in eq. (3.7):

$$\phi(x) \quad = \quad \phi_{\text{in}}(x) + \phi_{\text{out}}(x)\,. \tag{3.29}$$

Hence,

$$\begin{aligned}
\Delta_{\text{p}}^{(\text{free})}(x-y) &= -i\langle 0|T\{\phi(x)\phi(y)\}|0\rangle\,, && (3.30)\\
&= -i\int \frac{d^3\mathbf{p}}{(2\pi)^3}\frac{1}{2p_0}(\Theta(x_0-y_0)e^{-ip(x-y)} + \Theta(y_0-x_0)e^{ip(x-y)})\,, && (3.31)\\
&= \Theta(x_0-y_0)\Delta_{\text{p}}^{-(\text{free})}(x-y) + \Theta(y_0-x_0)\Delta_{\text{p}}^{+(\text{free})}(x-y)\,, && (3.32)
\end{aligned}$$

where Δ_{p} means Δ in position space. We have already shown that this function can be analytically continued into the complex p_0 plane. In this case, two poles appear at $p_0 = \pm E_{\mathbf{p}}$ and we can write the time part as a contour integral over p_0 with the indicated poles:

$$-\frac{1}{2\pi i}\oint_C \frac{e^{-ip_0(x_0-y_0)}}{(p_0-E_{\mathbf{p}})(p_0+E_{\mathbf{p}})} = \begin{cases} \dfrac{1}{2E_{\mathbf{p}}}e^{-ip_0(x_0-y_0)}|_{p_0=E_{\mathbf{p}}} & x_0 > y_0 \\ \dfrac{1}{2E_{\mathbf{p}}}e^{ip_0(x_0-y_0)}|_{p_0=E_{\mathbf{p}}} & x_0 < y_0 \end{cases}. \tag{3.33}$$

Combining this with the spatial part and using the Feynman prescription (which means p^μ is no longer on-shell) gives

$$\Delta_{\text{p}}^{(\text{free})}(x-y) = \int \frac{d^4p}{(2\pi)^4}\frac{e^{-ip(x-y)}}{p^2-m_0^2+i\epsilon}\,, \tag{3.34}$$

or in momentum space

$$\Delta^{(\text{free})}(p^2) = \frac{1}{p^2 - m_0^2 + i\epsilon}\,. \tag{3.35}$$

On the p^2 plane, there is a single pole which describes a stable state.

Källén-Lehman Representation

This time, let us consider a two-point function of interacting fields:

$$\Delta_{\text{p}}(x-y) = -i\langle\omega|T\{\phi(x)\phi(y)\}|\omega\rangle\,, \tag{3.36}$$

where $|\omega\rangle$ is the ground state of the interacting theory. Inserting the completeness relation which includes all single- and multi-particle states in between the fields and omitting the ground state gives

$$\Delta_{\text{p}}^{-}(x-y) = -i\sum_n \frac{d^3\mathbf{p}}{(2\pi)^3}\frac{e^{-ip(x-y)}}{2E_{\mathbf{p}}}|\langle\omega|\phi(0)|n\rangle|^2\,. \tag{3.37}$$

In the Källén-Lehman representation the spectral function $\rho(p^2)$ is defined as

$$\rho(p^2) = \sum_n \delta(p^2 - m_n^2)|\langle\omega|\phi(0)|n\rangle|^2\,, \tag{3.38}$$

which is normalized to one. The full two-point function has the form

$$\Delta_{\text{p}}(x-y) = \int \frac{d^4p}{(2\pi)^4}e^{-ip(x-y)}\int_{-\infty}^{\infty}dp'^2\frac{\rho(p'^2)}{p^2 - p'^2 - +i\epsilon}\,, \tag{3.39}$$

or in momentum space

$$\Delta(p^2) = \int_{-\infty}^{\infty}dp'^2\frac{\rho(p'^2)}{p^2 - p'^2 + i\epsilon}\,. \tag{3.40}$$

Note that $p'^2 = p_n^2 \geq (nm)^2$ which is the invariant mass squared for the state with mass m. Therefore, it cannot be negative so that the integration limit is actually from 0 to ∞. This limit means, eq. (3.40) defines a future light-cone as well. This representation of the two-point function is the Källén-Lehman representation.

The lowest possible contribution to the spectral function is the one-particle state

$$\rho(p^2) = (2\pi)^3\int\frac{d^3\mathbf{p}_n}{(2\pi)^3}\frac{\delta^4(p_n - p)}{2E_{\mathbf{p_n}}}|\langle 0|\phi(0)|p_n\rangle|^2 = \frac{\delta(p_{n0} - p_0)}{2E_{\mathbf{p_n}}} = \delta(m^2 - p^2)\,, \tag{3.41}$$

and the next contribution starts from the two-particle threshold, $4m^2$ and has a continuous spectrum afterwards. Consequently, the spectral function has the form

$$\rho(p^2) = Z\delta(m^2 - p^2) + \rho(p^2 \geq 4m^2)\,. \tag{3.42}$$

Hence, eq. (3.40) becomes

$$\Delta(p^2) = \frac{Z}{p^2 - m^2 + i\epsilon} + \int_{4m^2}^{\infty} dp'^2 \frac{\rho(p'^2)}{p^2 - p'^2 + i\epsilon} \,. \tag{3.43}$$

Z is the wave function renormalization constant which basically represents the probability for a state to be created by ϕ from the ground state of the theory.

The Analytic Properties of $\Delta(p^2)$

$\Delta(p^2)$ is analytic in the complex p^2 plane with a singularity at $p^2 = m^2$, a branch point at $p^2 = 4m^2$, and a cut starting at this which continues to infinity. The branch cut singularity causes a discontinuity along the real axis of p^2 starting from the branch point. The physical value of the two-point function is given by the real value of p^2 when it is approached from the upper half plane of p^2. Therefore, the discontinuity can be calculated as:

$$\begin{aligned} \mathrm{disc}\Delta(p^2) &= \Delta(p^2 + i\epsilon) - \Delta(p^2 - i\epsilon) \\ &= \int_{4m^2}^{\infty} dp'^2 \rho(p'^2 \geq 4m^2) \left(\frac{1}{p'^2 - p^2 - i\epsilon} - \frac{1}{p'^2 - p^2 + i\epsilon} \right) = 2i\pi\rho(p^2 \geq 4m^2) \\ &= 2i\mathrm{Im}\Delta(p^2 \geq 4m^2) \,. \end{aligned} \tag{3.44}$$

This is due to the fact that for complex values of p, we get a multi-valued function. Instead of considering a multi-valued function, we define branch cuts connecting the branch points and introduce Riemann sheets which are connected to each other along these branch cuts. Riemann sheets ensure that there is no discontinuity along the branch cuts. Branch cuts appearing due to the multi-particle thresholds of s-channel processes are called right-hand cuts (RHCs).

This can be seen from eq. (3.17). When there is a new opening channel, there must be an addition to the right-hand side of the equation. Hence, to preserve the equality, the left-hand side needs additional terms. These terms are additional singularities of the scattering amplitude, corresponding to branch points. Accordingly, branch cuts are sometimes called unitarity cuts since they are imposed on analyticity by unitarity.

Let us say that there is a complex function $f(z)$ which is defined on the first Riemann sheet. The continuation of this function to the second Riemann sheet is denoted as $f_{II}(z)$. They are connected to each other along the cut as

$$\lim_{\epsilon \to 0^+} f_{II}(z - i\epsilon) = \lim_{\epsilon \to 0^+} f(z + i\epsilon) \tag{3.45}$$

$$= \lim_{\epsilon \to 0^+} f(z - i\epsilon) + \mathrm{disc} f(z) \,. \tag{3.46}$$

By this definition, analytic continuation of a single valued function along a branch cut is also possible by changing from one Riemann sheet to another. The first sheet is usually called physical sheet and all other Riemann sheets are called unphysical sheets. There can be several unphysical sheets which are defined separately by how they are connected to physical sheet. For details of complex analysis we refer to [137]. Moreover,physical amplitudes satisfy the Schwartz reflection relation

$$T(s^*, t_0, u_0) = T^*(s, t_0, u_0) \,. \tag{3.47}$$

Therefore, if there is a complex pole on the first Riemann sheet, for a fixed t, there must be conjugated

pair of it on the second Riemann sheet for values of s over the RHC.

Besides the RHC, if we also consider the Mandelstam hypothesis and crossing symmetry, there are other cuts which appear on the real axis. This is due to the fact that when a single amplitude represents three channels and each channel has a RHC of its own, the physical threshold in one channel will appear as a left-hand cut (LHC) on another. For example, if $T(s,t,u)$ represents the scattering amplitude of two pions, there is a physical threshold for $u \geq 4m^2$. For a fixed $t = t_0$, this branch point will appear in the s plane at $s = -t_0$ (see eqs. (3.27) and (3.28)). To put it another way, the u-channel RHC will appear as a cut from $s = -\infty$ to $s = -t_0$ in the analytic structure of $T(s,t,u)$. A single pole at $u = m^2$ will appear on the s-plane at $s = -t_0 + 3m^2$. When partial-wave amplitudes are considered, t is integrated over, hence there is only one independent parameter. Therefore, the LHC falls into the negative axis of the p^2 or s plane, starting from $s = 0$ to $-\infty$. LHCs are below the physical threshold region, however, they can still influence the physical reactions.

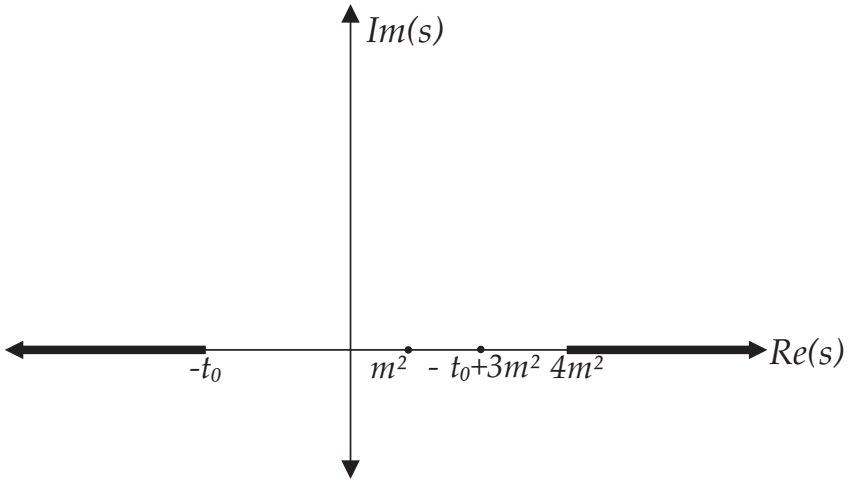

Figure 3.1: Analytic structure of $T(s,t_0,u)$ in the complex s-plane.

To summarize, in the inelastic region, if we consider eq. (3.12), T_{fi} and $T^{\dagger}_{if}$ are only connected via analytic continuation. If we are in the complex s-plane, T_{fi} is in the physical region (limit to the real s axis is approached from above, $\lim_{\epsilon\to 0} T(s+i\epsilon,t_0)$) and $T^{\dagger}_{if}$ is in the unphysical region (limit is approached from below $\lim_{\epsilon\to 0} T(s-i\epsilon,t_0)$). This property is called hermitian analyticity [138]. As a result, there is a discontinuity on the left-hand side of eq. (3.12). In the elastic region, eq. (3.19), T is real on the real axis below the threshold due to the Schwartz reflection principle, eq. (3.47). Finally, for a fixed $t = t_0$, crossing symmetry relates a value of $T(s+i\epsilon,t_0)$ in the physical region of s to a value of $T(s-i\epsilon,t_0)$ for $s < 0$ by crossing from the upper half-plane to the lower half-plane in between the branch cuts. Therefore, the lower half plane should also be analytic, since the u-channel reaction obeys causality as well. As a result, the scattering amplitude is an analytic function of the whole s-plane except for the singularities and branch cuts. The values for these two functions (reactions) are determined by the boundary values of $T(s,t,u)$. These properties are most easily represented in the form of dispersion relations. We will briefly introduce dispersion relations in section 3.3.

In a perturbative series, these branch points can be located in the complex plane of the unphysical Riemann sheets due to loop diagrams. If we study higher order diagrams like loop diagrams, there also appear other kinematic singularities. They are more complicated and called Landau singularities, such as the triangle singularity. The behaviour of these singularities, away or near threshold can be studied.

For a detailed discussion, we refer to [135], [139]. In summary, every singularity of Feynman diagrams has properties such as their position, which is exclusively related to the kinematics, and their behaviour, which is derived from the dynamics of the interaction.

3.2.2 Poles

Poles are rooted in the dynamics of an interaction. Causality and the Schwartz reflection theorem restrict the location of singularities on the physical Riemann sheet. They can only lie on the real axis. As stated, the interaction threshold lies above the unitarity cut. Therefore, poles on the real axis can be below the threshold and they are related to bound states. There can be also poles appearing on the unphysical Riemann sheet. If they lie on the real axis, they are called virtual states. Unlike the physical sheet, the unphysical sheets can have single poles in the complex plane as well. These poles correspond to unstable, non-normalizable states, identified as resonances. Due to hermitian analyticity, if there is a pole at a complex value of s, there should be a pole at the conjugate value s^* as well. Even though a pole is on the unphysical sheet, their effects can be seen on physical values since the scattering amplitude is analytically continuous. If a pole in the complex plane is isolated and far from threshold, its effect is seen as a peak in the scattering amplitude and the width of the peak is related to the lifetime of the resonance.

Bound States

We have seen in section 3.2.1 that single particle states are realized as poles whereas many-particle continuum states are realized as branch-cuts in the scattering amplitude. From eq. (3.40) we see that the spectral representation of the free scalar propagator is

$$\Delta_{\mathrm{p}}(x-y) = \int \frac{d^4p}{(2\pi)^4} e^{-ip(x-y)} \int_{-\infty}^{\infty} dp'^2 \frac{\rho(p'^2)}{p^2 - p'^2 - +i\epsilon}\,, \tag{3.48}$$

$$\Delta(p^2) = \int_0^{\infty} dp'^2 \frac{\rho(p'^2)}{p^2 - p'^2 + i\epsilon}\,. \tag{3.49}$$

Moreover, we know the equal-time commutation relations ($x^0 = y^0$) for interacting scalar field operators:

$$[\phi(x), \phi(y)] = 0\,, \tag{3.50}$$

$$\left[\frac{\partial\phi(x)}{\partial x^0}, \phi(y)\right] = i\delta^3(\mathbf{x}-\mathbf{y})\,. \tag{3.51}$$

If we take the derivative of eq. (3.48) with respect to x^0 with the equal-time relation and use the commutation relations above, we get:

$$\frac{\partial\Delta_{\mathrm{p}}(x-y)}{\partial x^0} = -i\frac{\partial\langle\omega|T\{\phi(x)\phi(y)\}|\omega\rangle}{\partial x^0}\,, \tag{3.52}$$

$$\int_0^{\infty} dp'^2 \rho(p'^2)\delta^3(\mathbf{x}-\mathbf{y}) = \delta^3(\mathbf{x}-\mathbf{y})\,. \tag{3.53}$$

This relation ensures the normalization of the spectral function $\rho(p^2)$:

$$\int_0^{\infty} dp'^2 \rho(p'^2) = 1\,. \tag{3.54}$$

When an interacting theory is considered, as stated, the spectral function becomes

$$\int_0^\infty dp'^2 \rho(p'^2) \to Z\delta(p'^2 - m^2) + \int_{4m^2}^\infty dp'^2 \rho(p'^2)\,. \tag{3.55}$$

Hence, eq. (3.54) puts a constraint on the renormalization constant Z:

$$1 = Z + \int_{4m^2}^\infty dp'^2 \rho(p'^2)\,. \tag{3.56}$$

Therefore, we can state that a single particle state contributes to the scattering amplitude proportional to its wave function renormalization constant which can be extracted from the residue of the pole as

$$Z = \lim_{p^2 \to m^2} (p^2 - m^2)\Delta(p^2)\,. \tag{3.57}$$

In an interacting theory, any contribution from the spectral function integration is non-zero. Therefore,

$$0 \leq Z \leq 1\,. \tag{3.58}$$

From field theory perspective, $Z = 1$ means a single free particle state. On the other hand, $Z = 0$ case can be interpreted as a possibility of the existence of a field with $Z = 0$ which does not appear in the Lagrangian. The corresponding states are called composite states. This case was first considered by Houard and Jouvet [140] (also see [141]) and applied to non-relativistic case by Weinberg, where the deuteron is explained as a proton-neutron bound state [142]. $Z = 0$ case is actually not applicable in QFT. Z must be interpreted as the coupling constant of a bound state to its constituent particles. However, this is not possible in perturbative sense since $Z = 0$ indicates that the bound state couples to its constituent particles in maximum possible limit of the interaction. The compositeness relation is derived in relativistic field theory approach in appendix F.

In his pioneering work, Weinberg found that the Z value has to be small for the deuteron and related this value to the compositeness of a particle in a non-relativistic approach [142]. This enables us to decide if a particle is elementary or not even in a low-energy scattering experiment. For small binding energies (hence, S-wave states only), these calculations are shown to be model-independent [142]. This work was then generalized to resonances and elaborated for various cases [143], [144], [145], [146] and references therein.

Resonances

It is easier to understand the nature of resonances in an elastic partial wave scattering. In this section, we will assume equal masses for the scattering particles. Since t_l has a complex value, it can be written in terms of its modulus and a phase as $t_l = |t_l|e^{i\delta_l}$. So, eq. (3.19) becomes:

$$\sin(\delta_l) = \rho(s)|t_l| \;\Rightarrow\; t_l = \frac{e^{i\delta_l}\sin(\delta_l)}{\rho(s)}\,, \tag{3.59}$$

$$t_l(s) = \frac{1}{2i\rho(s)}(e^{2i\delta_l} - 1) = \frac{\sin\delta_l e^{i\delta_l}}{\rho(s)}\,, \tag{3.60}$$

where δ_l is the scattering phase for angular momentum l. Due to the partial wave expansion (eq. (E.36)), we get

$$t_l(s) = \frac{1}{2}\int_{-1}^{1} d\cos\theta P_l(\cos\theta) T(s,t)\,. \tag{3.61}$$

Integration of the scattering angle from -1 to 1 is equivalent to integration of t from $-(s-4m^2)$ up to $t = 0$ (see eq. (D.9)). Therefore, $t_l(s)$ has the same analytic properties as $T(s,t)$ has. It is real on the real axis in the region $0 < s < 4m^2$ and complex otherwise. Since it has real values in a finite region it obeys Schwartz reflection principle, eq. (3.47). Hence, eq. (3.19) can be defined in terms of discontinuity of $t_l(s)$ as

$$\frac{1}{2i}(t_l(s+i\epsilon) - t_l(s-i\epsilon)) = \rho(s) t_l(s+i\epsilon) t_l(s-i\epsilon)\,. \tag{3.62}$$

This allows to give a formula for $t_l(s+i\epsilon)$:

$$t_l(s+i\epsilon) = \frac{t_l(s-i\epsilon)}{1 - 2i\rho(s) t_l(s-i\epsilon)}\,. \tag{3.63}$$

Let us interpret this equation in terms of complex functions and consider s as a complex number with sufficiently large negative imaginary part. In this case, $t_l(s-i\epsilon)$, which lies in the lower half plane of the physical sheet will shift to lower values in this plane. On the other hand, $t_l(s+i\epsilon)$, which is in the upper half plane of the physical sheet, has to cross the cut and therefore moves to the second Riemann sheet. Hence, eq. (3.63) defines the analytic continuation of partial waves from the physical sheet to the unphysical sheet. Accordingly, the analytic properties of $t_l(s)$ on the unphysical sheet can be deduced from its analytic properties on the physical sheet.

Both sheets contain the same cuts since $t_l(s+i\epsilon)$ and $t_l(s-i\epsilon)$ have the same cuts. However, due to eq. (3.63), $t_l(s+i\epsilon)$ contains poles with complex values unlike $t_l(s-i\epsilon)$. These poles are located at

$$1 - 2i\rho(s) t_l(s-i\epsilon) = 0\,. \tag{3.64}$$

To ensure the Schwartz reflection relation, in the upper half plane, the spectral function is the usual function $\rho(s)$ whereas in the lower half plane it is defined as $-\rho^*(s^*)$.

These poles, on the unphysical sheet, are defined as resonances and their contribution to the partial wave amplitude with angular momentum l can be defined as

$$t_l(s) = \frac{r}{s - m_{\text{res}}^2 + i\sqrt{s}\Gamma_{\text{res}}(s)}\,, \tag{3.65}$$

where r is the pole residue, m_{res} is the mass of the resonance and the imaginary part of the self-energy is related to the width of the resonance. The residue depends on the coupling constant, the coupling of the resonance to the initial state. Therefore, the position of a pole also depends on the coupling constant value. The pole position matters for the interaction amplitude. As the pole gets closer to a branch-cut, the interaction amplitude is increasingly affected. From the Schwartz reflection principle, we know that there are two poles in the complex plane. However, if its real s value is above the branch-point, then the pole in the lower half plane affects the interaction amplitude more, since it is closer to the physical sheet. If its real s value is below the threshold, both poles are at the equal distance point from the branch-point.

Resonances and Unitarity

Eq. (3.59) tells us that unitarity applies boundary conditions on the interaction amplitude:

$$|t_l| \leq \frac{1}{\rho} \xrightarrow{s \gg m^2} 1\,, \tag{3.66}$$

$$\mathrm{Re}t_l \leq \frac{1}{2\rho} \xrightarrow{s \gg m^2} \frac{1}{2}\,. \tag{3.67}$$

These bounds also hold for inelastic interactions. A strongly interacting theory can be identified by saturation of these bounds. We can state that unitarity relations indicate that partial waves shall be bounded as energy increases. Especially in sharp resonance regions, phase shift rapidly increases in energy from 0 degrees to around 180, see fig.2.4. This shows that in resonance regions an interaction becomes as strong as possible and that means resonances saturate the unitarity bounds. Therefore, unitarity is crucial in examining resonances and vice a versa.

Virtual States

The only other possible place for a pole to exist is on the real axis and below the threshold of the second Riemann sheet. These poles are called virtual states. By considering non-relativistic scattering theory, it can be seen that the wave function of virtual states is in an asymptotic form such that at large distances the wave function increases exponentially. Hence, they are non-normalizable. Especially for small energies of virtual states, they might have observable effects on scattering amplitudes, e.g. the neutron-neutron scattering pole in the isospin-1 and spin-0 channel.

3.3 Dispersion Relations

In section 3.1.3, we only defined how to apply Cauchy's theorem to an analytic function. This method is very useful once the analytic structure of a scattering amplitude is known since it relates a single value of a function to an entire contour integral of that function. However, Cauchy's theorem is valid only for single variable functions. Therefore, either one of the variables has to be fixed, $t = t_0$ (e.g. $t = 0$: forward dispersion relations) or partial waves dispersion relations (e.g. Roy equations) can be used since the scattering angle is integrated out in the partial waves expansion. In terms of the Mandelstam variables, dispersion relations read:

$$T(s,t,u) = \frac{1}{2\pi i} \oint ds' \frac{T(s',t,u')}{s'-s}\,. \tag{3.68}$$

Here, the complex integral is over a contour. We know from complex calculus that if $T(s,t,u)$ goes to zero faster than $1/s$ as s goes to infinity, the contribution from the circular path approaches zero as the radius approaches infinity.

We have already seen that for scattering of two same mass particles with partial wave expansion, there is a LHC from $-\infty$ to $s = 0$ and a RHC starting from the threshold of two identical particles $s_{\mathrm{th}} = 4m^2$ to ∞. This is the analytic structure without any poles. Its dispersion relation can be written as:

$$t_l(s) = \frac{1}{\pi}\int_{-\infty}^{0} ds' \frac{\mathrm{Im}(t_l(s'))}{s'-s} + \frac{1}{\pi}\int_{s_{\mathrm{th}}}^{\infty} ds' \frac{\mathrm{Im}(t_l(s'))}{s'-s}\,, \tag{3.69}$$

where the contour is depicted in fig.3.2. Integrals around cuts are in opposite directions above and below the real axis. Moreover, when the Schwartz reflection principle is used, we are left with twice the

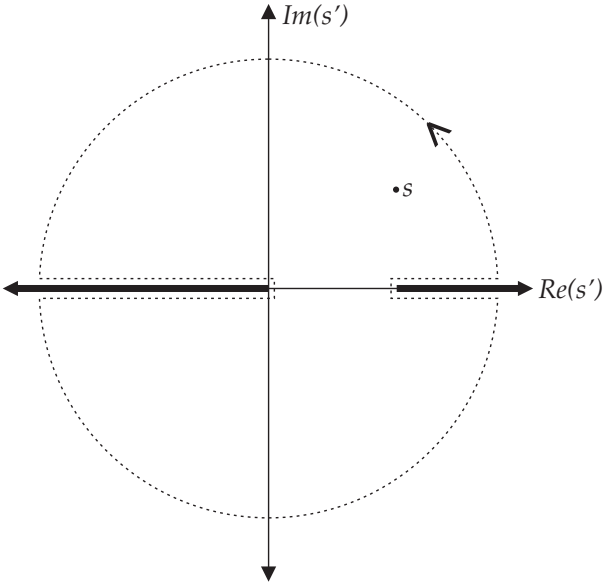

Figure 3.2: Contour for $t_l(s)$ in the complex plane, on the first Riemann sheet.

imaginary part of the amplitude and the real parts cancel each other. Hence, this relation provides partial wave amplitudes anywhere in the complex s plane except on cuts. On cuts (for real values of s), the $s' - s$ terms diverge. However, if the contour is deformed and the $s' - s \pm i\epsilon$ prescription is considered:

$$\frac{1}{s' - s' - i\epsilon} = \mathrm{PV}\frac{1}{s' - s} + i\pi\delta(s' - s)\,, \tag{3.70}$$

where PV stands for the principal value. The second term on the right-hand side of this equation takes $\mathrm{Im}t_l(s)$ of the second term on the right hand-side of eq. (3.69) out of the integral. This term cancels out with the imaginary part of the left-hand side of eq. (3.69). Thence, on the real axis dispersion relations provide $\mathrm{Re}(t_l)$ from $\mathrm{Im}(t_l)$:

$$\mathrm{Re}t_l(s) = \frac{1}{\pi}\int_{-\infty}^{0} ds' \frac{\mathrm{Im}(t_l(s'))}{s' - s} + \frac{1}{\pi}\mathrm{PV}\int_{s_{\mathrm{th}}}^{\infty} ds' \frac{\mathrm{Im}(t_l(s'))}{s' - s}\,. \tag{3.71}$$

In some cases $T(s,t)$ does not converge to zero faster than $1/s$ as s goes to infinity. In fact, it may even diverge. This can be cured with subtraction constants. When subtraction constants are used, Cauchy's theorem is not applied to $T(s,t,u)$ but to $T(s,t,u)/(s-s_0)$. Here, s_0 is a convenient subtraction point which is usually taken at $s = 0$ or at $s = s_{\mathrm{th}}$. Thus, it is enough for the circular part to vanish if $T(s,t,u)/(s - s_0)$ goes to zero faster than $1/s$. We can repeat this procedure as many times as required. However, Froissart's theorem tells that two hadron scattering amplitudes cannot grow faster than $\log^2(s)$ [147]. Therefore, to guarantee the convergence, two subtractions are enough. Nonetheless, we can do more subtractions. The more subtractions are used, the more high energy contributions are suppressed. All subtractions can be made at the same point, which is usually the case. The behaviour of functions should be well-known at each subtraction point to ensure convergence. The behaviour of amplitudes at subtraction points can be investigated from EFT. Therefore, to combine analyticity and EFT subtraction constants play a major

role. Once subtracted and twice subtracted dispersion relations are respectively given as:

$$\begin{aligned} t_l(s) &= t_l(s_0) + \frac{s-s_0}{\pi}\int_{-\infty}^{0} ds' \frac{\mathrm{Im}(t_l(s'))}{(s'-s)(s'-s_0)} + \frac{s-s_0}{\pi}\int_{s_{\mathrm{th}}}^{\infty} ds' \frac{\mathrm{Im}(t_l(s'))}{(s'-s)(s'-s_0)}\,, \\ t_l(s) &= t_l(s_0) + (s-s_1)t_l'(s_1) + \frac{(s-s_0)(s-s_1)}{2\pi i}\int_{-\infty}^{0} ds' \frac{\mathrm{Im}(t_l(s'))}{(s'-s)(s'-s_0)(s'-s_1)} \\ &+ \frac{(s-s_0)(s-s_1)}{2\pi i}\int_{s_{\mathrm{th}}}^{\infty} ds' \frac{\mathrm{Im}(t_l(s'))}{(s'-s)(s'-s_0)(s'-s_1)}\,. \end{aligned}$$

In case of different masses, there will be an additional circular cut with $s = |m_1^2 - m_2^2|$ and there can be poles related to bound states which should be encircled outside of the contour and their contribution is proportional to their residues (a once subtracted equation is considered):

$$\begin{aligned} t_l(s) &= \underbrace{t_l(s_0)}_{\text{subtraction constant}} + \underbrace{\frac{s-s_0}{\pi}\int_{-\infty}^{0} ds' \frac{\mathrm{Im}(t_l(s'))}{(s'-s)(s'-s_0)}}_{\text{LHC}} + \underbrace{\frac{s-s_0}{\pi}\int_{s_{\mathrm{th}}}^{\infty} ds' \frac{\mathrm{Im}(t_l(s'))}{(s'-s)(s'-s_0)}}_{\text{RHC}} \\ &+ \underbrace{C(s)}_{\text{Circular Cut}} + \underbrace{P(s)}_{\text{bound state poles}}\,. \end{aligned} \tag{3.72}$$

As a result, dispersion relations can give a rigorous scheme for calculating scattering amplitudes on the first Riemann sheet with relevant constraints. We can use partial wave S-matrix properties which allow for a continuation to the second Riemann sheet and investigate resonances and bound states. Since ChPT is accurate at low energies, subtraction constants can be obtained from it for low s values. Afterwards, we can use dispersion relations to obtain the higher energy behaviour of the interaction. We want to underline one thing before closing this chapter. Dispersion relations are consequences of causality; they include no interaction dynamics on their own.

3.4 Unitarization of ChPT

3.4.1 Unitarity in EFT

Let us start with a strong statement that any perturbation theory violates unitarity. It is straightforward to see the reason. Let us remember the elastic unitarity condition eq. (3.19):

$$\mathrm{Im}t_l(s) = \rho(s)|t_l(s)|^2\,. \tag{3.73}$$

Now, if a calculation is performed at the leading order in any EFT or QFT, the result is real. Once the next-to-leading order term is considered, with the inclusion of loop diagrams, the imaginary part comes in. Therefore, at the leading order, the left hand side of eq. (3.19) is zero whereas the right hand side is not and unitarity is violated. Hence, unitarity can only be satisfied perturbatively within a perturbative theory:

$$2\overbrace{\mathrm{Im}T}^{O(\lambda^n)} = \overbrace{T^\dagger T}^{O(\lambda^{2n})}\,. \tag{3.74}$$

However, in perturbative theories like QED, the perturbation parameter is small ($\lambda = \alpha \simeq 1/137$) so that this can be discarded.

On the other hand, in ChPT $\lambda = p$. That means that the amplitude is defined in polynomials of s.

Therefore, at some energy level unitarity will always be violated and this violation cannot be discarded anymore since the λ/Λ value is not small. To satisfy unitarity in ChPT we need to take into account the higher order terms in the power counting. Consider that $t_l(s) = t_l^{(2)}(s) + t_l^{(4)}(s) + t_l^{(6)}(s) + \cdots$ where $t^{(x)} \equiv O(p^x)$. Consequently, $t_l(s)$ has to be calculated up to a needed order. This termination in the power series prevents us from conserving unitarity exactly. Consequently, as stated before, unitarity has to be preserved perturbatively:

$$\begin{aligned} \mathrm{Im}t_l^{(2)}(s) &= 0\,, \\ \mathrm{Im}t_l^{(4)}(s) &= \rho(s)t_l^{(2)}(s)^2\,, \\ \mathrm{Im}t_l^{(6)}(s) &= 2\rho(s)t_l^{(2)}(s)\mathrm{Re}t_l^{(4)}(s)\,, \ldots \end{aligned}$$

If we are considering coupled channels, these relations can be written in matrix form:

$$\begin{aligned} \mathrm{Im}T^{(2)}(s) &= 0\,, \\ \mathrm{Im}T^{(4)}(s) &= T^{(2)}(s)\Sigma(s)T^{(2)}(s)\ \ldots \end{aligned}$$

The imaginary part of scattering amplitudes comes from loop diagrams with different intermediate states. According to the equations above, the imaginary part of these loops can be calculated from lower order amplitudes. It is expressed figuratively with unitarity cuts which are cuts that divide bubble diagrams into two as seen in fig.3.3. However, even if unitarity is not restored, ChPT can be used to provide subtraction constants in dispersion relations.

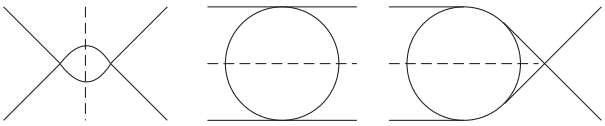

Figure 3.3: s-, t-, and u-channel unitarity cuts.

Unitarity Bounds and Resonances

3.4.2 Unitarization of EFTs

It turns out that analyzing the inverse of the interaction amplitude is useful [105–107, 148, 149]. Eq. (3.17) can be written as (using $\mathrm{Im}\left(\frac{1}{z}\right) = \frac{-\mathrm{Im}(z)}{|z|^2}$):

$$\mathrm{Im}\left(\frac{1}{t_l(s)}\right) = -\rho(s)\,. \tag{3.75}$$

This equation shows that the unitarity condition allows the imaginary part of the inverse of a partial wave amplitude to be known exactly. Moreover, we can say that the imaginary part of an inverse amplitude does not include any dynamics. It is just the phase space. Therefore, for physical values of s, any elastic partial wave should satisfy:

$$t(s) = \frac{1}{\mathrm{Re}(t(s))^{-1} - i\rho(s)}\,, \tag{3.76}$$

which has the form for n open, two-body state channel with an $n \times n$ T-matrix (again, for physical s values):

$$T(s) = \left[\mathrm{Re}(T(s)^{-1}) - i\Sigma(s)\right]^{-1} . \tag{3.77}$$

On the right hand side of eq. (3.77), $\mathrm{Re}(T(s)^{-1})$ is the only term which includes dynamics of the Lagrangian of an EFT. Hence, the effective Lagrangians provide only the dynamics for Eq. (3.77) and unitarity is preserved by the same equation even though the power expansion of the effective Lagrangian is not unitary. There are different unitarization methods with different approximations to calculate the interaction dynamics which are a part of eq. (3.77). These approximations should be considered carefully to calculate $\mathrm{Re}(T(s)^{-1})$ and applying the unitarization method in a specific energy region.

For example, the K-matrix method takes $K = \mathrm{Re}(T(s)^{-1})$ as a simple analytic and real function. This method is very simple since "any" function that explains resonances and thresholds of the system can be used with parameters to be fit by the data on real axis and an approximation for a pole can be achieved. Therefore, it is merely used in experimental data analyses. However, this method is valid only on the real axis above the threshold since no LHCs or circular cuts are considered. Moreover, the real part of an analytic function is not necessarily an analytic function. In many cases by considering only the real part analyticity might be violated. Therefore, these approximations are fair only if the poles are narrow and far from left cuts and thresholds.

The choice of method and its limitations should be carefully considered. This method dependence might look like vagueness in defining unitarization process, but these approximations can be constrained with the consideration of analyticity, terms from ChPT, symmetries of interactions, and so on [98]. The more constraints are considered, the better results will become. Consequently, a well motivated effective field theory, like ChPT, is needed to calculate $\mathrm{Re}(T(s)^{-1})$.

3.4.3 Chiral Unitary Approach

Unitary Chiral Perturbation Theory

Let us start with single channel scattering to calculate $\mathrm{Re}(t(s)^{-1})$ in eq. (3.76). Considering up to next-to-leading order (NLO) ChPT, the contributing diagrams are tree level diagrams from the leading order, loop diagrams which are constructed with vertices of leading order, and the tree level diagram with one NLO vertex. Loop diagrams include divergent integrals, and therefore they need to be regularized. This regularization introduces a scale parameter, which is represented by μ. Tree level diagrams with one NLO vertex include low-energy constants and also depend on the regulator. These constants, as explained before, absorb all divergences and contain information about the fundamental theory, in this case QCD. Moreover, the regulator dependence of NLO tree level diagram cancels out with regulator dependent terms of loop diagrams. Therefore, up to NLO, a renormalized calculation is finite and does not depend on any extra parameters except the parameters of ChPT itself.

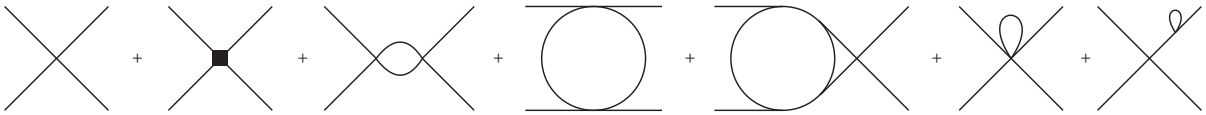

Figure 3.4: Up to NLO meson-meson scattering diagrams.

If all these factors are included in an elastic scattering process, up to NLO, ChPT amplitude in p^2

series can be written as

$$t = t^{(2)} + t^{(4)} + \cdots , \tag{3.78}$$

and expansion of $\mathrm{Re}(t^{-1})$ up to NLO is

$$\mathrm{Re}(t^{-1}) \approx \frac{1}{t^{(2)}} - \frac{\mathrm{Re}t^{(4)}}{{t^{(2)}}^2} + \cdots . \tag{3.79}$$

If we insert this in eq. (3.76) we get

$$t = \frac{1}{{t^{(2)}}^{-2}(t^{(2)} - \mathrm{Re}t^{(4)} + \cdots) - i\rho} = \frac{{t^{(2)}}^2}{t^{(2)} - \mathrm{Re}t^{(4)} - i\rho(t^{(2)})^2} . \tag{3.80}$$

Remember that the perturbative unitarity relation gives

$$\mathrm{Im}t^{(4)} = \rho|t^{(2)}|^2. \tag{3.81}$$

Hence,

$$t \approx \frac{{t^{(2)}}^2}{t^{(2)} - t^{(4)}}. \tag{3.82}$$

This equation is called the elastic inverse amplitude method (IAM) [105, 148, 150]. If this equation is expanded at low energies, it matches with the ChPT expansion.

As stated while discussing the K-matrix method, the real part of an analytic function is not necessarily analytic. Nevertheless, eq. (3.82) is an analytic function. Same formula can be derived by using dispersion relations [150]. However, there is an important difference. Eq. (3.76) is valid only on the real axis and above the threshold, whereas eq.(3.82), when derived from dispersion relations, is valid all over the complex plane. Since both $t^{(2)}$ and $t^{(4)}$ are calculated from EFT, both the RHC and LHC are present. In the IAM, the RHC is exact for the elastic case and the LHC is approximated up to NLO order of ChPT. In dispersion relations, the result of this approximation on the LHC can be suppressed by subtraction constants [150]. This might be an issue only if the pole of a resonance is very close to the LHC. The reason for this issue with the LHC is due to the violation of crossing symmetry when the unitarity condition is imposed on the real axis above the threshold. If the analyzed pole is observed to be close to the LHCs, in [151], they have proposed a method to combine the crossing symmetry constraints with the unitarity condition. In this method the LHC is calculated by ChPT, hence it is well-behaved in the low-energy regime.

Since eq.(3.82) is analytic in complex plane, analytic continuation is possible. By fitting the elastic $\pi\pi$ scattering data using IAM and considering analytic properties, the rho resonance can be identified as done in [105, 148, 150], see fig.2.4. As can be seen in the plot, by using only ChPT it is not possible to explain the rho-meson but it is explicit in NLO IAM. In the resonance region, unitarity bounds are saturated (see section 3.2.2). Since resonances are described by poles on the second Riemann sheet, they cannot be explained by polynomials but only by singularities as in eq. (3.65). Therefore, calculations performed only by using ChPT is not consistent with the data in higher energies when there is a pole. To generate the resonance behaviour of the scattering amplitude we need unitarization methods. As a result, it is possible in elastic IAM to calculate higher orders systematically. There are no scale-dependent parameters (except the ones coming from ChPT), since the calculation is renormalized and analytic. For a discussion on unitarization methods, see also [107].

If elastic scattering is generalized to coupled channels, eqs. (3.80) and (3.82) have the form, respect-

ively:

$$T = T^{(2)}(T^{(2)} - \mathrm{Re}T^{(4)} - iT^{(2)}\Sigma T^{(2)})^{-1}T^{(2)}\,, \tag{3.83}$$

$$T = T^{(2)}(T^{(2)} - T^{(4)})^{-1}T^{(2)}\,. \tag{3.84}$$

With full one-loop $SU(3)$ ChPT consideration in a unitarized form generates poles on the second Riemann sheet [108, 152]. These results are obtained by fitting the scattering data in inelastic IAM. Fitting error and systematic error for the LECs can be found in [152]. The LEC values are in good agreement with ChPT.

In coupled channel IAM, there is no dispersion relations based derivation available. The N/D method (we explain this method later in this section) which is, the closest form yet that can be gotten to coupled channel dispersion relations. Moreover, each LHC is unique to a specific channel and they are mixed when the inverse of the scattering amplitude matrix is calculated. Fortunately, the contribution from the LHC is numerically small most of the time. With all these problems, coupled channel IAM is not a very practical method and for some EFT or chiral Lagrangians, which are not as rigorous as ChPT, full one-loop calculations might be problematic. To have decent and convergent results, sometimes NNLO calculations are needed (for example in the EFT with nucleons), full one-loop calculations might lead to complicated functions or there might not be a systematic calculation at all (with chiral Lagrangians which are not EFTs) [152]. Therefore, simpler unitarization methods can be achieved by abandoning sound renormalized calculations.

Chiral Unitary Approach

As discussed above, if the pole of a resonance or a bound states is far from the LHCs, the contribution of LHCs will be small. Therefore, left-cut properties in NLO can be disregarded, while resonance properties are analyzed. This results in the elimination of crossed channel loop diagrams. The price to pay for this approximation is the full renormalization scheme. Divergences are not totally absorbed in the LECs anymore and calculations become cutoff (μ) (or subtraction constant), dependent. Thence, an NLO calculation is not fully renormalizable anymore. If renormalized values for masses and constants are used directly and as long as the origin of those values are not important for our purposes, tadpoles will not change the results. Therefore, tadpoles can be omitted as well. As a result, there are only three diagrams left to be calculated: tree diagrams with LO vertices, tree diagram with the NLO vertex and s-channel loop diagram:

$$t \sim t^{(2)} + t^{(4)}_{\text{tree}} + t^{(4)}_{\text{s-ch loop}}\,. \tag{3.85}$$

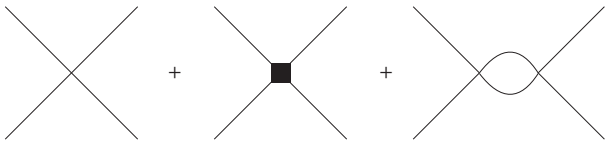

Figure 3.5: Chiral unitary approach diagrams.

Moreover, if we separate on- and off-shell parts of the amplitude as f(on-shell) and $f(q) - f$(on-shell), the loop term can be calculated with the on-shell factorization. Let us explain this statement briefly. If we consider the on-shell approximation ($p^2 = m^2$), the off-shell part (proportional to $p^2 - m^2$) cancels out with one of the meson propagators in the denominator of the loop integral. In this case this diagram becomes a

tadpole diagram. This part is explained in the next section. Thus, the integral over the momentum of the off-shell part can be factorized in physical values like mass and decay constant. Considering dispersion relations and unitarity, on-shell factorization can be derived for the inverse amplitude [109, 153]. As a result of this factorization, the s-channel loop diagram can be calculated by separating the external legs and the loop part:

$$t^{(4)}_{\text{s-ch loop}} = t^{(2)} G t^{(2)} \,, \tag{3.86}$$

where G is:

$$G = i \int \frac{d^4q}{(2\pi)^4} \frac{1}{q^2 - m_1^2 + i\epsilon} \frac{1}{(P-q)^2 - m_2^2 + i\epsilon} \,. \tag{3.87}$$

The loop diagram preserves the unitarity since $\text{Im}(G(s)) = \rho(s)$. G is not a convergent integral. Hence, we need to regularize it. This regularization brings a regulator term, a scale μ which the result is dependent on. Hence, the result is cutoff dependent which is expected since fully renormalized calculation is abandoned. We said that $\text{Im}(G)$ gives us the phase space where $\text{Re}G$ is used in the series expansion of eq. (3.79) as:

$$\text{Re}(t) = t^{(2)} + \text{Re}t^{(4)}_{\text{tree}} + t^{(2)}\text{Re}(G)t^{(2)} + \cdots \,. \tag{3.88}$$

Note that G is analytic. Therefore, analytic continuation to the second Riemann sheet is possible for resonance property investigation. Inverting eq. (3.88)

$$\text{Re}\left(\frac{1}{t}\right) = \frac{1}{t^{(2)}} \left(1 - \frac{\text{Re}t^{(4)}_{\text{tree}}}{t^{(2)}} - t^{(2)}\text{Re}(G)\cdots\right) , \tag{3.89}$$

and inserting it in (3.76) gives:

$$t = \frac{{t^{(2)}}^2}{t^{(2)} - t^{(4)}_{\text{tree}} - t^{(2)} G t^{(2)}} \,. \tag{3.90}$$

Keeping the $t^{(4)}_{\text{tree}}$ term ensures that the most general polynomial structure in NLO ChPT is preserved.

For coupled channels, eq. (3.90) becomes a matrix equation:

$$T \simeq T^{(2)} \cdot [T^{(2)} - T^{(4)}_{\text{tree}} - T^{(2)} \cdot G \cdot T^{(2)}]^{-1} \cdot T^{(2)} \,, \tag{3.91}$$

where G is now a diagonal matrix. With eq. (3.91), by using ChPT, all scalar-, isoscalar-, and vector-resonances have been produced in [112, 154].

In conclusion, there are no LHCs in this case. Moreover, there is cutoff dependence, which is different for each channel. However, by choosing a specific cutoff, usually named as natural cutoff, all parameters can be reduced to a single parameter for all channels. The LO diagrams set the scale of low-energy, whereas the NLO tree diagram gives information about resonances since it includes the LECs of ChPT and the unitarity condition is demanded with the imaginary part of the loop diagram. Its real part is contributing to the NLO with a cutoff dependence.

As discussed earlier, if we want to explain the ρ-meson, LECs should be used. On the other hand, scalar resonances are produced only by meson-meson interactions without the need for extra information that LECs contain. These are called dynamically generated resonances. Therefore, if only dynamically generated mesons are considered $t^{(4)}_{\text{tree}}$ can be omitted as well. These mesons usually do not have a $q\bar{q}$ structure. Hence, if we want to study hadronic molecules, we want them to be dynamically generated. Therefore this term is not crucial.

This might not seem reasonable since there are no counter terms left, yet the G function is still cutoff dependent which can sustain the energy dependent behaviour of omitted terms for up tp a natural cutoff

scale. In this case, eq. (3.90) reduces to

$$t = \frac{t^{(2)}}{1 - Gt^{(2)}}\,, \tag{3.92}$$

and coupled channel form is:

$$T = [1 - T^{(2)}G]^{-1}T^{(2)}\,. \tag{3.93}$$

These equations are called chiral unitary approach. If the cutoff is set to a natural cutoff (around the rho mass), some resonances are still produced from ChPT Lagrangian [111]. Again, this cutoff is, in principle, different for each channel, but one parameter is enough to reproduce all the light scalars which are not $q\bar{q}$ states. LHCs can be included perturbatively in the equation. However, the equations will not be algebraic anymore [98]. This method can be generalized with the N/D method which will be explained later in this section.

Bethe-Salpeter Equation

Eq. (3.92) can be obtained in a different way. If we consider the relativistic version of the Lippmann-Schwinger equation, which is called Bethe-Salpeter Equation (BSE), it enables us to study bound state and resonance regions in a field theoretic scheme. This method does not need any experimental scattering data and uses EFT scattering amplitudes in a geometric series.

$$T = V + \int VG'T\,, \tag{3.94}$$

where G' is the two particle propagator and V is the potential kernel. In this case, eq. (3.94) gives an

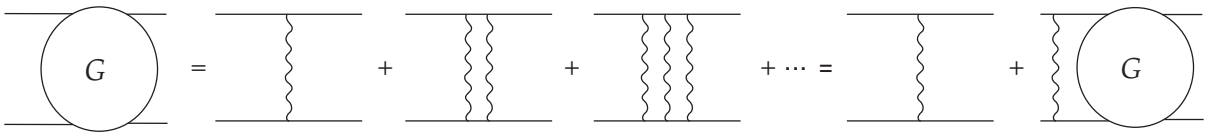

Figure 3.6: Bethe-Salpeter equation: diagramatic expression.

integral equation:

$$T = V + \int VG'T = V + i\int \frac{d^4q}{(2\pi)^4}\frac{V}{q^2 - {m_1}^2 + i\epsilon}\frac{T(q)}{(P-q)^2 - {m_2}^2 + i\epsilon}\,, \tag{3.95}$$

where m_1 and m_2 are the physical masses of the particles in the loop diagram and $P(= p_1 + p_2 = {p'}_1 + {p'}_2)$ is the total four-momentum of initial and final states whereas q is assigned as the momentum of the intermediate particle with mass m_1.

For simplicity, if we consider s-waves only (the partial wave formalism can be applied to interaction kernel and there is a BSE for each partial wave), V is a second order polynomial in momentum. If we separate the on and off-shell parts of V [5].:

$$V(p', p, P) = V_{\text{on}}(P^2) + (p_1^2 - m_1^2)V_{1\text{off}}(P^2) + (p_2^2 - m_2^2)V_{2\text{off}}(P^2) + ({p'}_1^2 - m_1^2)V_{3\text{off}}(P^2) + ({p'}_2^2 - m_2^2)V_{4\text{off}}(P^2)\,.$$

We have taken into account only non-mixed off-shell contributions for the sake of simplicity. Hence, the

[5] For the explicit investigation on this issue, see [155]

interaction matrix can be written as

$$T = V_{\text{on}} + \int \frac{d^4q}{(2\pi)^4} \frac{V_{\text{on}}}{q^2 - {m_1}^2 + i\epsilon} \frac{T_{\text{on}}}{(P-q)^2 - {m_2}^2 + i\epsilon} + \int \frac{d^4q}{(2\pi)^4} \frac{V_{3\text{off}}T_{\text{on}} + V_{\text{on}}T_{1\text{off}} + (q^2 - m_1^2)V_{3\text{off}}T_{1\text{off}}}{(P-q)^2 - {m_2}^2 + i\epsilon}$$
$$+ \int \frac{d^4q}{(2\pi)^4} \frac{V_{4\text{off}}T_{\text{on}} + V_{\text{on}}T_{2\text{off}} + ((P-q)^2 - m_2^2)V_{4\text{off}}T_{2\text{off}}}{(P-q)^2 - {m_2}^2 + i\epsilon} + \int \frac{d^4q}{(2\pi)^4} (V_{4\text{off}}T_{1\text{off}} + V_{3\text{off}}T_{2\text{off}}) .$$

Neither $V_{\text{on/off}}$ nor $T_{\text{on/off}}$ depends on q. Once they are taken out of the integral, the off-shell parts have the same structure as chiral logarithms. Hence, they are proportional to tadpole diagrams. These chiral logarithms can be omitted since they are numerically small in the meson-meson scattering region. The small contribution of these off-shell parts can be integrated into physical values of the EFT Lagrangian. When these off-shell parts are omitted, the equation becomes an algebraic equation:

$$T_{\text{on}} = V_{\text{on}} + V_{\text{on}} G T_{\text{on}} . \tag{3.96}$$

G is divergent again and the same regularization methods can be applied as in the chiral unitary approach. V is unknown in the BSE itself but it can be replaced by the LO amplitude from EFT to match with the chiral unitary approach. This replacement is straightforward since there are no cuts or logarithmic singularities in LO calculation. The NLO inclusion is also possible. Hence, the BSE can be written in a simplified form

$$T = T^{(2)} + T^{(2)} G T , \tag{3.97}$$

and G is the same as in eq. (3.87). If this equation is iterated:

$$T = T^{(2)} + T^{(2)} G T^{(2)} + T^{(2)} G T^{(2)} G T^{(2)} + \cdots = T^{(2)} (1 + G T^{(2)} + G T^{(2)} G T^{(2)} + \cdots) , \tag{3.98}$$

which is a geometric series and can be summed into:

$$T = (1 - T^{(2)} G)^{-1} \cdot T^{(2)} . \tag{3.99}$$

This corresponds to summing up the series of diagrams as in fig.3.6.

For single channel scattering, eq. (3.99) reads:

$$T(s) = \frac{V(s)}{1 - V(s) G(s)} . \tag{3.100}$$

This equation is equivalent to eq. (3.92).

The N/D Method

This method is derived from dispersion relations where LHCs are not exact, or are sometimes neglected and as in any unitarization method, amplitudes are unitary on the real axis. The N/D method was developed by Chew and Mandelstam [156]. It provides a solution to unitarization equations both for single and coupled channels. LHCs can be more systematically included with respect to chiral unitary approach and it performs better than the on-shell BSE, eq. (3.100).

The main idea in this method is to write the partial-wave amplitude in the form of:

$$t(s) = \frac{N(s)}{D(s)} . \tag{3.101}$$

RHCs are introduced in $D(s)$ and LHCs are contained in $N(s)$. Bound states and resonances can be investigated for $D(s) = 0$ and $D_{II}(s) = 0$, respectively, where the roman number II represents the second Riemann sheet. Both of these functions are analytic in complex s-plane, hence $D(s)$ is real on the real axis except on the RHC and $N(s)$ is real on the real axis except on the LHC. Moreover, due to unitarity, above threshold they satisfy

$$\mathrm{Im}D(s) = -\rho(s)N(s) = N(s)\mathrm{Im}t(s)^{-1}\,, \tag{3.102}$$

and on the LHC they satisfy

$$N(s) = D(s)\mathrm{Im}t(s)\,. \tag{3.103}$$

Using these two equations and knowing that both are analytic functions, they can be defined by dispersion relations as:

$$N(s) = \frac{1}{\pi}\int_{-\infty}^{s_{\mathrm{LHC}}} ds' \frac{D(s')\mathrm{Im}(t(s'))}{s'-s}\,, \tag{3.104}$$

$$D(s) = \frac{-1}{\pi}\int_{s_{\mathrm{th}}}^{\infty} \frac{\rho(s')N(s')}{s'-s}\,, \tag{3.105}$$

where no subtraction constant is considered, s_{LHC} is the branch point for the LHC and s_{th} indicates the threshold. The number of subtraction constants can be as many as needed and they will contain all the information about the amplitude except the imaginary part of it on the LHC. The LHC can easily be omitted by setting Im $t = 0$ on the LHC which makes things simpler since thereupon $N(s)$ can be set to 1 [131]. Furthermore, on the real axis above the threshold, the imaginary part of eq. (3.105) gives $-\rho(s)$ and the LHC can be studied perturbatively.

In [109], G is defined as

$$g(s) = -\frac{1}{\pi}\int_{s_{\mathrm{th}}}^{\infty} ds' \frac{\rho(s')}{s'-s}\,, \tag{3.106}$$

to get

$$t(s) = \left(\frac{1}{t^{(\mathrm{tree})}(s)} + g(s)\right)^{-1}\,, \tag{3.107}$$

where $t^{(\mathrm{tree})}(s)$ contains the tree level structure of the Lagrangian in consideration and unitarization is demanded by $g(s)$ since $\mathrm{Im}g(s) = -\rho(s) = \mathrm{Im}t^{-1}(s)$ on the real axis above threshold. As in the chiral unitary approach, $g(s)$ is divergent and needs to be regularized. For a more detailed study, we refer to [131, 157] and to [109] for an application to meson-meson scattering.

CHAPTER 4

Chiral Covariant $SU(2)$ and $SU(3)$ Vector Meson Interactions

4.1 Introduction[1]

It is now commonly accepted that some hadron resonances are generated by strong non-perturbative hadron-hadron interactions. Arguably the most famous example is the $\Lambda(1405)$, that arises from the coupled-channel dynamics of the strangeness $S = -1$ ground state octet meson-baryon channels in the vicinity of the $\pi\Sigma$ and $K^- p$ thresholds [159]. This resonance also has the outstanding feature of being actually the combination of two near poles, the so-called two-pole nature of the $\Lambda(1405)$. In a field-theoretic sense, we should consider this state as two particles. This fact was predicted theoretically [153, 160] and later unveiled experimentally [161] (see also the discussion in ref. [1]). Another example is the scalar meson $f_0(980)$ close to the $\bar{K}K$ threshold, that is often considered to arise due to the strong S-wave interactions in the $\pi\pi$-$\bar{K}K$ system with isospin zero [111, 162, 163]. A new twist was given to this field in ref. [115] where the S-wave vector-vector ($\rho\rho$) interactions were investigated and it was found that due to the strong binding in certain channels, the $f_2(1270)$ and the $f_0(1370)$ mesons could be explained as $\rho\rho$ bound states. This approach offered also an explanation why the tensor state f_2 is lighter than the scalar one f_0, as the leading order attraction in the corresponding $\rho\rho$ channel is stronger. This work was followed up by extensions to SU(3) [116], to account for radiative decays [164, 165] and many other works, see e.g the short review in ref. [166].

These results are certainly surprising and at odds with well-known features of the strong interactions. In this respect it is a text-book result that the $f_2(1270)$ fits very well within a nearly ideally-mixed P-wave $q\bar{q}$ nonet comprising as well the $a_2(1320)$, $f_2'(1525)$ and $K_s^*(1430)$ resonances [167–169]. Values for this mixing angle can be obtained from either the linear or quadratic mass relations as in ref. [169]. Non-relativistic quark model calculations [170], as well as with relativistic corrections [171], predict that the coupling of the tensor mesons to $\gamma\gamma$ should be predominantly through helicity two by an $E1$ transition. This simple $q\bar{q}$ picture for the tensor $f_2(1270)$ resonance has been recently validated by the analyses performed in ref. [172] of the high-statistics Belle data [173, 174] on $\gamma\gamma \to \pi\pi$ in both the neutral and charged pion channels. Another point of importance in support of the $q\bar{q}$ nature of the $f_2(1270)$ is Regge theory, since this resonance lays in a parallel linear exchange-degenerate Regge trajectory with a "universal" slope parameter of around 1 GeV [175–179]. Masses and widths of the first resonances with increasing spin laying on this Regge trajectory (ρ, f_2, ρ_3, f_4) are nicely predicted [180] by the dual-hadronic model of Lovelace-Shapiro-Veneziano [181–183].

[1] Most of the content of this chapter have been published in [158] and some parts are in preparation for publication.

One should stress that the results of ref. [115] were obtained based on extreme non-relativistic kinematics, $\mathbf{p}_i^2/m_\rho^2 \simeq 0$, with $\mathbf{p}$ the rho-meson three-momentum and m_ρ the vector meson mass. This approximation, however, leads to some severe simplifications:

- Due to the assumed threshold kinematics, the full ρ propagator was reduced to its scalar form, thus enabling the use of techniques already familiar from the pion-pion interaction [111]. This was applied when considering the iteration of the interactions in the Bethe-Salpeter equation.
- Based on the same argument, the algebra involving the spin and the isospin projectors of the two vector-meson states could considerably be simplified.

However, as $\sqrt{s_{\text{th}}} = 2m_\rho = 1540$ MeV, the lighter of the bound states is already quite far away from the 2ρ threshold. Moreover, the ρ-exchanging diagrams shrink to contact four-ρ interactions in ref. [115] and thus the left-hand cuts are neglected. It is therefore legitimate to question the assumptions made in ref. [115].

In a succedent work, i.e. ref. [184], the authors examine the relativistically covariant $\rho\rho$ interaction and question the disappearance of the tensor bound state in ref. [158]. They related it to the "on-shell" factorization of the potential done in the region where the dynamic singularity develops a large discontinuous and imaginary part. However, this argument is inconsistent since the presence of tensor bound state is done with the on-shell factorization in the same region as well [115, 184]. According to the N/D method [109, 156, 185], poles are identified as the zero points of the determinant of D functions which are free of any unphysical cut. In this sense, the on-shell approximation of the BSE, i.e. eq. (3.99), in the region near the left-hand cut is problematic, which indicates that eq. (3.99) can not be applied to energies below 1.34 GeV where the left-hand cut starts. The extreme non-relativistic limit is taken to avoid this left-hand cut in refs. [115, 184]. However, the extreme non-relativistic approximation leads to ignoring the energy-dependence of the interaction. This energy-dependence is crucial for the forming of a bound state. It seems to be surprising that a bound state appears in the sector $(I, J) = (0, 0)$, whereas we do not find a bound state in the $(I, J) = (0, 2)$ sector while the interaction is also attractive and with a strength more than twice of the scalar sector. As we know, in addition to the attraction strength, the effective interaction range r_0, which is sensitive to the energy-dependence of the interaction, is critical to form a bound state. The effective range is determined by

$$T(s) = \frac{8\pi\sqrt{s}}{-1/a + r_0\mathbf{p}^2 - i\mathbf{p}} \tag{4.1}$$

around the threshold with $\mathbf{p}$ the three-momentum and $s = E^2$ the total energy squared. It is easy to derive the r_0 proportionality to the derivative of $\sqrt{s}T^{-1}$ to the energy at the threshold.

$$\begin{aligned}
\mathbf{p} &= \frac{i}{2r_0}\left(1 \pm \sqrt{1 - 4r_0/a}\right) && (4.2)\\
&\overset{r_0 \ll a}{=} \frac{i}{2r_0}\left(1 \pm (1 - 2r_0/a - 2r_0^2/a^2 + \dots)\right) && (4.3)\\
&= \begin{cases} \frac{i}{r_0} - \frac{i}{a} - \frac{ir_0}{a^2} + \dots, & \text{for + sign}, \\ \frac{i}{a} + \frac{ir_0}{a^2} + \dots, & \text{for − sign}. \end{cases} && (4.4)
\end{aligned}$$

As a result, with the increase of the slope of the potential to the energy, the effective interaction range decreases. From the fig. 4 in ref. [158], it is easy to conclude that the effective interaction range for

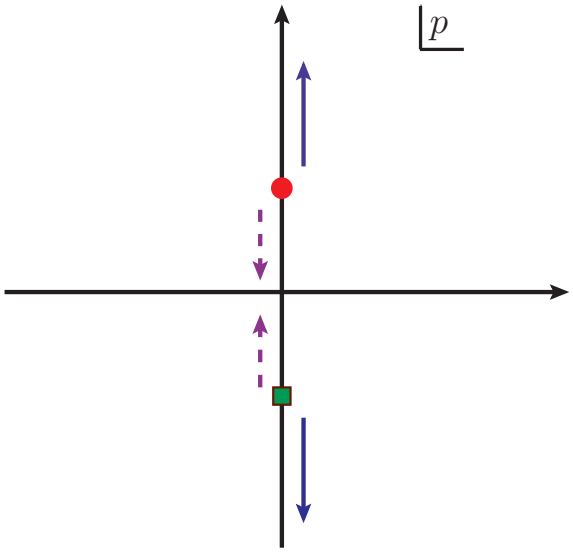

Figure 4.1: The effect of the r_0 correction. The blue solid curves $r_0 a > 0$ and the pink dashed curves $r_0 a < 0$. The red circle and green square points indicate a bound state $a > 0$ and a virtual state $a < 0$, respectively.

$(I, J) = (0, 0)$ is much larger than the tensor sector. A naive calculation with the tree-level potential shows that the tensor sector even has a negative effective interaction range. However, the scalar and tensor sector has same energy-dependence of the potential, see e.g. Table I in ref. [184] and thus same effective range. It accounts for the reason of the disappearance of the bound state in the tensor sector. It is easy to be misled that the disappearance of the tensor bound state happens due to the unexpected large imaginary part along the left-hand cut in the potential when we observe the determinant of BSE in fig. 11 of ref. [158]. The region we are interested in is beyond the scope of the eq. (3.99). To overcome this difficulty, an improved unitarization, i.e. the first iterated solution of the N/D method, is proposed in ref. [158]. The determinant of this method only contains the unitarity cut and agrees to the BSE up to $O(s^3)$. A matching condition (4.58) can be done in the physical region, and the resulting D functions have correct analytical structure and energy-dependence (mainly from ρ-exchange diagrams). We stress that the disappearance of the bound state in the tensor sector is not due to the left-hand cut itself, but due to the ρ-exchange contribution.

4.1.1 Formalism

In these works, we employ the hidden local symmetry formalism, see sec.2.3, in which the vectors are treated as gauge bosons of a hidden local symmetry transforming inhomogeneously. While in principle the tensor field formulation is preferable in the construction of chiral-invariant building blocks, an advantage of the hidden gauge symmetry approach is that the phenomenological success of naturally reproducing the low-energy theorems, e.g. KSFR relations, vector mesons dominance , the universality of ρ-couplings, and the Weinberg-Tomozawa theorem for the π-ρ scattering. Moreover, contrast to the corrections of the order p^3 in the CCWZ Lagrangian, any corrections to the leading $\rho\pi\pi$ coupling are of order p^5 or higher in the hidden local symmetry approach by an appropriate choice of the gauge coupling [186]. On the other hand, the main reason for us to employ this method is that it was used in [115, 116].

4.2 A chiral covariant approach to $\rho\rho$ scattering[2]

In this work, we will reanalyze the same reactions as in [115] using a fully covariant approach. This is technically much more involved than the formalism of the earlier works. However, as our aim is to scrutinize the approximations made there, we stay as much as possible close to their choice of parameters. Additionally, we also consider coupled-channel scattering interactions including channels with nonzero orbital angular momentum, that is, we go beyond the S-wave scattering approximation of ref. [115]. The inclusion of coupled channels is also important when moving away from threshold. The authors of this reference only considered scattering in S-wave because of the same type of near-threshold arguments. As will be shown, the near-threshold approximation is only reliable very close to threshold.

This section is organized as follows: In Sec. 4.2.1 we outline the formalism to analyze $\rho\rho$ scattering in a covariant fashion. In particular, we retain the full propagator structure of the ρ, which leads to a very different analytic structure of the scattering amplitude compared to the extreme non-relativistic framework. We also perform a partial-wave projection technique, that allows to perform the unitarization of tree-level scattering amplitudes using methods well established in the literature. An elaborate presentation of our results is given in Sec. 4.2.2, where we also give a detailed comparison to the earlier work based on the non-relativistic framework. Next, we consider the effect of the coupling between channels with different orbital angular momentum. We also improve the unitarization procedure by considering the first-iterated solution of the N/D method in Sec. 4.2.3, reinforcing our results obtained with the simpler unitarization method. We conclude with a summary and discussion in Sec. 4.2.4. A detailed account of the underlying projection formalism is given in App. E.

4.2.1 Formalism

To be specific, the Lagrangian for the interactions among vector mesons is taken from the pure gauge-boson part of eq. (2.118):

$$\mathcal{L}' = -\frac{1}{4}\langle F_{\mu\nu}F^{\mu\nu}\rangle \,. \tag{4.5}$$

Here, the coupling constant $g = M_V/2f_\pi$ and $f_\pi \approx 92$ MeV [1] the weak pion decay constant. The vector field V_μ is

$$V_\mu = \begin{pmatrix} \frac{1}{\sqrt{2}}\rho^0 & \rho^+ \\ \rho^- & -\frac{1}{\sqrt{2}}\rho^0 \end{pmatrix} \tag{4.6}$$

From the Lagrangian in eq. (4.5) we can derive the interaction between three and four vector mesons and the corresponding vertices. The corresponding Lagrangians are denoted as $\mathcal{L}'_3$ and $\mathcal{L}'_4$, respectively. The former one gives rise to $\rho\rho$ interactions through the exchange of a ρ meson and the latter corresponds to purely contact interactions. We did not include the ω resonance in eq. (4.6) since it does not contribute to the interaction part (in the isospin limit). Consider first the contact vertices for the 4ρ interaction:

$$\mathcal{L}'_4 = \frac{g^2}{2}\langle V_\mu V_\nu V^\mu V^\nu - V_\mu V^\mu V_\nu V^\nu\rangle \,. \tag{4.7}$$

The three different isospin (I) amplitudes for $\rho\rho$ scattering ($I = 0$, 1 and 2) can be worked out from the knowledge of the transitions $\rho^+(p_1)\rho^-(p_2) \to \rho^+(p_3)\rho^-(p_4)$ and $\rho^+(p_1)\rho^-(p_2) \to \rho^0(p_3)\rho^0(p_4)$ by

[2] The content of this section have been published in [158].

invoking crossing as well. We have indicated the different four-momenta by p_i, $i = 1, \ldots, 4$. The scattering amplitude for the former transition is denoted by $A(p_1, p_2, p_3, p_4)$ and the latter one by $B(p_1, p_2, p_3, p_4)$, which are shown in figs. 4.2 and 4.3, respectively.

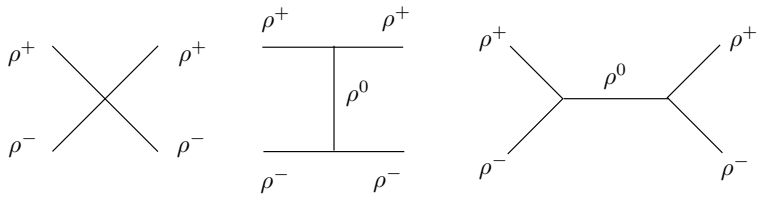

Figure 4.2: Feynman diagrams for the tree-level amplitude $\rho^+\rho^- \to \rho^+\rho^-$.

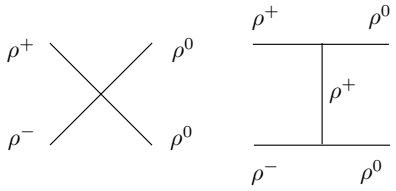

Figure 4.3: Feynman diagrams for the tree-level amplitude $\rho^+\rho^- \to \rho^0\rho^0$.

The contributions to those amplitudes from $\mathcal{L}'_4$, cf. eq. (4.7), are indicated by the subscript c and are given by:

$$\begin{aligned} A_c(k_1,k_2,k_3,k_4) =& -2g^2(2\epsilon(1)_\mu\epsilon(2)_\nu\epsilon(3)^\nu\epsilon(4)^\mu - \epsilon(1)_\mu\epsilon(2)^\mu\epsilon(3)_\nu\epsilon(4)^\nu - \epsilon(1)_\mu\epsilon(2)_\nu\epsilon(3)^\mu\epsilon(4)^\nu)\,, \\ B_c(k_1,k_2,k_3,k_4) =& 2g^2(2\epsilon(1)_\mu\epsilon(2)^\mu\epsilon(3)_\nu\epsilon(4)^\nu - \epsilon(1)_\mu\epsilon(2)_\nu\epsilon(3)^\mu\epsilon(4)^\nu - \epsilon(1)_\mu\epsilon(2)_\nu\epsilon(3)^\nu\epsilon(4)^\mu)\,. \end{aligned} \tag{4.8}$$

In this equation, the $\epsilon(i)_\mu$ corresponds to the polarization vector of the i^{th} ρ. Each polarization vector is characterized by its three-momentum $\mathbf{p}_i$ and third component of the spin σ_i in its rest frame, so that $\epsilon(i)_\mu \equiv \epsilon(\mathbf{p}_i, \sigma_i)_\mu$. Explicit expressions of these polarization vectors are given in eqs. (E.9) and (E.10) of appendix E. In the following, so as to simplify the presentation, tree-level scattering amplitudes are written for real polarization vectors. The same expressions are valid for complex ones by taking the complex conjugate of the polarization vectors attached to the final particles.[3] Considering the one-vector exchange terms, we need the three-vector interaction Lagrangian $\mathcal{L}'_3$. It reads

$$\mathcal{L}'_3 = ig\langle(\partial_\mu V_\nu - \partial_\nu V_\mu)V^\mu V^\nu\rangle\,. \tag{4.9}$$

The basic vertex is depicted in fig. 4.4 which after a simple calculation can be written as

$$\begin{aligned} V_3 = -\sqrt{2}g\Big[&(q_\mu\epsilon(1)_\nu - q_\nu\epsilon(1)_\mu)\epsilon(3)^\mu\epsilon(2)^\nu - (k_\mu\epsilon(2)_\nu - k_\nu\epsilon(2)_\mu)\epsilon(1)^\mu\epsilon(3)^\nu \\ &- (p_\mu\epsilon(3)_\nu - p_\nu\epsilon(3)_\mu)\epsilon(2)^\mu\epsilon(1)^\nu\Big]\,. \end{aligned} \tag{4.10}$$

In terms of this vertex, we can straightforwardly calculate the vector exchange diagrams in figs. 4.2 and 4.3. The expression for the t-channel ρ-exchange amplitude, the middle diagram in fig. 4.2, and denoted

[3] The polarization vectors $\epsilon(\mathbf{p}, \sigma)$ in the appendix E are complex, so that the polarization vectors associated with the final-state $\rho\rho$ should be complex conjugated in this case.

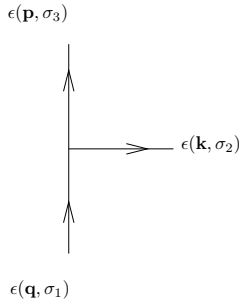

Figure 4.4: Three-ρ vertex from $\mathcal{L}_3'$.

by $A_t(p_1,p_2,p_3,p_4;\epsilon_1,\epsilon_2,\epsilon_3,\epsilon_4)$, is

$$\begin{aligned}A_t(p_1,p_2,p_3,p_4;\epsilon_1,\epsilon_2,\epsilon_3,\epsilon_4) = \frac{2g^2}{(p_1-p_3)^2-m_\rho^2+i0^+}[&(p_1(p_2+p_4)+p_3(p_2+p_4))\epsilon_1\cdot\epsilon_3\epsilon_2\cdot\epsilon_4\\ &+4(\epsilon_1\cdot k_3\epsilon_4\cdot k_2\epsilon_2\cdot\epsilon_3+\epsilon_1\cdot k_3\epsilon_2\cdot k_4\epsilon_3\cdot\epsilon_4+\epsilon_3\cdot k_1\epsilon_4\cdot k_2\epsilon_1\cdot\epsilon_2+\epsilon_2\cdot k_4\epsilon_3\cdot k_1\epsilon_1\cdot\epsilon_4)\\ &-2(\epsilon_1\cdot k_3(\epsilon_3\cdot k_2+\epsilon_3\cdot k_4)\epsilon_2\cdot\epsilon_4+\epsilon_3\cdot k_1(\epsilon_1\cdot k_2+\epsilon_1\cdot k_4)\epsilon_2\cdot\epsilon_4+\epsilon_2\cdot k_4(\epsilon_4\cdot k_1+\epsilon_4\cdot k_3)\epsilon_1\cdot\epsilon_3\\ &+\epsilon_4\cdot k_2(\epsilon_2\cdot k_1+\epsilon_2\cdot k_3)\epsilon_1\cdot\epsilon_3)]\,,\end{aligned} \tag{4.11}$$

where for short, we have rewritten $\epsilon(i)\to\epsilon_i$, and the scalar products involving polarization vectors are indicated with a dot. The u-channel ρ-exchange amplitude $A_u(p_1,p_2,p_3,p_4;\epsilon_1,\epsilon_2,\epsilon_3,\epsilon_4)$ can be obtained from the expression of A_t by exchanging $p_3\leftrightarrow p_4$ and $\epsilon_3\leftrightarrow\epsilon_4$. In the exchange for the polarization vectors they always refer to the same arguments of three-momentum and spin, that is, $\epsilon(\mathbf{p}_3,\sigma_3)\leftrightarrow\epsilon(\mathbf{p}_4,\sigma_4)$. In this way,

$$A_u(p_1,p_2,p_3,p_4;\epsilon_1,\epsilon_2,\epsilon_3,\epsilon_4) = A_t(p_1,p_2,p_4,p_3;\epsilon_1,\epsilon_2,\epsilon_4,\epsilon_3)\,. \tag{4.12}$$

Notice that the second diagram in fig. 4.3 is a sum of the t-channel and u-channel ρ-exchange diagrams.

The s-channel exchange amplitude (the last diagram in fig. 4.2) can also be obtained from A_t by performing the exchange $p_2\leftrightarrow -p_3$ and $\epsilon_2\leftrightarrow\epsilon_3$, with the same remark as above for the exchange of polarization vectors. We then have:

$$A_s(p_1,p_2,p_3,p_4;\epsilon_1,\epsilon_2,\epsilon_3,\epsilon_4) = A_t(p_1,-p_3,-p_2,p_4;\epsilon_1,\epsilon_3,\epsilon_2,\epsilon_4)\,. \tag{4.13}$$

The total amplitudes for $\rho^+\rho^-\to\rho^+\rho^-$ and $\rho^+\rho^-\to\rho^0\rho^0$ are

$$\begin{aligned}A &= A_c + A_t + A_s\,,\\ B &= B_c + A_t + A_u\,,\end{aligned} \tag{4.14}$$

with the usual arguments $(p_1,p_2,p_3,p_4;\epsilon_1,\epsilon_2,\epsilon_3,\epsilon_4)$. By crossing, we also obtain the amplitude for $\rho^+\rho^+\to\rho^+\rho^+$ [that we denote as $C(p_1,p_2,p_3,p_4;\epsilon_1,\epsilon_2,\epsilon_3,\epsilon_4)$] from the one for $\rho^+\rho^-\to\rho^+\rho^-$ by exchanging $p_2\leftrightarrow -p_4$ and $\epsilon_2\leftrightarrow\epsilon_4$, that is,

$$C(p_1,p_2,p_3,p_4;\epsilon_1,\epsilon_2,\epsilon_3,\epsilon_4) = A(p_1,-p_4,p_3,-p_2;\epsilon_1,\epsilon_4,\epsilon_3,\epsilon_2)\,. \tag{4.15}$$

The amplitude C is purely $I = 2$, that we denote as $T^{(2)}$. The amplitude B is an admixture of the $I = 0$, $T^{(0)}$, and $I = 2$ amplitudes,

$$B = \frac{1}{3}(T^{(0)} - T^{(2)}) \,, \tag{4.16}$$

from which we find that

$$T^{(0)} = 3B + C \,. \tag{4.17}$$

To isolate the $I = 1$ amplitude, $T^{(1)}$, we take the $\rho^+\rho^-$ elastic amplitude A which obeys the following isospin decomposition

$$A = \frac{1}{6}T^{(2)} + \frac{1}{2}T^{(1)} + \frac{1}{3}T^{(0)} \,. \tag{4.18}$$

Taking into account eq. (4.17), we conclude that

$$T^{(1)} = 2A - 2B - C \,. \tag{4.19}$$

In terms of these amplitudes with well-defined isospin the expression in eq. (E.48) for calculating the partial-wave amplitudes in the $\ell S\, JI$ basis (states with well-defined total angular momentum J, total spin S, orbital angular momentum ℓ and isospin I), denoted as $T^{(JI)}_{\ell S;\bar{\ell}\bar{S}}(s)$ for the transition $(\bar{\ell}\bar{S}\, JI) \to (\ell S\, JI)$, simplifies to

$$T^{(JI)}_{\ell S;\bar{\ell}\bar{S}}(s) = \frac{Y^0_{\bar{\ell}}(\hat{\mathbf{z}})}{2(2J+1)} \sum_{\substack{\sigma_1,\sigma_2,\bar{\sigma}_1\\ \bar{\sigma}_2,m}} \int d\hat{\mathbf{p}}''\, Y^m_\ell(\mathbf{p}'')^* \,(\sigma_1\sigma_2 M|s_1 s_2 S)(mM\bar{M}|\ell S\, J)(\bar{\sigma}_1\bar{\sigma}_2\bar{M}|\bar{s}_1\bar{s}_2\bar{S})(0\bar{M}\bar{M}|\bar{\ell}\bar{S}\, J)$$
$$\times T^{(I)}(p_1,p_2,p_3,p_4;\epsilon_1,\epsilon_2,\epsilon_3,\epsilon_4) \,, \tag{4.20}$$

with s the usual Mandelstam variable, $\mathbf{p}_1 = |\mathbf{p}|\hat{\mathbf{z}}$, $\mathbf{p}_2 = -|\mathbf{p}|\hat{\mathbf{z}}$, $\mathbf{p}_3 = \mathbf{p}''$ and $\mathbf{p}_4 = -\mathbf{p}''$, $M = \sigma_1 + \sigma_2$ and $\bar{M} = \bar{\sigma}_1 + \bar{\sigma}_2$. The Mandelstam variables t and u for $\rho\rho$ scattering in the isospin limit are given by $t = -2\mathbf{p}^2(1 - \cos\theta)$ and $u = -2\mathbf{p}^2(1 + \cos\theta)$, with θ the polar angle of the final momentum. The denominator in A_t due to the ρ propagator, cf. eq. (4.11), vanishes for $t = m_\rho^2$ and similarly the denominator in A_u for $u = m_\rho^2$. When performing the angular projection in eq. (4.20) these poles give rise to a left-hand cut starting at the branch point $s = 3m_\rho^2$. This can be easily seen by considering the integration on $\cos\theta$ of the fraction $1/(t - m_\rho^2 + i\varepsilon)$, which gives the same result both for the t and u channel exchange,

$$\frac{1}{2}\int_{-1}^{+1} d\cos\theta \frac{1}{-2\mathbf{p}^2(1-\cos\theta) - m_\rho^2 + i\varepsilon} = -\frac{1}{4\mathbf{p}^2}\log\left(\frac{4\mathbf{p}^2 + m_\rho^2}{m_\rho^2} + \frac{4\mathbf{p}^2}{m_\rho^4}i\varepsilon\right) , \tag{4.21}$$

with $\varepsilon \to 0^+$. The argument of the log becomes negative for $4\mathbf{p}^2 < -m_\rho^2$, which is equivalent to $s < 3m_\rho^2$. Because of the factor $\mathbf{p}^2\varepsilon$ the imaginary part of the argument of the log below the threshold is negative which implies that the proper value of the partial-wave amplitude on the physical axis below the branch point at $s = 3m_\rho^2$ is reached in the limit of vanishing negative imaginary part of s. The presence of this branch point and left-hand cut was not noticed in ref. [115], where only the extreme non-relativistic reduction was considered, so that the ρ propagators in the ρ-exchange amplitudes collapsed to just a

constant. Once we have calculated the partial-wave projected tree-level amplitude, we proceed to its unitarization making use of standard techniques within unitary chiral perturbation theory [109, 111, 153], see sec.3.4.3. It has been applied to many systems and resonances by now, e.g. in meson-meson, meson-baryon, nucleon-nucleon and WW systems. Among many others we list some pioneering works for these systems [111, 153, 160, 187–200]. In the last years, this approach has been applied also to systems containing mesons and baryons made from heavy quarks, some references on this topic are [201–205].

The basic equation to apply is eq. (3.99). We can rewrite this equation in the subspace of coupled channels $\ell S\, JI$, with the same JI, as [4]

$$T^{(JI)}(s) = \left[I - V^{(JI)}(s)\cdot G(s)\right]^{-1}\cdot V^{(JI)}(s)\,. \tag{4.22}$$

Here, $G(s)$ is a diagonal matrix, given in eq. (3.87), made up by the two-point loop function $G(s)$ with $\rho\rho$ as intermediate states. We have stated that $\mathrm{Im}\, G(s) = -|\mathbf{p}|/8\pi\sqrt{s}$. The loop function $G(s)$ is logarithmically divergent and it can be calculated once its value at a given reference point is subtracted. In this way, we can write down a once-subtracted dispersion relation for $G(s)$ whose result is[5]

$$G(s) = \frac{1}{(4\pi)^2}\left(a(\mu) + \log\frac{m_\rho^2}{\mu^2} + \sigma\left[\log(\sigma+1) - \log(\sigma-1)\right]\right), \tag{4.23}$$

with

$$\sigma = \sqrt{1 - \frac{4m_\rho^2}{s}}\,, \tag{4.24}$$

and μ is a renormalization scale typically taken around m_ρ, such the sum $a(\mu) + \log m_\rho^2/\mu^2$ is independent of μ. The subtraction constant in eq. (4.23) could depend on the quantum numbers ℓ, S and J, but not on I due to the isospin symmetry [160]. To compare with the results of ref. [115], we also evaluate the function $G(s)$ introducing a three-momentum cutoff $q_{\max}$, the resulting $G(s)$ function is denoted by $G_c(s)$,

$$G_c(s) = \frac{1}{2\pi^2}\int_0^{q_{\max}} dq \frac{q^2}{w(s - 4w^2 + i\varepsilon)}\,, \tag{4.25}$$

with $w = \sqrt{q^2 + m_\rho^2}$. This integral can be done algebraically [154]

$$\begin{aligned} G_c(s) = \frac{1}{(4\pi)^2}\Bigg(&\sigma\left[\log\left(\sigma\sqrt{1 + \frac{m_\rho^2}{q_{\max}^2}} + 1\right) - \log\left(\sigma\sqrt{1 + \frac{m_\rho^2}{q_{\max}^2}} - 1\right)\right] \\ &+ 2\log\left\{\frac{m_\rho}{q_{\max}}\left(1 + \sqrt{1 + \frac{m_\rho^2}{q_{\max}^2}}\right)\right\}\Bigg)\,. \end{aligned} \tag{4.26}$$

[4] In order to easier the comparison with ref. [115] we take the same sign convention for matrices $V(s)$ and $T(s)$ as in that reference.

[5] It is the same result as calculating $G(s)$ in dimensional regularization, $d = 4 + 2\epsilon$, and replacing the $1/\epsilon$ divergence by a constant, cf. [154].

Typical values of the cutoff are around 1 GeV. The unitarity loop function $G(s)$ has a branch point at the $\rho\rho$ threshold ($s = 4m_\rho^2$) and a unitarity cut above it ($s > 4m_\rho^2$). The physical values of the T-matrix $T^{(JI)}(s)$, with $s > 4m_\rho^2$, are reached in the limit of vanishing positive imaginary part of s. Notice that the left-hand cut present in $V^{(JI)}(s)$ for $s < 3m_\rho^2$ does not overlap with the unitarity cut, so that $V^{(JI)}(s)$ is analytic in the complex s-plane around the physical s-axis for physical energies. In this way, the sign of the vanishing imaginary part of s for $V^{(JI)}(s)$ is of no relevance in the prescription stated above for reaching its value on the real axis with $s < 3m_\rho^2$ according to the Feynman rules.

We can also get a natural value for the subtraction constant a in eq. (4.23) by matching $G(s)$ and $G_c(s)$ at threshold where $\sigma = 0$. For $\mu = m_\rho$, a usual choice, the final expression simplifies to

$$a = -2\log\frac{q_{\max}}{m_\rho}\left(1 + \sqrt{1 + \frac{m_\rho^2}{q_{\max}^2}}\right). \tag{4.27}$$

It is also worth noticing that eq. (4.22) gives rise to a T-matrix $T^{(IJ)}(s)$ that is gauge invariant in the hidden local symmetry theory because this equation just stems from the partial-wave projection of a complete on-shell tree-level calculation within that theory, which certainly is gauge invariant.

4.2.2 Results

One of our aims is to check the stability of the results of ref. [115] under relativistic corrections, particularly regarding the generation of the poles that could be associated with the $f_0(1370)$ and $f_2(1270)$ resonances as obtained in that paper. The main source of difference between our calculated $V^{(JI)}(s)$ and those in ref. [115] arises from the different treatment of the ρ-meson propagator. The point is that the authors of ref. [115] take the non-relativistic limit of this propagator so that from the expression $1/(t-m_\rho^2)$, cf. eq. (4.11), or $1/(u-m_\rho^2)$, only $-1/m_\rho^2$ is kept. This is the reason that the tree-level amplitudes calculated in ref. [115] do not have the branch point singularity at $s = 3m_\rho^2$ nor the corresponding left-hand cut for $s < 3m_\rho^2$. It turns out that for the isoscalar tensor case, the resonance $f_2(1270)$ is below this branch point, so that its influence cannot be neglected when considering the generation of this pole within this approach.

Uncoupled S-wave scattering

The issue on the relevance of this branch point singularity in the ρ-exchange amplitudes was not addressed in ref. [115] and it is indeed very important. This is illustrated in fig. 4.5 where we plot the potentials $V^{(JI)}(s)$ in S-wave ($\ell = 0$) (only S-wave scattering is considered in ref. [115]).[6] From top to bottom and left to right we show in the figure the potentials for the quantum numbers (J, I) equal to $(0, 0)$, $(2, 0)$, $(0, 2)$, $(2, 2)$ and $(1, 1)$. The red solid and black dotted lines correspond to the real and imaginary parts of our full covariant calculation of the $V^{(JI)}(s)$, respectively, while the blue dashed ones are the results of ref. [115]. The imaginary part in our results for $V^{(JI)}(s)$ appears below $s < 3m_\rho^2$ due to the left-hand cut that arises from the t- and u-channel ρ-exchanges.

It can be seen that our results and those of ref. [115] are typically close near threshold ($s = 4m_\rho^2$) but for lower values of s they typically depart quickly due to the onset of the branch point singularity at $s = 3m_\rho^2$. The strength of this singularity depends on the channel, being particularly noticeable in the $(J, I) = (2, 0)$ channel, while for the $(0, 0)$ channel it is comparatively weaker.

[6] Partial waves with $\ell \neq 0$ are considered in sec. 4.2.2.

$q_{\rm max}$ (MeV)	Pole Position (MeV) (Mass in ref. [115])	$(\gamma_{00}^{(00)})^2$ (GeV^2)	$X_{00}^{(00)}$
775	1515.9	55	0.73
875	1494.8 (1512)	64	0.63
1000	1467.2 (1491)	68	0.52
775 (conv.)	1521.9		
875 (conv.)	1501.6		
1000 (conv.)	1475.6		

Table 4.1: Pole position for the partial wave $T^{(00)}(s)$ (2nd column), residue (3rd column) and compositeness (4th column) as a function of the three-momentum cutoff q_{max} (1st column). In the last three rows we take into account the finite width of the ρ in the evaluation of the $G(s)$ function, as indicated between parenthesis by (conv). For details, see the text.

The strongest attractive potentials in the near threshold region occur for $(J, I) = (0, 0)$ and $(2, 0)$ and in every of these channels ref. [115] found a bound-state pole that the authors associated with the $f_0(1370)$ and $f_2(1270)$ resonances, respectively. For the $(0, 0)$ quantum numbers the pole position is relatively close to the $\rho\rho$ threshold, while for $(2, 0)$ it is much further away. Two typical values of the cutoff $q_{\rm max}$ were used in ref. [115], $q_{\rm max} = 875$ MeV and 1000 MeV. We employ these values here, too, together with $q_{\rm max} = m_\rho$ (so that we consider three values of $q_{\rm max}$ separated by around 100 MeV), and study the pole positions for our $T^{(JI)}(s)$ amplitudes in S wave. We only find a bound state for the isoscalar scalar case, while for the tensor case no bound state is found. In table 4.1 we give the values of the pole positions for our full calculation for $q_{\rm max} = m_\rho$ (first), 875 (second) and 1000 MeV (third row). For comparison we also give in round brackets the bound state masses obtained in ref. [115], when appropriate. As indicated above, the strong differences for $V^{(20)}(s)$ between our full covariant calculation and the one in ref. [115] in the extreme non-relativistic limit, cf. fig. 4.5(b), imply the final disappearance of the deep bound state for the isoscalar tensor case. The nominal three-momentum of a ρ around the mass of the $f_2(1270)$ has a modulus of about $0.6 m_\rho \simeq 460$ MeV and for such high values of three-momentum relativistic corrections are of importance, as explicitly calculated here. On the contrary, the $(0, 0)$ pole is located closer to the $\rho\rho$ threshold and the results are more stable against relativistic corrections, though one still finds differences of around 20 MeV in the bound state mass.

In addition we also show in the third column of table 4.1 the residue of $T^{(00)}(s)$ at the pole position s_P. For a generic partial wave $T^{(JI)}_{\ell S;\bar{\ell}\bar{S}}(s)$, its residue at a pole is denoted by $\gamma^{(JI)}_{\ell S}\gamma^{(JI)}_{\bar{\ell}\bar{S}}$ and is defined as

$$\gamma^{(JI)}_{\ell S}\gamma^{(JI)}_{\bar{\ell}\bar{S}} = -\lim_{s\to s_P}(s - s_P)T^{(JI)}_{\ell S;\bar{\ell}\bar{S}}(s)\,. \tag{4.28}$$

In terms of these couplings we can also calculate the compositeness $X^{(JI)}_{\ell S}$ associated with this bound state [146, 206, 207],

$$X^{(JI)}_{\ell S} = -\,\gamma^{(JI)\ 2}_{\ell S;\ell S}\ \left.\frac{\partial G(s)}{\partial s}\right|_{s_P}\,, \tag{4.29}$$

which in our case determines the $\rho\rho$ component in such bound state. Notice that the derivative of $G(s)$ from eq. (4.23) (which is negative below threshold) does not depend on the subtraction constant, the

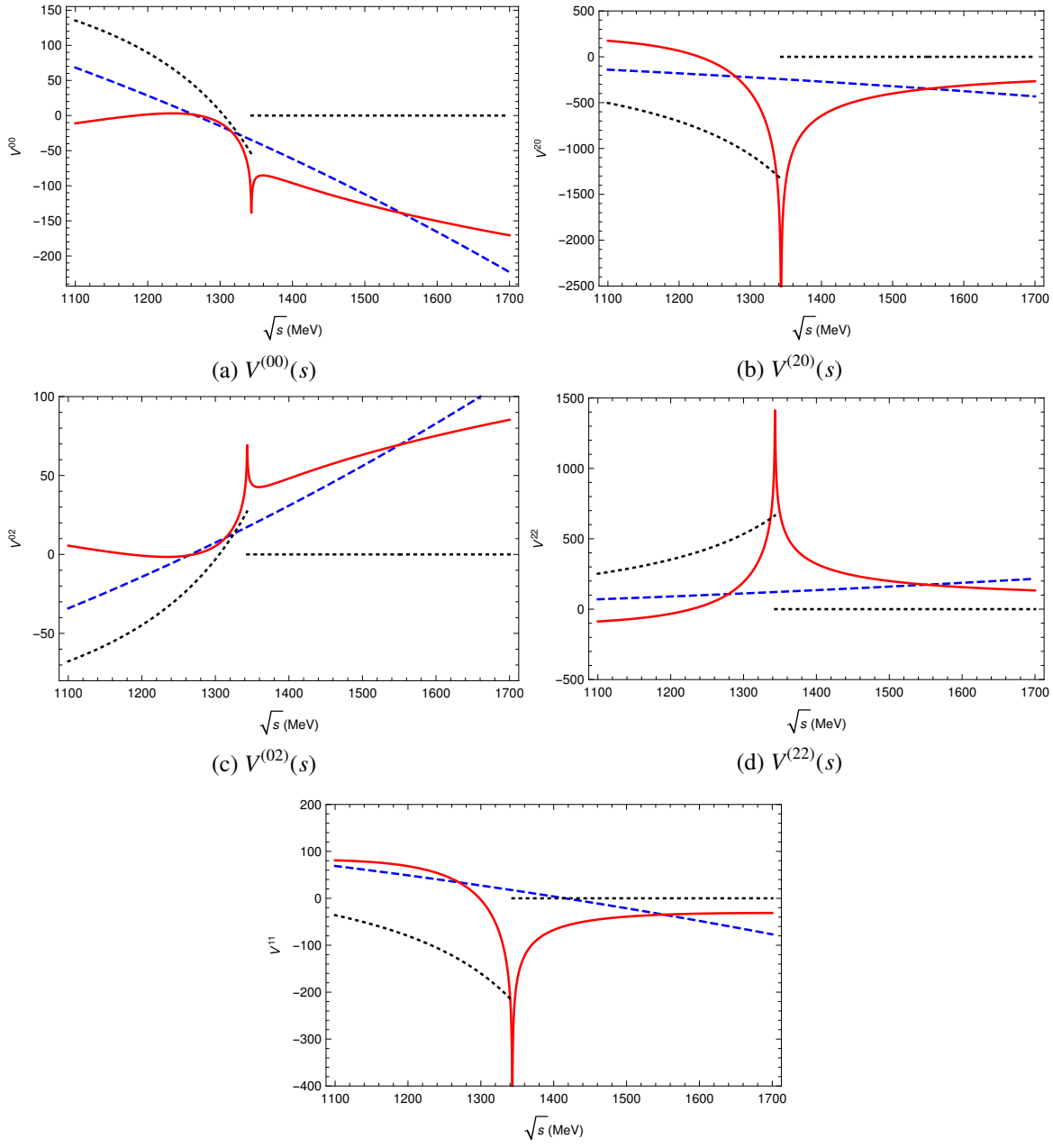

(a) $V^{(00)}(s)$ (b) $V^{(20)}(s)$

(c) $V^{(02)}(s)$ (d) $V^{(22)}(s)$

(e) $V^{(11)}(s)$

Figure 4.5: S-wave potentials $V^{(JI)}(s)$ (in MeV) for our calculation (real part: red solid line, imaginary part: black dotted line) and for the calculation of ref. [115] (blue dashed lines).

a	Pole Position (MeV)	$(\gamma_{00}^{(00)})^2$ (GeV^2)	$X_{00}^{(00)}$
-1.697	1525.7	43	0.80
-1.938	1500.4	56	0.69
-2.144	1474.5	62	0.58
-1.697 (conv.)	1546.0		
-1.938 (conv.)	1517.7		
-2.144 (conv.)	1491.1		

Table 4.2: Pole positions for the partial wave $T^{(00)}(s)$ (2nd column), residue (3rd column) and compositeness (4th column) as a function of the subtraction constant a (1st column). In the last three rows we take into account the finite width of the ρ in the evaluation of the $G(s)$ function, this is indicated between parenthesis by (conv).

dependence on the latter enters implicitly by the actual value of the pole position s_P. Of course, if one uses a three-momentum cutoff then $G_c(s)$ must be employed in the evaluation of $X_{\ell S}^{(JI)}$. The compositeness obtained for the pole positions in table 4.1 is given in the fourth column of the same table. As expected the $\rho\rho$ component is dominant, with $X_{00}^{(00)} > 0.5$, and increases as the pole moves closer to threshold, so that it is 73% for $q_{\max} = m_\rho$ and $\sqrt{s_P} = 1516$ MeV.

We can also determine the pole positions when $G(s)$ is calculated with exact analytical properties, eq. (4.23), and taking for a the values from eq. (4.27) as a function of $q_{\max}$. The results are given table 4.2, where we also give the residue at the pole position and the calculated compositeness, in the same order as in table 4.1. The results obtained are quite close to those in this table so that we refrain of further commenting on them. Nonetheless, we should stress again that we do not find any pole for the isoscalar tensor case.

We could try to enforce the generation of an isoscalar tensor pole by varying $q_{\max}$, when using $G_c(s)$, or by varying a, if eq. (4.23) is used. In the former case a much lower value of $q_{\max}$ is required than the chiral expansion scale around 1 GeV ($q_{\max} \lesssim 400$ MeV), while for the latter a qualitatively similar situation arises when taking into account the relationship between a and $q_{\max}$ of eq. (4.27). Even more serious are two facts that happen in relation with this isoscalar tensor pole. First we should stress that such a pole appears associated to the evolution with $q_{\max}$ or a of the pole in the first Riemann sheet, which violates analyticity. This is shown in fig. 4.6 where we exhibit the evolution of this pole as a function of $q_{\max}$. We start the series at a low value of $q_{\max} = 300$ MeV, where we have two poles on the real axis, and increase the cutoff in steps of $\delta q_{\max} = 50$ MeV. These two poles get closer and merge for $q_{\max} = 403.1$ MeV. For larger values of the cutoff the resulting pole moves deeper into the complex plane of the physical or first Riemann sheet. Second, we obtain that $X_{02}^{(20)}$ is larger than 1. For example, for $q_{\max} = 400$ MeV, there are two poles at 1422.4 and 1463.4 MeV with $X_{02}^{(20)} = 2.7$ and 3.8, in order, which of course makes no sense as compositeness factors have to be less or equal to one.

Next, we take into account the finite width of the ρ meson in the evaluation of the unitarity two-point loop function $G(s)$. As a result, the peak in the modulus squared of the isoscalar scalar amplitude now acquires some width due to the width of the ρ meson itself. To take that into account this effect we convolute the $G(s)$ function with a Lorentzian mass squared distribution for each of the two ρ mesons in the intermediate state [115, 191, 192]. The resulting unitarity loop function is denoted by $\mathfrak{g}(s)$ and is given by

$$\mathfrak{g}(s) = \frac{1}{N^2}\int_{(m_\rho-2\Gamma_\rho)^2}^{(m_\rho+2\Gamma_\rho)^2} dm_1^2 \frac{\Gamma m_1/\pi}{(m_1^2-m_\rho^2)^2+m_1^2\Gamma^2}\int_{(m_\rho-2\Gamma_\rho)^2}^{(m_\rho+2\Gamma_\rho)^2} dm_2^2 \frac{\Gamma m_2/\pi}{(m_2^2-m_\rho^2)^2+m_2^2\Gamma^2} G(s,m_1^2,m_2^2)\,. \quad (4.30)$$

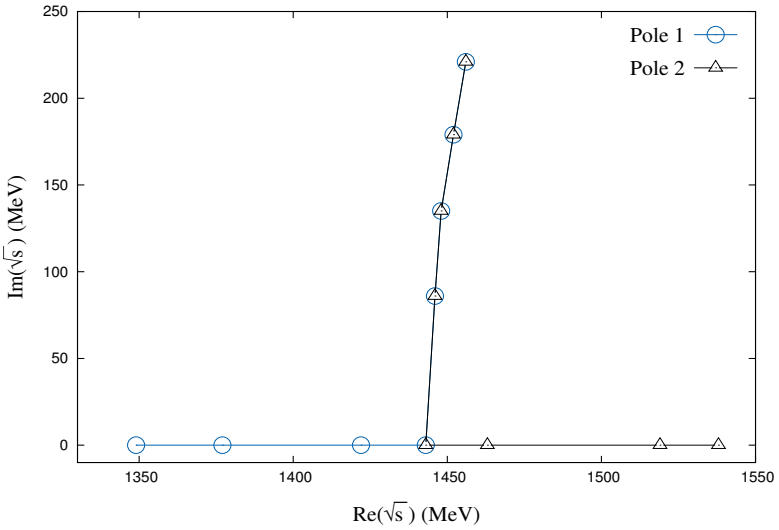

Figure 4.6: Evolution of the poles in the physical Riemann sheet for the isoscalar tensor channel as a function of $q_{\max}$. Two poles are present on the real axis for our starting value of $q_{\max} = 300$ MeV, and along the trajectory we increase $q_{\max}$ in steps of $\delta q_{\max} = 50$ MeV. The two poles merge at $q_{\max} = 403.1$ MeV and for larger values of the cutoff there is one pole that moves deeper into the complex plane.

The normalization factor N is

$$N = \int_{(m_\rho - 2\Gamma_\rho)^2}^{(m_\rho + 2\Gamma_\rho)^2} dm^2 \frac{\Gamma m/\pi}{(m^2 - m_\rho^2)^2 + m^2\Gamma^2} \,, \tag{4.31}$$

with $\Gamma(m)$ the width of the ρ meson with mass m. Due to the P-wave nature of this decay to $\pi\pi$, we take into account its strong cubic dependence on the decaying pion three-momentum and use the approximation

$$\Gamma(m) = \Gamma_\rho \left(\frac{m^2 - 4m_\pi^2}{m_\rho^2 - 4m_\pi^2} \right)^3 \theta(m - 2m_\pi) \tag{4.32}$$

with m_π the pion mass and $\Gamma_\rho \cong 148$ MeV [1]. The function $G(s, m_1^2, m_2^2)$ is the two-point loop function with different masses, while in eq. (4.23) we give its expression for the equal mass case. When evaluated in terms of a dispersion relation it reads,

$$\begin{aligned} G(s, m_1^2, m_2^2) = \frac{1}{16\pi^2} \Bigg\{ & a(\mu) + \log \frac{m_1^2}{\mu^2} + \frac{s - m_1^2 + m_2^2}{2s} \log \frac{m_2^2}{m_1^2} \\ & + \frac{\lambda^{1/2}(s)}{2s} \Big[\log \left(\lambda^{1/2}(s) + s - m_2^2 + m_1^2 \right) - \log \left(\lambda^{1/2}(s) - s + m_2^2 - m_1^2 \right) \\ & + \log \left(\lambda^{1/2}(s) + s + m_2^2 - m_1^2 \right) - \log \left(\lambda^{1/2}(s) - s - m_2^2 + m_1^2 \right) \Big] \Bigg\} \,, \end{aligned} \tag{4.33}$$

with $\lambda^{1/2}(s) = \sqrt{s^2 + m_1^4 + m_2^4 - 2sm_1^2 - 2sm_2^2 - 2m_1^2 m_2^2}$. The algebraic expression of this function when calculated with a three-momentum cutoff for different masses can be found in ref. [154], to which we

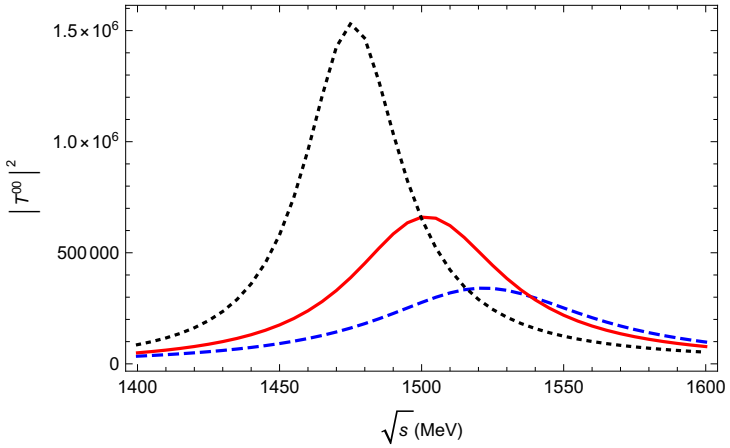

Figure 4.7: The amplitude squared $|T^{00}|^2$ when using the $\mathfrak{g}(s)$ function with a cutoff $q_{\max}$. The blue dashed line corresponds to $q_{\max} = 775$ MeV, the red solid one to 875 MeV and the black dotted one to 1000 MeV.

refer the interested reader.

When using the convoluted $G(s)$ function we find similar masses for the peak of $|T^{(00)}|^2$ in the $(0,0)$ channel compared to the case without convolution. The resulting peak positions are given in the last three rows of tables 4.1 and 4.2. The effects of the non-zero ρ width are clearly seen in fig. 4.7, where we plot $|T^{(00)}(s)|^2$ for the different values of $q_{\max}$ shown in table 4.1. The shape of the peaks follows quite closely a Breit-Wigner form, though it is slightly wider to the right side of the peak. We find that the width decreases with the increasing value of $q_{\max}$, being around 45, 65 and 95 MeV for $q_{\max} = 1000$, 875 and 775 MeV, respectively, of similar size as those found in ref. [115]. When using a subtraction constant instead of $q_{\max}$, relating them through eq. (4.27), the picture is quite similar. The peak positions are given in the last three columns of table 4.2 while the widths obtained are around 105, 70 and 50 MeV for $a = -1.70$, -1.94 and -2.14, in order. These widths are significantly smaller than the PDG values assigned to the $f_0(1370)$ resonance of 200-500 MeV [1].

Due to the coupling of the $\rho\rho$ and $\pi\pi$, this pole could develop a larger width. This is approximated in ref. [115] by considering the imaginary part of the $\pi\pi$ box diagram, with a $\rho \to \pi\pi$ vertex at each of the vertices of the box. These vertices are also worked out from the non-linear chiral Lagrangian with hidden gauge symmetry [124, 208]. We refer to ref. [115] for details on the calculation of this contribution. According to this reference one has to add to $V^{(00)}_{00;00}$ and to $V^{(20)}_{02;02}$ the contribution $V^{(JI)}_{2\pi}$, given by

$$\begin{aligned} V^{(00)}_{2\pi} &= 20i\ \mathrm{Im}\widetilde{V}_{\pi\pi}\ , \\ V^{(20)}_{2\pi} &= 8i\ \mathrm{Im}\widetilde{V}_{\pi\pi}\ . \end{aligned} \tag{4.34}$$

In the calculation of the function $\widetilde{V}_{\pi\pi}$, ref. [115] introduces a monopole form factor $F(q)$ for each of the four $\rho \to \pi\pi$ vertices in the pion box calculation,

$$F(q) = \frac{\Lambda^2 - m_\pi^2}{\Lambda^2 - (k-q)^2} \tag{4.35}$$

with $k^0 = \sqrt{s}/2$, $\mathbf{k} = 0$, $q^0 = \sqrt{s}/2$ and $\mathbf{q}$ the integration variables. This introduces a sizeable dependence of the results on the value of Λ. Nonetheless, in order to compare with ref. [115] we follow the very same

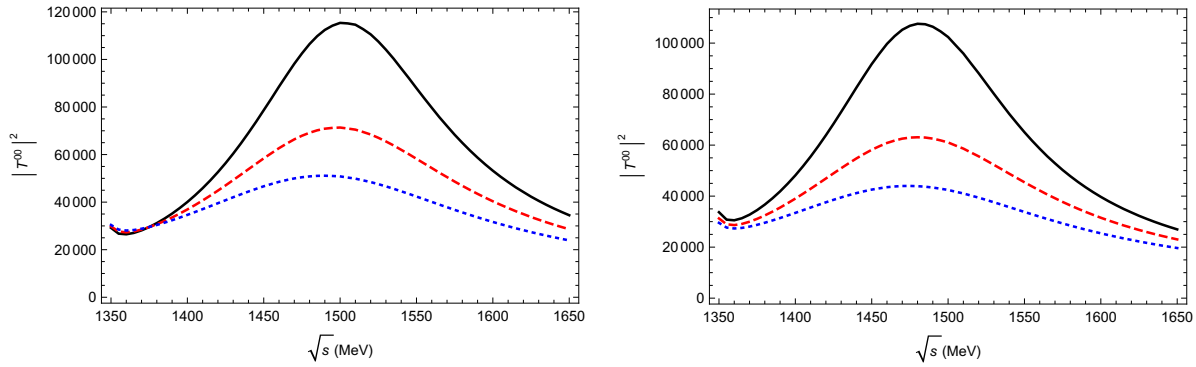

Figure 4.8: $|T^{(00)}(s)|^2$ with the $\pi\pi$ box diagram contribution included for different values of Λ in $F(q)$, cf. eq. (4.35). Specifically, $\Lambda = 1200$ (black solid line), 1300 (red dashed line) and 1400 MeV (blue dotted line), for $q_{\,\rm max} = 875$ (left panel) and $q_{\,\rm max} = 1000$ MeV (right panel).

(J, I)	(ℓ, S) channels
$(0, 0)$	$(0, 0)$, $(2, 2)$
$(2, 0)$	$(0, 2)$, $(2, 0)$, $(2, 2)$

Table 4.3: Coupled-channels with different orbital angular momentum.

scheme of calculation and take the same values for Λ, that is, 1200, 1300 and 1400 MeV.[7]

The inclusion of the $\pi\pi$ box diagram, on top of the convolution with the ρ mass squared distribution for calculating the $G(s)$ function, does not alter the previous conclusion on the absence of a pole in the isoscalar tensor channel. However, the isoscalar scalar pole develops a larger width around 200-300 MeV, that increases with Λ, as can be inferred from fig. 4.8, where we plot $|T^{(00)}(s)|^2$. On the other hand, the position of the peak barely changes compared to the one given in the last two rows of table 4.1.Tentatively this pole could be associated to the $f_0(1370)$ resonance, which according to refs. [209, 210] decays mostly to $\pi\pi$ with a width around 200 MeV. In the PDG [1] the total width of the $f_0(1370)$ is given with a large uncertainty, within the range 200-500 MeV and the $\pi\pi$ decay mode is qualified as dominant. The nearby $f_0(1500)$ resonance has a much smaller width, around 100 MeV, and its coupling and decay to $\pi\pi$ is suppressed. These properties of the $f_0(1500)$ are discussed in detail in ref. [209].

Coupled-channel scattering

We now consider the impact on our results when allowing for the coupling between channels with different orbital angular momenta, an issue not considered in ref. [115]. In table 4.3 we show the different channels that couple for given JI quantum numbers and pay special attention to the $(J, I) = (0, 0)$ and $(2, 0)$ channels. Apart from the conservation of J and I, one also has to impose invariance under parity, which avoids the mixing between odd and even ℓ's.

When including coupled channel effects, we find two poles in the channels with $(J, I) = (0, 0)$, that are reported in table 4.4 for various values of $q_{\,\rm max}$ (shown in the first column). We give from left to right the

[7] Another more complete scheme is to work explicitly with coupled-channel scattering as done in ref. [209], where $\rho\rho$ and $\pi\pi$ channels, among many others, were explicitly included. In this way resonances develop decay widths in a full nonperturbative fashion because of the coupling between channels.

$q_{\,\mathrm{max}}$ (MeV)	Mass (MeV)	$(\gamma_{00}^{(00)})^2$ (GeV^2)	$(\gamma_{22}^{(00)})^2$ (GeV^2)	$X_{00}^{(00)}$	$X_{22}^{(00)}$
775	1515.3	57.2	0.2	0.75	0.00
	1386.6	−7.6	−20.2	< 0	< 0
875	1492.4	72.1	1.0	0.69	0.01
	1396.8	−13.5	−19.4	< 0	< 0
1000	1455.3	116.2	8.3	0.80	0.06
	1415.7	−53.1	−25.1	< 0	< 0

Table 4.4: Bound state poles in the partial wave amplitudes of quantum numbers $(J, I) = (0, 0)$ with varying cutoff $q_{\,\mathrm{max}}$, which is indicated in the first column. The masses (2nd column), the residues to $(\ell, S) = (0, 0)$ and $(2, 2)$ (3rd and 4th columns) and the compositeness coefficients $X_{00}^{00)}$ and $X_{22}^{00)}$ (6th and 7th columns) are also given. For the lighter poles the compositeness coefficients are small and negative, so that they cannot be interpreted as physical states contrary to common wisdom [146, 206, 207].

pole mass (second column), residues (third and fourth ones) and compositeness coefficients (fifth and sixth ones) of different channels, $(\ell, S) = (0, 0)$ and $(2, 2)$, respectively. One of the poles is heavier and closer to the $\rho\rho$ threshold with similar properties as the pole in the uncoupled case, compare with table 4.1, particularly for $q_{\,\mathrm{max}} = 775$ MeV. Nonetheless, as $q_{\,\mathrm{max}}$ increases the difference of the properties of this pole between the coupled and uncoupled cases is more pronounced. In particular let us remark that now $X_{00}^{(00)}$ is always $\gtrsim 0.7$ and for $q_{\,\mathrm{max}} = 1$ GeV the residue to the channel $(\ell, S) = (0, 0)$ is much larger than in the uncoupled case. Additionally, we find now a lighter pole which lays above the branch point singularity at $\sqrt{3}\, m_\rho \simeq 1343$ MeV. For lower values of the cutoff $q_{\,\mathrm{max}}$ this pole couples more strongly to the $(\ell, S) = (2, 2)$ channel, but as the cutoff increases its residue for the channel $(\ell, S) = (0, 0)$ also increases in absolute value and it is the largest for $q_{\,\mathrm{max}} = 1$ GeV. It is then clear that both channels $(\ell, S) = (0, 0)$ and $(2, 2)$ are relevant for the origin of this pole. Note that the residues for this lighter pole are negative, which is at odds with the standard interpretation of the residue $(\gamma_{\ell S}^{(00)})^2$ of a bound state as the coupling squared. This implies that the compositeness coefficients $X_{\ell S}^{(00)}$ are all negative, which is at odds with a probabilistic interpretation as suggested in refs. [146, 206, 207] for bound states. The moduli of the $|X_{\ell S}^{(00)}|$ are all small because this lighter pole lays quite far from the $\rho\rho$ threshold. The fact that its mass is not far from the strong branch point singularity at $\sqrt{3}\, m_\rho$ makes that this pole is very much affected by the left-hand cut discontinuity. In this respect, it might well be that the presence of this pole with anomalous properties is just an artefact of the unitarization formula of eq. (4.22), that treats the left-hand cut discontinuity of the potential perturbatively. One can answer this question by solving exactly the N/D method [211–214], so that the left-hand cut discontinuity of the potential is properly treated and the resulting amplitude has the right analytical properties. Let us recall that eq. (4.22) is an approximate algebraic solution of the N/D method by treating perturbatively the left-hand cut discontinuities of the coupled partial waves [109, 195, 197]. For the uncoupled scattering such effects are further studied in detail in the next section.

For the $(J, I) = (2, 0)$ partial waves we have three coupled channels, $(\ell, S) = (0, 2)$, $(2, 0)$ and $(2, 2)$ and, contrary to the uncoupled case, we now find a pole that lays above the branch point singularity. We give its mass and residues for different $q_{\,\mathrm{max}}$ in table 4.5, with the same notation as in table 4.4. Notice that these pole properties are very stable under the variation of $q_{\,\mathrm{max}}$. This pole couples by far much more strongly to the channel with $(\ell, S) = (2, 2)$ than to any other channel. This indicates that it is mainly due to the dynamics associated with the $(\ell, S) = (2, 2)$ channel. But the same comments are in order here as given above for the lighter isoscalar scalar pole, because its residues shown in table 4.5 are negative and

$q_{\max}$ (MeV)	Mass (MeV)	$(\gamma_{02}^{(20)})^2$ (GeV^2)	$(\gamma_{20}^{(20)})^2$ (GeV^2)	$(\gamma_{22}^{(20)})^2$ (GeV^2)
775	1355.1	−0.8	−0.0	−8.6
875	1358.2	−0.7	−0.0	−8.3
1000	1361.8	−0.6	−0.0	−7.9

Table 4.5: Bound state poles in the partial wave amplitudes of quantum numbers $(J, I) = (2, 0)$ with different cutoffs $q_{\max}$, indicated in the first column. The masses (2nd column) and the residues to $(\ell, S) = (0, 2)$, $(2, 0)$ and $(2, 2)$ (3rd, 4th and 5th columns) are shown. Here, "−0.0" denotes a small but negative number.

so are the corresponding compositeness coefficients. Hence, the lighter pole for $(J, I) = (0, 0)$ and the one found for $(2, 2)$ cannot be considered as robust results of our analysis. This has to be contrasted to the case of the heavier isoscalar scalar pole that is stable under relativistic corrections, coupled-channel effects and has quite standard properties regarding its couplings and compositeness coefficients.

4.2.3 First iterated solution of the N/D method

In this section for definiteness we only consider uncoupled scattering. We have in mind the $(J, I) = (0, 0)$ and $(J, I) = (2, 0)$ quantum numbers to which special attention has been paid in the literature concerning the generation of poles that could be associated with the $f_0(1370)$ and $f_2(1270)$ resonances, as discussed above. Further applications of the improved unitarization formalism presented in this section are left for future work.

According to the N/D method [156], see 3.4.3 a partial-wave amplitude can be written as

$$T = \frac{N(s)}{D(s)} \,, \tag{4.36}$$

where the function $D(s)$ has only the unitarity or right-hand cut (RHC) while $N(s)$ only has the left-hand cut (LHC). The secular equation for obtaining resonances and bound states corresponds to look for the zeros of $D(s)$,

$$D(s_i) = 0 \,. \tag{4.37}$$

Below threshold along the real s axis this equation is purely real because $D(s)$ has a non-vanishing imaginary part only for $s > s_{\rm th}$.

However, with our unitarization procedure from leading-order unitary chiral perturbation theory (UChPT) we have obtained the approximation

$$T^{(JI)}(s) = \frac{V^{(JI)}(s)}{1 - V^{(JI)}(s) G_c(s)} \,, \tag{4.38}$$

and the resulting equation to look for the bound states is, cf eq. (3.100)

$$D_U(s) = 1 - V(s) G_c(s) = 0 \,. \tag{4.39}$$

Notice that eq. (4.38), contrary to the general eq. (4.37), has an imaginary part below the branch-point singularity at $s = 3m^2$. Nonetheless, if the LHC were perturbative this imaginary part would not have prevented having a strong peak in the amplitude if there were already a bound state below the branch-point singularity when the LHC is neglected. However, this is by far not the case for the pole associated with

the $f_2(1270)$ in ref. [115], which clearly indicates the instability of this approach under the inclusion of relativistic corrections.

We can go beyond this undesired situation by considering the first-iterated solution to the N/D method. This is indeed similar to eq. (4.38) but improving upon it because it allows us to go beyond the on-shell factorization employed in this equation. In the first-iterated N/D solution one identifies the numerator function $N(s)$ to the tree-level calculation $V^{(JI)}(s)$ and employs the exact dispersive expression for $D(s)$. Namely, it reads[8]

$$\begin{aligned} N(s) &= V^{(JI)}(s)\,, \\ D(s) &= \gamma_0 + \gamma_1(s - s_{th}) + \frac{1}{2}\gamma_2(s - s_{th})^2 + \frac{(s - s_{th})s^2}{\pi}\int_{s_{th}}^{\infty} ds' \frac{\rho(s')V^{(JI)}(s')}{(s' - s_{th})(s' - s)(s')^2}\,, \\ T_{ND}(s) &= \frac{N(s)}{D(s)}\,, \end{aligned} \tag{4.40}$$

with the phase space factor $\rho(s)$ given by $\rho(s) = \sigma(s)/16\pi$. We have taken three subtractions in the dispersion relation for $D(s)$ because $V^{(JI)}(s)$ diverges as s^2 for $s \to \infty$.

From our present study we have concluded that $T^{(JI)}(s)$ is stable in the threshold region under relativistic corrections as well as under the addition of coupled channels. Because of the stability of the results in this region under relativistic corrections and by visual inspection of the potentials in fig. 4.5 we conclude that the near-threshold region is quite safe of the problem related to the branch-point singularity of the LHC associated with one-ρ crossed-channel exchanges. We then determine the subtractions constants, γ_0, γ_1 and γ_2 in $D(s)$ by matching $T_{ND}(s)$, eq. (4.40), and $T^{(JI)}(s)$, eq. (4.38), around threshold (s_{th}). At the practical level it is more convenient to match $1/T(s)$, so that in the threshold region up to $O(s^3)$ one has:

$$\begin{aligned} \gamma_0 + \gamma_1(s - s_{th}) + \frac{1}{2}\gamma_2(s - s_{s_{th}})^2 &= 1 - V(s)G_c(s) - \frac{(s - s_{th})s^2}{\pi}\int_{s_{th}}^{\infty} ds' \frac{\rho(s')V(s')}{(s' - s_{th})(s' - s)(s')^2} \\ &\equiv \omega(s)\,. \end{aligned} \tag{4.41}$$

In this way,

$$\begin{aligned} \gamma_0 &= 1 - V(s_{th})G_c(s_{th})\,, \\ \gamma_1 &= \omega'(s_{th})\,, \\ \gamma_2 &= \omega''(s_{th})\,. \end{aligned} \tag{4.42}$$

The dependence of our present results on the cutoff used in $T^{(JI)}(s)$ stems from the matching conditions of eq. (4.42). However, let us stress that the analytical properties of $D(s)$ and $N(s)$ are correct, they have the RHC and LHC with the appropriate extent and branch point singularities, respectively, and the resulting amplitude is unitarized.

Results $J = 0$, $I = 0$

We plot $D(s)$ for $(J, I) = (0, 0)$ in fig. 4.9 for $q_{\max} = 0.7$, 1 and 1.3 GeV by the red solid, green dashed and blue dash-dotted lines, in order. The crossing with the zero line (dotted one) indicates the mass of the bound state. This mass decreases with increasing $q_{\max}$, being around 1.4 GeV for the largest cutoff and

[8] A comprehensive introduction to the N/D method is given in refs. [109, 131, 211–214].

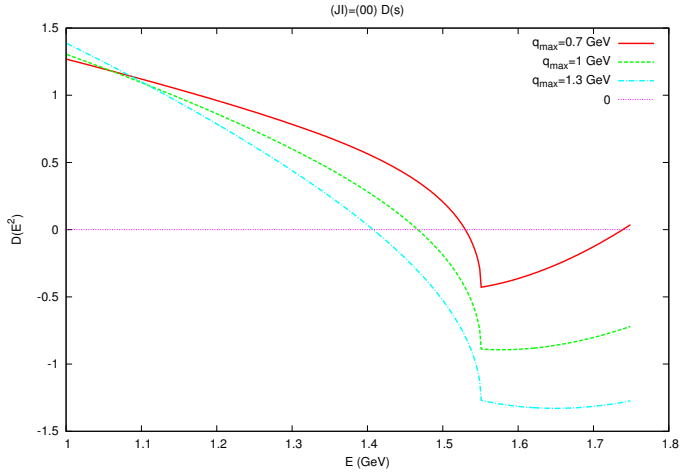

Figure 4.9: $D(s)$ function, eq. (4.40), for $(J, I) = (0, 0)$. Above threshold only the real part is shown.

very close to threshold for the smallest. In fig. 4.10 we compare the real (left) and imaginary parts (right panel) of $D(s)$ and $D_U(s) = 1 - V(s)G_c(s)$ for a cutoff of 1 GeV. We do not show more values of the cutoff because the same behavior appears. The function $D(s)$ and $D_U(s)$ match up to around the branch-point singularity at $\sqrt{s} = 3m_\rho^2$. Below this, $D_U(s)$ becomes imaginary, cf. eq. (4.39), while $D(s)$ remains real and has the right property by construction, cf. eq. (4.40). Above threshold the imaginary parts of both functions coincide as demanded by unitarity. We see that for these quantum numbers our new improved unitarization formalism and the one used to derive eq. (4.22) agree very well. The bound-state mass remains the same as given in table 4.1 because the functions $D(s)$ and $D_U(s)$ match perfectly well in the region where these poles occur, as it is clear from fig. 4.10. This should be expected because for $(J, I) = (0, 0)$ the branch point singularity was much weaker than for other cases, e.g. $(J, I) = (2, 0)$, as discussed above.

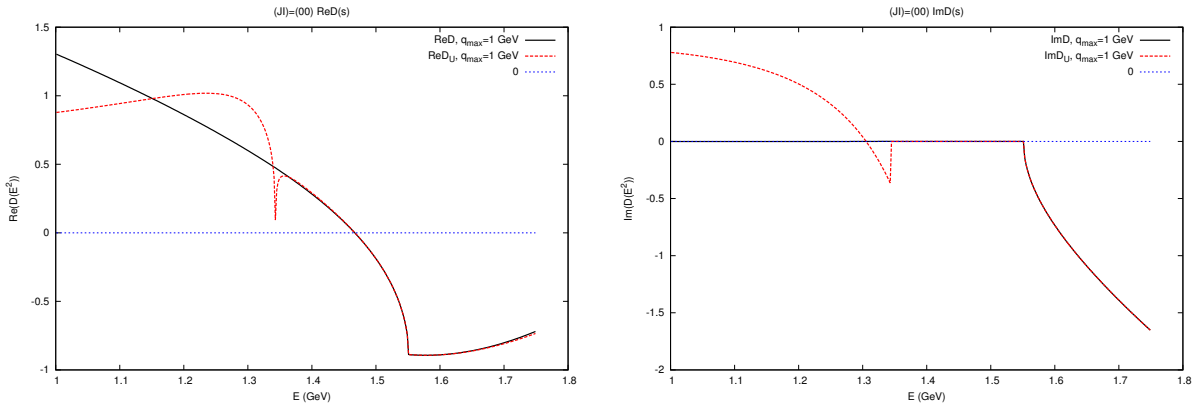

Figure 4.10: $(J, I) = (0, 0)$. Real (left) and imaginary (right panel) parts of $D(s)$ compared also with $D_U(s) = 1 - V^{(00)}(s)G_c(s)$ from leading-order UChPT.

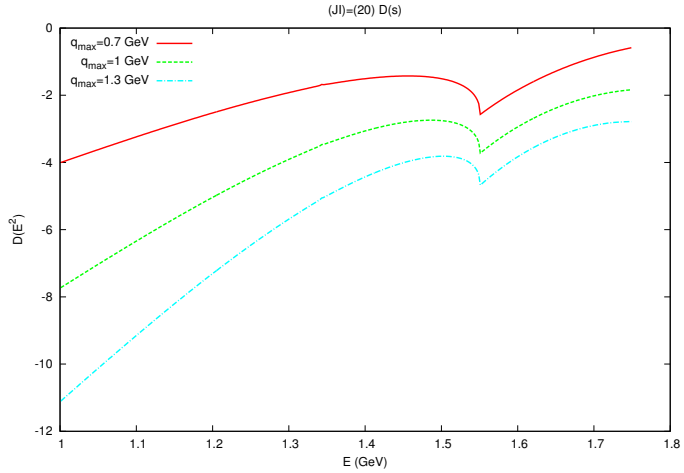

Figure 4.11: $D(s)$ function, eq. (4.40), for $(J, I) = (2, 0)$. Above threshold only the real part is shown.

Results $J = 2$, $I = 0$

We plot $D(s)$ for $(J, I) = (2, 0)$ in fig. 4.11 for $q_{\max} = 0.7$, 1 and 1.3 GeV by the red solid, green dashed and blue dash-dotted lines, respectively. We can see that in this region the function $D(s)$ is large and negative so that there is by far no pole in the $f_2(1270)$ region. In order to show the curves more clearly we use only $q_{\max} = 1$ GeV in fig. 4.12, for other values of $q_{\max}$ the behavior is the same. In the left panel we compare the real parts of $T_{ND}(s)$ (black solid) and $T^{(20)}(s)$ (red dashed) while in the right panel we proceed similarly for the real parts of $D(s)$ and $D_U(s) = 1 - V^{(20)}(s)G_c(s)$, with the same type of lines in order. All the functions match near the threshold region and above it, but they strongly depart once we approach the LHC branch-point singularity at $s = 3m_\rho^2$ and beyond (for smaller values of s). Notice that $D(s)$, which has not such branch-point singularity, follows then the smooth decreasing trend already originated for $3m^2 < s < 4m^2$. For $(J, I) = (0, 0)$ the corresponding smooth trend is that of a decreasing function, cf. fig. 4.9. The branch-point singularity is clearly seen in $T^{(20)}(s)$ because it is proportional to $V^{(20)}(s)$.

In summary, the conclusions obtained in Sec. 4.2.2 regarding the generation of the pole that could be identified with the $f_0(1370)$ and the absence of that associated with the $f_2(1270)$ as claimed in ref. [115] fully hold. As a matter of fact, they get reinforced after considering the more elaborated unitarization process that is obtained here by taking the first-iterated N/D solution.

4.2.4 Summary and conclusions

In this section, we have revisited the issue of resonance generation in unitarized $\rho\rho$ scattering using a chiral covariant formalism. The main results of our study can be summarized as follows:

i) We have developed a partial-wave projection formalism that is applicable to the covariant treatment of $\rho\rho$ scattering. In particular, we point out that accounting for the full ρ-meson propagator leads to a branch point in the partial wave projected amplitudes at $s = 3m_\rho^2 \simeq 1.8\,\text{GeV}^2$, about 208 MeV below the 2ρ threshold. This branch point does not appear in the extreme non-relativistic treatment of the propagator.

ii) Evaluating the T-matrix using the standard form, see eq. (4.22) that treats the left-cut perturbatively,

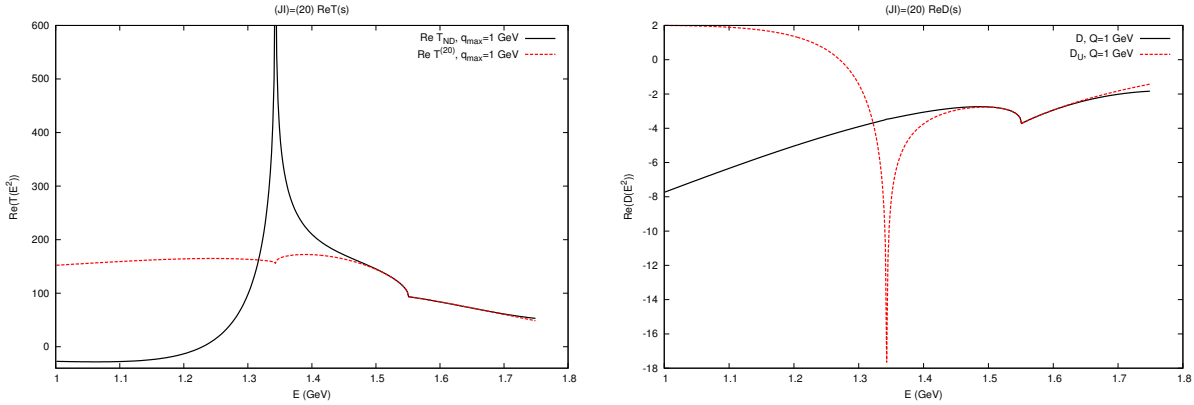

Figure 4.12: $(J, I) = (2, 0)$. Left panel: real part of $T_{ND}(s)$ (black solid) compared with that of $T^{(20)}(s)$ (red dashed). Right panel: comparison between the real parts of $D(s)$ (black solid) and $D_U(s) = 1 - V^{(20)}(s)G_c(s)$ (red dashed).

we find a pole in the scalar isoscalar channel close to the $\rho\rho$ threshold that can be associated with the $f_0(1370)$ resonance, in agreement with the findings of ref. [115], though there are minor quantitative differences.

iii) In contrast to ref. [115], we do not find a tensor state below the scalar one. This can be traced back to the influence of the aforementioned branch point. We therefore conclude that the state that is identified in ref. [115] with the $f_2(1270)$ is an artifact of the non-relativistic approximation and its generation does not hold from the arguments given in that reference.

iv) We have also worked out the effects of the coupling between channels with different orbital angular momenta, which lead to additional states. These, however, have negative composite coefficients and are thus not amenable to a simple bound state interpretation. As these states are close to the branch point at $s = 3m_\rho^2$, the perturbative treatment of the left-hand cut, as employed here, is certainly not sufficient to decide about their relevance.

v) We have improved the treatment of the left-hand cut by employing the first-iterated N/D method, in particular this method avoids the factorization approach of leading order UChPT. We worked the solutions that follow for uncoupled scattering in the $(J, I) = (0, 0)$ and $(2, 0)$ channels. The outcome fully agrees with the conclusions already obtained from UChPT and, notably, the absence of a pole that could be associated with the $f_2(1270)$ is firmly reinforced.

A lesson from points iii) and v) is clear. A strongly attractive interaction in a given channel is a necessary but by far not sufficient condition to generate a multi-hadron bound state. This argument, as used in ref. [115], is in general terms too naive because it does not take into account the possible raise of a singularity in the true potential between the range of validity of the approximation used and the predicted bound-state mass from the latter. It could be rephrased as trying to deduce the values of the function $1/(1 + x)$ for $x < -1$ by knowing its values for x around 0.

We conclude that the approach presented here should be used to investigate the possible generation of meson resonances from the interaction of vector mesons. In the next section, we will investigate how the relativistic effects affect the conclusions of the SU(3) calculation of ref. [116] and will further sharpen the framework along the lines mentioned, in particular by solving exactly the N/D equations [212–

214].On top of this, a realistic treatment of the meson spectroscopy in the region above 1 GeV definitely requires the inclusion of more channels than just $\rho\rho$ (or more generally vector-vector ones). However, the formalism developed developed here could be very useful to accomplish this aim phenomenologically if implemented in multi-channel studies, e.g. by extending the work of ref. [209].

4.3 Covariant vector meson-vector meson interactions and dynamically generated resonances[9]

The extension of vector-vector interaction to SU(3) is given in ref. [116], however, in an extreme non-relativistic form as in ref. [115]. Up to 11 dynamically generated states were reported. While six of them are assigned to the $f_0(1370)$, $f_0(1710)$, $f_2(1270)$, $f_2'(1525)$, $a_2(1320)$ and $K_2^*(1430)$ resonances, the other states with the quantum numbers as h_1, a_0, b_1, K_0^* and K_1 could be tested by future experiments. Since the work employed is the same extreme non-relativistic formalism as in ref. [115], a relativistic covariant revision is needed.

This section is devoted to the extension to SU(3) case in a covariant formalism. It is worth mentioning that for each single channel the left-hand cut is located below the corresponding unitarity cut. The nearby left-hand cut may plague the determination of the pole positions [215]. Therefore, the poles associated are reliable as long as they are sufficiently far away from the left-hand cuts. In the coupled-channel interactions, dynamic left-hand cuts associated with the t- and u-channel vector-exchange diagrams overlap with the unitarity cut. Thus, this invalidate the unitarization formula (3.100). A more systematic way to deal with the unitarity and the dynamic singularities is provided by the N/D method [109, 156, 185]. However, a complete solution of the coupled-channel N/D is extremely difficult. Therefore, we will use the first-iterated solution of the N/D method as proposed in ref. [158], in sec. 4.2, which has the correct analytic structure.

This section is organized as follows. In section 4.3.1, the effective Lagrangian in the hidden local symmetry approach is briefly introduced for $SU(3)$ case and the scattering amplitudes are calculated. Then the partial wave projection for a relativistic system is performed. The on-shell factorization of the BSE is applied to the single-channels with different masses to generate dynamical resonances outside of the left-hand cuts. The improved unitarization formula, i.e. the first iterated solution of the N/D method, is employed in section 4.3.2 to single-channels and to coupled-channels as well. Finally, section 4.3.3 comprises a summary and outlook.

4.3.1 Formalism

We can use eq. (2.118) with U and V_μ being 3×3 matrices and defined as:

$$\Phi = \begin{pmatrix} \frac{1}{\sqrt{2}}\pi^0 + \frac{1}{\sqrt{6}}\eta & \pi^+ & K^+ \\ \pi^- & -\frac{1}{\sqrt{2}}\pi^0 + \frac{1}{\sqrt{6}}\eta & K^0 \\ K^- & \bar{K}^0 & -\frac{2}{\sqrt{6}}\eta \end{pmatrix}, \tag{4.43}$$

[9]The content of this section is in preparation for publication.

and

$$V_\mu = \begin{pmatrix} \frac{1}{\sqrt{2}}\rho^0 + \frac{1}{\sqrt{2}}\omega & \rho^+ & K^{*+} \\ \rho^- & -\frac{1}{\sqrt{2}}\rho^0 + \frac{1}{\sqrt{2}}\omega & K^{*0} \\ K^{*-} & \bar{K}^{*0} & \phi \end{pmatrix}_\mu . \tag{4.44}$$

Expanding the Lagrangian (2.118) up to two pseudoscalars for the relevant terms, we find

$$\begin{aligned} \mathcal{L}_{\text{mass}} &= ag^2 f_\pi^2 \langle V_\mu V^\mu \rangle, \\ \mathcal{L}_{V\Phi\Phi} &= -i\frac{a}{2} g \langle V^\mu [\Phi, \partial_\mu \Phi] \rangle, \\ \mathcal{L}_{VVV} &= ig \langle (\partial_\mu V_\nu - \partial_\nu V_\mu) V^\mu V^\nu \rangle, \\ \mathcal{L}_{VVVV} &= \frac{1}{2} g^2 \langle V_\mu V_\nu V^\mu V^\nu - V_\mu V^\mu V_\nu V^\nu \rangle. \end{aligned} \tag{4.45}$$

Again, we choose $a = 2$ to get the vector-coupling universality and KSRF relations.

Unlike the last section, we have plenty of combinations for allowed scatterings. Therefore, we define general amplitudes. At tree level, the Feynman diagrams needed are displayed in fig. 4.13, The amplitude

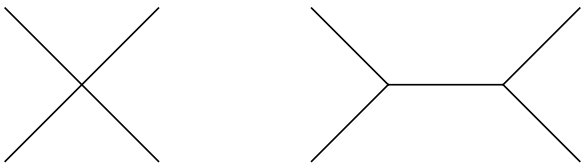

Figure 4.13: Possible Feynman diagrams for the tree-level amplitudes for the vector-vector scattering. The u- and t-channel vector-exchange diagrams are not shown explicitly.

for the process $V_1(p_1)V_2(p_2) \to V_3(p_3)V_4(p_4)$ can be written as

$$A(s,t,u) = A_c(s,t,u) + A_t(s,t,u) + A_u(s,t,u) + A_s(s,t,u), \tag{4.46}$$

where A_c, A_t, A_u and A_s correspond to the four-vector-contact diagrams, i.e. (a) in fig. 4.13, t-, u- and s-channel vector-exchange diagrams, respectively.

The contributions to the contact amplitudes from $\mathcal{L}_{VVVV}$ which are independent of the momenta of vectors are given by

$$\begin{aligned} A_c(s,t,u) &= g^2 C_1 \left(2\epsilon_1 \cdot \epsilon_2\, \epsilon_3^* \cdot \epsilon_4^* - \epsilon_1 \cdot \epsilon_3^*\, \epsilon_2 \cdot \epsilon_4^* - \epsilon_1 \cdot \epsilon_4^*\, \epsilon_2 \cdot \epsilon_3^*\right) \\ &\quad -g^2 C_2 \left(2\epsilon_1 \cdot \epsilon_4^*\, \epsilon_2 \cdot \epsilon_3^* - \epsilon_1 \cdot \epsilon_2\, \epsilon_3^* \cdot \epsilon_4^* - \epsilon_1 \cdot \epsilon_3^*\, \epsilon_2 \cdot \epsilon_4^*\right), \\ &= C_1 A_c^1 + C_2 A_c^2, \end{aligned} \tag{4.47}$$

where $\epsilon_i^{(*)}$ is the polarization vector of the i^{th} external vector meson. The polarization vector can be characterized by the corresponding three-momentum $\mathbf{p}_i$ and the third component of the spin in its rest frame, and the explicit expression for the polarization vectors can be found in app. E. The two structures in eq. (4.47) which are symmetric by exchanging $\epsilon_2 \leftrightarrow \epsilon_4^*$ is due to the two operators in $\mathcal{L}_{VVVV}$.

Considering the vector-exchange amplitudes, for the s-channel diagram exchanging a vector V with mass M_V, it has the form

$$\begin{aligned} A(s,t,u) &= C_s^V A_s^V(s,t,u) \\ &\equiv C_s^V \frac{g^2}{s-M_V^2}\Big[\epsilon_1\cdot\epsilon_2\,\epsilon_3^*\cdot\epsilon_4^*\left(u-t-\frac{(M_1^2-M_2^2)(M_3^2-M_4^2)}{M_V^2}\right) \\ &+ 4\Big(\epsilon_3^*\cdot\epsilon_4^*\,(\epsilon_1\cdot p_2\,\epsilon_2\cdot p_3-\epsilon_1\cdot p_3\,\epsilon_2\cdot p_1)+\epsilon_2\cdot p_1\,(\epsilon_4^*\cdot p_3\,\epsilon_1\cdot\epsilon_3^*-\epsilon_3^*\cdot p_4\,\epsilon_1\cdot\epsilon_4^*) \\ &+ \epsilon_1\cdot p_2(\epsilon_3^*\cdot p_4\,\epsilon_2\cdot\epsilon_4^*-\epsilon_4^*\cdot p_3\,\epsilon_2\cdot\epsilon_3^*)\Big)-4\epsilon_1\cdot\epsilon_2\,(\epsilon_3^*\cdot p_1\,\epsilon_4^*\cdot p_3-\epsilon_3^*\cdot p_4\,\epsilon_4^*\cdot p_1)\Big], \end{aligned} \tag{4.48}$$

with M_i the mass of the i^{th} external vector meson. The t- and u-channel amplitudes A_t^V and A_u^V can be obtained from A_s^V by performing the exchange $p_2 \leftrightarrow -p_3$, $\epsilon_2 \leftrightarrow \epsilon_3^*$ and $p_2 \leftrightarrow -p_4$, $\epsilon_2 \leftrightarrow \epsilon_4^*$, respectively.

We study the scattering amplitudes in the isospin basis instead of the particle basis as in the previous section. The scattering processes can be classified by the strangeness S and isospin I of the system. There are 7 independent channels in total. The corresponding quantum numbers (S,I) of the scattering systems are $(0,0)$, $(0,1)$, $(0,2)$, $(1,1/2)$, $(1,3/2)$, $(2,0)$ and $(2,1)$, among which $(0,2)$, $(1,3/2)$, $(2,0)$ and $(2,1)$ are single-channels. For $(S,I)=(0,0)$, there are five channels: $\rho\rho$, $K^*\bar{K}^*$, $\omega\omega$, $\omega\phi$ and $\phi\phi$. The $(S,I)=(0,1)$ has four channels: $\rho\rho$, $K\bar{K}^*$, $\rho\omega$ and $\rho\phi$, and the $(S,I)=(1,1/2)$ has three channels: ρK^*, $K^*\omega$ and $K^*\phi$. The phase convention we use is

$$\left|\rho^+\right\rangle = -\left|1,+1\right\rangle, \quad \left|\bar{K^*}^0\right\rangle = -\left|\frac{1}{2},+\frac{1}{2}\right\rangle. \tag{4.49}$$

Expressed in (S,I) basis, the tree level scattering amplitudes are given by

$$A^{(S,I)}(s,t,u) = \sum_{i=1,2} C_i^{(S,I)} A_c^i(s,t,u) + \sum_{\substack{V=\rho,K^*,\omega,\phi \\ j=s,t,u}} C_j^{V(S,I)} A_j^V(s,t,u), \tag{4.50}$$

where the coefficients are collected in table 4.6.

In this section, we only consider the $S-$wave scattering interactions. Angular momentum coupled-channel effect is considered in the last section 4.2. We have seen that it led to the presence of an artificial pole with anomalous properties. It has a negative residue and compositeness coefficient, which is at odds with the probabilistic interpretation of a bound state. The presence of the extra pole is attributed to the unitarization which treats the left-hand cut perturbatively. Apart from the extra artificial pole, including coupled-channel effects reproduce the pole with close properties of that in the uncoupled case. For simplicity, the coupled-channel effect from the different possible orbital angular momenta is not taken into account. We only focus on the channels with angular momenta. Therefore, $\ell=\bar{\ell}=0$ in eq. (4.20).

If we generalize eq. (4.21) to two different masses for a t-channel amplitude, we get

$$\begin{aligned} \frac{1}{2}\int_{-1}^{1} d\cos\theta\,\frac{1}{t-m^2+i\epsilon} &= -\frac{s}{\sqrt{\lambda(s,m_1^2,m_2^2)\lambda(s,m_3^2,m_4^2)}} \\ &\times\log\frac{m_1^2+m_3^2-\frac{(s+m_1^2-m_2^2)(s+m_3^2-m_4^2)}{2s}-\frac{\sqrt{\lambda(s,m_1^2,m_2^2)\lambda(s,m_3^2,m_4^2)}}{2s}-m^2+i\epsilon}{m_1^2+m_3^2-\frac{(s+m_1^2-m_2^2)(s+m_3^2-m_4^2)}{2s}+\frac{\sqrt{\lambda(s,m_1^2,m_2^2)\lambda(s,m_3^2,m_4^2)}}{2s}-m^2+i\epsilon}, \end{aligned} \tag{4.51}$$

Table 4.6: The coefficients of the tree-level vector-vector scattering in the (S, I) basis.

(S,I)	Channel	C_1	C_2	C_t^{ρ}	$C_t^{K^*}$	C_t^{ω}	C_t^{ϕ}	C_u^{ρ}	$C_u^{K^*}$	C_u^{ω}	C_u^{ϕ}	C_s^{ρ}	$C_s^{K^*}$	C_s^{ω}	C_s^{ϕ}
$(0,0)$	$\rho\rho \to \rho\rho$	4	0	-4	0	0	0	-4	0	0	0	0	0	0	0
	$\rho\rho \to K^*\bar{K}^*$	$\sqrt{\frac{3}{2}}$	0	0	$-\sqrt{\frac{3}{2}}$	0	0	0	$-\sqrt{\frac{3}{2}}$	0	0	0	0	0	0
	$\rho\rho \to \omega\omega$	0	0	0	0	0	0	0	0	0	0	0	0	0	0
	$\rho\rho \to \omega\phi$	0	0	0	0	0	0	0	0	0	0	0	0	0	0
	$\rho\rho \to \phi\phi$	0	0	0	0	0	0	0	0	0	0	0	0	0	0
	$K^*\bar{K}^* \to K^*\bar{K}^*$	0	3	$-\frac{3}{2}$	0	$-\frac{1}{2}$	-1	0	0	0	0	0	0	-1	-2
	$K^*\bar{K}^* \to \omega\omega$	$-\frac{1}{\sqrt{2}}$	0	0	$\frac{1}{\sqrt{2}}$	0	0	0	$\frac{1}{\sqrt{2}}$	0	0	0	0	0	0
	$K^*\bar{K}^* \to \omega\phi$	1	0	0	-1	0	0	0	-1	0	0	0	0	0	0
	$K^*\bar{K}^* \to \phi\phi$	$-\sqrt{2}$	0	0	$\sqrt{2}$	0	0	0	$\sqrt{2}$	0	0	0	0	0	0
	$\omega\omega \to \omega\omega$	0	0	0	0	0	0	0	0	0	0	0	0	0	0
	$\omega\omega \to \omega\phi$	0	0	0	0	0	0	0	0	0	0	0	0	0	0
	$\omega\omega \to \phi\phi$	0	0	0	0	0	0	0	0	0	0	0	0	0	0
	$\omega\phi \to \omega\phi$	0	0	0	0	0	0	0	0	0	0	0	0	0	0
	$\omega\phi \to \phi\phi$	0	0	0	0	0	0	0	0	0	0	0	0	0	0
	$\phi\phi \to \phi\phi$	0	0	0	0	0	0	0	0	0	0	0	0	0	0
$(0,1)$	$\rho\rho \to \rho\rho$	-2	4	-2	0	0	0	2	0	0	0	-4	0	0	0
	$\rho\rho \to K^*\bar{K}^*$	-1	2	0	-1	0	0	0	1	0	0	-2	0	0	0
	$\rho\rho \to \rho\omega$	0	0	0	0	0	0	0	0	0	0	0	0	0	0
	$\rho\rho \to \rho\phi$	0	0	0	0	0	0	0	0	0	0	0	0	0	0
	$K^*\bar{K}^* \to K^*\bar{K}^*$	0	1	$\frac{1}{2}$	0	$-\frac{1}{2}$	-1	0	0	0	0	-1	0	0	0
	$K^*\bar{K}^* \to \rho\omega$	$\frac{1}{\sqrt{2}}$	0	0	$-\frac{1}{\sqrt{2}}$	0	0	0	$-\frac{1}{\sqrt{2}}$	0	0	0	0	0	0
	$K^*\bar{K}^* \to \rho\phi$	-1	0	0	1	0	0	0	1	0	0	0	0	0	0
	$\rho\omega \to \rho\omega$	0	0	0	0	0	0	0	0	0	0	0	0	0	0
	$\rho\omega \to \rho\phi$	0	0	0	0	0	0	0	0	0	0	0	0	0	0
	$\rho\phi \to \rho\phi$	0	0	0	0	0	0	0	0	0	0	0	0	0	0
$(0,2)$	$\rho\rho \to \rho\rho$	-2	0	2	0	0	0	2	0	0	0	0	0	0	0
$(1,\frac{1}{2})$	$\rho K^* \to \rho K^*$	$\frac{1}{2}$	$\frac{3}{2}$	-2	0	0	0	0	$-\frac{1}{2}$	0	0	0	$-\frac{3}{2}$	0	0
	$\rho K^* \to K^*\omega$	0	$-\frac{\sqrt{3}}{2}$	0	$\frac{\sqrt{3}}{2}$	0	0	0	0	0	0	0	$\frac{\sqrt{3}}{2}$	0	0
	$\rho K^* \to K^*\phi$	0	$\sqrt{\frac{3}{2}}$	0	$-\sqrt{\frac{3}{2}}$	0	0	0	0	0	0	0	$-\sqrt{\frac{3}{2}}$	0	0
	$K^*\omega \to K^*\omega$	$-\frac{1}{2}$	$\frac{1}{2}$	0	0	0	0	0	$\frac{1}{2}$	0	0	0	$-\frac{1}{2}$	0	0
	$K^*\omega \to K^*\phi$	$\frac{1}{\sqrt{2}}$	$-\frac{1}{\sqrt{2}}$	0	0	0	0	0	$-\frac{1}{\sqrt{2}}$	0	0	0	$\frac{1}{\sqrt{2}}$	0	0
	$K^*\phi \to K^*\phi$	-1	1	0	0	0	0	0	1	0	0	0	-1	0	0
$(0,\frac{3}{2})$	$\rho K^* \to \rho K^*$	-1	0	1	0	0	0	0	1	0	0	0	0	0	0
$(2,0)$	$K^*K^* \to K^*K^*$	0	0	$-\frac{3}{2}$	0	$\frac{1}{2}$	1	$\frac{3}{2}$	0	$-\frac{1}{2}$	-1	0	0	0	0
$(2,1)$	$K^*K^* \to K^*K^*$	-2	0	$\frac{1}{2}$	0	$\frac{1}{2}$	1	$\frac{1}{2}$	0	$\frac{1}{2}$	1	0	0	0	0

with $\lambda(a,b,c) = a^2 + b^2 + c^2 - 2ab - 2bc - 2ac$ the Källén function. A projection for a u-channel can be obtained from eq. (4.51) by the crossing symmetry $p_3 \leftrightarrow p_4$. The locations of the left-hand branch points of the partial wave amplitudes depend on the channel. In an algebraic method of unitarization, e.g. on-shell factorization of Bethe-Salpeter equation, an unphysical left-hand cut of a given channel is transported into other channels as long as the transition amplitude is non-vanishing. As a result, all left-hand cuts are retained in all processes for a coupled-channel via the determinant. In general, the presence of left-hand cuts is not fatal as long as all left-hand cuts are located below the lowest threshold. The associated poles are reliable unless they are located sufficiently near left-hand cuts. However, once a left-hand branch point is located above the lowest threshold, the algebraic approach start to be problematic. Unfortunately, it happens in our case and an improved unitarization has to be used to investigate the possible dynamically generated resonances and bound states.

On-shell factorization of the Bethe-Salpeter equation

When we use the BSE, eq. (4.22) to obtain the unitary partial wave amplitude, $G(s)$ can be written for two different masses as

$$G_i(s) = i \int \frac{d^4q}{(2\pi)^4} \frac{1}{(q^2 - M_1^2 + i\epsilon)((P-q)^2 - M_2^2 + i\epsilon)}, \tag{4.52}$$

and its explicit expression in dimensional regularization becomes

$$\begin{aligned} G_i(s) &= \frac{1}{16\pi^2}\Big(a(\mu) + \log\frac{M_1^2}{\mu^2} + \frac{s - M_1^2 + M_2^2}{2s}\log\frac{M_2^2}{M_1^2} + \frac{\sigma}{2s}\big[\log(s - M_2^2 + M_1^2 + \sigma) \\ &\quad - \log(-s + M_2^2 - M_1^2 + \sigma) + \log(s + M_2^2 - M_1^2 + \sigma) - \log(-s - M_2^2 + M_1^2 + \sigma)\big]\Big), \end{aligned} \tag{4.53}$$

with

$$\sigma = \sqrt{(s - (M_1 + M_2)^2)(s - (M_1 - M_2)^2)} \tag{4.54}$$

and $a(\mu)$ is a renormalization scale μ-dependent subtraction constant. The subtraction constant $a(\mu)$ depends on the quantum numbers S and J, but not on I due to the isospin symmetry.

When we use the cutoff regularization, we obtain two different particle version of eq. (4.26):

$$\begin{aligned} G_i^c(s) &= \frac{1}{32\pi^2}\Big\{ -\frac{\Delta}{s}\log\frac{M_1^2}{M_2^2} + \frac{\sigma}{s}\Big[\log\frac{s - \Delta + \sigma\sqrt{1 + \frac{M_1^2}{q_{\max}^2}}}{-s + \Delta + \sigma\sqrt{1 + \frac{M_1^2}{q_{\max}^2}}} + \log\frac{s + \Delta + \sigma\sqrt{1 + \frac{M_2^2}{q_{\max}^2}}}{-s - \Delta + \sigma\sqrt{1 + \frac{M_2^2}{q_{\max}^2}}}\Big] \\ &\quad + 2\frac{\Delta}{s}\log\frac{1 + \sqrt{1 + \frac{M_1^2}{q_{\max}^2}}}{1 + \sqrt{1 + \frac{M_2^2}{q_{\max}^2}}} - 2\log\Big[\Big(1 + \sqrt{1 + \frac{M_1^2}{q_{\max}^2}}\Big)\Big(1 + \sqrt{1 + \frac{M_2^2}{q_{\max}^2}}\Big)\Big] + \log\frac{M_1^2 M_2^2}{q_{\max}^4}\Big\}, \end{aligned} \tag{4.55}$$

with $\Delta = M_2^2 - M_1^2$. In this section, to investigate the dependence of the associated pole on the cutoff, we employ the values $q_{\max} = 0.775$ GeV, 0.875 GeV and 1.0 GeV successively as in previous works [115, 116] and as in the last section.

Before unitarizing the amplitudes, we first investigate the left-hand cuts of amplitudes to make sure that the they are located lower than the right-hand branch point (the lowest right-hand branch point for coupled-channels). The coupling constant $g = \frac{M_V}{2f_\pi} = 4.596$ is evaluated with the average mass of vectors and $f_\pi = 92.4$ MeV. The locations of the left-hand branch points can be easily calculated by making use of eq. (4.51) and (4.50). For the channel $(S, I) = (0, 0)$, while the lowest threshold is $2M_\rho = 1.550$ GeV, the left-hand cuts start from 1.606 GeV and 1.602 GeV for t-channel ρ- and ω-exchange diagrams, respectively, for $K^*\bar{K}^* \to K^*\bar{K}^*$, see e.g. in fig. 4.14. In addition, the left-hand branch points are located at 1.558 GeV and 1.673 GeV for $K^*\bar{K}^* \to \omega\phi$ and $\phi\phi$, respectively, which are above the $\rho\rho$ threshold. The overlap of the left-hand cut and right hand cut makes the coupled-channel unitarization, (3.99), problematic. Therefore associated poles become problematic as well. A naive use

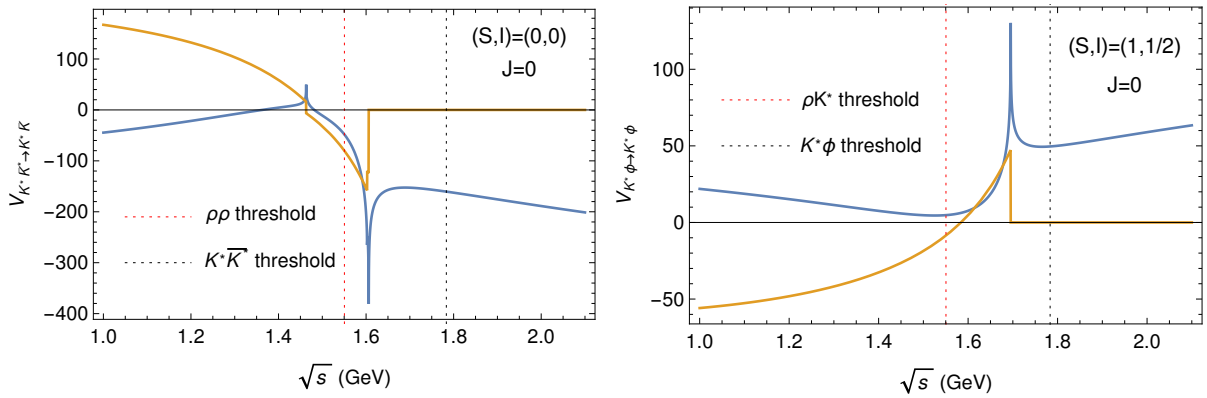

Figure 4.14: S-wave potentials for $K^*\bar{K}^* \to K^*\bar{K}^*$ with $(S, I, J) = (0, 0, 0)$ and $K^*\phi \to K^*\phi$ with $(S, I, J) = (1, 1/2, 0)$ for our calculation (real part: blue line, imaginary part: yellow line). The corresponding threshold and the lowest threshold for coupled-channels are represented by the black and red dotted lines, respectively.

of eq. (3.99) to the coupled-channel leads to a branch cut along the whole real axis. The pole found in the single channel below the $\rho\rho$ threshold is not reproduced in the coupled-channel case, see in fig. 4.15, where the determinant for the single $\rho\rho$ channel and the coupled-channel cases are plotted with the cutoff $q_{\max} = 0.875$ GeV. It confirms the invalidation of eq. (3.99) for coupled-channel with the overlap of the left- hand and right-hand cut.

The overlap of the left-hand cut and the right-hand cut is present for all the coupled-channels, i.e. $(S, I) = (0, 1)$ and $(1, 1/2)$, see e.g. in fig. 4.14. For the $(S, I) = (0, 1)$, the left-hand cuts start from 1.606 GeV and 1.554 GeV for $K^*\bar{K}^* \to K^*\bar{K}^*$ and $K^*\bar{K}^* \to \rho\phi$, respectively, which are located above the lowest threshold, i.e. $2M_\rho = 1.551$ GeV. The lowest threshold for the channel $(S, I) = (1, 1/2)$ is 1.667 GeV, while the left-hand branch point of $K^*\phi \to K^*\phi$ is located at 1.689 GeV. It is worth mentioning, however, that not all the left-hand cuts are present for all partial-wave projected amplitudes. For some angular momenta J, the partial wave amplitude vanishes. In particular, for $(S, I, J) = (0, 0, 1)$, the only non-vanishing potential is for $K^*\bar{K}^* \to K^*\bar{K}^*$, such that it reduces to a single-channel with the threshold 1.783 GeV, above the corresponding left-hand cuts. As a result, the unitarization formula (3.99) can be employed in this case.

In the $SU(3)$ case, we are only interested in pole structures of the unitarized amplitudes. Poles located on the physical Riemann sheets are associated with possible bound states, and those on the unphysical sheets are associated to possible resonances (including virtual states), see sec.3.2.2. Each loop function $G_i(s)$ has two Riemann sheets: the first/physical and the second/unphysical sheets, denoted as $G_i^I(s)$ and

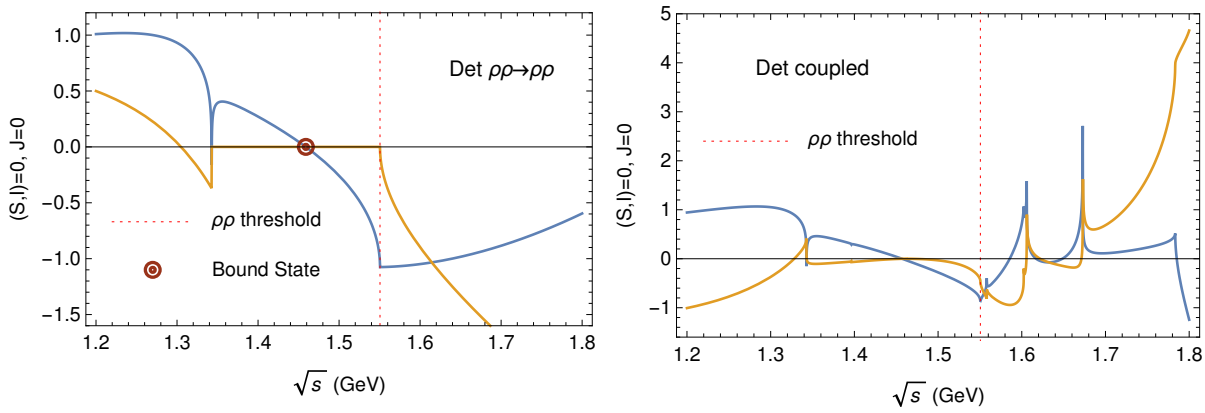

Figure 4.15: The determinant of the unitarized amplitudes for the single channel ($\rho\rho$) and the coupled-channel evaluated with the cutoff 0.875 GeV (real part: blue line, imaginary part: yellow line). Note that no pole is reproduced below the $\rho\rho$ threshold.

$G_i^{\rm II}(s)$, respectively. Different sheets can be characterized by the sign of the imaginary part of the loop function on the right hand cut. The expression in eq. (4.53) and (4.55) define the physical Riemann sheet, while the expression for the second sheet can be obtained by analytic continuation via, cf eq. (3.62)

$$G_i^{\rm II}(s+i\epsilon) = G_i^I(s+i\epsilon) - 2i\ {\rm Im}\ G_i^I(s+i\epsilon). \tag{4.56}$$

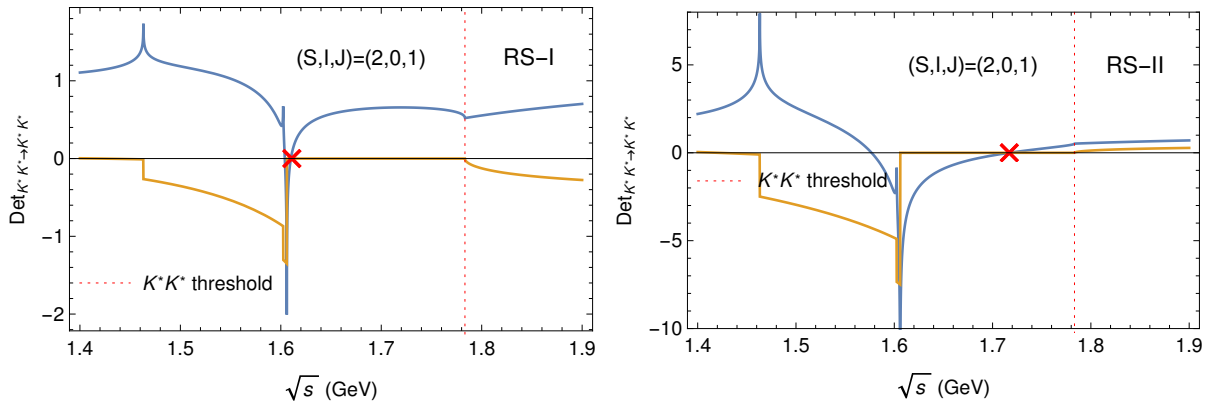

Figure 4.16: The determinant of $K^*K^* \to K^*K^*$ with $(S,I,J) = (2,0,1)$ on the real axis of physical sheet (RS-I) and unphysical sheet (RS-II). The artificial pole due to the unphysical left-hand cut is denoted by the red cross.

In this part, we focus on the single-channels, i.e. $(S,I) = (0,2), (1,3/2), (2,0), (2,1)$ with $J = 0,1,2$ and $(S,I,J) = (0,0,1)$. For channel $(S,I) = (0,2), (1,3/2)$ and $(2,1)$, no pole is found on both physical and unphysical sheets. For the $(S,I) = (2,0)$, only the system with $J = 1$ survives under the partial-wave projection. A pole located at 1.613 GeV (calculated with the cutoff $q_{\rm max} = 0.875$ GeV), lower than the K^*K^* threshold 1.783 GeV, is found on the physical Riemann sheet, see e.g. in fig. 4.16. It is naively expected to be associated with a bound state of K^*K^*. However, inspection of the pole position shows

that its existence is attributed to the presence of the left-hand cut, starting from 1.606 GeV, which is very close to the pole position. The left-hand cut is the result of the on-shell approximation, and should be absent in a complete solution of Bethe-Salpeter equation (at least in the determinant). In addition, the N/D method shows that the determinant of the unitarized amplitude is free of any left-hand cut. In fig. 4.16, it is easy to see that the zero point of the determinant, denoted by the red cross, which is identified as the pole of the amplitude is caused by the sharp dip due to the left-hand cut of t- and u-channel ρ-exchange diagrams. In this respect, the presence of the pole near the left-hand cut is just an artifact of the unitarization formula (3.99) that treats the left-hand cut perturbatively. Furthermore, a pole at 1.724 GeV is found on the second Riemann sheet. However, from the fig. 4.16, it may be a remnant of the dynamic singularity.

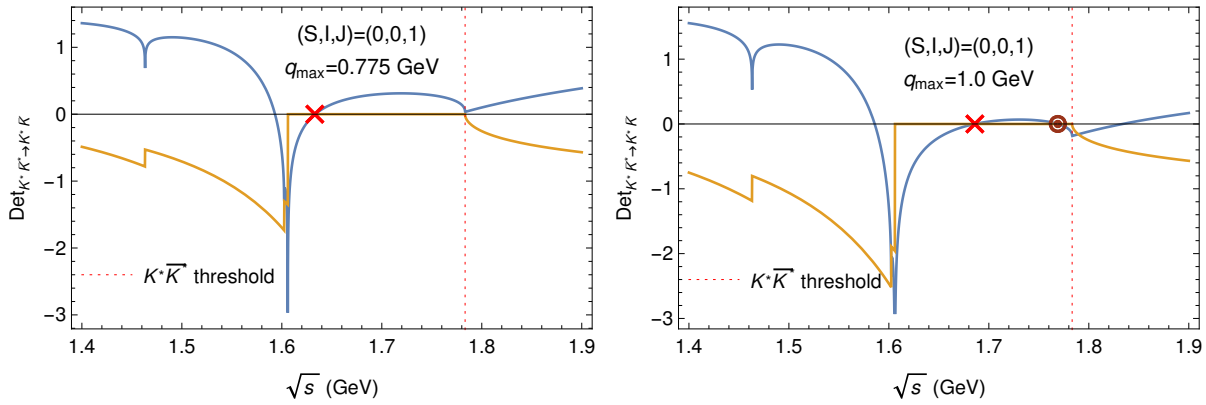

Figure 4.17: The determinant of $K^*\bar{K}^* \to K^*\bar{K}^*$ with $(S, I, J) = (0, 0, 1)$ on the real axis with the cutoff $q_{\max} = 0.775$ GeV and 1.0 GeV, respectively. The artificial pole is denoted as a red cross and the pole associated with a bound state is denoted as a ring.

The same situation can be found in the channel $(S, I, J) = (0, 0, 1)$ as well, see e.g. in fig. 4.17. Besides a pole near the left-hand cut, however, with the cutoff $q_{\max} = 0.875$ GeV, an additional pole at 1.782 GeV which is very close to the threshold 1.783 GeV is found. This pole is subtle since its position and its presence is sensitive to the cutoff we use. As the cutoff increases, the pole position moves deeper below the threshold, while if we decrease the cutoff the pole moves towards the threshold and at $q_{\max} = 0.808$ GeV, the pole disappears on the first Riemann sheet and shows up on the second sheet as a virtual state (on the real axis below the threshold). The determinants are plotted in fig. 4.17 with cutoff $q_{\max} = 0.775$ and 1.0 GeV, respectively. The situation for the pole near the threshold on the first Riemann sheet and on the second sheet are shown in fig. 4.18. For different choices of the cutoff, the pole shows itself either as a bound state or a virtual state near the threshold. The dependence of the pole on the coupling constant g is motivated by its sensitivity to the cutoff. As a comparison, we study the pole using the coupling evaluated at $g_2 = 2M_\rho/f_\pi = 4.168$. The pole is found on the second Riemann sheet for each cutoff $q_{\max} = 0.775$, 0.875 and 1.0 GeV. It turns to be a virtual state at $q_{\max} = 1.033$ GeV. A comparison of different choices of the coupling and cutoff can be found in table 4.7. For other channels, pole structures are insensitive to the coupling constant and cutoff. Apart from poles located close to the left-hand cut and thus are ruled out, results for single-channels in this section are consistent with the result of ref. [116] where a pole at $1.802 - 0.078i$ GeV is reported which corresponds to the pole in

table 4.7 [10]. It is expected since this pole is very close to the corresponding threshold and the extreme non-relativistic approximation works without a problem.

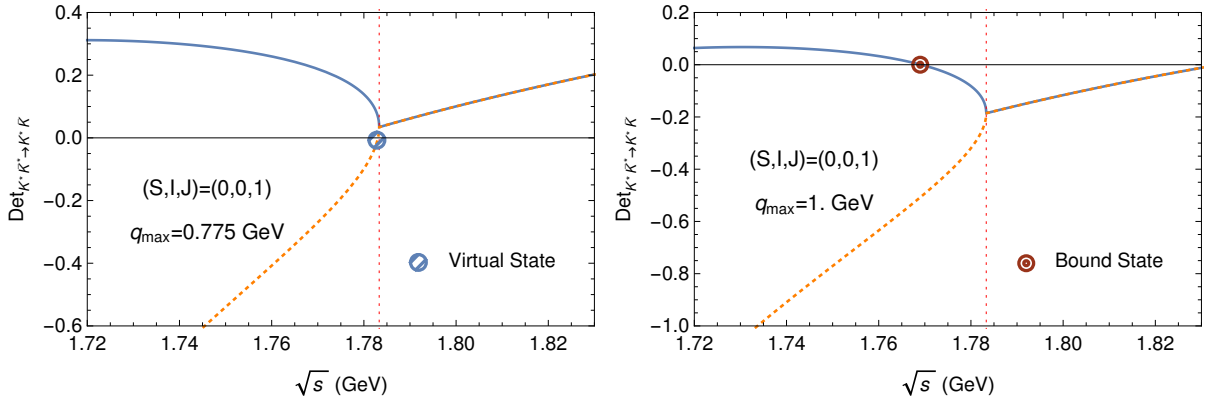

Figure 4.18: The part part of the determinant of $K^*\bar{K}^* \to K^*\bar{K}^*$ with $(S, I, J) = (0, 0, 1)$ on the real axis of the first (blue line) and the second Riemann sheet (yellow dotted line) with the cutoff $q_{\max} = 0.775$ GeV and 1.0 GeV, respectively.

Table 4.7: Pole positions (in GeV) evaluated with different cutoffs $q_{\max}$ (in GeV) and couplings. The subscript B and V stand for bound state and virtual state, respectively.

$(S, I, J) = (0, 0, 1)$	$q_{\max} = 0.775$	$q_{\max} = 0.875$	$q_{\max} = 1.0$
$g = 4.596$	1.783_{V}	1.782_{B}	1.769_{B}
$g = 4.168$	1.774_{V}	1.779_{V}	1.783_{V}

4.3.2 First iterated solution of the N/D method

In general, the overlap of the artificial unphysical cut and the right-hand cut breaks the unitarity and analyticity, and thus leads to the invalidation of the unitarization formula (3.99). One way to avoid this problem is to employ the N/D method [109, 156, 158, 185] to the coupled-channel systems, see sec. 3.4.3.

For the first iterated solution, see eq. (4.40) and for the matching condition eq (4.41). If we extend this to coupled channels, we have

$$N(s)_{ij} = V(s)_{ij}, \tag{4.57}$$

$$D(s)_{ij} = \gamma_{0ij} + \gamma_{1ij}(s - s^i_{\mathrm{thr}}) + \frac{1}{2}\gamma_{2ij}(s - s^i_{\mathrm{thr}})^2 + \frac{(s - s^i_{\mathrm{thr}})s^2}{\pi}\int_{s^i_{\mathrm{thr}}}^{\infty} ds' \frac{\rho(s')_i V(s')_{ij}}{(s' - s^i_{\mathrm{thr}})(s' - s)s'^2},$$

with γ the subtraction constants and the subscript i and j the channel indices whereas matching conditions

[10] Notice that the pole position has an imaginary part in ref. [116] due to the convoluted propagators in loop functions.

has the form

$$\gamma_{0ij} + \gamma_{1ij}(s - s^i_{\rm thr}) + \frac{1}{2}\gamma_{2ij}(s - s^i_{\rm thr})^2 = -g_i(s)V(s)_{ij} - \frac{(s - s^i_{\rm thr})s^2}{\pi}\int_{s^i_{\rm thr}}^{\infty} ds' \frac{\rho(s')_i V(s')_{ij}}{(s' - s^i_{\rm thr})(s' - s)s'^2}$$
$$\equiv w(s)_{ij}, \tag{4.58}$$

where the contributions of $O((s - s_{\rm thr})^3)$ is neglected. The subtraction constants depend on the cutoff $q_{\rm max}$ via the matching conditions (4.58). Note that for each scattering process, the left-hand branch point associated with the t- and u-channel diagrams are located lower than its own threshold, although they may be above the lowest threshold with the same quantum numbers.

The continuation of D function to the second Riemann sheet has the form [11]

$$D^{\rm II}(s)_{ij} = \gamma^{\rm II}_{0ij} + \gamma^{\rm II}_{1ij}(s - s^i_{\rm thr}) + \frac{1}{2}\gamma^{\rm II}_{2ij}(s - s^i_{\rm thr})^2 - \frac{(s - s^i_{\rm trh})s^2}{\pi}\int_{s^i_{\rm thr}}^{\infty} ds' \frac{\rho(s')_i V(s')_{ij}}{(s' - s^i_{\rm thr})(s' - s)s'^2}. \tag{4.59}$$

Likewise, the subtraction constants $\gamma^{\rm II}$s can be determined by matching

$$\gamma^{\rm II}_{0ij} + \gamma^{\rm II}_{1ij}(s - s^i_{\rm thr}) + \frac{1}{2}\gamma^{\rm II}_{2ij}(s - s^i_{\rm thr})^2 = -g^{\rm II}_i(s)V(s)_{ij} + \frac{(s - s^i_{\rm thr})s^2}{\pi}\int_{s^i_{\rm thr}}^{\infty} ds' \frac{\rho(s')_i V(s')_{ij}}{(s' - s^i_{\rm thr})(s' - s)s'^2}$$
$$\equiv w^{\rm II}(s)_{ij}. \tag{4.60}$$

In this way, we have

$$\gamma^{\rm (II)}_{0ij} = w^{\rm (II)}(s_{\rm thr})_{ij},$$
$$\gamma^{\rm (II)}_{1ij} = w^{\rm (II)\prime}(s^i_{\rm thr})_{ij},$$
$$\gamma^{\rm (II)}_{2ij} = w^{\rm (II)\prime\prime}(s^i_{\rm thr})_{ij}. \tag{4.61}$$

The Obtained D functions have the correct analytical properties on both the first and second Riemann sheets, see e.g. in fig. 4.21, where the associated zero points correspond to possible dynamically generated resonances or bound states. For comparison, the real parts of the determinants of N/D and of (3.99), denoted by $\mathrm{Det}_{N/D}$ and Det_U respectively, are ploted in fig. 4.21.

Single-channels

In this section, we first consider single-channels. In the N/D method, the determinant of amplitudes is free of any unphysical cut. Thus, it is expected that the poles, due to the presence of left-hand cuts found in the unitarization formula, see e.g. in Figs. 4.16 and 4.17, should be absent in the N/D method. It is the case for the pole on the first Riemann sheet, see e.g. 4.16, in channel $(S, I, J) = (2, 0, 1)$, see in fig. 4.19. For $(S, I, J) = (0, 0, 1)$, the pole on the first Riemann sheet is found much deeper than that in BSE, see in fig. 4.19. It stems from the matching condition (4.58) where the contribution from t- and u-channel diagrams still play a role to let the determinant eventually to vanish at some point. The position of this pole dramatically depends on the coupling and the cutoff we use and much below the threshold. Therefore, these strongly indicate that it is an artificial pole due to the perturbative treatment of the left-hand cut. However, the pole on the second Riemann sheet for $(S, I, J) = (2, 0, 1)$ is changed

[11] The usual continuation $T^{\rm II}(s) = \dfrac{1}{(\frac{N}{D})^{-1} - 2i\rho}$ would introduce unexpected left-hand cuts into unphysical Riemann sheets.

barely. The fig. 4.20 indicates that the formation of the virtue state stems from the t- and u-channel diagrams via the matching condition (4.58). The pole corresponding to either a bound state or virtual state in channel $(S, I, J) = (0, 0, 1)$, which is close to the threshold, changes barely. It is not a surprise since the difference between the two methods is of $O((s - s_{\text{thr}})^3)$.

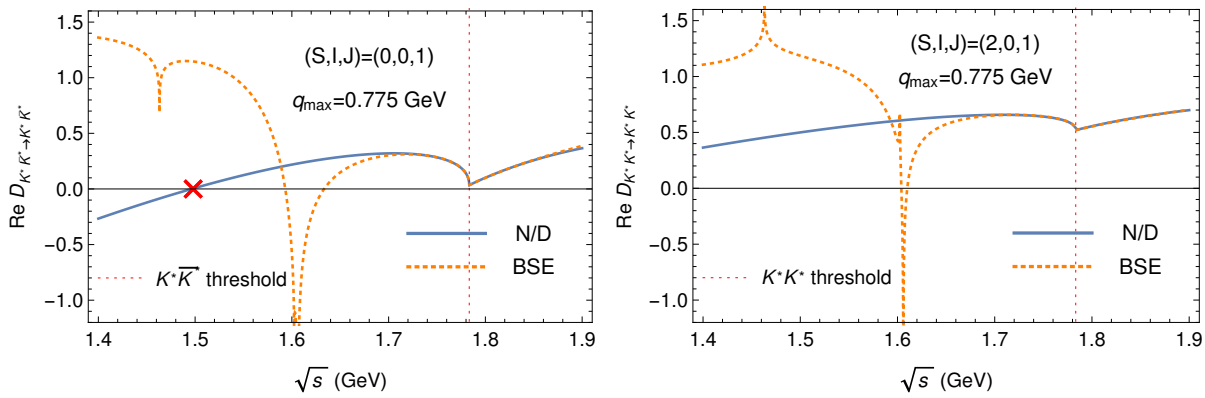

Figure 4.19: The real part of the determinant of $(0, 0, 1)$ and $(2, 0, 1)$ based on the N/D and algebraic approximation of BSE. The pole due to the left-hand cut is absent for $(2, 0, 1)$, and is moved to very deep (around 1.49 GeV) below the threshold where the matching (4.58) applicability is in question.

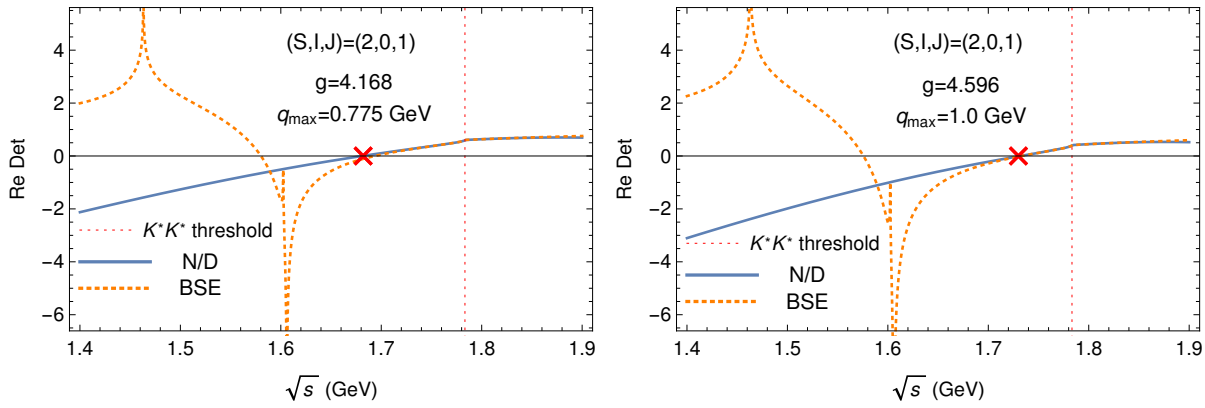

Figure 4.20: The real part of the determinant on the second Riemann sheet of $(2, 0, 1)$ based on the N/D and BSE.

Apart from above poles, additional poles are found on the second Riemann sheet for channels $(S, I, J) = (0, 2, 2)$, $(1, 3/2, 2)$ and $(2, 1, 2)$, which are absent in the algebraic approximation of the BSE, see e.g. table 4.8. All of them are located on the unphysical Riemann sheet in the tensor sector. An inspection shows that the discrepancy stems from the badly matching of eq. (4.58) far away from the threshold on the second Riemann sheet in the corresponding channels. The matching condition eq. (4.58) works well sufficiently for the $J = 0$ and $J = 1$ channel. However, for the tensor sector, the matching is much worse, especially for the second Riemann sheet, see e.g. in Figs. 4.21 and 4.22, where the Det_U represents the determinant of eq. (3.99). The poles in table 4.8 are located around 0.3 GeV away from their threshold, and thus beyond the reliability. As a consequence, we do not relate these poles to physical

resonances.

Table 4.8: The pole positions (in GeV) on the second Riemann sheet evaluated with $g = 4.596$ and $q_{\max} = 0.875$ GeV for the first iterated solution of the N/D method.

Channel	Process	Threshold [GeV]	Pole position [GeV]
$(S, I, J) = (0, 2, 2)$	$\rho\rho \to \rho\rho$	1.55	$1.73 \pm 0.21i$
$(S, I, J) = (1, 3/2, 2)$	$\rho K^* \to \rho K^*$	1.67	$1.85 \pm 0.21i$
$(S, I, J) = (2, 1, 2)$	$K^* K^* \to K^* K^*$	1.78	$1.97 \pm 0.22i$

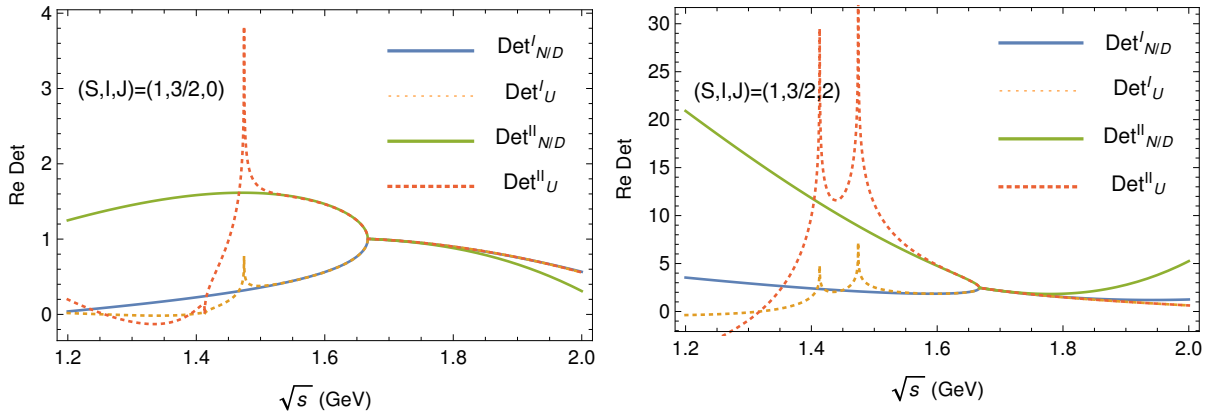

Figure 4.21: The real part of the determinant of channel $(S, I, J) = (1, 3/2, 0)$ and $(1, 3/2, 0)$ on the first and second Riemann sheet evaluated with the cutoff $q_{\max} = 0.875$ GeV. The superscript I and II indicate on which Riemann sheet are plotted, and the subscript denotes the unitarization formula.

Coupled-channels

The bound state in channel $(S, I, J) = (0, 0, 0)$, which is absent in the BSE, is obtained in the coupled-channel version, see in fig. 4.23. It is consistent with the extreme non-relativistic limit in ref. [116] and with results of the previous section. One may wonder the reliability of this pole since it is deeply below the $\phi\phi$ threshold where the $D(s)_{55}$ is matched via eq. (4.58). To show that this pole is reasonable, we calculate its residues which stand for its coupling to various channels. They are defined as

$$T_{ij} = \frac{g_i g_j}{s - s_{\text{pole}}}, \tag{4.62}$$

with i the channel index and g_i is the effective coupling to channel i. A calculation shows that the coupling of the bound state to the $\rho\rho$ channel dominates and the channels with higher thresholds are negligible. In addition, a pole located at $1.68 \pm 0.02i$ GeV is found on an unphysical Riemann sheet which is associated to a possible resonances. It corresponds to the pole $1.726 \pm 0.028i$ GeV which is assigned to $f_0(1710)$. It is not surprising since the channel $K^* \bar{K}^*$ dominates whose threshold is close to the pole position and thus the non-relativistic limit makes sense. It is worth stressing that its position largely

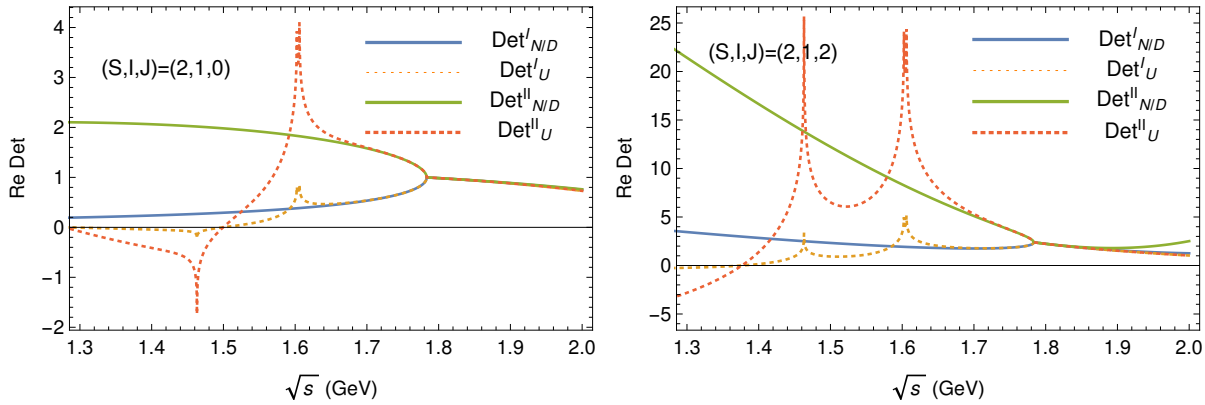

Figure 4.22: The real part of the determinant of channel $(S, I, J) = (2, 1, 0)$ and $(2, 1, 0)$ on the first and second Riemann sheet evaluated with the cutoff $q_{\max} = 0.875$ GeV. The superscript I and II indicate on which Riemann sheet are plotted, and the subscript denotes the unitarization formula.

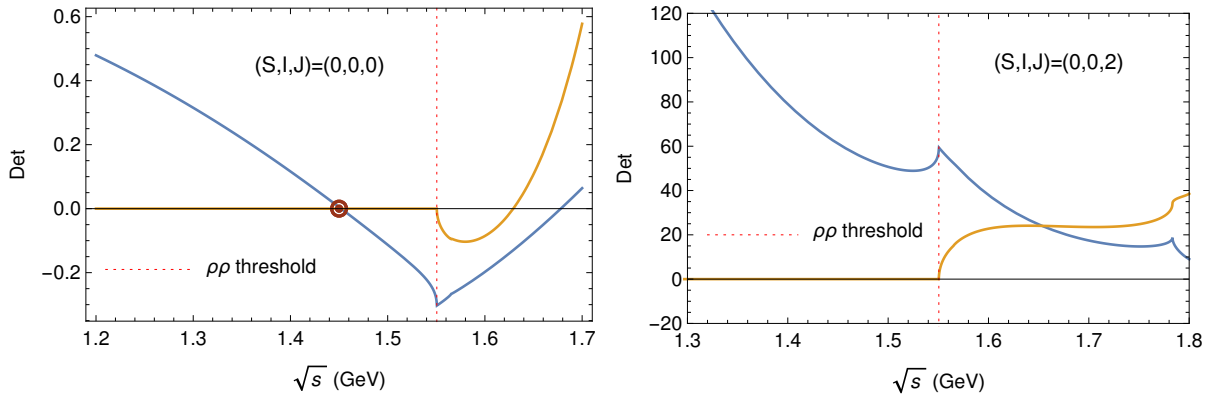

Figure 4.23: The determinant of channel $(S, I, J) = (0, 0, 0)$ and $(0, 0, 2)$ on the first Riemann sheet evaluated with the cutoff $q_{\max} = 0.875$ GeV.

depends on the coupling and cutoff. So far, the scalar and vector sectors of $(S, I) = (0, 0)$ are consistent with the non-relativistic result in ref. [116]. In ref. [116], two bound states, assigned to $f_2(1270)$ and $f_2'(1525)$, are reported in the tensor sector. However, no bound state is found in this channel fig.4.23, which agrees with the SU(2) relativistic result in the previous section. Instead, a resonance located at $1.93 \pm 0.15i$ GeV is found. As discussed in section 4.3.2, the matching condition (4.58) does not work very well on the unphysical Riemann sheet for the tensor sectors. From table 4.9, it is easy to see that all poles in the tensor sector are found on the unphysical Riemann sheet, in particular for the dominating channel. The relative distant positions of the poles from thresholds (of the dominating channels) indicate that these poles are "artificial". Hence, we do not relate them to physical resonances. For the channel $(S, I) = (1, 1/2)$, a pole around 1.64 GeV is found, see e.g. table 4.9, which corresponds to the bound state at $1.643 \pm 0.047i$ GeV in ref. [116] [12]. However, the bound state in the tensor sector reported in ref. [116] is not found in this work, see e.g. fig. 4.24.

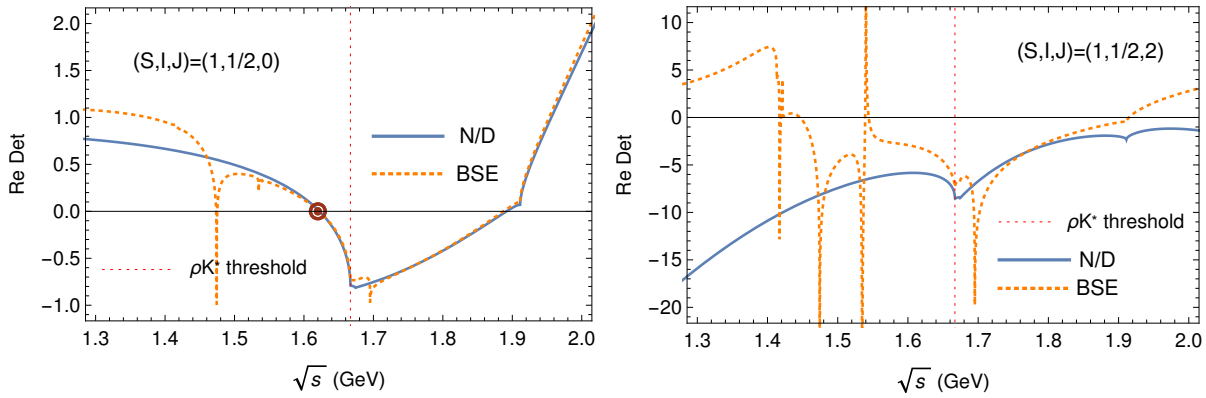

Figure 4.24: The real part of the determinant of channels $(S, I, J) = (1, 1/2, 0)$ and $(1, 1/2, 2)$ on the physical Riemann sheet evaluated with the cutoff $q_{\max} = 0.875$ GeV. A bound state is found in the scalar sector for the first iterated solution of N/D, while no bound state is there in the tensor sector.

To investigate the dependence of the pole position on the coupling and cutoff, we search the poles with different choices of g and $q_{\max}$. A list of the poles in the region we are interested in is given in table 4.9. Resonances in the scalar and vector sectors having small width is due to that we neglect the width of ρ and K^*. A convolution of G functions over the mass distribution of vector mesons will give a width to bound states and resonances related to the $\rho \to \pi\pi$ and $K^* \to \pi K$ decays. In addition, box diagrams with four intermediate pseudoscalars give a width to resonances/bound states due to decaying to two pseudoscalars [115, 116]. However, to that end, we have to introduce model-dependent form factors and the width strongly depends on the cutoff we use in form factors. However, the real part of pole positions is merely affected. In this section, only the possible dynamically generated resonances are considered. Thus, we will not introduce the convolution of loop functions and the box diagrams to broaden the width of resonances, which is sensitive to form factors.

4.3.3 Summary and conclusions

We have briefly reviewed the $\rho\rho$ interaction and the dynamically generated resonances with the conclusion that the disappearance of the tensor bound state in the non-relativistic formalism [115] stems from missing

[12] Note that the imaginary part corresponding to the width is due to the convolution of the loop functions in ref. [116].

Table 4.9: The pole positions (in GeV) evaluated with different choice of coupling and cutoff for coupled-channels. Here $g_1 = 4.596$ and $g_2 = 4.168$, and $q_{\rm max1,2,3} = 0.775$, 0.875 and 1.0 GeV, respectively. Only poles located on the physical sheet and unphysical sheet connected to the physical one are listed. The dominating channels (DCs) are listed in the second column. The subscript B and V stand for bound state and virtual state, respectively.

(S, I, J)	DC	$g_1, q_{\rm max1}$	$g_1, q_{\rm max2}$	$g_1, q_{\rm max3}$	$g_2, q_{\rm max1}$	$g_2, q_{\rm max2}$	$g_2, q_{\rm max3}$
$(0, 0, 0)$	$\rho\rho$	1.47_B	1.44_B	1.41_B	1.50_B	1.48_B	1.45_B
	$K^*\bar{K}^*$	$1.68 \pm 0.02i$	$1.63 \pm 0.02i$	$1.56 \pm 0.01i$	$1.73 \pm 0.02i$	$1.69 \pm 0.02i$	$1.63 \pm 0.02i$
$(0, 0, 2)$	$K^*\bar{K}^*$	$1.93 \pm 0.15i$	$1.92 \pm 0.16i$	$1.91 \pm 0.16i$	$1.93 \pm 0.15i$	$1.92 \pm 0.16i$	$1.91 \pm 0.16i$
$(0, 1, 1)$	$\rho\rho$	1.47_V	1.48_V	1.50_V	1.44_V	1.45_V	1.46_V
$(0, 1, 2)$	$K^*\bar{K}^*$	$1.84 \pm 0.2i$	$1.83 \pm 0.2i$	$1.83 \pm 0.2i$	$1.84 \pm 0.2i$	$1.84 \pm 0.2i$	$1.83 \pm 0.2i$
$(1, 1/2, 0)$	ρK^*	1.64_B	1.62_B	1.58_B	1.66_B	1.65_B	1.63_B
$(1, 1/2, 1)$	ρK^*	$1.89 \pm 0.06i$	$1.88 \pm 0.07i$	$1.86 \pm 0.07i$	$1.92 \pm 0.05i$	$1.88 \pm 0.07i$	$1.88 \pm 0.06i$
$(1, 1/2, 2)$	ρK^*	$1.85 \pm 0.13i$	$1.85 \pm 0.14i$	$1.84 \pm 0.15i$	$1.85 \pm 0.13i$	$1.85 \pm 0.13i$	$1.84 \pm 0.14i$

the important energy-dependence of the potential. To deal with left-hand cut associated with the on-shell factorization, the first iterated solution of the N/D method is employed. Later on, scattering amplitudes between vector mesons are calculated in the hidden local symmetry approach in the SU(3) frame. The partial-wave projection is implemented to scattering amplitudes in order to perform unitarization procedures. The projection for on-shell scattering amplitudes leads to unphysical left-hand cuts, which overlap with the unitarity cut for coupled-channels in an algebraic unitarization, i.e. on-shell factorization of the BSE. However, for single-channels the unitarization is still reliable as long as only the region sufficiently far away from the left-hand cuts is investigated.

In order to avoid left-hand cuts, an improved unitarization, i.e. the first iterated solution of the N/D method, is employed. Without the left-hand cut in the determinant, the method can be applied to coupled-channels as well. An analyses of the pole structure shows that relativistic effects are important when the pole is far away from the threshold. The possible dynamically generated resonances (including bound states) are listed in Table 4.10. Compared to the non-relativistic result [116], bound states in tensor sectors, i.e. $I(J^P) = 0(2^+)$ and $1/2(2^+)$, disappear in the covariant formalism. We stress that the the disappearance of those bound states is due to the contribution from covariant t- and u-channel amplitudes via the matching condition (4.58) performed around the threshold which is far away from the left-hand cuts. For the unphysical Riemann sheet in tensor sectors, the matching only works well in a small region around the threshold. Poles, that are found in those channels with relatively large imaginary parts, are dropped due to the discrepancies between the two unitarization methods.

In this section, the left-hand cut is considered perturbatively. Subtraction constants are determined by matching to the algebraic approximation of the BSE at the threshold. In practice, differences between the two methods is of order $O((s - s_{\rm thr})^3)$, thus the associated poles outside this region is beyond the scope of the method. In fact, the extension to a broader energy region needs higher order effective Lagrangians as well. In addition, the contribution from the large width of ρ and K^* are not considered, as well as the box diagrams with intermediate pseudoscalars. A complete considerations of the meson spectroscopy requires the inclusion of more channels than just vector-vector scatterings. However, this formalism is phenomenologically valuable only to simply investigate the possible dynamically generated resonances due to the vector-vector interactions.

Table 4.10: Only the real parts of the pole positions (in GeV) are listed. Uncertainties are determined by different choices of coupling g=g_1, g_2, and the cutoff $q_{\max}$ = 0.775, 0.875 and 1.0 GeV. The PDG part shows which particle can be identified as the pole and the Mass part shows the estimated mass value of that particle in the PDG [1].

S	$I^G(J^{PC})$	Pole position [GeV]	PDG	Mass[GeV]
0	$0^+(0^{++})$	[1.41 – 1.50]	$f_0(1370)$	[1.2 – 1.5]
	$0^+(0^{++})$	[1.56 – 1.73]	$f_0(1710)$	[1.72 – 1.73]
	$0^-(1^{+-})$	[1.77 – 1.78]	–	–
	$1^+(1^{+-})$	[1.44 – 1.50]	–	–
1	$1/2(0^+)$	[1.58 – 1.66]	–	–
	$1/2(1^+)$	[1.86 – 1.92]	$K_1(1650)$?	[1.62 – 1.72]
2	$0(1^+)$	[1.68 – 1.74]	–	–

Outlook

At the end of each section of the previous chapter, we have summarized and discussed our results. Therefore, instead of listing them once again, we would like to provide a few extra comments on the results and possible future continuations.

We have shown that while a scattering potential is examined for possible bound states or resonances, it is crucial that the form of the potential is examined properly. In the non-relativistic approach, the LHCs of scattering amplitudes are neglected by construction. However, these LHCs are shown to be in the vicinity of some of the poles. These LHCs have a physical meaning. The LHCs start when $t-$ and $u-$channel exchange particles become on-shell. As a result, these LHCs should always be present. Moreover, it was shown in [212] that in low-energy nucleon-nucleon scattering, one-pion exchange (OPE) has the highest contribution to the LHCs and that this contribution exists for energies $s < 4(m_N - m_\pi^2/4)$. If we apply this to the $\rho\rho$ scattering, we get $s < 3m_\rho^2$. This is exactly where the LHCs start in fig. 4.5. Therefore, the LHC contributions should be taken into account for a proper investigation of dynamically generated resonances and bound states. Finally, we have also argued that not only the consideration of LHCs but also the consideration of effective ranges is important for the behaviour of the pole. We did not find any pole in none of the tensor channels unlike in the non-relativistic approach (this can be easily seen in table 4.11). We argued that the reason for this is the effective range, which is the same for both scalar and tensor channels in the non-relativistic calculation, whereas they have opposite signs in our results.

Table 4.11: Only the real parts of the pole positions (in GeV) are listed in the second column. Uncertainties are determined by different choices of coupling g=g_1, g_2, and the cutoff $q_{\max}$ = 0.775, 0.875 and 1.0 GeV. The dominating channels (DC) are listed in the first column. The pole positions II part shows the results of the non-relativistic calculations in [116]. The PDG part shows which particle can be associated with the founded pole and the mass part shows the estimated range of mass value for that particle by the PDG collaboration [1].

DC	$I^G(J^{PC})$	Pole positions [GeV]	Pole positions II [GeV]	PDG	Mass[GeV]
$\rho\rho$	$0^+(0^{++})$	[1.41 – 1.50]	1.51	$f_0(1370)$	[1.2 – 1.5]
$K^*\overline{K}^*$	$0^+(0^{++})$	[1.56 – 1.73]	1.73	$f_0(1710)$	[1.72 – 1.73]
$K^*\overline{K}^*$	$0^-(1^{+-})$	[1.77 – 1.78]	1.80	–	–
$\rho\rho$	$0^+(2^{++})$	–	1.28	$f_2(1270)$	[1.28]
$K^*\overline{K}^*$	$0^+(2^{++})$	–	1.53	$f_2'(1525)$	[1.52 – 1.53]
$K^*\overline{K}^*$	$1^-(0^{++})$	–	1.78	–	–
$\rho\rho$	$1^+(1^{+-})$	[1.44 – 1.50]	1.68	–	–
$K^*\overline{K}^*$	$1^-(2^{++})$	–	1.57	–	–
ρK^*	$1/2(0^+)$	[1.58 – 1.66]	1.64	–	–
ρK^*	$1/2(1^+)$	[1.86 – 1.92]	1.74	$K_1(1650)$	[1.62 – 1.72]
ρK^*	$1/2(2^+)$	–	1.43	$K_2^*(1430)$	[1.42 – 1.43]

If we combine our results (from table 4.10) and the non-relativistic results (from [116]), we get table 4.11. This table shows us that we are able to generate 6 out of 11 poles generated in the non-relativistic method. We can see that 4 out of 5 of these disagreements are in tensor channels.

We are able to associate 3 of the generated poles with some resonances in the PDG. For the $0^+(0^{++})$ channel we can associate two resonances with the poles that we discovered. $f_0(1370)$ is found as a bound state whereas $f_0(1710)$ is found on the unphysical sheet. Even though $f_0(1500)$ is closer to the pole position of the bound state that we discovered, the width of $f_0(1500)$ is too small to be associated with the bound state. We mentioned that the calculated width of states with the consideration of convoluted ρ and box diagrams highly depend on the form factor values. However, the calculated width for this state is at least double the width of $f_0(1500)$. Moreover, the dominant decay mode of $f_0(1370)$ is $\rho\rho$.

There is no associated particle in the PDG in the channel $0^-(1^{+-})$. This channel has the quantum numbers of h_1 and it only includes $K^*\overline{K}^*$ interaction and does not couple to two pseudoscalars (since it is spin 1). Therefore, observation of this state in an experiment is difficult.

The $1^+(1^{+-})$ channel has the quantum numbers of b_1. The pole we found strongly couples to $\rho\rho$ and it is not allowed to couple to two pseudoscalars. There is no associated particle with this pole, but it was proposed in [116] to look at the $\rho\rho$ invariant mass distribution of J/ψ decay.

Lastly, we would like to comment on the $1^+(1^{+-})$ channel. The discovered pole can be associated with the $K_1(1650)$ with overlapping decay widths. There is no observed decay mode to two pseudoscalars in the PDG for this resonance which is in agreement with our calculations.

As a result, we have shown that the chosen unitarization methods should be applied carefully, considering their limitations. Otherwise, they lead to incorrect analytic properties of the scattering amplitudes. Moreover, the overlapping of LHCs with RHCs should be avoided in coupled channel interactions. Hence, we need a unitarization method in which the LHCs can be considered properly. Therefore, a full N/D analysis is crucial to investigate the deep-lying bound-states and other interactions can be investigated as well, depending on the results. E.g. vector octet-baryon octet interactions, vector octet-baryon decuplet interactions.

APPENDIX **A**

Used Conventions and Some Formulas

- Natural units

$$c = \hbar = 1.$$

- Minkowski metric

$$ds^2 = dt^2 - d\mathbf{x}^2\,, \qquad g_{\mu\nu} = \mathrm{diag}(1,-1,-1,-1)\,. \tag{A.1}$$

- Normalization of states and commutator relations

$$|\mathbf{p}\rangle = \sqrt{2p_0}a^\dagger_{\mathbf{p}}|0\rangle\,, \tag{A.2}$$

$$\langle\mathbf{p}|\mathbf{q}\rangle = 2p_0(2\pi)^3\delta^{(3)}(\mathbf{p}-\mathbf{q})\,, \tag{A.3}$$

$$\phi(x) = \int \frac{d^3\mathbf{p}}{(2\pi)^3}\frac{1}{\sqrt{2p_0}}(a^\dagger_{\mathbf{p}}e^{ipx} + a_{\mathbf{p}}e^{-ipx})\,, \tag{A.4}$$

$$\left[a_{\mathbf{p}}, a^\dagger_{\mathbf{q}}\right] = (2\pi)^3\delta^3(\mathbf{p}-\mathbf{q})\,. \tag{A.5}$$

- Fourier transformation

$$f(\mathbf{x}) = \int \frac{d^3k}{(2\pi^3)}e^{i\mathbf{k}\cdot\mathbf{x}}\tilde{f}(\mathbf{k})\,, \tag{A.6}$$

$$\tilde{f}(\mathbf{k}) = \int d^3x e^{i\mathbf{k}\cdot\mathbf{x}}f(x)\,, \tag{A.7}$$

$$\delta^{(3)}(\mathbf{k}-\mathbf{q}) = \int \frac{d^3x}{(2\pi)^3}e^{-i(\mathbf{k}-\mathbf{q})\cdot\mathbf{x}} \tag{A.8}$$

$$f(x) = \int \frac{d^4k}{(2\pi^4)}e^{-ikx}\tilde{f}(k)\,, \tag{A.9}$$

$$\tilde{f}(k) = \int d^4x e^{ikx}f(x)\,, \tag{A.10}$$

$$\delta^{(4)}(k-q) = \int \frac{d^4x}{(2\pi)^4}e^{i(k-q)\cdot x}\,. \tag{A.11}$$

APPENDIX B

Building Blocks and Gauge Invariance of QCD

B.1 Building Blocks of QCD

If we start with eq. (1.12) and check global invariance of $\mathcal{L}_0$, quarks should transform as

$$q_i \rightarrow q'_i = U_{ij} q_j \,, \tag{B.1}$$

where U are unitary matrices, $UU^\dagger = U^\dagger U = 1$. Taking into account the color property of QCD we are left with the special unitary group $SU(3)$ which is the subgroup of $U(3)$. Any unitary matrix can be defined as a Hermitian matrix H in the way that $U = e^{iH}$. Since $U \in SU(3)$, it should satisfy $\det(U) = 1$. If we use $\det e^{iH} = e^{i\mathrm{tr}H}$, we conclude that H must be traceless. Therefore, the generators of $SU(3)$ should be a set of Hermitian and traceless three dimensional matrices with eight independent parameters, denoted by ϵ_a:

$$U(\epsilon_a) = \exp\left(-i \sum_{a=1}^{8} \epsilon_a \frac{\lambda_a}{2}\right). \tag{B.2}$$

Here, λ are Gell-Mann matrices which are traceless and hermitian. They are normalized as

$$\mathrm{tr}(\lambda_a \lambda_b) = 2\delta_{ab}, \tag{B.3}$$

and their commutation relations are:

$$[\lambda_a, \lambda_b] = 2i f_{abc} \lambda_c \tag{B.4}$$

where f_{abc} are anti-symmetric structure constants. These generators are conventionally expressed as

$$\lambda_1 = \begin{pmatrix} 0 & 1 & 0 \\ 1 & 0 & 0 \\ 0 & 0 & 0 \end{pmatrix} \quad \lambda_2 = \begin{pmatrix} 0 & -i & 0 \\ i & 0 & 0 \\ 0 & 0 & 0 \end{pmatrix} \quad \lambda_3 = \begin{pmatrix} 1 & 0 & 0 \\ 0 & -1 & 0 \\ 0 & 0 & 0 \end{pmatrix}$$
$$\lambda_4 = \begin{pmatrix} 0 & 0 & 1 \\ 0 & 0 & 0 \\ 1 & 0 & 0 \end{pmatrix} \quad \lambda_5 = \begin{pmatrix} 0 & 0 & -i \\ 0 & 0 & 0 \\ i & 0 & 0 \end{pmatrix} \quad \lambda_6 = \begin{pmatrix} 0 & 0 & 0 \\ 0 & 0 & 1 \\ 0 & 1 & 0 \end{pmatrix}$$
$$\lambda_7 = \begin{pmatrix} 0 & 0 & 0 \\ 0 & 0 & -i \\ 0 & i & 0 \end{pmatrix} \quad \lambda_8 = \frac{1}{\sqrt{3}} \begin{pmatrix} 1 & 0 & 0 \\ 0 & 1 & 0 \\ 0 & 0 & -2 \end{pmatrix} \quad \lambda_0 = \sqrt{\frac{2}{3}} \begin{pmatrix} 1 & 0 & 0 \\ 0 & 1 & 0 \\ 0 & 0 & 1 \end{pmatrix}$$

where λ_0 is a generator of $U(3)$ and is not an element of $SU(3)$. Their other properties are given as:

$$\begin{aligned} \mathrm{tr}(\lambda_a\lambda_b\lambda_c) &= 2(d_{abc} + if_{abc}), \\ \{\lambda_a, \lambda_b\} &= \frac{4}{3}\delta_{ab}I + 2d_{abc}\lambda_c, \\ f_{abc} &= \frac{1}{4i}\mathrm{tr}([\lambda_a, \lambda_b]\lambda_c), \\ d_{abc} &= \frac{1}{4}\mathrm{tr}(\{\lambda_a, \lambda_b\}\lambda_c). \end{aligned}$$

Here, d_{abc} are totally symmetric structure constants. The anti-symmetric structure constants are given by

abc	123	147	156	246	257	345	367	458	678
f_{abc}	1	$\frac{1}{2}$	$-\frac{1}{2}$	$\frac{1}{2}$	$\frac{1}{2}$	$\frac{1}{2}$	$-\frac{1}{2}$	$\frac{1}{2}\sqrt{3}$	$\frac{1}{2}\sqrt{3}$

whereas, the symmetric ones are given by

abc	118	146	157	228	247	256	338	344
d_{abc}	$\frac{1}{\sqrt{3}}$	$\frac{1}{2}$	$\frac{1}{2}$	$\frac{1}{\sqrt{3}}$	$-\frac{1}{2}$	$\frac{1}{2}$	$\frac{1}{\sqrt{3}}$	$\frac{1}{2}$
abc	355	366	377	448	558	668	778	888
d_{abc}	$\frac{1}{2}$	$-\frac{1}{2}$	$-\frac{1}{2}$	$-\frac{1}{2\sqrt{3}}$	$-\frac{1}{2\sqrt{3}}$	$-\frac{1}{2\sqrt{3}}$	$-\frac{1}{2\sqrt{3}}$	$-\frac{1}{\sqrt{3}}$

To ensure colorless bound states in QCD, quarks and antiquarks should not transform in the same way and color charges should be connected via gauge transformations. Considering these rules, quarks are in the fundamental representation (F) with $a = 1, 2, 3$ whereas gluons are in the adjoint representation (A) with $a = 1, 2, ..., 8$, respectively:

$$t_a^F = \frac{\lambda_a}{2}, \qquad t_a^A = -if_{abc}. \tag{B.5}$$

The commutation relations of these representations define the Lie algebra of $SU(3)$:

$$[t_a, t_b] = if_{abc}t_c. \tag{B.6}$$

B.2 Gauge Invariance

Demanding local gauge invariance, a covariant derivative has to be introduced like in eq. (1.7), but this time we have eight gauge fields $G_{a,\mu}(x)$ rather than a single one.

$$(D^\mu q)_i = \left(\partial^\mu\delta_{ij} + ig_s\sum_{a=1}^{8} G_a^\mu\frac{\lambda_{a,ij}}{2}q_j\right) = ((\partial^\mu + ig_sG^\mu)q)_i \tag{B.7}$$

is the form of the covariant derivative where the second term introduces quark-gluon field interactions with coupling strength g_s and using summation convention, $G_{ij}^\mu = G_a^\mu\frac{\lambda_{a,ij}}{2}$. In order for $(D^\mu q)_i$ to transform like quarks, G_μ should transform as

$$G_\mu \to G'_\mu = U(\epsilon)G_\mu U^\dagger(\epsilon) + \frac{i}{g_s}(\partial_\mu U(\epsilon))U^\dagger(\epsilon). \tag{B.8}$$

Immediately, the infinitesimal transformations of gauge fields can be written as:

$$G_a^\mu \to G'^\mu_a = G_a^\mu + \frac{1}{g_s}\partial^\mu \epsilon_a + f_{abc}\epsilon_b G_c^\mu + O(\epsilon)\,. \tag{B.9}$$

This is more complicated than eq. (1.8). The main reason is the non-abelian property of the Lie algebra of $SU(3)$ caused by the third term of (B.9). This term gives rise to three and four gluon interaction vertices. Again a mass term for vector fields cannot be introduced since it is not invariant under gauge symmetry like in the $U(1)$ case. As in eq. (1.11), we need to introduce kinetic terms for gluon fields to obtain an analogue of the field strength tensor of $U(1)$:

$$[D_\mu, D_\nu] = [\partial_\mu + ig_s G_\mu, \partial_\nu + ig_s G_\nu] =: ig_s F_{\mu\nu}\,. \tag{B.10}$$

The explicit form of $F_{\mu\nu}$ is then:

$$\begin{aligned} F_{a,\mu\nu} &= \partial_\mu G_{a,\nu} - \partial_\nu G_{a,\mu} + ig_s G_{b,\mu} G_{c,\nu} \frac{1}{2}[\lambda_b, \lambda_c]\,, \\ F_{a,\mu\nu} &= \partial_\mu G_{a,\nu} - \partial_\nu G_{a,\mu} - g_s f_{abc} G_{b,\mu} G_{c,\nu}\,, \qquad \text{(B.11)} \\ F_{\mu\nu} &= \partial_\mu G_\nu - \partial_\nu G_\mu + ig_s[G_\mu, G_\nu]\,. \qquad \text{(B.12)} \end{aligned}$$

The transformation of the field strength tensor under $SU(3)$ is

$$F_{\mu\nu} \to F'_{\mu\nu} = U(\epsilon) F_{\mu\nu} U^\dagger(\epsilon)\,. \tag{B.13}$$

With this transformation, all the building blocks of eq. (1.13) are introduced.

B.2.1 Fixing the Gauge

To use perturbation theory, gauge has to be fixed to get rid of the extra degrees of freedom. One of the ways of doing this is to replace the $\mathcal{L}_{\text{QCD}}$ of (1.13) with

$$\mathcal{L}_{\text{QCD}} - \frac{\alpha}{2}(\partial_\mu G_a^\mu)^2 + \mathcal{L}_{\text{ghost}}\,. \tag{B.14}$$

The additional $\mathcal{L}_{\text{ghost}}$ term fixes the affect of gauge fixing term on $\mathcal{L}_{\text{QCD}}$. eq. (B.14) gives us gluon propagator in the form of

$$\Delta_{ab}^{\mu\nu}(k) = \delta_{ab}\frac{-i}{k^2 + i\epsilon}\left(g^{\mu\nu} + \left(\frac{1}{\alpha} - 1\right)\frac{k^\mu k^\nu}{k^2}\right). \tag{B.15}$$

There are different choices for α. The choice of α determines form of the breaking of gauge invariance. However, even though Green functions are gauge-dependent, physical observables are still independent of α. Hence, it does not matter for physical results. The choice of α is usually made which ever simplifies the calculations to be made. One of the most common choice is the Feynman gauge, $\alpha = 1$. With this choice, gluon propagator gets the form of

$$\Delta_{ab}^{\mu\nu}(k) = \delta_{ab}\frac{-ig^{\mu\nu}}{k^2 + i\epsilon}\,. \tag{B.16}$$

APPENDIX C

Noether's Theorem and Spontaneous Symmetry Breaking

C.1 Noether's Theorem

If we consider a scalar field ϕ transform under a chosen representation of a Lie group A, a small transformation of that field is given as

$$\phi \to \phi' = \phi + \delta\phi = \phi + i\theta_a(t^a)\phi\,, \tag{C.1}$$

where θ are some parameters and t are the generators of the chosen representation of A. For example, for $SU(3)$, the representation of the infinitesimal generators are the Gell-Mann matrices. Let us first take into account the case where global transformations are considered, hence θ are spacetime independent. Moreover, we assume the Lagrangian is a function of ϕ and its first derivative $\partial\phi$ only, and vanish on the boundary ∂B. In this case, we can write the action as

$$S[\phi] = \int_B d^4x \mathcal{L}(\phi, \partial\phi)\,, \tag{C.2}$$

and the equations of motion can be obtained by variation principle as

$$\delta S[\phi] = 0\,, \tag{C.3}$$

$$\frac{\partial\mathcal{L}}{\partial\phi} = \partial_\mu \frac{\partial\mathcal{L}}{\partial(\partial_\mu\phi)}\,. \tag{C.4}$$

If the transformation is a symmetry of the action, we have

$$S[\phi] = S[\phi + \delta\phi] \tag{C.5}$$

which is equivalent to

$$\delta\mathcal{L} = 0\,. \tag{C.6}$$

If we neglect terms in θ^2, we can write the variation of the Lagrangian as

$$\begin{aligned}
\delta\mathcal{L} &= \mathcal{L}(\phi', \partial\phi') - \mathcal{L}(\phi, \partial\phi) && \text{(C.7)}\\
&= \frac{\partial\mathcal{L}}{\partial\phi}\delta\phi + \frac{\partial\mathcal{L}}{\partial(\partial_\mu\phi)}\partial_\mu\delta\phi && \text{(C.8)}\\
&= \theta_a\left(-i\frac{\partial\mathcal{L}}{\partial\phi}t^a - i\frac{\partial\mathcal{L}}{\partial(\partial_\mu\phi)}\partial_\mu t^a\right) && \text{(C.9)}\\
&= \theta_a\partial_\mu J^{\mu,a}\,, && \text{(C.10)}
\end{aligned}$$

where we have defined a current density for each transformation as

$$J^{\mu,a} = -i\frac{\partial\mathcal{L}}{\partial(\partial_\mu\phi)}t^a\,. \tag{C.11}$$

From eqs. (C.10) and (C.6), we get

$$\partial_\mu J^{\mu,a} = 0\,. \tag{C.12}$$

This is known as the Noether's theorem which states that for every continuous symmetry of the Lagrangian there is a conserved current.

If we consider the classical level and let charges have continuous values, we can define the charges of the currents as

$$Q^a(t) = \int d\mathbf{x} J^{0,a}\,, \tag{C.13}$$

and applying Noether's theorem and the Gauss theorem we get

$$dQ^a(t)/dt = 0\,. \tag{C.14}$$

As a consequence, the charges of Noether currents are constants of motion.

Let us now consider the local transformations and the the quantum level. For local transformations $\theta \to \theta(x)$, hence eq. (C.9) gets the form

$$\begin{aligned}
\delta\mathcal{L} &= \theta_a(x)\left(-i\frac{\partial\mathcal{L}}{\partial\phi}t^a - i\frac{\partial\mathcal{L}}{\partial(\partial_\mu\phi)}\partial_\mu t^a\right) + (\partial_\mu\theta_a(x))\left(-i\frac{\partial\mathcal{L}}{\partial(\partial_\mu\phi)}t^a\right) && \text{(C.15)}\\
&= \theta_a(x)\partial_\mu J^{\mu,a} + (\partial_\mu\theta_a(x))J^{\mu,a}\,. && \text{(C.16)}
\end{aligned}$$

Now, the divergence of the current gives

$$\begin{aligned}
\partial_\mu J^{\mu,a} &= -i\frac{\partial\mathcal{L}}{\partial\phi}t^a - i\frac{\partial\mathcal{L}}{\partial(\partial_\mu\phi)\partial_\mu t^a} && \text{(C.17)}\\
&= \frac{\partial\delta\mathcal{L}}{\partial\theta_a(x)}\,. && \text{(C.18)}
\end{aligned}$$

If we consider quantum theory and use canonical quantization with the fields and their conjugate momenta $\Pi = \partial\mathcal{L}/\partial(\partial_0\phi)$, their commutation relations for equal time are

$$[\phi_i(\mathbf{x}), \Pi_k(\mathbf{y})] = i\delta^3(\mathbf{x}-\mathbf{y})\delta_{ij} \tag{C.19}$$

and zero otherwise. In this case both $J^{\mu,a}$ and Q^a are operators and obtained from:

$$J^{\mu,a} = -it^a \frac{\partial \mathcal{L}}{\partial(\partial_\mu \phi_i)} \phi_j \,, \tag{C.20}$$

$$Q^a(t) = -i \int d^3\mathbf{x} \Pi_i(x) t^a \phi_j(x) \,. \tag{C.21}$$

By using these equations, we can find the equal time commutation relations for the charge operator:

$$[Q^a, \phi] = -t^a \phi \,, \tag{C.22}$$

$$[Q^a, Q^b] = \frac{t^a_{ij} t^b_{jk} - t^b_{ij} t^a_{jk}}{t^c_{ik}} Q^c \,, \tag{C.23}$$

where the last line can be interpreted as $[Q^a, Q^b] = i f_{abc} Q^C$ with structure constants f_{abc}. If we have conserved current operators, they correspond to time independent charge operators. Hence, these charge operators commute with the Hamiltonian.

C.1.1 Chiral Symmetry and Noether's Theorem in QCD

If we define $U_{L/R} = e^{i\alpha_a t_a} P_{L/R} q \backsimeq 1 + P_{L/R} \delta\alpha_a t_a q + \cdots$, where t_a are the generators of $SU(3)$ ($t_a = \lambda_a/2$), and since $\delta\alpha_a$ is arbitrary we get currents:

$$j^\mu_{L,a} = \bar{q}_L \gamma^\mu t_a q_L \,, \tag{C.24}$$

$$j^\mu_{R,a} = \bar{q}_R \gamma^\mu t_a q_R \,. \tag{C.25}$$

Hence, vector and axial vector currents are

$$j^\mu_{R,a} + j^\mu_{L,a} = V^\mu_a = \bar{q} \gamma^\mu t_a q \tag{C.26}$$

$$j^\mu_{R,a} - j^\mu_{L,a} = A^\mu_a = \bar{q} \gamma^\mu \gamma_5 t_a q \,. \tag{C.27}$$

At tree level, with on-shell external particles ($(\not{p} - m)q = 0$ & $\bar{q}(\not{p} - m) = 0$), we can write the derivatives of these currents as

$$\partial_\mu V^\mu_a \rightarrow q^\mu V_{\mu,a} = (p_1 - p_2)^\mu \bar{q} \gamma_\mu t_a q \tag{C.28}$$

$$= \bar{q}(\not{p}_1 - \not{p}_2) t_a q = (m_1 - m_2) \bar{q} t_a q \,, \tag{C.29}$$

$$\partial_\mu A^\mu_a \rightarrow q^\mu A_{\mu,a} = (m_1 + m_2) \bar{q} t_a q \,. \tag{C.30}$$

$$\tag{C.31}$$

These equations are equivalent to eq. (1.33). Hence, the axial current is conserved only if the quark masses are zero whereas the vector current is conserved in the equal quark mass case as well.

C.2 Symmetry Realization

In the quantum theory, time independent charge operators are guaranteed if the system has a continuous symmetry. These charge operators are the generators of the unitary symmetry group representation U. U commutes with Hamiltonian,

$$UHU^\dagger = H \,. \tag{C.32}$$

C.2.1 Wigner-Weyl Realization

In this case, we say the charge operator annihilates the vacuum, $Q|0\rangle = 0$. Therefore, it remains invariant under the group transformations $U|0\rangle = |0\rangle$. Therefore, this gives us degenerate states ϕ_1 and ϕ_2 when they are related via the symmetry transformation $U\phi_1 U^\dagger = \phi_2$:

$$E_{\phi_2} = \langle\phi_2|H|\phi_2\rangle = \langle 0|\phi_2 H\phi_2^\dagger|0\rangle = \langle 0|U^\dagger U\phi_2 U^\dagger UHU^\dagger U\phi_2^\dagger U^\dagger U|0\rangle = \langle 0|\phi_1 H\phi_1^\dagger|0\rangle = E_{\phi_1}\,. \tag{C.33}$$

If the vacuum is not symmetric under the group transformations this equation is not valid anymore. Moreover, the charge operator is not well defined either.

C.2.2 Spontaneous Symmetry Breaking and the Nambu-Goldstone Theorem

Above, we have assumed that $U|0\rangle = |0\rangle$, which implies $Q|0\rangle = 0$. If that were the case for QCD, there should be multiplets with the same mass and opposite parity. However, this is not the case. We need an alternative picture to explain the chiral symmetry realization in QCD.

We can ask the question that what if $Q|0\rangle \neq 0$? In this case, $U|0\rangle \neq 0$, hence eq. (C.33) is not valid and $E_{\phi_2} \neq E_{\phi_1}$. Therefore, we can state for any operator ϕ that[1]

$$\langle 0|\phi Q|0\rangle \neq 0\,, \tag{C.34}$$

whereas, since the charge is still conserved,

$$\frac{d}{dt}\langle 0|\phi Q|0\rangle\,. \tag{C.35}$$

We can write this in terms of the currents as ($P_\mu = (E, \mathbf{P})$)

$$\begin{aligned}
\frac{d}{dt}\int d\mathbf{x}\langle 0|\phi\, j_0(t,\mathbf{x})|0\rangle &= \frac{d}{dt}\sum_n \int d\mathbf{x}\langle 0|\phi|n\rangle\langle n|j_0(t,\mathbf{x})|0\rangle && \text{(C.36)}\\
&= \frac{d}{dt}\sum_n (2\pi)^3\delta^3(\mathbf{P}_n)e^{iE_n t}\langle 0|\phi|n\rangle\langle n|j_0(0)|0\rangle && \text{(C.37)}\\
&= \sum_n (2\pi)^3\delta^3(\mathbf{P}_n)iE_n e^{iE_n t}\langle 0|\phi|n\rangle\langle n|j_0(0)|0\rangle && \text{(C.38)}\\
&= 0\,. && \text{(C.39)}
\end{aligned}$$

The only possibility to satisfy eq. (C.39) is when the produced states, by applying Q on the vacuum, are massless ($E_n = 0$). In this case, we say that Nambu-Goldstone bosons emerge. Accordingly, there is a different Nambu-Goldstone boson for each charge operator which does not annihilate the vacuum of the system. Quantum numbers of the Goldstone boson should agree with those of Q. This is the Goldstone theorem. In this case we speak of spontaneous breaking of symmetry. As in the case of electroweak theory, Goldstone bosons are not necessarily physical particles.

If we consider QCD, $SU(3)_L \times SU(3)_R$ chiral symmetry is spontaneously broken and the Goldstone bosons refer to physical particles, which are defined as in eq. (1.41). Therefore, if we consider eq. (1.41), the pion decay constant should not vanish for QCD to have spontaneous symmetry breaking:

$$\lim_{m\to 0} F_\pi = F_0 \neq 0\,. \tag{C.40}$$

[1] Here, we ignore a precise formulation that requires a study of the infinite-volume limit.

APPENDIX D

Kinematics and Mandelstam variables

Let us consider a scattering processes of a two-particle interaction: $a + b \to c + d$. This interaction amplitude have three independent four momentum vectors, hence there are 12 independent parameters. All particles are considered to be on-mass shell. This is satisfied by the condition $p^2 = m^2$. Thence, we are left with $12 - 4 = 8$ parameters. The choice of reference frame does not affect the interaction amplitude. The reference frame is characterized by rotations and Lorentz boosts in each space dimension. Therefore, we are left with $8 - 3 - 3 = 2$ independent parameters.

If we consider the process in the center-of-mass frame (CM), we have

$$\begin{aligned} p_a &= (-E_a, \mathbf{p}_a)\,, \qquad p_b = (-E_b, \mathbf{p}_b)\,, \\ p_c &= (E_c, -\mathbf{p}_c)\,, \qquad p_d = (E_d, -\mathbf{p}_d)\,, \end{aligned} \tag{D.1}$$

with $E_i = \sqrt{m_i^2 + |\mathbf{p_i}^2|}$, $\mathbf{p}_a = -\mathbf{p}_b$, and $\mathbf{p}_c = -\mathbf{p}_d$. The Mandelstam variables are convenient to use:

$$\begin{aligned} s &= (p_a + p_b)^2 = (p_c + p_d)^2\,, \quad \text{in CM:} \quad s = (E_a + E_b)^2 = (E_c + E_d)^2 = E_{\text{CM}}^2\,, \\ t &= (p_a - p_c)^2 = (p_b - p_d)^2\,, \quad \text{in CM:} \quad t = (E_a - E_c)^2 - (\mathbf{p}_a - \mathbf{p}_c)^2 = m_a^2 + m_c^2 - 2E_aE_c + 2|\mathbf{p}_a||\mathbf{p}_c|\cos\theta\,, \\ u &= (p_a - p_d)^2 = (p_b - p_c)^2\,, \quad \text{in CM:} \quad u = (E_a - E_d)^2 - (\mathbf{p}_a - \mathbf{p}_d)^2 = m_a^2 + m_d^2 - 2E_aE_d - 2|\mathbf{p}_a||\mathbf{p}_c|\cos\theta\,, \end{aligned} \tag{D.2}$$

where θ is the angle between the particles a and c

$$\cos\theta = \frac{\mathbf{p}_a \cdot \mathbf{p}_c}{|\mathbf{p}_a||\mathbf{p}_c|}\,. \tag{D.3}$$

There are two independent variables in a two-body scattering but we have defined three parameters. Therefore, they are not independent. The relation between the Mandelstam variables is

$$s + t + u = m_a^2 + m_b^2 + m_c^2 + m_d^2\,. \tag{D.4}$$

This relation is what makes the Mandelstam variables convenient. Hence, the kinematics can be represented on the Mandelstam plane as in fig.D.1. If we use eq. (D.2) and express three momentums in

terms of the scattering angle, we get

$$\begin{aligned} |\mathbf{p}_a| = q &= \frac{(s-(m_a+m_b)^2)(s-(m_a-m_b)^2)}{4s}\,, \\ |\mathbf{p}_c| = q' &= \frac{(s-(m_c+m_d)^2)(s-(m_c-m_d)^2)}{4s}\,. \end{aligned} \tag{D.5}$$

If we consider a scattering with $m_a = m_c$, t is simplified and if all masses are equal, the u channel is simplified as well:

$$t = -2q^2(1-\cos\theta)\,, \tag{D.6}$$

$$u = -2q^2(1+\cos\theta)\,. \tag{D.7}$$

Therefore, we can identify the physical regions of the interaction $a+b \to c+d$ on a Mandelstam plane. As a first case, let us assume all masses to be equal: $a+a \to a+a$. In this case, the Mandelstam plane will form an equilateral triangle as can be seen in fig.D.1. The physical region can be identified by using eq. (D.2), (D.6), (D.7) as:

$$s \geq 4m^2\,, \quad t \leq 0\,, \quad u \leq 0\,. \tag{D.8}$$

As we have seen in sec. 3.1.4, the same amplitude is equal also to different interactions which are called as t-channel and u-channel. In this case, the physical boundaries for each channel are given as

$$\begin{aligned} \text{s-channel:} \quad & s \geq 4m^2\,, t \leq 0\,, u \leq 0\,, \\ \text{t-channel:} \quad & t \geq 4m^2\,, s \leq 0\,, u \leq 0\,, \\ \text{u-channel:} \quad & u \geq 4m^2\,, s \leq 0\,, t \leq 0\,, \end{aligned} \tag{D.9}$$

and the Mandelstam plane is now extended as in fig.D.1.

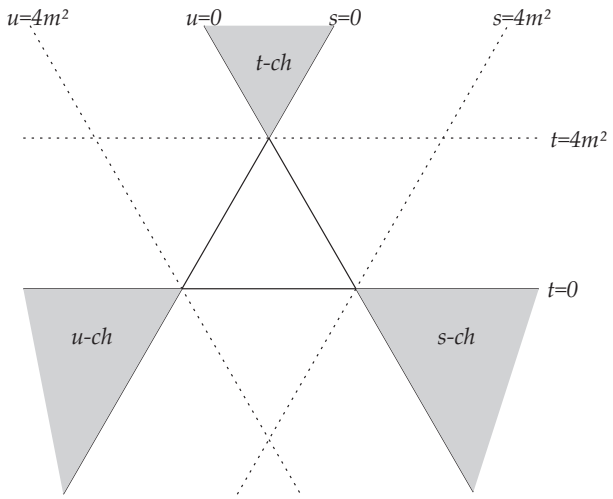

Figure D.1: Mandelstam plane and physical regions for equal mass elastic scattering.

A more complicated interaction would be $a + b \to a + b$. In this case boundaries can be written as:

$$\begin{aligned} \text{s-channel: } & a + b \to a + b \quad s \geq (m_a + m_b)^2 \,, t \leq 0 \,, u \leq 0 \,, \\ \text{t-channel: } & \bar{b} + b \to a + \bar{a} \quad t \geq 4m_b^2 \,, s \leq 0 \,, u \leq 0 \,, \\ \text{u-channel: } & \bar{a} + b \to \bar{a} + b \quad u \geq (m_a + m_b)^2 \,, s \leq 0 \,, t \leq 0 \,. \end{aligned} \tag{D.10}$$

APPENDIX E

Partial-wave projection formalism [1]

In this appendix, we detail the projection formalism used in this work to calculate the different $\rho\rho$ partial waves. First, we give the expression for the polarization vectors for a massive spin-one particle with a three-momentum $\mathbf{p}$ and third component of spin σ in the z axis of its rest frame, that we denote by $\varepsilon(\mathbf{p},\sigma)$. In the rest frame they are given by

$$\varepsilon(\mathbf{0},\sigma) = \begin{pmatrix} 0 \\ \boldsymbol{\varepsilon}_\sigma \end{pmatrix} , \tag{E.1}$$

with

$$\boldsymbol{\varepsilon}_0 = \begin{pmatrix} 0 \\ 0 \\ 1 \end{pmatrix} , \; \boldsymbol{\varepsilon}_{\pm 1} = \frac{\mp 1}{\sqrt{2}} \begin{pmatrix} 1 \\ \pm i \\ 0 \end{pmatrix} . \tag{E.2}$$

Next, we take a Lorentz transformation $U(\mathbf{p})$ along the vector $\mathbf{p}$ that takes the particle four-momentum at rest to its final value,

$$U(\mathbf{p}) \begin{pmatrix} m \\ \mathbf{0} \end{pmatrix} = \begin{pmatrix} E_p \\ \mathbf{p} \end{pmatrix} , \tag{E.3}$$

with $E_p = \sqrt{m^2 + \mathbf{p}^2}$. We also introduce the rotation $R(\hat{\mathbf{p}})$ that takes $\hat{\mathbf{z}}$ to $\hat{\mathbf{p}}$,

$$R(\hat{\mathbf{p}})\hat{\mathbf{z}} = \hat{\mathbf{p}} . \tag{E.4}$$

In terms of the polar (θ) and azimuthal (ϕ) angles of $\hat{\mathbf{p}}$ this rotation is defined as

$$R(\hat{\mathbf{p}}) = R_z(\phi) R_y(\theta) , \tag{E.5}$$

with the subscripts z and y indicating the axis of rotation. For latter convenience we write the Lorentz transformation $U(\mathbf{p})$ as

$$U(\mathbf{p}) = R(\hat{\mathbf{p}}) B_z(|\mathbf{p}|) R(\hat{\mathbf{p}})^{-1} , \tag{E.6}$$

[1] This formalism has been published in [158]

where $B_z(|\mathbf{p}|)$ is a boost along the $\hat{\mathbf{z}}$ axis with velocity $v = -\beta$ and $\beta = |\mathbf{p}|/E_p$. Namely,

$$B_z(|\mathbf{p}|) = \begin{pmatrix} \gamma & 0 & 0 & \gamma\beta \\ 0 & 0 & 0 & 0 \\ 0 & 0 & 0 & 0 \\ \gamma\beta & 0 & 0 & \gamma \end{pmatrix} \tag{E.7}$$

and

$$\gamma = \frac{1}{\sqrt{1-\beta^2}} \, . \tag{E.8}$$

Notice that we could also include any arbitrary rotation around the $\hat{\mathbf{z}}$ axis to the right hand side of eq. (E.5). Of course, this does not have any affect on either eqs. (E.4) and (E.6) (for the latter one let us note that $B_z(|\mathbf{p}|)$ commutes with a rotation around the $\hat{\mathbf{z}}$ axis).

The action of $U(\mathbf{p})$ on $\epsilon(\mathbf{0}, \sigma_i)$ gives us the polarization vectors with definite three-momentum $\mathbf{p}$, whose expressions are

$$\varepsilon(\mathbf{p}, 0) = \begin{pmatrix} \gamma\beta\cos\theta \\ \frac{1}{2}(\gamma-1)\sin 2\theta\cos\phi \\ \frac{1}{2}(\gamma-1)\sin 2\theta\sin\phi \\ \frac{1}{2}\left(1+\gamma+(\gamma-1)\cos 2\theta\right) \end{pmatrix} , \; \varepsilon(\mathbf{p}, \pm 1) = \mp\frac{1}{\sqrt{2}} \begin{pmatrix} \gamma\beta e^{\pm i\phi}\sin\theta \\ 1+(\gamma-1)e^{\pm i\phi}\sin^2\theta\cos\phi \\ \pm i+(\gamma-1)e^{\pm i\phi}\sin^2\theta\sin\phi \\ \frac{1}{2}(\gamma-1)e^{\pm i\phi}\sin 2\theta \end{pmatrix} . \tag{E.9}$$

The previous equation can be written in a more compact form as

$$\varepsilon(\mathbf{p}, \sigma) = \begin{pmatrix} \gamma\beta\hat{\mathbf{p}}\cdot\boldsymbol{\varepsilon}_\sigma \\ \boldsymbol{\varepsilon}_\sigma + \hat{\mathbf{p}}\,(\gamma-1)\hat{\mathbf{p}}\cdot\boldsymbol{\varepsilon}_\sigma \end{pmatrix} . \tag{E.10}$$

In terms of the polarization vectors in eq. (E.10), we can write the vector field for the neutral ρ^0 particle, $\rho^0_\mu(x)$, as

$$\rho^0_\mu(x) = \sum_\sigma \int \frac{d^3p}{(2\pi)^3 2E_p} \left\{ \varepsilon(\mathbf{p},\sigma)_\mu e^{-ip\,x} a(\mathbf{p},\sigma) + \varepsilon(\mathbf{p},\sigma)^*_\mu e^{ip\,x} a(\mathbf{p},\sigma)^\dagger \right\} , \tag{E.11}$$

with the corresponding similar expressions for the $\rho^\pm(x)$ fields. Here, $a(\mathbf{p},\sigma)$ and $a(\mathbf{p},\sigma)^\dagger$ refer to the annihilation and creation operators, with the canonical commutation relation

$$[a(\mathbf{p}',\sigma'), a(\mathbf{p},\sigma)^\dagger] = \delta_{\sigma\sigma'}(2\pi)^3 2E_p \delta(\mathbf{p}-\mathbf{p}') \, . \tag{E.12}$$

In order to check the time-reversal and parity-invariance properties of the vector-vector scattering amplitudes worked out from the chiral Lagrangians in eq. (2.78), we notice that the polarization vectors in eq. (E.9) satisfy the following transformation properties:

$$\begin{aligned} \varepsilon(-\mathbf{p},\sigma)^* &= (-1)^\sigma(-\varepsilon(\mathbf{p},\sigma)_0, \boldsymbol{\varepsilon}(\mathbf{p},\sigma)) \, , \\ \varepsilon(-\mathbf{p},\sigma) &= (-\varepsilon(\mathbf{p},\sigma)_0, \boldsymbol{\varepsilon}(\mathbf{p},\sigma)) \, . \end{aligned} \tag{E.13}$$

A one-particle state $|\mathbf{p},\sigma\rangle$ is obtained by the action of the creation operators on the vacuum state,

$$|\mathbf{p},\sigma\rangle = a(\mathbf{p},\sigma)^\dagger|\mathbf{0},0\rangle\,. \tag{E.14}$$

From eq. (E.12) it follows the following normalization for such states

$$\langle\mathbf{p}',\sigma'|\mathbf{p},\sigma\rangle = \delta_{\sigma'\sigma}(2\pi)^3 2E_p\delta(\mathbf{p}'-\mathbf{p})\,. \tag{E.15}$$

Next, we consider a two-body state characterized by the CM three-momentum $\mathbf{p}$ and the third components of spin σ_1 and σ_2 in their respective rest frames. This state is denoted by $|\mathbf{p},\sigma_1\sigma_2\rangle$. Associated to this, we can define the two-body state with orbital angular momentum ℓ with its third component of orbital angular momentum m, denoted by $|\ell m,\sigma_1\sigma_2\rangle$ as

$$|\ell m,\sigma_1\sigma_2\rangle = \frac{1}{\sqrt{4\pi}}\int d\hat{\mathbf{p}}\, Y_\ell^m(\hat{\mathbf{p}})|\mathbf{p},\sigma_1\sigma_2\rangle\,. \tag{E.16}$$

Let us show first that this definition is meaningful because the state $|\ell m,\sigma_1\sigma_2\rangle$ transforms under the rotation group as the direct product of the irreducible representations associated to the orbital angular momentum ℓ and the spins s_1 and s_2 of the two particles.

Every single-particle state $|\mathbf{p},\sigma\rangle$ under the action of a rotation R transforms as

$$R|\mathbf{p},\sigma\rangle = RU(\mathbf{p})|\mathbf{0},\sigma\rangle = U(\mathbf{p}')U(\mathbf{p}')^{-1}RU(\mathbf{p})|\mathbf{0},\sigma\rangle\,, \tag{E.17}$$

and $\mathbf{p}' = R\mathbf{p}$.[2] It is straightforward to show that

$$R = U(\mathbf{p}')^{-1}RU(\mathbf{p})\,. \tag{E.18}$$

For that, we explicitly write the Lorentz transformations $U(\mathbf{p}')$ and $U(\mathbf{p})$ as in eq. (E.6):

$$U(\mathbf{p}')^{-1}RU(\mathbf{p}) = R(\hat{\mathbf{p}}')B_z(|\mathbf{p}|)^{-1}R(\hat{\mathbf{p}}')^{-1}RR(\hat{\mathbf{p}})B_z(|\mathbf{p}|)R(\hat{\mathbf{p}})^{-1}\,. \tag{E.19}$$

Next, the product of rotations $R(\hat{\mathbf{p}}')^{-1}RR(\hat{\mathbf{p}})$ is a rotation around the z axis, $R_z(\gamma)$, since it leaves invariant $\hat{\mathbf{z}}$. Thus,

$$R(\hat{\mathbf{p}}')^{-1}RR(\hat{\mathbf{p}}) = R_z(\gamma)\,, \tag{E.20}$$

or, in other terms,

$$R(\hat{\mathbf{p}}') = RR(\hat{\mathbf{p}})R_z(\gamma)^{-1}\,, \tag{E.21}$$

Taking into account eqs. (E.20) and (E.21) in eq. (E.19) it follows the result given in eq. (E.18) because $B_z(|\mathbf{p}|)$ and $R_z(\gamma)$ commute. Then, eq. (E.17) implies that

$$R|\mathbf{p},\sigma\rangle = U(\mathbf{p}')R|\mathbf{0},\sigma\rangle = \sum_{\sigma'} D^{(s)}(R)_{\sigma'\sigma}|\mathbf{p}',\sigma'\rangle\,, \tag{E.22}$$

with $D^{(s)}(R)$ the rotation matrix in the irreducible representation of the rotation group with spin s.

Now, we can use this result to find the action of the rotation R on the state $|\mathbf{p},\sigma_1\sigma_2\rangle$ which is the direct

[2] For a general Lorentz transformation these manipulations give rise to the Wigner rotation [131].

product of the states $|\mathbf{p}, \sigma_1\rangle$ and $|-\mathbf{p}, \sigma_2\rangle$ (once the trivial CM movement is factorized out [131]). In this way,

$$R|\mathbf{p}, \sigma_1\sigma_2\rangle = \sum_{\sigma_1', \sigma_2'} D^{(s_1)}(R)_{\sigma_1'\sigma_1} D^{(s_2)}(R)_{\sigma_2'\sigma_2} |\mathbf{p}', \sigma_1'\sigma_2'\rangle \,. \tag{E.23}$$

We are now ready to derive the action R on $|\ell m, \sigma_1\sigma_2\rangle$,

$$\begin{aligned} R|\ell m, \sigma_1\sigma_2\rangle &= \sum_{\sigma_1', \sigma_2'} D^{(s_1)}(R)_{\sigma_1'\sigma_1} D^{(s_2)}(R)_{\sigma_2'\sigma_2} \frac{1}{\sqrt{4\pi}} \int d\hat{\mathbf{p}}'\, Y_\ell^m(R^{-1}\hat{\mathbf{p}}')|\mathbf{p}', \sigma_1'\sigma_2'\rangle \\ &= \sum_{\sigma_1', \sigma_2', m'} D^{(\ell)}(R)_{m'm} D^{(s_1)}(R)_{\sigma_1'\sigma_1} D^{(s_2)}(R)_{\sigma_2'\sigma_2} |\ell m', \sigma_1'\sigma_2'\rangle \,. \end{aligned} \tag{E.24}$$

In this equation we have made use of the property of the spherical harmonics

$$Y_\ell^m(R^{-1}\hat{\mathbf{p}}') = \sum_{m'} D^{(\ell)}(R)_{m'm} Y_\ell^{m'}(\hat{\mathbf{p}}') \,. \tag{E.25}$$

Equation (E.24) shows that under rotation the states defined in eq. (E.16) has the right transformation under the action of a rotation R, and our proposition above is shown to hold.

Now, because of the transformation in eq. (E.24), corresponding to the direct product of spins s_1, s_2 and ℓ, we can combine these angular momentum indices and end with the LSJ basis. In the latter every state is labelled by the total angular momentum J, the third component of the total angular momentum μ, orbital angular momentum ℓ and total spin S (resulting from the composition of spins s_1 and s_2). Namely, we use the notation $|J\mu, \ell S\rangle$ for these states which are then given by

$$|J\mu, \ell S\rangle = \sum_{\sigma_1, \sigma_2, m, M} (\sigma_1\sigma_2 M|s_1 s_2 S)(mM\mu|\ell S J)|\ell m, \sigma_1\sigma_2\rangle \,, \tag{E.26}$$

where we have introduced the standard Clebsch-Gordan coefficients for the composition of two angular momenta.[3] Next, we introduce the isospin indices α_1 and α_2 corresponding to the third components of the isospins τ_1 and τ_2. This does not modify any of our previous considerations since isospin does not transform under the action of spatial rotations. Within the isospin formalism, the $\rho\rho$ states obey Bose-Einstein statistics and these symmetric states are defined by

$$|\mathbf{p}, \sigma_1\sigma_2, \alpha_1\alpha_2\rangle_S = \frac{1}{\sqrt{2}} \left(|\mathbf{p}, \sigma_1\sigma_2, \alpha_1\alpha_2\rangle + |-\mathbf{p}, \sigma_2\sigma_1, \alpha_2\alpha_1\rangle\right) \,, \tag{E.27}$$

with the subscript S indicating the symmetrized nature of the state under the exchange of the two particles. We can invert eq. (E.16) and give the momentum-defined states in terms of those with well-defined orbital

[3] The Clebsch-Gordan coefficient $(m_1 m_2 m_3|j_1 j_2 j_3)$ is the composition for $\mathbf{j}_1 + \mathbf{j}_2 = \mathbf{j}_3$, with m_i referring to the third components of the spins.

angular momentum,

$$|\mathbf{p},\sigma_1\sigma_2,\alpha_1\alpha_2\rangle = \sqrt{4\pi}\sum_{\ell,m} Y_\ell^m(\hat{\mathbf{p}})^*|\ell m,\sigma_1\sigma_2,\alpha_1\alpha_2\rangle$$
$$= \sqrt{4\pi}\sum_{\substack{J,\mu,\ell,m\\ S,M,I,t_3}} Y_\ell^m(\hat{\mathbf{p}})^*(\sigma_1\sigma_2 S_3|s_1s_2S)(mM\mu|\ell S J)(\alpha_1\alpha_2t_3|\tau_1\tau_2 I)|J\mu,\ell S,It_3\rangle\,, \tag{E.28}$$

with I the total isospin of the particle pair and t_3 is third component. Taking into account this result, we can write the symmetrized states as

$$|\mathbf{p},\sigma_1\sigma_2,\alpha_1\alpha_2\rangle_S = \sqrt{4\pi}\sum_{\substack{J,\mu,\ell,m\\ S,M,I,t_3}} \frac{1+(-1)^{\ell+S+I}}{\sqrt{2}}(\sigma_1\sigma_2M|s_1s_2S)(mM\mu|\ell S J)(\alpha_1\alpha_2t_3|\tau_1\tau_2 I)Y_\ell^m(\hat{\mathbf{p}})^*|J\mu,\ell S,It_3\rangle\,. \tag{E.29}$$

In deducing this expression, we have taken into account the following symmetric properties of the Clebsch-Gordan coefficients

$$\begin{aligned}(\sigma_2\sigma_1M|s_2s_1S) &= (-1)^{S-s_1-s_2}(\sigma_1\sigma_2M|s_1s_2S)\,,\\ (\alpha_2\alpha_1t_3|t_2t_1T) &= (-1)^{T-t_1-t_2}(\alpha_1\alpha_2t_3|\tau_1\tau_2T)\,,\\ Y_\ell^m(-\hat{\mathbf{p}}) &= (-1)^\ell Y_\ell^m(\hat{\mathbf{p}})\,.\end{aligned} \tag{E.30}$$

Of course, due to the fact that we are dealing with indistinguishable bosons within the isospin formalism, it follows that $s_1 = s_2$, $\tau_1 = \tau_2$ as well as that $2\tau_1$ and $2s_1$ are even numbers. The combination $(1+(-1)^{\ell+S+I})/\sqrt{2}$ in eq. (E.29) is denoted in the following as $\chi(\ell S T)$ and takes into account the Bose-Einstein symmetric character of the two-particles, so that only states with even $\ell+S+I$ are allowed.

The inversion of eq. (E.29) gives (we assume in the following that $\ell+S+I$ =even, so that $\chi(\ell S T) = \sqrt{2}$)

$$|J\mu,\ell S,It_3\rangle = \frac{1}{\sqrt{8\pi}}\sum_{\substack{\sigma_1,\sigma_2\\ M,m\\ \alpha_1,\alpha_2}}\int d\hat{\mathbf{p}}\,Y_\ell^m(\hat{\mathbf{p}})(\sigma_1\sigma_2M|s_1s_2S)(mM\mu|\ell S J)(\alpha_1\alpha_2t_3|\tau_1\tau_2 I)|\mathbf{p},\sigma_1\sigma_2,\alpha_1\alpha_2\rangle_S\,. \tag{E.31}$$

We can also express the state $|J\mu,\ell S,It_3\rangle$ in terms of the states $|\mathbf{p},\sigma_1\sigma_2,\alpha_1\alpha_2\rangle$ without symmetrization by inverting eq. (E.28). We would obtain the same expression as eq. (E.31) but with a factor $1/\sqrt{4\pi}$ instead of $1/\sqrt{8\pi}$, namely,

$$|J\mu,\ell S,It_3\rangle = \frac{1}{\sqrt{4\pi}}\sum_{\substack{\sigma_1,\sigma_2\\ M,m\\ \alpha_1,\alpha_2}}\int d\hat{\mathbf{p}}\,Y_\ell^m(\hat{\mathbf{p}})(\sigma_1\sigma_2M|s_1s_2S)(mM\mu|\ell S J)(\alpha_1\alpha_2t_3|\tau_1\tau_2 I)|\mathbf{p},\sigma_1\sigma_2,\alpha_1\alpha_2\rangle\,. \tag{E.32}$$

The extra factor of $1/\sqrt{2}$ in eq. (E.31) is a symmetrization factor because of the Bose-Einstein symmetry properties of the two-particle state in the symmetrized states $|\mathbf{p},\sigma_1\sigma_2,\alpha_1\alpha_2\rangle_S$, which disappears when employing the nonsymmetrized states. In order to obtain the normalization of the states $|J\mu,\ell S,Tt_3\rangle$, it is

indeed simpler to use eq. (E.32) though, of course, the same result is obtained if we start from eq. (E.31). The two-body particle states with definite three-momentum satisfy the normalization

$$\langle \mathbf{p}', \sigma_1'\sigma_2', \alpha_1'\alpha_2' | \mathbf{p}, \sigma_1\sigma_2, \alpha_1\alpha_2 \rangle = \frac{16\pi^2\sqrt{s}}{|\mathbf{p}|}\delta(\hat{\mathbf{p}}' - \hat{\mathbf{p}}) \,, \tag{E.33}$$

The total energy conservation guarantees that the modulus of the final and initial three-momentum in eq. (E.34) is the same, that we denote by $|\mathbf{p}|$. In terms of this result and eq. (E.32), it follows straightforwardly by taking into account the orthogonal properties of the Clebsch-Gordan coefficients and the spherical harmonics that

$$\langle J'\mu', \ell' S', I' t_3' | J\mu, \ell S, I t_3 \rangle = \frac{4\pi\sqrt{s}}{|\mathbf{p}|}\delta_{J'J}\delta_{\mu'\mu}\delta_{\ell'\ell}\delta_{S'S}\delta_{I'I}\delta_{t_3' t_3} \tag{E.34}$$

We are interested in the partial-wave amplitude corresponding to the transition between states with quantum numbers $J\bar{\ell}\bar{S}\,I$ to states $J\ell S\,I$, that corresponds to the matrix element

$$T^{(JI)}_{\ell S;\bar{\ell}\bar{S}} = \langle J\mu, \ell S, I t_3 | \hat{T} | J\mu, \bar{\ell}\bar{S}, I t_3 \rangle \,, \tag{E.35}$$

with $\hat{T}$ the T-matrix scattering operator. Here, we take the convention that the quantum numbers referring to the initial state are barred. Of course, the matrix element in eq. (E.35) is independent of μ and t_3 because of invariance under rotations in ordinary and isospin spaces, respectively. We can calculate this scattering matrix element in terms of those in the basis with definite three-momentum by replacing in eq. (E.35) the states in the $J\ell S$ basis as given in eq. (E.31). We then obtain in a first step

$$\begin{aligned} T^{(JI)}_{\ell S;\bar{\ell}\bar{S}} =& \frac{1}{8\pi}\sum \int d\hat{\mathbf{p}} \int d\hat{\mathbf{p}}' \, Y_\ell^m(\hat{\mathbf{p}}')^* Y_{\bar{\ell}}^{\bar{m}}(\hat{\mathbf{p}}) (\sigma_1\sigma_2 M | s_1 s_2 S)(m M\mu | \ell S\, J)(\alpha_1\alpha_2 t_3 | \tau_1\tau_2 I) \\ & \times (\bar{\sigma}_1\bar{\sigma}_2\bar{M} | \bar{s}_1\bar{s}_2 S)(\bar{m}\bar{M}\mu | \bar{\ell}\bar{S}\, J)(\bar{\alpha}_1\bar{\alpha}_2 t_3 | \bar{\tau}_1\bar{\tau}_2 I)_S \langle \mathbf{p}', \sigma_1\sigma_2, \alpha_1\alpha_2 | \hat{T} | \mathbf{p}, \bar{\sigma}_1\bar{\sigma}_2, \bar{\alpha}_1\bar{\alpha}_2 \rangle_S \,, \end{aligned} \tag{E.36}$$

Here, we have not shown the explicit indices over which the sum is done in order not to overload the notation.[4] We use, next, the rotation invariance of the T-matrix operator $\hat{T}$ to simplify the previous integral so that, in the end, we have just the integration over the final three-momentum angular solid. There are several steps involved that we give in quite detail. The referred rotational invariance of $\hat{T}$ implies that it remains invariant under the transformation $\hat{T} \to R(\hat{\mathbf{p}})\hat{T}R(\hat{\mathbf{p}})^\dagger$, which implies at the level of the matrix elements that

$${}_S\langle \mathbf{p}', \sigma_1\sigma_2, \alpha_1\alpha_2 | \hat{T} | \mathbf{p}, \bar{\sigma}_1\bar{\sigma}_2, \bar{\alpha}_1\bar{\alpha}_2 \rangle_S = {}_S\langle \mathbf{p}', \sigma_1\sigma_2, \alpha_1\alpha_2 | R(\hat{\mathbf{p}})\hat{T}R(\hat{\mathbf{p}})^\dagger | \mathbf{p}, \bar{\sigma}_1\bar{\sigma}_2, \bar{\alpha}_1\bar{\alpha}_2 \rangle_S \,. \tag{E.37}$$

Under the action of the rotation $R(\hat{\mathbf{p}})^\dagger$ ($R(\hat{\mathbf{p}})^\dagger\hat{\mathbf{p}} = \hat{\mathbf{z}}$ and $R(\hat{\mathbf{p}})^\dagger\hat{\mathbf{p}}' = \hat{\mathbf{p}}''$), the final and initial states transform as, cf. eq. (E.23),

$$\begin{aligned} R(\hat{\mathbf{p}})^\dagger | \mathbf{p}, \bar{\sigma}_1\bar{\sigma}_2, \bar{\alpha}_1\bar{\alpha}_2 \rangle_S &= \sum_{\bar{\sigma}_1', \bar{\sigma}_2'} D^{(\bar{s}_1)}_{\bar{\sigma}_1'\bar{\sigma}_1}(R^\dagger) D^{(\bar{s}_2)}_{\bar{\sigma}_2'\bar{\sigma}_2}(R^\dagger) | \hat{\mathbf{z}}, \bar{\sigma}_1'\bar{\sigma}_2', \bar{\alpha}_1\bar{\alpha}_2 \rangle_S \,, \\ R(\hat{\mathbf{p}})^\dagger | \mathbf{p}', \sigma_1\sigma_2, \alpha_1\alpha_2 \rangle_S &= \sum_{\sigma_1', \sigma_2'} D^{(s_1)}_{\sigma_1'\sigma_1}(R^\dagger) D^{(s_2)}_{\sigma_2'\sigma_2}(R^\dagger) | \hat{\mathbf{p}}'', \sigma_1'\sigma_2', \alpha_1\alpha_2 \rangle_S \,, \end{aligned} \tag{E.38}$$

with the convention that R inside the argument of the rotation matrices refers to $R(\hat{\mathbf{p}})$. We insert eqs. (E.37)

[4] They correspond to those indicated under the summation symbol in eq. (E.31) both for the initial and final states.

and (E.38) into eq. (E.36), and next transform $\hat{\mathbf{p}}' \to \hat{\mathbf{p}}''$ as integrations variables, take into account the invariance of the solid angle measure under such rotation and use eq. (E.25) for

$$\begin{aligned} Y_{\bar{\ell}}^{\bar{m}}(\hat{\mathbf{p}}) =& Y_{\bar{\ell}}^{\bar{m}}(R(\hat{\mathbf{p}})\hat{\mathbf{z}}) = \sum_{\bar{m}'} D^{(\bar{\ell})}_{\bar{m}'\bar{m}}(R^\dagger) Y_{\bar{\ell}}^{\bar{m}'}(\hat{\mathbf{z}}) \,, \\ Y_{\ell}^{m}(\hat{\mathbf{p}}') =& Y_{\ell}^{m}(R(\hat{\mathbf{p}})\hat{\mathbf{p}}'') = \sum_{m'} D^{(\ell)}_{m'm}(R^\dagger) Y_{\ell}^{m'}(\hat{\mathbf{p}}'') \,. \end{aligned} \tag{E.39}$$

Then, eq. (E.36) for $T^{(JI)}_{\ell S;\bar{\ell}\bar{S}}$ can be rewritten as

$$\begin{aligned} T^{(JI)}_{\ell S;\bar{\ell}\bar{S}} =& \frac{1}{8\pi} \sum \int d\hat{\mathbf{p}} \int d\hat{\mathbf{p}}''(\sigma_1\sigma_2 M|s_1 s_2 S)(mM\mu|\ell S J)(\alpha_1\alpha_2 t_3|\tau_1\tau_2 I) D^{(s_1)}_{\sigma_1'\sigma_1}(R^\dagger)^* D^{(s_2)}_{\sigma_2'\sigma_2}(R^\dagger)^* \\ & \times D^{(\ell)}_{m'm}(R^\dagger)^* Y_{\ell}^{m'}(\hat{\mathbf{p}}'')^*(\bar{\sigma}_1\bar{\sigma}_2\bar{M}|\bar{s}_1\bar{s}_2\bar{S})(\bar{m}\bar{M}\mu|\bar{\ell}\bar{S}J)(\bar{\alpha}_1\bar{\alpha}_2 t_3|\bar{\tau}_1\bar{\tau}_2 I) \\ & \times D^{(\bar{s}_1)}_{\bar{\sigma}_1'\bar{\sigma}_1}(R^\dagger) D^{(\bar{s}_2)}_{\bar{\sigma}_2'\bar{\sigma}_2}(R^\dagger) D^{(\bar{\ell})}_{\bar{m}'\bar{m}}(R^\dagger) Y_{\bar{\ell}}^{\bar{m}'}(\hat{\mathbf{z}})_S \langle \mathbf{p}'', \sigma_1'\sigma_2', \alpha_1\alpha_2|\hat{T}|\,|\mathbf{p}|\hat{\mathbf{z}}, \bar{\sigma}_1'\bar{\sigma}_2', \bar{\alpha}_1\bar{\alpha}_2\rangle_S \,. \end{aligned} \tag{E.40}$$

Let us recall that from the composition of two rotation matrices we have [131]

$$\sum_{m_1,m_2} (m_1 m_2 M|\ell_1\ell_2 L) D^{(\ell_1)}_{m_1'm_1}(R) D^{(\ell_2)}_{m_2'm_2}(R) = \sum_{M'} (m_1' m_2' M'|\ell_1\ell_2 L) D^{(L)}_{M'M}(R) \,. \tag{E.41}$$

We apply this result first to two combinations in eq. (E.40):

$$\begin{aligned} \sum_{\sigma_1,\sigma_2} (\sigma_1\sigma_2 M|s_1 s_2 S) D^{(s_1)}_{\sigma_1'\sigma_1}(R^\dagger) D^{(s_2)}_{\sigma_2'\sigma_2}(R^\dagger) &= \sum_{M'} (\sigma_1'\sigma_2' M'|s_1 s_2 S) D^{(S)}_{M'M}(R^\dagger) \\ \sum_{\bar{\sigma}_1,\bar{\sigma}_2} (\bar{\sigma}_1\bar{\sigma}_2\bar{M}|\bar{s}_1\bar{s}_2\bar{S}) D^{(\bar{s}_1)}_{\bar{\sigma}_1'\bar{\sigma}_1}(R^\dagger) D^{(\bar{s}_2)}_{\bar{\sigma}_2'\bar{\sigma}_2}(R^\dagger) &= \sum_{\bar{M}'} (\bar{\sigma}_1'\bar{\sigma}_2'\bar{M}'|\bar{s}_1\bar{s}_2\bar{S}) D^{(\bar{S})}_{\bar{M}'\bar{M}}(R^\dagger) \,, \end{aligned} \tag{E.42}$$

so that eq. (E.40) becomes

$$\begin{aligned} T^{(JI)}_{\ell S;\bar{\ell}\bar{S}} =& \frac{1}{8\pi} \sum \int d\hat{\mathbf{p}} \int d\hat{\mathbf{p}}''(\sigma_1'\sigma_2' M'|s_1 s_2 S) D^{(S)}_{M'M}(R^\dagger)^* D^{(\ell)}_{m'm}(R^\dagger)^*(mM\mu|\ell S J)(\alpha_1\alpha_2 t_3|\tau_1\tau_2 I) Y_{\ell}^{m'}(\hat{\mathbf{p}}'')^* \\ & \times (\bar{\sigma}_1'\bar{\sigma}_2'\bar{M}'|\bar{s}_1\bar{s}_2\bar{S}) D^{(\bar{S})}_{\bar{M}'\bar{M}}(R^\dagger) D^{(\bar{\ell})}_{\bar{m}'\bar{m}}(R^\dagger)(\bar{m}\bar{M}\mu|\bar{\ell}\bar{S}J)(\bar{\alpha}_1\bar{\alpha}_2 t_3|\bar{\tau}_1\bar{\tau}_2 I) Y_{\bar{\ell}}^{\bar{m}'}(\hat{\mathbf{z}}) \\ & \times_S \langle \mathbf{p}'', \sigma_1'\sigma_2', \alpha_1\alpha_2|\hat{T}|\,|\mathbf{p}|\hat{\mathbf{z}}, \bar{\sigma}_1'\bar{\sigma}_2', \bar{\alpha}_1\bar{\alpha}_2\rangle_S \,. \end{aligned} \tag{E.43}$$

The same relation in eq. (E.41) is applied once more to the following combinations in eq. (E.43):

$$\begin{aligned} \sum_{m,M} (mM\mu|\ell S J) D^{(S)}_{M'M}(R^\dagger) D^{(\ell)}_{m'm}(R^\dagger) &= \sum_{\mu'} (m' M'\mu'|\ell S J) D^{(J)}_{\mu'\mu}(R^\dagger) \,, \\ \sum_{\bar{m},\bar{M}} (\bar{m}\bar{M}\mu|\bar{\ell}\bar{S}J) D^{(\bar{S})}_{\bar{M}'\bar{M}}(R^\dagger) D^{(\bar{\ell})}_{\bar{m}'\bar{m}}(R^\dagger) &= \sum_{\bar{\mu}'} (\bar{m}'\bar{M}'\bar{\mu}'|\bar{\ell}\bar{S}J) D^{(J)}_{\bar{\mu}'\mu}(R^\dagger) \,. \end{aligned} \tag{E.44}$$

We take eq. (E.44) into eq. (E.43) which now reads

$$\begin{aligned} T^{(JI)}_{\ell S;\bar{\ell}\bar{S}} =& \frac{1}{8\pi}\sum\int d\hat{\mathbf{p}}\int d\hat{\mathbf{p}}''(\sigma_1'\sigma_2'M'|s_1s_2S)(m'M'\mu'|\ell S J)(\alpha_1\alpha_2t_3|\tau_1\tau_2I)Y^{m'}_{\ell}(\hat{\mathbf{p}}'')^* \\ &\times(\bar{\sigma}_1'\bar{\sigma}_2'\bar{M}'|\bar{s}_1\bar{s}_2\bar{S})(\bar{m}'\bar{M}'\bar{\mu}'|\bar{\ell}\bar{S}J)(\bar{\alpha}_1\bar{\alpha}_2t_3|\bar{\tau}_1\bar{\tau}_2I)Y^{\bar{m}'}_{\bar{\ell}}(\hat{\mathbf{z}})D^{(J)}_{\mu'\mu}(R^\dagger)^*D^{(J)}_{\bar{\mu}'\mu}(R^\dagger) \\ &\times{}_S\langle\mathbf{p}'',\sigma_1'\sigma_2',\alpha_1\alpha_2|\hat{T}|\,|\mathbf{p}|\hat{\mathbf{z}},\bar{\sigma}_1'\bar{\sigma}_2',\bar{\alpha}_1\bar{\alpha}_2\rangle_S \end{aligned} \tag{E.45}$$

Now, the partial wave amplitude $T^{(JI)}_{\ell S;\bar{\ell}\bar{S}}$ is independent of μ so that we have that

$$T^{(JI)}_{\ell S;\bar{\ell}\bar{S}} = \frac{1}{2J+1}\sum_{\mu=-J}^{J} T^{(JI)}_{\ell S;\bar{\ell}\bar{S}}\ . \tag{E.46}$$

The same result in eq. (E.45) is obtained with the product $D^{(J)}_{\mu'\mu}(R^\dagger)^*D^{(J)}_{\bar{\mu}'\mu}(R^\dagger)$ replaced by

$$\frac{1}{2J+1}\sum_{\mu=-J}^{J} D^{(J)}_{\mu'\mu}(R^\dagger)^*D^{(J)}_{\bar{\mu}'\mu}(R^\dagger) = \frac{\delta_{\bar{\mu}'\mu'}}{2J+1}\ , \tag{E.47}$$

as follows from the unitarity of the rotation matrices. As a consequence, any dependence in $\hat{\mathbf{p}}$ present in the integrand of eq. (E.45) disappears in the average of eq. (E.46), the integration in the solid angle $\hat{\mathbf{p}}$ is trivial and it gives a factor 4π. Taking into account the Kronecker delta from eq. (E.47) in the third component of the total angular momentum and a new one that arises because $Y^{\bar{m}'}_{\bar{\ell}}(\hat{\mathbf{z}})$ is not zero only for $\bar{m}' = 0$. We, then, end with the following expression for $T^{(JI)}_{\ell S;\bar{\ell}\bar{S}}$:

$$\begin{aligned} T^{(JI)}_{\ell S;\bar{\ell}\bar{S}} = \frac{Y^0_{\bar{\ell}}(\hat{\mathbf{z}})}{2(2J+1)} \sum_{\substack{\sigma_1,\sigma_2,\bar{\sigma}_1\\ \bar{\sigma}_2,\alpha_1,\alpha_2\\ \bar{\alpha}_1,\bar{\alpha}_2,m}} &\int d\hat{\mathbf{p}}''(\sigma_1\sigma_2M|s_1s_2S)(mM\bar{M}|\ell S J)(\bar{\sigma}_1\bar{\sigma}_2\bar{M}|\bar{s}_1\bar{s}_2\bar{S})(0\bar{M}\bar{M}|\bar{\ell}\bar{S}J) \\ &\times(\alpha_1\alpha_2t_3|\tau_1\tau_2I)(\bar{\alpha}_1\bar{\alpha}_2t_3|\bar{\tau}_1\bar{\tau}_2I)_S\langle\mathbf{p}'',\sigma_1\sigma_2,\alpha_1\alpha_2|\hat{T}|\,|\mathbf{p}|\hat{\mathbf{z}},\bar{\sigma}_1\bar{\sigma}_2,\bar{\alpha}_1\bar{\alpha}_2\rangle_S\ , \end{aligned} \tag{E.48}$$

where we have removed useless primes on top of the spin and orbital angular momentum third-component symbols and in the previous sum $M = \sigma_1 + \sigma_2$ and $\bar{M} = \bar{\sigma}_1 + \bar{\sigma}_2$.

Next, we derive the unitarity relation corresponding to our normalization for the partial-wave projected amplitudes $T^{(JI)}_{\ell S;\bar{\ell}\bar{S}}$. We write the $\hat{S}$ matrix as

$$\hat{S} = I + i\hat{T}\ , \tag{E.49}$$

which satisfies the standard unitarity relation

$$\hat{S}\cdot\hat{S}^\dagger = \mathbb{I}\ , \tag{E.50}$$

with $\mathbb{I}$ the identity matrix. In terms of the T-matrix, cf. (E.49), this implies that

$$\hat{T} - \hat{T}^\dagger = i\hat{T}\hat{T}^\dagger\ . \tag{E.51}$$

Expressed with the matrix elements in the basis $\ell S\, J$, this relation becomes

$$2\,\mathrm{Im}\hat{T}^{(JI)}_{\ell S;\bar{\ell}\bar{S}} = \langle J\mu, \ell S, Tt_3|\hat{T}\hat{T}^{\dagger}|J\mu, \bar{\ell}\bar{S}, Tt_3\rangle\,. \tag{E.52}$$

In deriving the left-hand side of this equation, we have taken into account that because of time-reversal symmetry $T^{(JI)}_{\ell S;\bar{\ell}\bar{S}} = T^{(JI)}_{\bar{\ell}\bar{S};\ell S}$. On the right-hand side, we introduce a two-body resolution of the identity of states $|J\mu, \ell S, It_3\rangle$ (we have restricted our vector space to the one generated by these states) such that, taking into account their normalization in eq. (E.34), we end with

$$\mathrm{Im}T^{(JI)}_{\ell S;\bar{\ell}\bar{S}} = \sum_{\ell'',S''} \frac{|\mathbf{p}''|}{8\pi\sqrt{s}} T^{(JI)}_{\ell,S;\ell'',S''} T^{(JI)^*}_{\ell'',S'';\bar{\ell}\bar{S}}\,. \tag{E.53}$$

The phase space factor is included in the diagonal matrix

$$\rho_{ij} = \frac{|\mathbf{p}|_i}{8\pi\sqrt{s}}\delta_{ij}\,. \tag{E.54}$$

A more standard definition of the S-matrix implies to redefine it as

$$\hat{S} \to S = 2\rho^{\frac{1}{2}}\hat{S}\rho^{\frac{1}{2}} = I + 2i\rho^{\frac{1}{2}}\hat{T}\rho^{\frac{1}{2}}\,, \tag{E.55}$$

such that now the diagonal matrix elements of the identity operator I and S are just 1 and $\eta_i e^{2i\delta_i}$, in order, where η_i is the inelasticity for channel i and δ_i its phase shift.

APPENDIX F

Compositeness in Relativistic Field Theory

The relativistic compositeness was first defined in [216]. We follow the arguments in [146]. Consider a field theory of a pseudoscalar meson (ϕ) and a bare scalar meson σ_0:

$$\mathcal{L} = \frac{1}{2}(\partial_\mu\phi\partial^\mu\phi - m^2\phi^2) + (\partial_\mu\sigma_0\partial^\mu\sigma_0 - m^2_{\sigma_0}\sigma_0^2) + g_0\sigma_0\phi^2\,, \tag{F.1}$$

where g_0 is the bare coupling constant of the three-point interaction vertex. Let us assume that there is a scalar meson bound state σ in the spectrum of the theory. The Green's function at $s = m^2_\sigma$, where s is the Mandelstam variable, is

$$\Delta(s) = \frac{Z}{s - m^2_\sigma}\,. \tag{F.2}$$

Z is the field renormalization constant and the bound state mass is related to the binding energy (V_0), $m_\sigma = m_\phi + m_\phi - V_0$.

Eq. (F.2) shows that Z is the residue of the full green function at $s = m_\sigma$. To calculate Z, let us consider the free Green's function

$$\Delta_0(s) = \frac{1}{s - m^2_{\sigma_0}} \tag{F.3}$$

and the full Green's function is related to the free Green's function via

$$\Delta(s) = \Delta_0(s) + \Delta_0(s)g_0G(s)\Delta(s) \tag{F.4}$$

where G is the two meson loop function as in eq. (3.105). The solution to eq. (F.4) is

$$\Delta(s) = \frac{1}{s - m^2_{\sigma_0} - g_0^2G(s)}\,. \tag{F.5}$$

Again, $G(s)$ is divergent. The divergence of the loop function is canceled by the infinite scalar bare mass m_{σ_0}. The renormalization condition is $s = m^2_\sigma$. After renormalization, eq. (F.5) can be written as

$$\Delta(s) = \frac{1}{s - g_0^2G(s,\mu)}\,, \tag{F.6}$$

where μ dependence of G denotes renormalization scale. Hence, the field renormalization constant can

be calculated by using eqs. (F.2) and (F.6):

$$Z = \lim_{s \to m_\sigma^2} \frac{s - m_\sigma^2}{s - g_0^2 G(s,\mu)} = \frac{1}{1 - g_0^2 \frac{\partial G(s,\mu)}{\partial s}|_{s=m_\sigma^2}} \,. \tag{F.7}$$

The residue of the scattering amplitude at the bound state pole is equal to the square of the physical coupling constant squared: $g^2 = g_0^2 Z$. Using this relation in eq. (F.7), we get

$$1 - Z = -g^2 G'(m_\sigma^2, \mu) \,. \tag{F.8}$$

This is analog of eq. (3.58) and definition of compositeness in the relativistic field theory. Since the square of the physical coupling constant is positive and derivative of loop function is negative, we get $Z \leq 1$. Eq. (F.8) can be used for resonances as well [146]:

$$1 - Z = -g^2 G'_{II}(m_\sigma^2, \mu) \,, \tag{F.9}$$

where G_{II} is the loop function on the second Riemann sheet. However, compositeness is not always well defined for resonances since $1 - Z$ might have a complex value. Eq. (F.9) approaches to eq. (F.8) as the width of the resonance /approaches to zero. Hence, for narrow resonances eq. (F.9) can be used.

References

[1] C. Patrignani et al., *Review of Particle Physics*, http://dx.doi.org/10.1088/1674-1137/40/10/100001Chin. Phys. **C40** (2016) 100001 (cit. on pp. 3, 5, 12, 27, 29, 62, 65, 74–76, 98, 99, 134).

[2] J. Erler and A. Freitas, *Electroweak Model and Constraints on New Physics*, http://dx.doi.org/10.1088/1674-1137/40/10/100001Chin. Phys. **C40** (2016) 100001, URL: http://pdg.lbl.gov/2017/reviews/rpp2017-rev-standard-model.pdf (cit. on p. 3).

[3] S. Weinberg, *What is Quantum Field Theory, and What Did We Think It Is?*, (1997), arXiv: 9702027 [hep-th], URL: http://arxiv.org/abs/hep-th/9702027 (cit. on p. 3).

[4] S. Weinberg, *The Quantum theory of fields. Vol. 1: Foundations*, Cambridge University Press, 2005, ISBN: 9780521670531 (cit. on pp. 3, 7).

[5] R. Gupta, "Introduction to lattice QCD: Course", *Probing the standard model of particle interactions. Proceedings, Summer School in Theoretical Physics, NATO Advanced Study Institute, 68th session, Les Houches, France, July 28-September 5, 1997. Pt. 1, 2*, 1997 83, arXiv: hep-lat/9807028 [hep-lat] (cit. on p. 4).

[6] A. S. Kronfeld, *Uses of effective field theory in lattice QCD: Chapter 39 in At the Frontiers of Particle Physics, Handbook of QCD*, http://dx.doi.org/10.1142/9789812777270_0004(2002), arXiv: hep-lat/0205021 [hep-lat] (cit. on p. 4).

[7] J. J. Dudek et al., *Toward the excited meson spectrum of dynamical QCD*, http://dx.doi.org/10.1103/PhysRevD.82.034508Phys. Rev. **D82** (2010) 034508, arXiv: 1004.4930 [hep-ph] (cit. on p. 4).

[8] A. Ali Khan et al., *Light hadron spectroscopy with two flavors of dynamical quarks on the lattice*, http://dx.doi.org/10.1103/PhysRevD.65.054505, 10.1103/PhysRevD.67.059901Phys. Rev. **D65** (2002) 054505, [Erratum: Phys. Rev.D67,059901(2003)], arXiv: hep-lat/0105015 [hep-lat] (cit. on p. 4).

[9] A. Karch et al., *Linear confinement and AdS/QCD*, http://dx.doi.org/10.1103/PhysRevD.74.015005Phys. Rev. **D74** (2006) 015005, arXiv: hep-ph/0602229 [hep-ph] (cit. on p. 4).

[10] J. Erlich et al., *QCD and a holographic model of hadrons*, http://dx.doi.org/10.1103/PhysRevLett.95.261602Phys. Rev. Lett. **95** (2005) 261602, arXiv: hep-ph/0501128 [hep-ph] (cit. on p. 4).

[11] R. Baron et al., *Light hadrons from lattice QCD with light (u,d), strange and charm dynamical quarks*, http://dx.doi.org/10.1007/JHEP06(2010)111JHEP **06** (2010) 111, arXiv: 1004.5284 [hep-lat] (cit. on pp. 4, 15).

[12] C. Liu, *Review on Hadron Spectroscopy*, PoS **LATTICE2016** (2017) 006, arXiv: 1612.00103 [hep-lat] (cit. on p. 4).

[13] S. Weinberg, *Phenomenological Lagrangians*, http://dx.doi.org/10.1016/0378-4371(79)90223-1Physica **A96** (1979) 327 (cit. on pp. 4, 15, 16, 18, 25).

[14] J. Gasser and H. Leutwyler, *Chiral Perturbation Theory to One Loop*, http://dx.doi.org/10.1016/0003-4916(84)90242-2Annals Phys. **158** (1984) 142 (cit. on pp. 4, 15, 19, 23, 28).

[15] J. Gasser and H. Leutwyler, *Chiral Perturbation Theory: Expansions in the Mass of the Strange Quark*, http://dx.doi.org/10.1016/0550-3213(85)90492-4Nucl. Phys. **B250** (1985) 465 (cit. on pp. 4, 15, 19, 23, 25, 28, 29).

[16] V. Bernard, N. Kaiser and U.-G. Meißner, *Chiral dynamics in nucleons and nuclei*, http://dx.doi.org/10.1142/S0218301395000092Int. J. Mod. Phys. **E4** (1995) 193, arXiv: hep-ph/9501384 [hep-ph] (cit. on pp. 4, 15, 19, 31).

[17] A. V. Manohar, *Introduction to Effective Field Theories*, (2018), arXiv: 1804.05863, URL: http://arxiv.org/abs/1804.05863 (cit. on p. 4).

[18] A. Pich, *Effective Field Theory with Nambu-Goldstone Modes*, (2018), arXiv: 1804.05664, URL: http://arxiv.org/abs/1804.05664 (cit. on p. 4).

[19] S. Scherer and M. R. Schindler, *A Chiral perturbation theory primer*, (2005), arXiv: hep-ph/0505265 [hep-ph] (cit. on pp. 4, 10, 15, 19).

[20] A. De Rujula, *Archeology and evolution of QCD*, http://dx.doi.org/10.1051/epjconf/201713701007(2016), ISSN: 2100014X, arXiv: 1610.07466, URL: http://arxiv.org/abs/1610.07466 (cit. on p. 4).

[21] L. H. Hoddeson et al., eds., *The Rise of the standard model: Particle physics in the 1960s and 1970s. Proceedings, Conference, Stanford, USA, June 24-27, 1992*, 1997, URL: http://www.cambridge.org/uk/catalogue/catalogue.asp?isbn=0521570824 (cit. on p. 4).

[22] M. Gell-Mann, *A Schematic Model of Baryons and Mesons*, http://dx.doi.org/10.1016/S0031-9163(64)92001-3Phys. Lett. **8** (1964) 214 (cit. on p. 4).

[23] G. Zweig, "An SU(3) model for strong interaction symmetry and its breaking. Version 2", *Developments in the Quark Theory of Hadrons vol. 1. 1964 - 1978*, ed. by D. Lichtenberg and S. P. Rosen, 1964 22, URL: http://inspirehep.net/record/4674/files/cern-th-412.pdf (cit. on p. 4).

[24] G. Miller et al., *Inelastic electron-Proton Scattering at Large Momentum Transfers*, http://dx.doi.org/10.1103/PhysRevD.5.528Phys. Rev. **D5** (1972) 528 (cit. on pp. 4, 5).

[25] A. Manohar and C. Sachrajda, *Quark Masses*, http://dx.doi.org/10.1088/1674-1137/40/10/100001Chin. Phys. **C40** (2016) 100001, URL: http://pdg.lbl.gov/2012/reviews/rpp2012-rev-quark-masses.pdf (cit. on p. 5).

[26] R. Aaij et al., *Observation of the resonant character of the $Z(4430)^-$ state*, http://dx.doi.org/10.1103/PhysRevLett.112.222002Phys. Rev. Lett. **112** (2014) 222002, arXiv: 1404.1903 [hep-ex] (cit. on p. 5).

[27] R. Aaij et al., *Observation of $J/\psi p$ Resonances Consistent with Pentaquark States in $\Lambda_b^0 \to J/\psi K^- p$ Decays*, http://dx.doi.org/10.1103/PhysRevLett.115.072001Phys. Rev. Lett. **115** (2015) 072001, arXiv: 1507.03414 [hep-ex] (cit. on p. 5).

[28] H.-X. Chen et al., *The hidden-charm pentaquark and tetraquark states*, http://dx.doi.org/10.1016/j.physrep.2016.05.004Phys. Rept. **639** (2016) 1, arXiv: 1601.02092 [hep-ph] (cit. on p. 5).

[29] N. Brambilla et al., *QCD and Strongly Coupled Gauge Theories: Challenges and Perspectives*, http://dx.doi.org/10.1140/epjc/s10052-014-2981-5Eur. Phys. J. **C74** (2014) 2981, arXiv: 1404.3723 [hep-ph] (cit. on p. 5).

[30] A. Ali, J. S. Lange and S. Stone, *Exotics: Heavy Pentaquarks and Tetraquarks*, http://dx.doi.org/10.1016/j.ppnp.2017.08.003Prog. Part. Nucl. Phys. **97** (2017) 123, arXiv: 1706.00610 [hep-ph] (cit. on p. 5).

[31] S. Weinberg, *The quantum theory of fields. Vol. 2: Modern applications*, Cambridge University Press, 2013, ISBN: 9781139632478, 9780521670548, 9780521550024 (cit. on pp. 5, 7, 10).

[32] F. Halzen and A. D. Martin, *Quarks and Leptons: An Introductory Course in Modern Particle Physics*, 1984, ISBN: 0471887412, 9780471887416 (cit. on p. 5).

[33] J. Steinberger, *On the Use of Subtraction Fields and the Lifetimes of Some Types of Meson Decay*, http://dx.doi.org/10.1103/PhysRev.76.1180Phys. Rev. **76** (8 1949) 1180, URL: https://link.aps.org/doi/10.1103/PhysRev.76.1180 (cit. on p. 5).

[34] J. F. Donoghue, E. Golowich and B. R. Holstein, *Dynamics of the standard model*, Camb. Monogr. Part. Phys. Nucl. Phys. Cosmol. **2** (1992) 1, [Camb. Monogr. Part. Phys. Nucl. Phys. Cosmol.35(2014)] (cit. on pp. 5, 10).

[35] R. P. Feynman, *Very High-Energy Collisions of Hadrons*, http://dx.doi.org/10.1103/PhysRevLett.23.1415Phys. Rev. Lett. **23** (24 1969) 1415, URL: https://link.aps.org/doi/10.1103/PhysRevLett.23.1415 (cit. on p. 5).

[36] H. D. Politzer, *Reliable Perturbative Results for Strong Interactions?*, http://dx.doi.org/10.1103/PhysRevLett.30.1346Phys. Rev. Lett. **30** (26 1973) 1346, URL: https://link.aps.org/doi/10.1103/PhysRevLett.30.1346 (cit. on p. 6).

[37] D. J. Gross and F. Wilczek, *Ultraviolet Behavior of Non-Abelian Gauge Theories*, http://dx.doi.org/10.1103/PhysRevLett.30.1343Phys. Rev. Lett. **30** (26 1973) 1343, URL: https://link.aps.org/doi/10.1103/PhysRevLett.30.1343 (cit. on p. 6).

[38] G. 't Hooft, *Renormalizable Lagrangians for Massive Yang-Mills Fields*, http://dx.doi.org/10.1016/0550-3213(71)90139-8Nucl. Phys. **B35** (1971) 167, [,201(1971)] (cit. on p. 6).

[39] A. Zee, *Study of the Renormalization Group for Small Coupling Constants*, http://dx.doi.org/10.1103/PhysRevD.7.3630Phys. Rev. D **7** (12 1973) 3630, URL: https://link.aps.org/doi/10.1103/PhysRevD.7.3630 (cit. on p. 6).

[40] R. K. Ellis, W. J. Stirling and B. R. Webber, *QCD and collider physics*, vol. 8, 1996 1 (cit. on p. 6).

[41] D. H. Perkins, *Introduction to high energy physics*, 1982, ISBN: 9780521621960 (cit. on pp. 7, 26).

[42] F.-K. Guo et al., *The electric dipole moment of the neutron from 2+1 flavor lattice QCD*, http://dx.doi.org/10.1103/PhysRevLett.115.062001Phys. Rev. Lett. **115** (2015) 062001, arXiv: 1502.02295 [hep-lat] (cit. on p. 8).

[43] C. A. Baker et al., *An Improved experimental limit on the electric dipole moment of the neutron*, http://dx.doi.org/10.1103/PhysRevLett.97.131801Phys. Rev. Lett. **97** (2006) 131801, arXiv: hep-ex/0602020 [hep-ex] (cit. on p. 8).

[44] R. D. Peccei and H. R. Quinn, *CP Conservation in the Presence of Instantons*, http://dx.doi.org/10.1103/PhysRevLett.38.1440Phys. Rev. Lett. **38** (1977) 1440, [,328(1977)] (cit. on p. 8).

[45] H. Banerjee, D. Chatterjee and P. Mitra, *Is there still a strong CP problem?*, http://dx.doi.org/10.1016/j.physletb.2003.08.058Phys. Lett. **B573** (2003) 109, arXiv: hep-ph/0012284 [hep-ph] (cit. on p. 8).

[46] A. I. Vainshtein et al., *ABC's of Instantons*, http://dx.doi.org/10.1070/PU1982v025n04ABEH004533Sov. Phys. Usp. **25** (1982) 195, [,201(1981)] (cit. on p. 8).

[47] N. R. Acharya et al., *-dependence of the lightest meson resonances in QCD*, http://dx.doi.org/10.1103/PhysRevD.92.054023Phys. Rev. **D92** (2015) 054023, arXiv: 1507.08570 [hep-ph] (cit. on p. 8).

[48] Y. Nambu, *Quasiparticles and Gauge Invariance in the Theory of Superconductivity*, http://dx.doi.org/10.1103/PhysRev.117.648Phys. Rev. **117** (1960) 648 (cit. on p. 10).

[49] J. Goldstone, *Field Theories with Superconductor Solutions*, http://dx.doi.org/10.1007/BF02812722Nuovo Cim. **19** (1961) 154 (cit. on p. 10).

[50] C. Vafa and E. Witten, *Restrictions on Symmetry Breaking in Vector-Like Gauge Theories*, http://dx.doi.org/10.1016/0550-3213(84)90230-XNucl. Phys. **B234** (1984) 173 (cit. on p. 10).

[51] S. L. Adler and R. F. Dashen, eds., *Current Algebras and Applications to Particle Physics*, Benjamin, 1968 (cit. on pp. 13, 15).

[52] H. Leutwyler, *Chiral effective Lagrangians*, http://dx.doi.org/10.1007/3-540-54978-1_8(1991) 97, [Lect. Notes Phys.396,1(1991)] (cit. on p. 15).

[53] U.-G. Meißner, *Low-Energy Hadron Physics from Effective Chiral Lagrangians with Vector Mesons*, http://dx.doi.org/10.1016/0370-1573(88)90090-7Phys. Rept. **161** (1988) 213 (cit. on pp. 15, 32, 33, 36, 37).

[54] V. Bernard and U.-G. Meißner, *Chiral perturbation theory*, http://dx.doi.org/10.1146/annurev.nucl.56.080805.140449Ann. Rev. Nucl. Part. Sci. **57** (2007) 33, arXiv: hep-ph/0611231 [hep-ph] (cit. on pp. 15, 19).

[55] S. Narison, *QCD as a Theory of Hadrons*, vol. 17, Cambridge University Press, 2007, ISBN: 9780521037310, 9780521811644, 9780511189487, URL: http://www.cambridge.org/zw/academic/subjects/physics/particle-physics-and-nuclear-physics/qcd-theory-hadrons-partons-confinement?format=PB (cit. on p. 15).

[56] M. A. Shifman, A. I. Vainshtein and V. I. Zakharov,
QCD and Resonance Physics. Theoretical Foundations,
http://dx.doi.org/10.1016/0550-3213(79)90022-1Nucl. Phys. **B147** (1979) 385
(cit. on pp. 15, 29).

[57] H.-X. Chen, A. Hosaka and S.-L. Zhu,
QCD sum rule study of the masses of light tetraquark scalar mesons,
http://dx.doi.org/10.1016/j.physletb.2007.05.031Phys. Lett. **B650** (2007) 369,
arXiv: hep-ph/0609163 [hep-ph] (cit. on p. 15).

[58] F. J. Yndurain, *Low-energy pion physics*, (2002), arXiv: hep-ph/0212282 [hep-ph]
(cit. on p. 15).

[59] C. D. Roberts and A. G. Williams,
Dyson-Schwinger equations and their application to hadronic physics,
http://dx.doi.org/10.1016/0146-6410(94)90049-3Prog. Part. Nucl. Phys. **33** (1994) 477,
arXiv: hep-ph/9403224 [hep-ph] (cit. on p. 15).

[60] S. R. Cotanch and P. Maris,
QCD based quark description of pi pi scattering up to the sigma and rho region,
http://dx.doi.org/10.1103/PhysRevD.66.116010Phys. Rev. **D66** (2002) 116010,
arXiv: hep-ph/0210151 [hep-ph] (cit. on p. 15).

[61] G. Eichmann, C. S. Fischer and W. Heupel, *The light scalar mesons as tetraquarks*,
http://dx.doi.org/10.1016/j.physletb.2015.12.036Phys. Lett. **B753** (2016) 282,
arXiv: 1508.07178 [hep-ph] (cit. on p. 15).

[62] R. G. Edwards et al., *Excited state baryon spectroscopy from lattice QCD*,
http://dx.doi.org/10.1103/PhysRevD.84.074508Phys. Rev. **D84** (2011) 074508,
arXiv: 1104.5152 [hep-ph] (cit. on p. 15).

[63] J. J. Dudek, R. G. Edwards and D. J. Wilson,
An a_0 resonance in strongly coupled $\pi\eta$, $K\overline{K}$ scattering from lattice QCD,
http://dx.doi.org/10.1103/PhysRevD.93.094506Phys. Rev. **D93** (2016) 094506,
arXiv: 1602.05122 [hep-ph] (cit. on p. 15).

[64] E. Epelbaum, W. Gloeckle and U.-G. Meißner, *Nuclear forces from chiral Lagrangians using the method of unitary transformation. 1. Formalism*,
http://dx.doi.org/10.1016/S0375-9474(98)00220-6Nucl. Phys. **A637** (1998) 107,
arXiv: nucl-th/9801064 [nucl-th] (cit. on p. 15).

[65] E. Epelbaum, W. Gloeckle and U.-G. Meißner, *Nuclear forces from chiral Lagrangians using the method of unitary transformation. 2. The two nucleon system*,
http://dx.doi.org/10.1016/S0375-9474(99)00821-0Nucl. Phys. **A671** (2000) 295,
arXiv: nucl-th/9910064 [nucl-th] (cit. on p. 15).

[66] E. Epelbaum, H.-W. Hammer and U.-G. Meißner, *Modern Theory of Nuclear Forces*,
http://dx.doi.org/10.1103/RevModPhys.81.1773Rev. Mod. Phys. **81** (2009) 1773,
arXiv: 0811.1338 [nucl-th] (cit. on p. 15).

[67] J. Bijnens and G. Ecker, *Mesonic low-energy constants*,
http://dx.doi.org/10.1146/annurev-nucl-102313-025528Ann. Rev. Nucl. Part. Sci. **64** (2014) 149,
arXiv: 1405.6488 [hep-ph] (cit. on pp. 15, 30).

[68] H. Leutwyler, "Principles of chiral perturbation theory", *Hadrons 94 Workshop Gramado, Brazil, April 10-14, 1994*, 1994 1, arXiv: hep-ph/9406283 [hep-ph] (cit. on pp. 16, 22).

[69] E. Fermi, *An attempt of a theory of beta radiation. 1.*, http://dx.doi.org/10.1007/BF01351864Z. Phys. **88** (1934) 161 (cit. on p. 17).

[70] R. P. Feynman and M. Gell-Mann, *Theory of the Fermi Interaction*, http://dx.doi.org/10.1103/PhysRev.109.193Phys. Rev. **109** (1 1958) 193, URL: https://link.aps.org/doi/10.1103/PhysRev.109.193 (cit. on p. 17).

[71] J. Zinn-Justin, *Quantum field theory and critical phenomena*, Int. Ser. Monogr. Phys. **77** (1989) 1 (cit. on p. 17).

[72] T. Appelquist and J. Carazzone, *Infrared Singularities and Massive Fields*, http://dx.doi.org/10.1103/PhysRevD.11.2856Phys. Rev. **D11** (1975) 2856 (cit. on p. 18).

[73] S. Weinberg, *Nonlinear realizations of chiral symmetry*, http://dx.doi.org/10.1103/PhysRev.166.1568Phys. Rev. **166** (1968) 1568 (cit. on pp. 19, 33).

[74] S. R. Coleman, J. Wess and B. Zumino, *Structure of phenomenological Lagrangians. 1.*, http://dx.doi.org/10.1103/PhysRev.177.2239Phys. Rev. **177** (1969) 2239 (cit. on p. 19).

[75] C. G. Callan Jr. et al., *Structure of phenomenological Lagrangians. 2.*, http://dx.doi.org/10.1103/PhysRev.177.2247Phys. Rev. **177** (1969) 2247 (cit. on p. 19).

[76] J. Gasser, *Chiral perturbation theory*, http://dx.doi.org/10.1016/S0920-5632(00)00573-9Nucl. Phys. Proc. Suppl. **86** (2000) 257, arXiv: hep-ph/9912548 [hep-ph] (cit. on p. 19).

[77] U.-G. Meißner and G. Schierholz, "Lattice QCD, Chiral Perturbation Theory and Hadron Phenomenology", *ECT* Workshop on Lattice QCD, Chiral Perturbation Theory and Hadron Phenomenology Trento, Italy, October 2-6, 2006*, 2006, arXiv: hep-ph/0611072 [hep-ph] (cit. on p. 19).

[78] U.-G. Meißner, H.-W. Hammer and A. Wirzba, eds., *Chiral dynamics: Theory and experiment (CD2003). Mini-Proceedings, Fourth International Workshop*, 2003, arXiv: hep-ph/0311212 [hep-ph] (cit. on p. 19).

[79] G. Colangelo and G. Isidori, "An Introduction to ChPT", *Nuclear, subnuclear and astroparticle physics. Proceedings, 5th LNF Spring School, Frascati, Italy, May 15-20, 2000*, 2000 333, arXiv: hep-ph/0101264 [hep-ph] (cit. on p. 19).

[80] H. Leutwyler, "Theoretical chiral dynamics", *Chiral dynamics: Theory and experiment. Proceedings, 3rd Workshop, Newport News, USA, July 17-22, 2000*, 2000 3, arXiv: hep-ph/0011140 [hep-ph] (cit. on p. 19).

[81] A. S. Kronfeld, *Twenty-first Century Lattice Gauge Theory: Results from the QCD Lagrangian*, http://dx.doi.org/10.1146/annurev-nucl-102711-094942Ann. Rev. Nucl. Part. Sci. **62** (2012) 265, arXiv: 1203.1204 [hep-lat] (cit. on p. 19).

[82] S. Scherer, *Introduction to chiral perturbation theory*, Adv. Nucl. Phys. **27** (2003) 277, arXiv: hep-ph/0210398 [hep-ph] (cit. on pp. 19, 22, 23).

[83] H. Leutwyler, *Nonrelativistic effective Lagrangians*, http://dx.doi.org/10.1103/PhysRevD.49.3033Phys. Rev. **D49** (1994) 3033, arXiv: hep-ph/9311264 [hep-ph] (cit. on p. 21).

[84] S. Weinberg, *Strong interactions at low-energies*, http://dx.doi.org/10.1007/3-540-59279-2_61(1994) 0003, [Lect. Notes Phys.452,1(1995)], arXiv: hep-ph/9412326 [hep-ph] (cit. on p. 21).

[85] M. Gell-Mann and M. Levy, *The axial vector current in beta decay*, http://dx.doi.org/10.1007/BF02859738Nuovo Cim. **16** (1960) 705 (cit. on p. 21).

[86] O. Cata and V. Mateu, *Chiral perturbation theory with tensor sources*, http://dx.doi.org/10.1088/1126-6708/2007/09/078JHEP **09** (2007) 078, arXiv: 0705.2948 [hep-ph] (cit. on p. 22).

[87] M. Gell-Mann, R. J. Oakes and B. Renner, *Behavior of current divergences under SU(3) x SU(3)*, http://dx.doi.org/10.1103/PhysRev.175.2195Phys. Rev. **175** (1968) 2195 (cit. on p. 26).

[88] S. Okubo and B. Sakita, *Unitary Symmetry and Decay of eta Meson*, http://dx.doi.org/10.1103/PhysRevLett.11.50Phys. Rev. Lett. **11** (1963) 50 (cit. on p. 26).

[89] M. Gell-Mann, *The Eightfold Way: A Theory of strong interaction symmetry*, (1961) (cit. on p. 26).

[90] J. Gomis and S. Weinberg, *Are nonrenormalizable gauge theories renormalizable?*, http://dx.doi.org/10.1016/0550-3213(96)00132-0Nucl. Phys. **B469** (1996) 473, arXiv: hep-th/9510087 [hep-th] (cit. on p. 27).

[91] J. Wess and B. Zumino, *Consequences of anomalous Ward identities*, http://dx.doi.org/10.1016/0370-2693(71)90582-XPhys. Lett. **37B** (1971) 95 (cit. on p. 28).

[92] E. Witten, *Global Aspects of Current Algebra*, http://dx.doi.org/10.1016/0550-3213(83)90063-9Nucl. Phys. **B223** (1983) 422 (cit. on p. 28).

[93] L. Maiani, G. Pancheri and N. Paver, eds., *The second DAPHNE physics handbook. Vol. 1, 2*, INFN, 1995, ISBN: 9788886409025, URL: http://www.lnf.infn.it/theory/hcm/dafne2006.html (cit. on p. 30).

[94] S. Aoki et al., *Review of lattice results concerning low-energy particle physics*, http://dx.doi.org/10.1140/epjc/s10052-016-4509-7Eur. Phys. J. **C77** (2017) 112, arXiv: 1607.00299 [hep-lat] (cit. on p. 30).

[95] G. Ecker et al., *The Role of Resonances in Chiral Perturbation Theory*, http://dx.doi.org/10.1016/0550-3213(89)90346-5Nucl. Phys. **B321** (1989) 311 (cit. on pp. 31, 32).

[96] G. Ecker et al., *Chiral Lagrangians for Massive Spin 1 Fields*, http://dx.doi.org/10.1016/0370-2693(89)91627-4Phys. Lett. **B223** (1989) 425 (cit. on pp. 31, 32).

[97] J. F. Donoghue, C. Ramirez and G. Valencia, *The Spectrum of QCD and Chiral Lagrangians of the Strong and Weak Interactions*, http://dx.doi.org/10.1103/PhysRevD.39.1947Phys. Rev. **D39** (1989) 1947 (cit. on p. 31).

[98] J. R. Pelaez, *From controversy to precision on the sigma meson: a review on the status of the non-ordinary $f_0(500)$ resonance*, http://dx.doi.org/10.1016/j.physrep.2016.09.001Phys. Rept. **658** (2016) 1, arXiv: 1510.00653 [hep-ph] (cit. on pp. 31, 39, 55, 59).

[99] V. Bernard, N. Kaiser and U.-G. Meißner, *Threshold parameters of pi K scattering in QCD*, Phys. Rev. **D43** (1991) 2757 (cit. on p. 31).

[100] V. Bernard, N. Kaiser and U.-G. Meißner,
pi K scattering in chiral perturbation theory to one loop,
http://dx.doi.org/10.1016/0550-3213(91)90461-6Nucl. Phys. **B357** (1991) 129 (cit. on p. 31).

[101] V. Bernard, N. Kaiser and U.-G. Meißner, *pi eta scattering in QCD*,
http://dx.doi.org/10.1103/PhysRevD.44.3698Phys. Rev. **D44** (1991) 3698 (cit. on p. 31).

[102] G. Colangelo, J. Gasser and H. Leutwyler, *$\pi\pi$ scattering*,
http://dx.doi.org/10.1016/S0550-3213(01)00147-XNucl. Phys. **B603** (2001) 125,
arXiv: hep-ph/0103088 [hep-ph] (cit. on p. 31).

[103] J. Bijnens, P. Dhonte and P. Talavera, *Pi pi scattering in three flavor ChPT*,
http://dx.doi.org/10.1088/1126-6708/2004/01/050JHEP **01** (2004) 050,
arXiv: hep-ph/0401039 [hep-ph] (cit. on p. 31).

[104] J. Bijnens, P. Dhonte and P. Talavera, *pi K scattering in three flavor ChPT*,
http://dx.doi.org/10.1088/1126-6708/2004/05/036JHEP **05** (2004) 036,
arXiv: hep-ph/0404150 [hep-ph] (cit. on p. 31).

[105] T. N. Truong, *Chiral Perturbation Theory and Final-State Theorem*,
http://dx.doi.org/10.1103/PhysRevLett.61.2526Phys. Rev. Lett. **61** (22 1988) 2526,
URL: https://link.aps.org/doi/10.1103/PhysRevLett.61.2526
(cit. on pp. 31, 54, 56).

[106] J. Gasser and U.-G. Meißner, *On the phase of epsilon-prime*,
http://dx.doi.org/10.1016/0370-2693(91)91235-NPhys. Lett. **B258** (1991) 219
(cit. on pp. 31, 32, 54).

[107] J. Gasser and U.-G. Meißner, *Chiral expansion of pion form-factors beyond one loop*,
http://dx.doi.org/10.1016/0550-3213(91)90460-FNucl. Phys. **B357** (1991) 90
(cit. on pp. 31, 32, 54, 56).

[108] J. R. Pelaez et al., *Unitarized Chiral Perturbation Theory and the Meson Spectrum*,
http://dx.doi.org/10.1063/1.3483311AIP Conf. Proc. **1257** (2010) 141,
arXiv: 1003.0364 [hep-ph] (cit. on pp. 32, 57).

[109] J. A. Oller and E. Oset, *N/D description of two meson amplitudes and chiral symmetry*,
http://dx.doi.org/10.1103/PhysRevD.60.074023Phys. Rev. **D60** (1999) 074023, [,165(1998)],
arXiv: hep-ph/9809337 [hep-ph] (cit. on pp. 32, 58, 61, 63, 69, 77, 79, 83, 91).

[110] A. Gomez Nicola and J. R. Pelaez,
Meson meson scattering within one loop chiral perturbation theory and its unitarization,
http://dx.doi.org/10.1103/PhysRevD.65.054009Phys. Rev. **D65** (2002) 054009,
arXiv: hep-ph/0109056 [hep-ph] (cit. on p. 32).

[111] J. A. Oller and E. Oset, *Chiral symmetry amplitudes in the S wave isoscalar and isovector channels and the σ, $f_0(980)$, $a_0(980)$ scalar mesons*,
http://dx.doi.org/10.1016/S0375-9474(99)00427-3, 10.1016/S0375-9474(97)00160-7Nucl. Phys. **A620** (1997) 438, [Erratum: Nucl. Phys.A652,407(1999)], arXiv: hep-ph/9702314 [hep-ph]
(cit. on pp. 32, 59, 62, 63, 69).

[112] J. A. Oller, E. Oset and J. R. Pelaez,
Nonperturbative approach to effective chiral Lagrangians and meson interactions,
http://dx.doi.org/10.1103/PhysRevLett.80.3452Phys. Rev. Lett. **80** (1998) 3452,
arXiv: hep-ph/9803242 [hep-ph] (cit. on pp. 32, 58).

[113] T. Fujiwara et al., *Nonabelian Anomaly and Vector Mesons as Dynamical Gauge Bosons of Hidden Local Symmetries*, http://dx.doi.org/10.1143/PTP.73.926Prog. Theor. Phys. **73** (1985) 926 (cit. on p. 32).

[114] P. Jain et al., *Realistic Pseudoscalar Vector Chiral Lagrangian and Its Soliton Excitations*, http://dx.doi.org/10.1103/PhysRevD.37.3252Phys. Rev. **D37** (1988) 3252 (cit. on p. 32).

[115] R. Molina, D. Nicmorus and E. Oset, *The rho rho interaction in the hidden gauge formalism and the f(0)(1370) and f(2)(1270) resonances*, http://dx.doi.org/10.1103/PhysRevD.78.114018Phys. Rev. **D78** (2008) 114018, arXiv: 0809.2233 [hep-ph] (cit. on pp. 32, 62–65, 68–73, 75, 76, 79, 81–83, 87, 96).

[116] L. S. Geng and E. Oset, *Vector meson-vector meson interaction in a hidden gauge unitary approach*, http://dx.doi.org/10.1103/PhysRevD.79.074009Phys. Rev. **D79** (2009) 074009, arXiv: 0812.1199 [hep-ph] (cit. on pp. 32, 62, 64, 82, 83, 87, 90, 91, 94, 96, 97, 99, 100).

[117] D. Djukanovic et al., *Universality of the rho-meson coupling in effective field theory*, http://dx.doi.org/10.1103/PhysRevLett.93.122002Phys. Rev. Lett. **93** (2004) 122002, arXiv: hep-ph/0407239 [hep-ph] (cit. on p. 33).

[118] P. C. Bruns and U.-G. Meißner, *Infrared regularization for spin-1 fields*, http://dx.doi.org/10.1140/epjc/s2005-02118-0Eur. Phys. J. **C40** (2005) 97, arXiv: hep-ph/0411223 [hep-ph] (cit. on p. 33).

[119] M. Bando, T. Kugo and K. Yamawaki, *Composite Gauge Bosons and 'Low-energy Theorems' of Hidden Local Symmetries*, http://dx.doi.org/10.1143/PTP.73.1541Prog. Theor. Phys. **73** (1985) 1541 (cit. on pp. 33, 35, 37).

[120] G. J. Gounaris and J. J. Sakurai, *Finite width corrections to the vector meson dominance prediction for rho —> e+ e-*, http://dx.doi.org/10.1103/PhysRevLett.21.244Phys. Rev. Lett. **21** (1968) 244 (cit. on p. 33).

[121] K. Kawarabayashi and M. Suzuki, *Partially conserved axial vector current and the decays of vector mesons*, http://dx.doi.org/10.1103/PhysRevLett.16.255Phys. Rev. Lett. **16** (1966) 255 (cit. on pp. 33, 35, 37).

[122] Riazuddin and Fayyazuddin, *Algebra of current components and decay widths of rho and K* mesons*, http://dx.doi.org/10.1103/PhysRev.147.1071Phys. Rev. **147** (1966) 1071 (cit. on pp. 33, 35, 37).

[123] A. D'Adda, M. Luscher and P. Di Vecchia, *A 1/n Expandable Series of Nonlinear Sigma Models with Instantons*, http://dx.doi.org/10.1016/0550-3213(78)90432-7Nucl. Phys. **B146** (1978) 63 (cit. on p. 34).

[124] M. Bando, T. Kugo and K. Yamawaki, *Nonlinear Realization and Hidden Local Symmetries*, http://dx.doi.org/10.1016/0370-1573(88)90019-1Phys. Rept. **164** (1988) 217 (cit. on pp. 34, 36, 38, 75).

[125] J. Sakurai, *Collision Theory*, University of Chicago Press, 1969 (cit. on p. 36).

[126] M. Bando, T. Kugo and K. Yamawaki, *On the Vector Mesons as Dynamical Gauge Bosons of Hidden Local Symmetries*, http://dx.doi.org/10.1016/0550-3213(85)90647-9Nucl. Phys. **B259** (1985) 493 (cit. on p. 37).

[127] U.-G. Meißner et al., *Skyrmions With ρ and ω Mesons as Dynamical Gauge Bosons*, http://dx.doi.org/10.1103/PhysRevLett.57.1676Phys. Rev. Lett. **57** (1986) 1676 (cit. on p. 37).

[128] N. Kaiser and U.-G. Meißner, *Generalized hidden symmetry for low-energy hadron physics*, http://dx.doi.org/10.1016/0375-9474(90)90431-KNucl. Phys. **A519** (1990) 671 (cit. on p. 38).

[129] W. Heisenberg, *The "Observable Quantities" in the Theory of Elementary Particles*, Z. Phys. **120** (1943) 513 (cit. on p. 39).

[130] R. Omnès and G. Barton, *Introduction to particle physics*, Translation of: Introduction à l'étude des particules élémentaires, London ; New York : Wiley-Interscience, 1971 (cit. on pp. 39, 42, 43).

[131] A. Martin and T. Spearman, *Elementary Particle Theory*, North-Holland Pub. Co., 1970 (cit. on pp. 40, 42, 43, 61, 79, 114, 115, 118).

[132] H. M. Nussenzveig, *Causality and dispersion relations*, New York : Academic Press, 1972, ISBN: 0125230508 (cit. on p. 41).

[133] S. Mandelstam, *Determination of the Pion-Nucleon Scattering Amplitude from Dispersion Relations and Unitarity. General Theory*, http://dx.doi.org/10.1103/PhysRev.112.1344Phys. Rev. **112** (1958) 1344, URL: https://link.aps.org/doi/10.1103/PhysRev.112.1344 (cit. on p. 42).

[134] S. Mandelstam, *Analytic Properties of Transition Amplitudes in Perturbation Theory*, http://dx.doi.org/10.1103/PhysRev.115.1741Phys. Rev. **115** (6 1959) 1741, URL: https://link.aps.org/doi/10.1103/PhysRev.115.1741 (cit. on p. 42).

[135] V. N. Gribov, *Strong interactions of hadrons at high emnergies: Gribov lectures on*, ed. by Y. L. Dokshitzer and J. Nyiri, Cambridge University Press, 2012, ISBN: 9781107411302, 9780521856096, 9780511451454, URL: http://cambridge.org/catalogue/catalogue.asp?isbn=9780521856096 (cit. on pp. 42, 43, 48).

[136] F.-K. Guo et al., *Hadronic molecules*, http://dx.doi.org/10.1103/RevModPhys.90.015004Rev. Mod. Phys. **90** (2018) 015004, arXiv: 1705.00141 [hep-ph] (cit. on p. 44).

[137] R. Vance. Churchill and J. Ward Brown, *Complex variables and applications / Ruel V. Churchill, James Ward Brown*, 1990 (cit. on p. 46).

[138] D. I. Olive, *Unitarity and the evaluation of discontinuities*, http://dx.doi.org/10.1007/BF02754344Il Nuovo Cimento (1955-1965) **26** (1962) 73, URL: https://doi.org/10.1007/BF02754344 (cit. on p. 47).

[139] R. J. Eden et al., *The analytic S-matrix*, Cambridge Univ. Press, 1966, URL: https://cds.cern.ch/record/98637 (cit. on p. 48).

[140] J. Houard and B. Jouvet, *Etude d'un modèle de champ à constante de renormalisation nulle*, http://dx.doi.org/10.1007/BF02732720Il Nuovo Cimento (1955-1965) **18** (1960) 466, ISSN: 1827-6121, URL: https://doi.org/10.1007/BF02732720 (cit. on p. 49).

[141] A. Salam, *Lagrangian theory of composite particles*, http://dx.doi.org/10.1007/BF02733330Il Nuovo Cimento **25** (1962) 224 (cit. on p. 49).

[142] S. Weinberg, *Evidence That the Deuteron Is Not an Elementary Particle*, http://dx.doi.org/10.1103/PhysRev.137.B672Phys. Rev. **137** (3B 1965) B672, URL: https://link.aps.org/doi/10.1103/PhysRev.137.B672 (cit. on p. 49).

[143] V. Baru et al., *Evidence that the a(0)(980) and f(0)(980) are not elementary particles*, http://dx.doi.org/10.1016/j.physletb.2004.01.088Phys. Lett. **B586** (2004) 53, arXiv: hep-ph/0308129 [hep-ph] (cit. on p. 49).

[144] Z.-H. Guo and J. A. Oller, *Probabilistic interpretation of compositeness relation for resonances*, http://dx.doi.org/10.1103/PhysRevD.93.096001Phys. Rev. **D93** (2016) 096001, arXiv: 1508.06400 [hep-ph] (cit. on p. 49).

[145] J. A. Oller, *New results from a number operator interpretation of the compositeness of bound and resonant states*, (2017), arXiv: 1710.00991 [hep-ph] (cit. on p. 49).

[146] T. Hyodo, D. Jido and A. Hosaka, *Compositeness of dynamically generated states in a chiral unitary approach*, http://dx.doi.org/10.1103/PhysRevC.85.015201Phys. Rev. **C85** (2012) 015201, arXiv: 1108.5524 [nucl-th] (cit. on pp. 49, 71, 77, 121, 122).

[147] M. Froissart, *Asymptotic behavior and subtractions in the Mandelstam representation*, http://dx.doi.org/10.1103/PhysRev.123.1053Phys. Rev. **123** (1961) 1053 (cit. on p. 52).

[148] T. N. Truong, *Remarks on unitarization methods*, http://dx.doi.org/10.1103/PhysRevLett.67.2260Phys. Rev. Lett. **67** (17 1991) 2260, URL: https://link.aps.org/doi/10.1103/PhysRevLett.67.2260 (cit. on pp. 54, 56).

[149] A. Dobado and J. R. Pelaez, *Unitarity and $\gamma\gamma \to \pi\pi$ in chiral perturbation theory*, http://dx.doi.org/10.1007/BF01474345Z. Phys. **C57** (1993) 501 (cit. on p. 54).

[150] A. Dobado and J. R. Pelaez, *The Inverse amplitude method in chiral perturbation theory*, http://dx.doi.org/10.1103/PhysRevD.56.3057Phys. Rev. **D56** (1997) 3057, arXiv: hep-ph/9604416 [hep-ph] (cit. on p. 56).

[151] Z. Y. Zhou et al., *The Pole structure of the unitary, crossing symmetric low energy pi pi scattering amplitudes*, http://dx.doi.org/10.1088/1126-6708/2005/02/043JHEP **02** (2005) 043, arXiv: hep-ph/0406271 [hep-ph] (cit. on p. 56).

[152] J. R. Pelaez, *Light scalars as tetraquarks or two-meson states from large N(c) and unitarized chiral perturbation theory*, http://dx.doi.org/10.1142/S0217732304016160Mod. Phys. Lett. **A19** (2004) 2879, arXiv: hep-ph/0411107 [hep-ph] (cit. on p. 57).

[153] J. A. Oller and U.-G. Meißner, *Chiral dynamics in the presence of bound states: Kaon nucleon interactions revisited*, http://dx.doi.org/10.1016/S0370-2693(01)00078-8Phys. Lett. **B500** (2001) 263, arXiv: hep-ph/0011146 [hep-ph] (cit. on pp. 58, 62, 69).

[154] J. A. Oller, E. Oset and J. R. Pelaez, *Meson meson interaction in a nonperturbative chiral approach*, http://dx.doi.org/10.1103/PhysRevD.59.074001, 10.1103/PhysRevD.60.099906, 10.1103/PhysRevD.75.099903Phys. Rev. **D59** (1999) 074001, [Erratum: Phys. Rev.D75,099903(2007)], arXiv: hep-ph/9804209 [hep-ph] (cit. on pp. 58, 69, 74).

[155] B. Borasoy et al., *A Gauge invariant chiral unitary framework for kaon photo- and electroproduction on the proton*, http://dx.doi.org/10.1140/epja/i2007-10492-4Eur. Phys. J. **A34** (2007) 161, arXiv: 0709.3181 [nucl-th] (cit. on p. 59).

[156] G. F. Chew and S. Mandelstam, *Theory of low-energy pion pion interactions*, http://dx.doi.org/10.1103/PhysRev.119.467Phys. Rev. **119** (1960) 467 (cit. on pp. 60, 63, 78, 83, 91).

[157] M. Goldberger and K. Watson, *Collision Theory*, John Wiley and Sons Inc., 1970 (cit. on p. 61).

[158] D. Gülmez, U.-G. Meißner and J. A. Oller, *A chiral covariant approach to ρρ scattering*, http://dx.doi.org/10.1140/epjc/s10052-017-5018-zEur. Phys. J. **C77** (2017) 460, arXiv: 1611.00168 [hep-ph] (cit. on pp. 62–65, 83, 91, 112).

[159] R. H. Dalitz and S. F. Tuan, *A possible resonant state in pion-hyperon scattering*, http://dx.doi.org/10.1103/PhysRevLett.2.425Phys. Rev. Lett. **2** (1959) 425 (cit. on p. 62).

[160] D. Jido et al., *Chiral dynamics of the two Lambda(1405) states*, http://dx.doi.org/10.1016/S0375-9474(03)01598-7Nucl. Phys. **A725** (2003) 181, arXiv: nucl-th/0303062 [nucl-th] (cit. on pp. 62, 69).

[161] H. Y. Lu et al., *First Observation of the* $\Lambda(1405)$ *Line Shape in Electroproduction*, http://dx.doi.org/10.1103/PhysRevC.88.045202Phys. Rev. **C88** (2013) 045202, arXiv: 1307.4411 [nucl-ex] (cit. on p. 62).

[162] J. D. Weinstein and N. Isgur, *K anti-K Molecules*, http://dx.doi.org/10.1103/PhysRevD.41.2236Phys. Rev. **D41** (1990) 2236 (cit. on p. 62).

[163] G. Janssen et al., *On the structure of the scalar mesons f0 (975) and a0 (980)*, http://dx.doi.org/10.1103/PhysRevD.52.2690Phys. Rev. **D52** (1995) 2690, arXiv: nucl-th/9411021 [nucl-th] (cit. on p. 62).

[164] H. Nagahiro et al., *The gamma gamma decay of the f(0)(1370) and f(2)(1270) resonances in the hidden gauge formalism*, http://dx.doi.org/10.1103/PhysRevD.79.114023Phys. Rev. **D79** (2009) 114023, arXiv: 0809.3717 [hep-ph] (cit. on p. 62).

[165] J.-J. Xie, E. Oset and L.-S. Geng, *Photoproduction of the* $f_2'(1525), a_2(1320)$*, and* $K_2^*(1430)$, http://dx.doi.org/10.1103/PhysRevC.93.025202Phys. Rev. **C93** (2016) 025202, arXiv: 1509.06469 [nucl-th] (cit. on p. 62).

[166] E. Oset, L. S. Geng and R. Molina, *Vector meson-vector meson interaction and dynamically generated resonances*, http://dx.doi.org/10.1088/1742-6596/348/1/012004J. Phys. Conf. Ser. **348** (2012) 012004 (cit. on p. 62).

[167] M. Koll et al., *A Relativistic quark model for mesons with an instanton induced interaction*, http://dx.doi.org/10.1007/PL00013675Eur. Phys. J. **A9** (2000) 73, arXiv: hep-ph/0008220 [hep-ph] (cit. on p. 62).

[168] R. Ricken et al., *The Meson spectrum in a covariant quark model*, http://dx.doi.org/10.1007/s100500070041Eur. Phys. J. **A9** (2000) 221, arXiv: hep-ph/0008221 [hep-ph] (cit. on p. 62).

[169] C. Amsler, T. DeGrand and B. Krusche, *Quark Model*, Review in [1] (), URL: http://www-pdg.lbl.gov/2017/reviews/rpp2017-rev-quark-model.pdf (cit. on p. 62).

[170] M. Krammer and H. Krasemann, *Two Gluon Jets from Upsilon-prime (10)*, http://dx.doi.org/10.1016/0370-2693(78)90171-5Phys. Lett. **73B** (1978) 58 (cit. on p. 62).

[171] Z. P. Li, F. E. Close and T. Barnes,
Relativistic effects in gamma gamma decays of P wave positronium and q anti-q systems,
http://dx.doi.org/10.1103/PhysRevD.43.2161Phys. Rev. **D43** (1991) 2161 (cit. on p. 62).

[172] L.-Y. Dai and M. R. Pennington,
Comprehensive amplitude analysis of $\gamma\gamma \to \pi^+\pi^-, \pi^0\pi^0$ and $\overline{K}K$ below 1.5 GeV,
http://dx.doi.org/10.1103/PhysRevD.90.036004Phys. Rev. **D90** (2014) 036004,
arXiv: 1404.7524 [hep-ph] (cit. on p. 62).

[173] T. Mori et al.,
High statistics study of f(0)(980) resonance in gamma gamma —> pi+ pi- production,
http://dx.doi.org/10.1103/PhysRevD.75.051101Phys. Rev. **D75** (2007) 051101,
arXiv: hep-ex/0610038 [hep-ex] (cit. on p. 62).

[174] T. Mori et al.,
High statistics measurement of the cross-sections of gamma gamma —> pi+ pi- production,
http://dx.doi.org/10.1143/JPSJ.76.074102J. Phys. Soc. Jap. **76** (2007) 074102,
arXiv: 0704.3538 [hep-ex] (cit. on p. 62).

[175] J. A. Carrasco et al., *Dispersive calculation of complex Regge trajectories for the lightest f_2 resonances and the $K^*(892)$*,
http://dx.doi.org/10.1016/j.physletb.2015.08.019Phys. Lett. **B749** (2015) 399,
arXiv: 1504.03248 [hep-ph] (cit. on p. 62).

[176] J. T. Londergan et al., *Identification of non-ordinary mesons from the dispersive connection between their poles and their Regge trajectories: The $f_0(500)$ resonance*,
http://dx.doi.org/10.1016/j.physletb.2013.12.061Phys. Lett. **B729** (2014) 9,
arXiv: 1311.7552 [hep-ph] (cit. on p. 62).

[177] J. R. Pelaez and F. J. Yndurain,
*Regge analysis of pion pion (and pion kaon) scattering for energy s**1/2 > 1.4-GeV*,
http://dx.doi.org/10.1103/PhysRevD.69.114001Phys. Rev. **D69** (2004) 114001,
arXiv: hep-ph/0312187 [hep-ph] (cit. on p. 62).

[178] R. Garcia-Martin et al., *The Pion-pion scattering amplitude. IV: Improved analysis with once subtracted Roy-like equations up to 1100 MeV*,
http://dx.doi.org/10.1103/PhysRevD.83.074004Phys. Rev. **D83** (2011) 074004,
arXiv: 1102.2183 [hep-ph] (cit. on p. 62).

[179] A. V. Anisovich, V. V. Anisovich and A. V. Sarantsev,
*Systematics of q anti-q states in the (n, M**2) and (J, M**2) planes*,
http://dx.doi.org/10.1103/PhysRevD.62.051502Phys. Rev. **D62** (2000) 051502,
arXiv: hep-ph/0003113 [hep-ph] (cit. on p. 62).

[180] B. Ananthanarayan et al., *Roy equation analysis of pi pi scattering*,
http://dx.doi.org/10.1016/S0370-1573(01)00009-6Phys. Rept. **353** (2001) 207,
arXiv: hep-ph/0005297 [hep-ph] (cit. on p. 62).

[181] G. Veneziano,
Construction of a crossing-symmetric, Regge behaved amplitude for linearly rising trajectories,
http://dx.doi.org/10.1007/BF02824451Nuovo Cim. **A57** (1968) 190 (cit. on p. 62).

[182] C. Lovelace, *A novel application of regge trajectories*,
http://dx.doi.org/10.1016/0370-2693(68)90255-4Phys. Lett. **28B** (1968) 264 (cit. on p. 62).

[183] J. A. Shapiro, *Narrow-resonance model with regge behavior for pi pi scattering*, http://dx.doi.org/10.1103/PhysRev.179.1345Phys. Rev. **179** (1969) 1345 (cit. on p. 62).

[184] L.-S. Geng, R. Molina and E. Oset, *On the chiral covariant approach to ρρ scattering*, http://dx.doi.org/10.1088/1674-1137/41/12/124101Chin. Phys. **C41** (2017) 124101, arXiv: 1612.07871 [nucl-th] (cit. on pp. 63, 64).

[185] J. D. Bjorken, *Construction of Coupled Scattering and Production Amplitudes Satisfying Analyticity and Unitarity*, http://dx.doi.org/10.1103/PhysRevLett.4.473Phys. Rev. Lett. **4** (1960) 473 (cit. on pp. 63, 83, 91).

[186] M. C. Birse, *Effective chiral Lagrangians for spin 1 mesons*, http://dx.doi.org/10.1007/s002180050105Z. Phys. **A355** (1996) 231, arXiv: hep-ph/9603251 [hep-ph] (cit. on p. 64).

[187] N. Kaiser, P. B. Siegel and W. Weise, *Chiral dynamics and the low-energy kaon - nucleon interaction*, http://dx.doi.org/10.1016/0375-9474(95)00362-5Nucl. Phys. **A594** (1995) 325, arXiv: nucl-th/9505043 [nucl-th] (cit. on p. 69).

[188] N. Kaiser, P. B. Siegel and W. Weise, *Chiral dynamics and the S11 (1535) nucleon resonance*, http://dx.doi.org/10.1016/0370-2693(95)01203-3Phys. Lett. **B362** (1995) 23, arXiv: nucl-th/9507036 [nucl-th] (cit. on p. 69).

[189] Z.-H. Guo, J. A. Oller and J. Ruiz de Elvira, *Chiral dynamics in form factors, spectral-function sum rules, meson-meson scattering and semi-local duality*, http://dx.doi.org/10.1103/PhysRevD.86.054006Phys. Rev. **D86** (2012) 054006, arXiv: 1206.4163 [hep-ph] (cit. on p. 69).

[190] L. Roca, E. Oset and J. Singh, *Low lying axial-vector mesons as dynamically generated resonances*, http://dx.doi.org/10.1103/PhysRevD.72.014002Phys. Rev. **D72** (2005) 014002, arXiv: hep-ph/0503273 [hep-ph] (cit. on p. 69).

[191] L. Alvarez-Ruso, J. A. Oller and J. M. Alarcon, *On the phi(1020) f0(980) S-wave scattering and the Y(2175) resonance*, http://dx.doi.org/10.1103/PhysRevD.80.054011Phys. Rev. **D80** (2009) 054011, arXiv: 0906.0222 [hep-ph] (cit. on pp. 69, 73).

[192] L. Alvarez-Ruso, J. A. Oller and J. M. Alarcon, *The $\phi(1020)$ $a_0(980)$ S-wave scattering and hints for a new vector-isovector resonance*, http://dx.doi.org/10.1103/PhysRevD.82.094028Phys. Rev. **D82** (2010) 094028, arXiv: 1007.4512 [hep-ph] (cit. on pp. 69, 73).

[193] S. Sarkar, E. Oset and M. J. Vicente Vacas, *Baryonic resonances from baryon decuplet-meson octet interaction*, http://dx.doi.org/10.1016/j.nuclphysa.2005.01.006, 10.1016/j.nuclphysa.2006.09.019Nucl. Phys. **A750** (2005) 294, [Erratum: Nucl. Phys.A780,90(2006)], arXiv: nucl-th/0407025 [nucl-th] (cit. on p. 69).

[194] J. A. Oller, *Nucleon nucleon interactions from effective field theory*, http://dx.doi.org/10.1016/S0375-9474(03)01448-9Nucl. Phys. **A725** (2003) 85 (cit. on p. 69).

[195] J. A. Oller, *The Case of a WW dynamical scalar resonance within a chiral effective description of the strongly interacting Higgs sector*, http://dx.doi.org/10.1016/S0370-2693(00)00185-4Phys. Lett. **B477** (2000) 187, arXiv: hep-ph/9908493 [hep-ph] (cit. on pp. 69, 77).

[196] A. Dobado et al., *CERN LHC sensitivity to the resonance spectrum of a minimal strongly interacting electroweak symmetry breaking sector*, http://dx.doi.org/10.1103/PhysRevD.62.055011Phys. Rev. **D62** (2000) 055011, arXiv: hep-ph/9912224 [hep-ph] (cit. on p. 69).

[197] U.-G. Meißner and J. A. Oller, *Chiral unitary meson baryon dynamics in the presence of resonances: Elastic pion nucleon scattering*, http://dx.doi.org/10.1016/S0375-9474(00)00150-0Nucl. Phys. **A673** (2000) 311, arXiv: nucl-th/9912026 [nucl-th] (cit. on pp. 69, 77).

[198] M. Albaladejo, J. A. Oller and L. Roca, *Dynamical generation of pseudoscalar resonances*, http://dx.doi.org/10.1103/PhysRevD.82.094019Phys. Rev. **D82** (2010) 094019, arXiv: 1011.1434 [hep-ph] (cit. on p. 69).

[199] P. C. Bruns, M. Mai and U.-G. Meißner, *Chiral dynamics of the S11(1535) and S11(1650) resonances revisited*, http://dx.doi.org/10.1016/j.physletb.2011.02.008Phys. Lett. **B697** (2011) 254, arXiv: 1012.2233 [nucl-th] (cit. on p. 69).

[200] M. Mai and U.-G. Meißner, *Constraints on the chiral unitary $\bar{K}N$ amplitude from $\pi\Sigma K^+$ photoproduction data*, http://dx.doi.org/10.1140/epja/i2015-15030-3Eur. Phys. J. **A51** (2015) 30, arXiv: 1411.7884 [hep-ph] (cit. on p. 69).

[201] D. Gamermann and E. Oset, *Axial resonances in the open and hidden charm sectors*, http://dx.doi.org/10.1140/epja/i2007-10435-1Eur. Phys. J. **A33** (2007) 119, arXiv: 0704.2314 [hep-ph] (cit. on p. 69).

[202] J. M. Dias, F. Aceti and E. Oset, *Study of $B\bar{B}^*$ and $B^*\bar{B}^*$ interactions in $I = 1$ and relationship to the $Z_b(10610)$, $Z_b(10650)$ states*, http://dx.doi.org/10.1103/PhysRevD.91.076001Phys. Rev. **D91** (2015) 076001, arXiv: 1410.1785 [hep-ph] (cit. on p. 69).

[203] O. Romanets et al., *Charmed and strange baryon resonances with heavy-quark spin symmetry*, http://dx.doi.org/10.1103/PhysRevD.85.114032Phys. Rev. **D85** (2012) 114032, arXiv: 1202.2239 [hep-ph] (cit. on p. 69).

[204] X.-W. Kang and J. A. Oller, *P-wave coupled-channel scattering of $B_s\pi$, $B_s^*\pi$, $B\overline{K}$, $B^*\overline{K}$ and the puzzling $X(5568)$*, http://dx.doi.org/10.1103/PhysRevD.94.054010Phys. Rev. **D94** (2016) 054010, arXiv: 1606.06665 [hep-ph] (cit. on p. 69).

[205] L. Roca et al., *Predictions for the $\Lambda_b \to J/\psi\,\Lambda(1405)$ decay*, http://dx.doi.org/10.1140/epjc/s10052-015-3438-1Eur. Phys. J. **C75** (2015) 218, arXiv: 1503.02936 [hep-ph] (cit. on p. 69).

[206] F. Aceti and E. Oset, *Wave functions of composite hadron states and relationship to couplings of scattering amplitudes for general partial waves*, http://dx.doi.org/10.1103/PhysRevD.86.014012Phys. Rev. **D86** (2012) 014012, arXiv: 1202.4607 [hep-ph] (cit. on pp. 71, 77).

[207] T. Sekihara, T. Hyodo and D. Jido,
Comprehensive analysis of the wave function of a hadronic resonance and its compositeness,
http://dx.doi.org/10.1093/ptep/ptv081PTEP **2015** (2015) 063D04, arXiv: 1411.2308 [hep-ph]
(cit. on pp. 71, 77).

[208] M. Bando et al., *Is rho Meson a Dynamical Gauge Boson of Hidden Local Symmetry?*,
http://dx.doi.org/10.1103/PhysRevLett.54.1215Phys. Rev. Lett. **54** (1985) 1215 (cit. on p. 75).

[209] M. Albaladejo and J. A. Oller, *Identification of a Scalar Glueball*,
http://dx.doi.org/10.1103/PhysRevLett.101.252002Phys. Rev. Lett. **101** (2008) 252002,
arXiv: 0801.4929 [hep-ph] (cit. on pp. 76, 83).

[210] D. V. Bugg, *A Study in Depth of f0(1370)*,
http://dx.doi.org/10.1140/epjc/s10052-007-0389-1Eur. Phys. J. **C52** (2007) 55,
arXiv: 0706.1341 [hep-ex] (cit. on p. 76).

[211] M. Albaladejo and J. A. Oller,
Nucleon-nucleon interactions from dispersion relations: Elastic partial waves,
http://dx.doi.org/10.1103/PhysRevC.84.054009Phys. Rev. **C84** (2011) 054009,
arXiv: 1107.3035 [nucl-th] (cit. on pp. 77, 79).

[212] Z.-H. Guo, J. A. Oller and G. Ríos,
Nucleon-Nucleon scattering from the dispersive N/D method: next-to-leading order study,
http://dx.doi.org/10.1103/PhysRevC.89.014002Phys. Rev. **C89** (2014) 014002,
arXiv: 1305.5790 [nucl-th] (cit. on pp. 77, 79, 82, 99).

[213] J. A. Oller,
Nucleon-Nucleon scattering from dispersion relations: next-to-next-to-leading order study,
http://dx.doi.org/10.1103/PhysRevC.93.024002Phys. Rev. **C93** (2016) 024002,
arXiv: 1402.2449 [nucl-th] (cit. on pp. 77, 79, 82).

[214] D. R. Entem and J. A. Oller,
The N/D method with non-perturbative left-hand-cut discontinuity and the $^1S_0$ NN partial wave,
http://dx.doi.org/10.1016/j.physletb.2017.09.012Phys. Lett. **B773** (2017) 498,
arXiv: 1610.01040 [nucl-th] (cit. on pp. 77, 79, 82).

[215] A. M. Badalian et al., *Resonances in Coupled Channels in Nuclear and Particle Physics*,
http://dx.doi.org/10.1016/0370-1573(82)90014-XPhys. Rept. **82** (1982) 31 (cit. on p. 83).

[216] D. Lurié and A. J. Macfarlane, *Equivalence Between Four-Fermion and Yukawa Coupling, and the $Z_3 = 0$ Condition for Composite Bosons*,
http://dx.doi.org/10.1103/PhysRev.136.B816Phys. Rev. **136** (3B 1964) B816,
URL: https://link.aps.org/doi/10.1103/PhysRev.136.B816 (cit. on p. 121).

Acknowledgements

First of all, I express my gratitude to Prof. Dr. Ulf Meißner who gave me the opportunity to do this research in his research group. I am thankful to him for his important remarks on the thesis, for carefully correcting this thesis and for his guidance during my research project. I am also grateful to Prof. Dr. Christoph Hanhart for his support in being my second thesis advisor.

I would like to express my special thanks to Prof. Dr. Jose Oller for his patience with me and for discussions on the topic. I am grateful for the time he spared for Skype meetingsö for his answers to all my questions and for precious his collaboration.

I thank Dr. Feng-Kun Guo, Dr. Menglin Du and Dr. Qian Wang for their comments, discussions and collaboration on the subject.

My special thank goes to Barbara Kraus and Dr. Serdar Elhatisari. They were willing to help with any problem I had during my time in HISKP. I am grateful to Prof. Dr. Bastian Kubis, PD Dr. Akaki Rusetsky, and Matthias Frink for all their help during all this time.

I would like to thank Ripunjay Acharya for his corrections regarding the grammar and structure of this thesis. Moreover, I thank Ertan Sinan Şahin for his bits of help with generating the figures of this thesis.

Benim için yaptıkları bütün fedakarlıklar için, beni her zaman destekledikleri ve sevgilerini hiçbir zaman esirgemedikleri için ve anneme ve babama minnettarım.

I would like to thank all my friends who made me feel home here. Especially, I would like to thank Ripunjay Acharya for his precious companionship all these years, İlkin Deniz Özer for all her dear friendship, support, help and for all the time we have been through together, Emrah Özkan for the priceless TLH nights and talks and for all the effort he made and time he spent for me, Roberto Cota for the joy that he shares without hesitation and for all his help, Jan-Matthis Lückmann for his kindness and help, Arthur Speiser for all the fruitful discussions and help, Thorsten Schimannek for his friendship and making last 5 years more interesting.

Hayatımı renklendiren, neşe ve heyecan katan, zor zamanlarda huzur ve güç veren dostluğu ve desteği için sevgili Cansu Tekin'e minnettarım.

Zor zamanlarda karşılıksız yardımlarını sunan, her zaman destek olan ve dostluklarını esirgemeyen Cansu Tekin, Gül Tuçaltan, Emre Kanpolat, Ezgi Erdoğan, Emrah Özkan, İlkin Deniz Özer, Marie Miglianico, Ayça Yıldırım ve Özgür Kızılay'a minnettarlığımı belirtmek isterim ve teşekkür ederim.

Her zaman yanımda olduklarını bildiğim, boşluğa düştüğümde dostluklarına sığındığım, varlıkları ile bana huzur veren Ayşegül Turupcu ve Arman Konukçu'ya minnettarım.

Mesafeleri umursamadan ve karşılık beklemeden dostluklarını ve sevgilerini her zaman paylaşan, hayatımı zenginleştiren benim için çok değerli ve güzel insanlar İbrahim Çağlar Şakar, Ezgi Erdoğan, Anıl

Yüksel, Ulaş Özdem, Ece Özbey, Hakan Çetinkaya, Didem Türe, Hasan Küçükalpelli, Tuna Demircik, Arif Emre Taş, Burçin İçdem ve Aybike Alkan'a teşekkür ederim.